THE UNIVERSITY
of EDINBURGH

Modelling Adipose Tissue Expansion in Zebrafish

Rebecca Wafer

Doctor of Philosophy (PhD)

The University of Edinburgh

2020

Abstract

Obesity has been classified as a global epidemic by the World Health Organisation, with 13% of the world's adult population estimated to be obese in 2016. An increased risk of multiple diseases is associated with obesity, including cardiovascular disease and type two diabetes. Obesity itself is defined as an excess of white adipose tissue (AT) and a body mass index of over 30 kg/m^2. The excess adipose tissue present in obesity can become dysfunctional and display increased hypoxia, fibrosis, and necrotic adipocyte death. It is AT dysfunction which is thought to be responsible for obesity associated disease and the primary cause of AT dysfunction is a limited capacity of adipose tissue to expand. Obesity and by proxy adipose tissue expansion are known to be partially genetically regulated, with heritability estimates ranging from 40% to 70%. In order to identify the genetic variation underlying obesity, genome wide association studies (GWAS) have been utilised. Multiple GWAS studies, including a study into BMI by Kichaev et al (2019), have found that genetic variation at the *FOXP1* locus is associated with adiposity levels. However, whether *FOXP1* directly regulates adipose levels is entirely unknown. Here I generated a series of predicted loss of function *foxp1* alleles in zebrafish. My goal was to determine whether *foxp1* influenced AT growth and expansion *in vivo*. To this end a CRISPR/Cas9 system was employed to generate stable *foxp1* mutant zebrafish. Changes in AT expansion were then assessed in the F2 generation, with live imaging of total AT area providing information on changes in growth dynamics between wild type and mutant fish. Mutant fish were found to have reduced levels of adipose tissue during normal development and also accumulated less AT in response to a high fat diet. In addition to generating *foxp1* mutants I also generated a novel transgenic line which labels both adipocytes and adipose progenitor cells. Using the transgenic line, I performed high resolution *in vivo* imaging of zebrafish AT and compiled novel information about adipose progenitor cell behaviour. Adipose progenitor cell behaviour was also assessed in *foxp1* mutant zebrafish. In summary, I have tested the role of *foxp1* in adipose tissue expansion and found evidence to suggest that *foxp1* is required for adipose tissue expansion. I have also generated a novel transgenic line which has allowed for unprecedented *in vivo* imaging of adipose tissue expansion. This is the first data to suggest that *foxp1* plays an *in vivo* role in adipose tissue expansion. Further investigations into the mechanisms by which *foxp1* influences AT expansion could lead to the creation of prediction strategies to prevent the development of unhealthy obesity.

Lay summary

Obesity is now a global health epidemic with 13% of the world's adult population classified as obese in 2016. Multiple diseases are associated with obesity, including cardiovascular disease and type two diabetes. Obesity is characterised by excess fat, also known as adipose tissue, and is defined as a body mass index (BMI) of over 30 kg/m^2. Not everyone with obesity will develop associated diseases and therefore it is not excess fat alone which influences disease susceptibility. While obesity is primarily thought of as a lifestyle disease it is also known to be influenced by an individual's genetic makeup. However, which genes control fat levels and which genes lead to increased risks of developing obesity associated diseases are largely unknown. In this project I have investigated how a gene called *foxp1* influences fat levels and have found that *foxp1* is required for fat expansion. Further investigations into how *foxp1* acts to influence fat levels could lead to the creation of prediction strategies to prevent the development of obesity associated disease.

Declaration

I, Rebecca Wafer, hereby certify that this thesis has been composed by me and that the work is my own unless otherwise stated. The work undertaken was undertaken as part of a research group and some experiments were conducted with the assistance of masters students under my supervision. Two masters students, Jason Lam and Katy McDonald, contributed to some of the data presented in chapter 5.

Jason Lam performed *cebpa* transcript level measurements, the *cebpa* mutant survival assay and helped to perform Nile Red imaging. All raw data was reanalysed by me and all figures and text complied by me. Katy McDonald helped to perform liver imaging, the *cebpa* HFD, some confocal imaging of *cebpa*$^{(+/ed19)}$ and *cebpa*$^{(+/ed10)}$ PVAT and LSAT depots and the *Foxp1:eGFP:cebpa*$^{(+/ed19)}$ imaging. All raw data was analysed by me and all figures and text were compiled by me. The Nile Red imaging, HFD and *Foxp1:eGFP:cebpa*$^{(+/ed19)}$ imaging were also performed on live fish post 5 dpf and so a home office license was required for this work and so I was present and helped to perform all of these experiments.

Finally, this work has not been submitted for any other degree or professional qualification.

01.04.20

Acknowledgements

I would like to thank the following people who have helped me undertake this research project. I would first like to thank my supervisor Dr James Minchin for providing guidance and advice over the course of my PhD. I would also like to thank the other members of the lab group Dr Panna Tadon and Loes Elemans. I would like to especially thank Panna for all of her help and advice during my PhD. Thankyou also to previous students Jason Lam, Katy McDonald and Rosalind Fong who provided invaluable help in the lab in collecting data. Thankyou to the members of my thesis committee, Dr John Mullins, Dr Will Cawthorn and Dr Yi Feng for all of their advice and encouragement. Thankyou to all the members of the BVS aquatics facility. Finally, thank you to the BHF and the BHF centre of research excellence for providing funding.

List of abbreviations

ACTB	Beta actin
AT	Adipose Tissue
ATG	ATG translational start site
BAT	Brown Adipose Tissue
BMI	Body Mass Index
bZIP	Basic Leucine Zipper
CD	Control Diet
CD29	Integrin Beta 1
CD31	Platelet endothelial cell adhesion molecule
CD45	Protein tyrosine phosphatase receptor type C
CEBP	CCAT enhancer binding protein
CFRSAT	Caudal Fin Ray SAT
ChIP	Chromatin immunoprecipitation
CNE	Conserved non-coding element
CTBP1	C-terminal binding protein 1
CXCR4	Chemokine Receptor type 4
DALYs	Disability adjusted life years
DHS	Dnase hypersensitive site
dpf	Days post fertilisation
DR1	Direct repeat 1
DSAT	Dorsal SAT
ECM	Extracellular Matrix
eQTL	expression Quantitative Trait Locus
ESCs	Embryonic Stem Cells
FACS	Fluorescence Activated Cell Sorting
FHD	Forkhead Domain
FOXP1	Forkhead box P1
gDNA	Genomic DNA
GFP	Green Fluorescent Protein
GH	Growth Hormone
GO	Gene Ontology
GTEx	Genotype-tissue expression
GWAS	Genome Wide Association Study

HFD	High Fat Diet
HISAT	Hierarchical Indexing for Spliced Alignment
HOXA5	Homeobox A5
hpf	hours post fertilisation
HYD	Hyoid Apparatus
H2B	Histone 2B
KLF	Kruppel Like Factor
Krox20	Early Growth Response 2, Egr2
LB	Lysogeny Broth
LSAT	Lateral Subcutaneous Adipose Tissue
METSIM	Metabolic Syndrome In Men
MSC	Mesenchymal Stem Cell
NEFAs	Non-esterified fatty acids
NR3C1	Nuclear Receptor Subfamily 3 Group C member 1
OCU	Eye
OPC	Operculum
PCR	Polymerase Chain Reaction
PDGFRa	Platelet Derived Growth Factor Receptor alpha
PLXND1	Plexin D1
PVAT	Pancreatic Visceral Adipose Tissue
PPARG	Peroxisome Proliferator Activated Receptor Gamma
RIN	RNA Integrity Number
RNA-Seq	RNA Sequencing
RT-qPCR	Reverse Transcription Quantitative PCR
RXRA	Retinoid X Receptor Alpha
SAT	Subcutaneous Adipose Tissue
Sca1	Ataxin 1
sgRNA	single guide RNA
SL	Standard Length
SNPs	Single Nucleotide Polymorphisms
SOC	Super Optimal Broth
SREBP1c	Sterol Regulatory Element Binding Protein 1c
STAT5a	Signal Transducer and Activator of Transcription 5a
SVF	Stromal Vascular Fraction

TAD	Transactivation Domain
T7E1	T7 Endonuclease 1
UCP1	Uncoupling Protein 1
VAT	Visceral Adipose Tissue
VEGF	Vascular Endothelial Growth Factor
VSAT	Ventral SAT
WAT	White Adipose Tissue
WT	Wild Type
zCNE	Zebrafish Conserved Non-Coding Element
ZFD	Zinc Finger Domain
ZFP423	Zinc Finger Protein 423

Table of Contents

Chapter 1 – Introduction

1.1 – Obesity, obesity associated disease and adipose tissue dysfunction

1.1.1 – The global prevalence of obesity is increasing

Levels of overweight and obesity, defined by Body Mass Indexes (BMI) of over 25 kg/m^2 and 30 kg/m^2 respectively, are currently a global epidemic **(Figure 1.1A & B)** (Collaborators et al., 2017, WHO). Previously considered an issue confined to the developed world, obesity has now become a truly global problem with the worldwide prevalence of obesity nearly tripling between 1975 and 2016 **(Figure 1.1A, B & C)** (WHO). For example, in Africa the prevalence of obesity has nearly doubled between 1980 and 2015, going from 6.2% to 12.7% (**Figure 1.1C)** (Collaborators et al., 2017). Despite the global reach of obesity, it is still much more common in the west. In 2015 28.3% of Americans were obese, as were 22.9% of Europeans **(Figure 1.1A & B)** (Collaborators et al., 2017). Among adults the prevalence of obesity is generally higher amongst women and if current trends continue 18% of men and 21% of women are predicted to be obese by 2025 (Collaborators et al., 2017, Collaboration, 2016). Together these statistics highlight the extent to which obesity is now a global phenomenon.

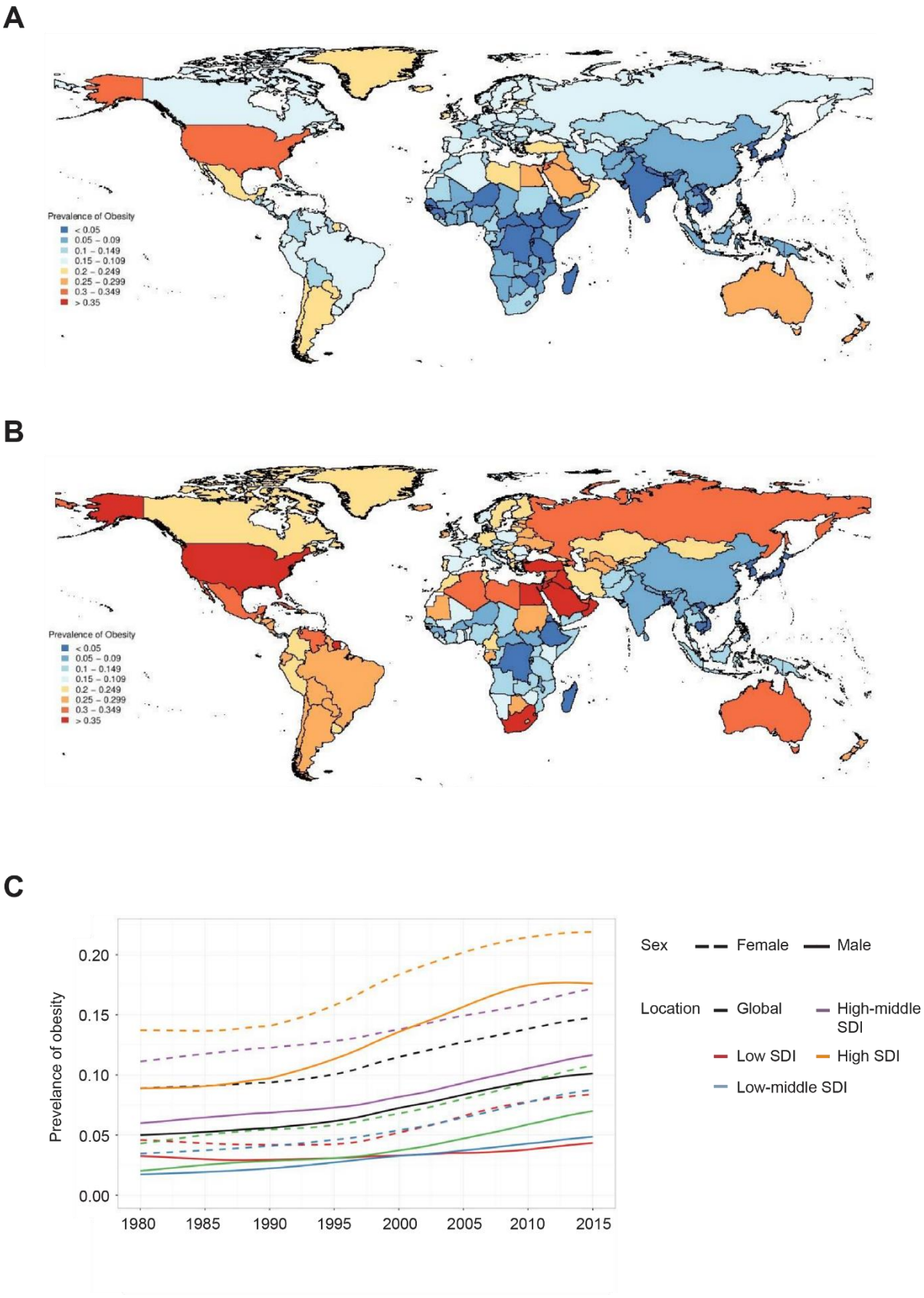

Figure 1.1 – The global prevalence of obesity

Figure 1.1 – The global prevalence of obesity. A. Schematic of global obesity levels in adult males, adapted from GBD 2015 obesity collaborators (2017). **B.** Schematic of global obesity levels in adult females, adapted from GBD 2015 obesity collaborators (2017). **C.** Trends in age standardized prevalence of obesity among adults, adapted from GBD 2015 obesity collaborators (2017). SDI (Sociodemographic Index).

1.1.2 – Obesity is linked to increased disease risk

Obesity is classified as a health problem due to the increased disease risk which it confers (Martin et al., 2015). For example, in 2015 excess weight contributed to 4 million deaths and 120 million disability adjusted life years (DALYs) **(Figure 1.2A)** (Collaborators et al., 2017). In the UK 9000 premature deaths occur each year as the result of obesity, accounting for 8.7% of all deaths (Agha and Agha, 2017). Numerous medical complications are associated with obesity and these extend to nearly every organ system, with cardiovascular disease, diabetes and cancer being common complications (Martin et al., 2015, Haffner, 2006). Cardiovascular disease has been shown to be the leading cause of deaths and DALYs relating to high BMI, and was responsible for 2.7 million deaths and 66.3 million DALYs in 2015 **(Figure 1.2A)** (Collaborators et al., 2017). Diabetes was the second leading cause, responsible for 0.9 million deaths and 39.1 million DALYs **(Figure 1.2A)** (Collaborators et al., 2017). Overall obesity is linked to multiple diseases, with cardiovascular disease and diabetes being leading causes of obesity related death.

Numerous studies have examined the links between obesity and disease. For example, multiple epidemiological studies have shown that obesity is an independent cardiovascular disease predictor (Hubert et al., 1983, Rabkin et al., 1977, Manson et al., 1990, Kenchaiah et al., 2002). Cardiovascular diseases associated with obesity include, coronary heart disease, heart failure, hypertension, and sudden cardiac death (Koliaki et al., 2019). Obesity is thought to lead to cardiovascular disease by inducing maladaptive adaptations in cardiovascular structure and function **(Figure 1.2B)** (Koliaki et al., 2019). These alterations increase cardiac workload and predispose obese individuals to heart failure **(Figure 1.2B)** (Koliaki et al., 2019). Obesity is also linked to type two diabetes (Al-Goblan et al., 2014). Briefly type 1 diabetes is caused by an inability of the body to produce insulin due to the autoimmune destruction of pancreatic β-cells, while type two diabetes is caused by the absence of insulin secretion, due to low amounts of insulin production from pancreatic β-cells and peripheral insulin resistance **(Figure 1.2C)** (Al-Goblan et al., 2014). Insulin sensitivity varies across BMI, however there is a strong association between obesity and insulin sensitivity (Al-Goblan et al., 2014). Diabetes occurs in individuals who lack sufficient insulin secretion to match the degree of insulin resistance (Al-Goblan et al., 2014). Obesity causes increased secretion of leptin, cytokines, and nonesterified fatty acids (NEFAs) (Al-Goblan et al., 2014). Increased

levels of NEFAs are associated with both insulin resistance and a decline in pancreatic β-cell function (Al-Goblan et al., 2014). Increased levels of NEFAs are therefore one way in which obesity can lead to the development of diabetes (Al-Goblan et al., 2014). Finally, obesity is associated with an increased risk of developing various cancers, with strong epidemiological evidence linking obesity to increased cancer risk and mortality (Park et al., 2014, Barlow et al., 2006, Calle et al., 2003). Secretion of adipokines from adipocytes has been shown to influence the tumour microenvironment and to influence the progression of cancer (Park et al., 2014). Furthermore, cytokines released from AT during obesity have been shown to stimulate cancer stem cell growth and survival (Park et al., 2014). In summary obesity causes changes in the body which increase the likelihood of developing diseases including cardiovascular disease, diabetes and cancer.

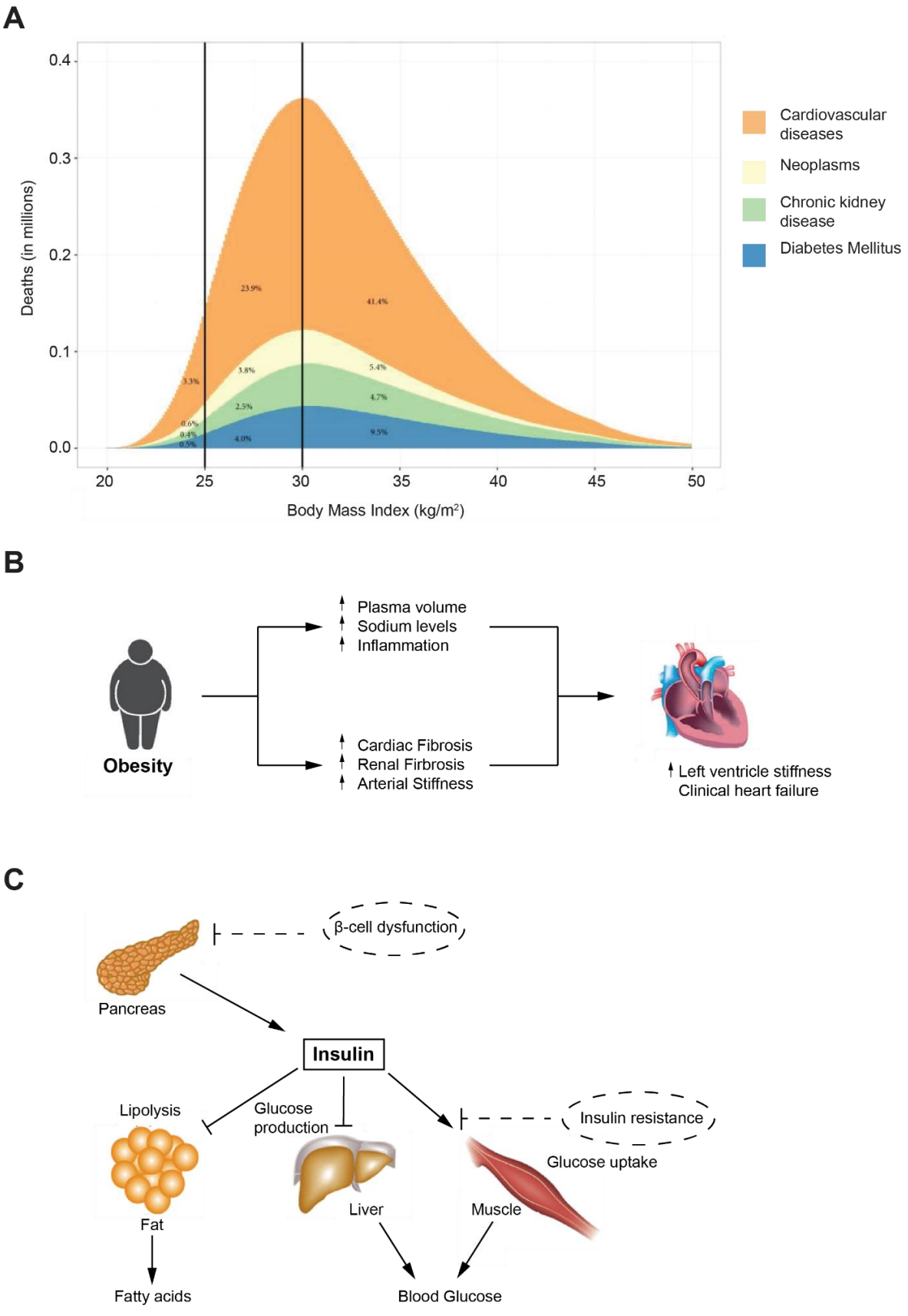

Figure 1.2 – Obesity is associated with increased disease risk

Figure 1.2 – Obesity is associated with increased disease risk A. Graph showing deaths in 2015 due to obesity associated disease. Adapted from GBD 2015 obesity collaborators (2015). **B.** Schematic showing how obesity can lead to heart failure. Adapted from (Pandey et al., 2018). **C.** Schematic showing the effect of β-cell dysfunction and peripheral insulin resistance. Adapted from (Stumvoll et al., 2005).

1.1.3 – Adipose tissue acts primarily as an energy storage organ

Obesity is characterised by over nutrition and the accumulation of fat (Collaborators et al., 2017). Nearly every species of animal has found a way to store excess energy in the form of fat (Gesta et al., 2007). For example, *Caenorhabditis elegans* stores fat in the intestinal epithelium, while sharks store fat in the liver (Gesta et al., 2007). However, in most species excess energy is stored in white adipose tissue (WAT) (Gesta et al., 2007). WAT acts as a dynamic energy store, storing lipid in times of energy excess and mobilising lipid in times of energy deficit (Ma et al., 2015). In addition to it's energy storage role, WAT also has several additional functions including providing mechanical cushioning in regions of high stress such as the palm and heel, and providing cushioning to organs such as the heart and kidneys (Ghaben and Scherer, 2019). Adipose tissue also acts as an endocrine organ and secretes a variety of signalling proteins, known as adipokines (Ghaben and Scherer, 2019). Overall white adipose tissue has multiple functions, with its function as an energy store being the focus of this chapter.

In addition to WAT, mammals also possess brown and beige adipose tissue (Gesta et al., 2007). No tissue resembling brown adipose tissue (BAT) has yet been described in reptiles, amphibians or fish (Gesta et al., 2007). BAT is characterised by the expression of uncoupling protein 1 (UCP1) and generates heat through adaptive thermogenesis (Gesta et al., 2007). In rodents and humans BAT is most abundant during early development (Gesta et al., 2007). BAT is found in the interscapular region in rodents and in axillary, cervical, perirenal and periadrenal locations in humans (Gesta et al., 2007). Beige adipose tissue has been described as typical WAT tissue which contains some brown adipocytes and has been observed following cold exposure (Gesta et al., 2007). In summary, in addition to WAT mammals also possess thermogenic BAT however the remainder of this chapter will focus on the role of white adipose tissue.

1.1.4 – Adipose tissue is comprised of multiple cell types

Adipose tissue is comprised primarily of adipocytes **(Figure 1.3A)** (Ma et al., 2015). Within adipose tissue, adipocytes are found tightly packed together and surrounded by a richly vascularised loose connective tissue **(Figure 1.3A)** (Ma et al., 2015). Other cell types found in adipose tissue include, preadipocytes, fibroblasts,

endothelial cells and immune cells **(Figure 1.3A)** (Ma et al., 2015). Adipocytes are the specialised cells within adipose tissue which store energy within lipid droplets **(Figure 1.3B)** (Ma et al., 2015). Although some lipid accumulation can occur in other cell types, adipocytes differ from other cells due to the presence of large lipid droplets which are surrounded by the protein perilipin **(Figure 1.3B)** (Gesta et al., 2007). Adipocytes are characterised by the presence of a singular lipid droplet, a peripheral nucleus and their large size, with cells typically being 100 μm in diameter **(Figure 1.3B)** (Ma et al., 2015). In summary adipose tissue is comprised of multiple cell types, with adipocytes acting to store energy.

Adipocytes store energy in response to insulin **(Figure 1.3C)** (Haczeyni et al., 2018). Elevations in blood glucose occur in response to food intake and this stimulates the secretion of insulin from pancreatic β-cells (Haczeyni et al., 2018). In response, adipocytes take up and convert glucose into neutral lipid for later use **(Figure 1.3C)** (Haczeyni et al., 2018). This process, known as lipogenesis, involves long chain fatty acid synthesis and the formation of triglycerides **(Figure 1.3C)** (Haczeyni et al., 2018). The reverse process of lipolysis also takes place in response to insulin signalling, with insulin signalling inhibiting lipolysis **(Figure 1.3C)** (Haczeyni et al., 2018). Here triglycerides are broken down into glycerol and free fatty acids and are released from the cell **(Figure 1.3C)** (Haczeyni et al., 2018). In addition to storing triglycerides, adipocytes can also store cholesterol (Haczeyni et al., 2018). Adipose tissue behaves as a cholesterol sink, with 25% of total bodily cholesterol stored within the adipose of normal weight individuals (Haczeyni et al., 2018). Both cholesterol and triglycerides enter adipocytes via specific transporter molecules, which are often found within caveolae (Haczeyni et al., 2018). Caveolae are lipid dense domains within the plasma membrane enriched with glycosphingolipids, proteins and cholesterol molecules, and they are abundant in adipocytes (Haczeyni et al., 2018). Overall adipocytes act in response to insulin signalling to store energy within lipid droplets.

1.1.5 – Adipose tissue is found throughout the body

Adipose tissue is generally thought to be mesodermal in origin (Gesta et al., 2007). In rodents WAT develops mainly after birth, while in humans WAT development begins early in the second trimester of gestation (Gesta et al., 2007). WAT location also differs between species with invertebrates, amphibians and many

reptiles storing most adipose intraabdominally (Gesta et al., 2007). In contrast mammals, birds and some species of fish have both intraabdominal and subcutaneous adipose tissue (SAT), which is located beneath the skin **(Figure 1.3D)** (Gesta et al., 2007, Minchin and Rawls, 2017b). In humans WAT is found throughout the body with major intraabdominal depots being the omentum, which is a fold of fat around the stomach, and mesenteric AT, which surrounds the intestines **(Figure 1.3D)** (Gesta et al., 2007). Major subcutaneous depots are found in the buttocks, thighs and abdomen **(Figure 1.3D)** (Gesta et al., 2007). In mice major intraabdominal depots are the mesenteric and perigonadal depots and major SAT depots include inguinal SAT, which is located near the hindlimbs **(Figure 1.3D)** (Cleal et al., 2017, Gesta et al., 2007). In addition to being stored intraabdominally and subcutaneously, WAT can also be found in many other areas such as the retro-orbital space and within the bone marrow (Gesta et al., 2007). In summary WAT is found throughout the body and can be broadly classified as intraabdominal AT and SAT.

Intraabdominal adipose tissue, also known as visceral adipose tissue (VAT), and SAT are known to have different properties (Gesta et al., 2007). For example, expression profiling has revealed significant differences in the expression of 100s of genes between subcutaneous and visceral depots in both mice and humans (Gesta et al., 2006, Vidal, 2001, Vohl et al., 2004). Differentially expressed genes include genes involved in cell differentiation and adipogenesis (Vohl et al., 2004). For example, CEBPA expression has been shown to be higher in SAT, while CEBPD expression is higher in VAT (Vohl et al., 2004). VAT and SAT also show altered secretion of adipokines, rates of lipolysis and thermogenic potential (Ghaben and Scherer, 2019). The differing properties of VAT and SAT mean that SAT is considered to be broadly protective (Cleal et al., 2017). For example, numerous human and rodent studies have correlated increased SAT relative to VAT with preserved metabolic function, for subjects of similar weights (Ghaben and Scherer, 2019). Furthermore, transplantation of SAT into visceral adipose regions in mice has been shown to improve metabolic parameters (Tran et al., 2008). Taken together this data suggests that VAT and SAT have slightly different properties and that SAT is broadly protective.

While the heterogeneity of adipocytes from different depots has been established, more recent data has suggested that adipocytes within the same depot also display heterogeneity (Hepler et al., 2018, Schwalie et al., 2018, Sempere et al.,

2014). These studies have isolated adipose progenitor cells from within adipose tissue and have then used single cell RNA-Seq to look at differences in gene expression (Hepler et al., 2018, Schwalie et al., 2018, Sempere et al., 2014). Adipose progenitor cells are fibroblast like cells which differentiate to form adipocytes (Siersbaek et al., 2012). A study by Schwalie et al (2018) identified multiple populations of adipose progenitor cells and found that one population was capable of inhibiting adipocyte differentiation. Another study used single cell RNA-Seq to identify three adipose progenitor cell populations in one human adipose depot and found these cells to show differing rates of lipolysis (Raajendiran et al., 2019). In summary there is not only heterogeneity between adipose depots but also heterogeneity within adipose depots.

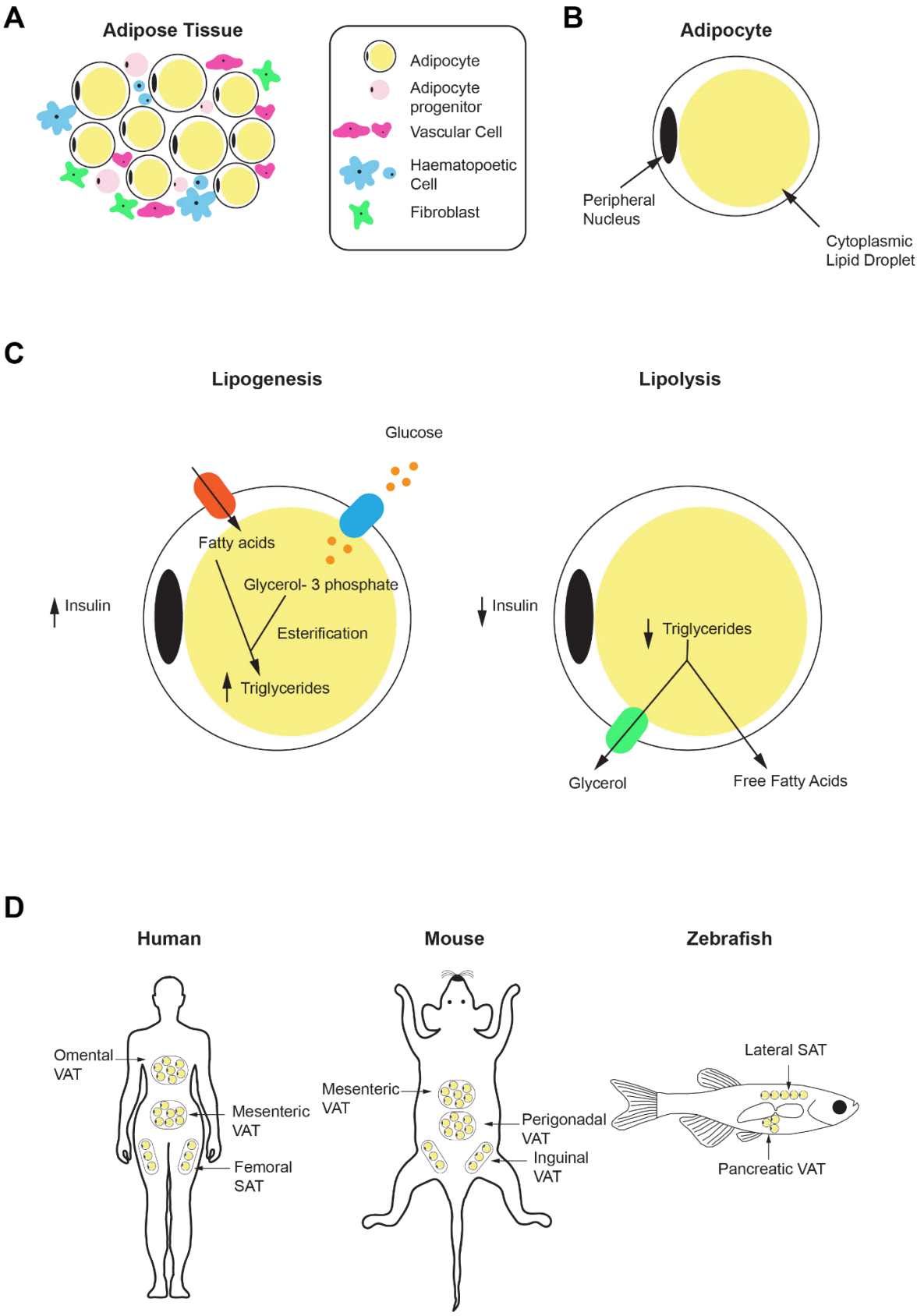

Figure 1.3 – Adipose tissue is composed primarily of adipocytes and is located throughout the body

Figure 1.3 – Adipose tissue is composed primarily of adipocytes and is located throughout the body. A. Schematic showing the cell types present in adipose tissue. **B.** Schematic of a white adipocyte with a singular lipid droplet. **C.** Schematic of lipolysis and lipogenesis. Adapted from Badimon et al (2015). **D.** Schematic showing some of the major adipose depots found in human, mouse and zebrafish. Mouse schematic adapted from (Schoettl et al., 2018). Human schematic adapted from (Zwick et al., 2018). VAT (Visceral adipose tissue). SAT (Subcutaneous adipose tissue).

1.1.6 – Obesity leads to adipose tissue dysfunction

Obesity is characterised by excess adipose tissue accumulation and adipose tissue dysfunction during obesity is thought to confer disease risk (Lafontan, 2014). Under a normal state, nutrient excess causes adipocytes to store lipid and expand in size (Crewe et al., 2017). These adipocytes will then reach the diffusional limit of oxygen, resulting in mild hypoxia which induces a stress signal to drive angiogenesis and remodelling of the extracellular matrix **(Figure 1.4A)** (Crewe et al., 2017). This response leads to healthy adipose tissue expansion **(Figure 1.4)**. However, lipodystrophy, ageing and obesity can all lead to dysfunctional adipose tissue expansion (Crewe et al., 2017). At some point during obesity adipose tissue depots expand beyond the tissues capacity for adequate angiogenesis, resulting in persistent hypoxia **(Figure 1.4B)** (Crewe et al., 2017). This in turn leads to necrotic adipocyte death, which triggers inflammation and the initiation of a wound healing response **(Figure 1.4B)** (Crewe et al., 2017). Macrophages and neutrophils are then recruited and produce toxic products such as reactive oxygen species which further injure surrounding cells and promote fibrosis **(Figure 1.4B)** (Crewe et al., 2017). During normal wound healing this process would end following the removal of the injury signal (Crewe et al., 2017). However, during obesity this injury signal persists and causes the chronic activation of immune cells which results in further tissue damage, fibrosis and AT dysfunction **(Figure 1.4B)** (Crewe et al., 2017). The resulting dysfunctional adipose tissue then loses its ability to store lipid, resulting in ectopic deposition of lipid in the liver and insulin resistance (Lafontan, 2014). The disease risk associated with obesity can therefore be explained by dysfunctional adipose tissue.

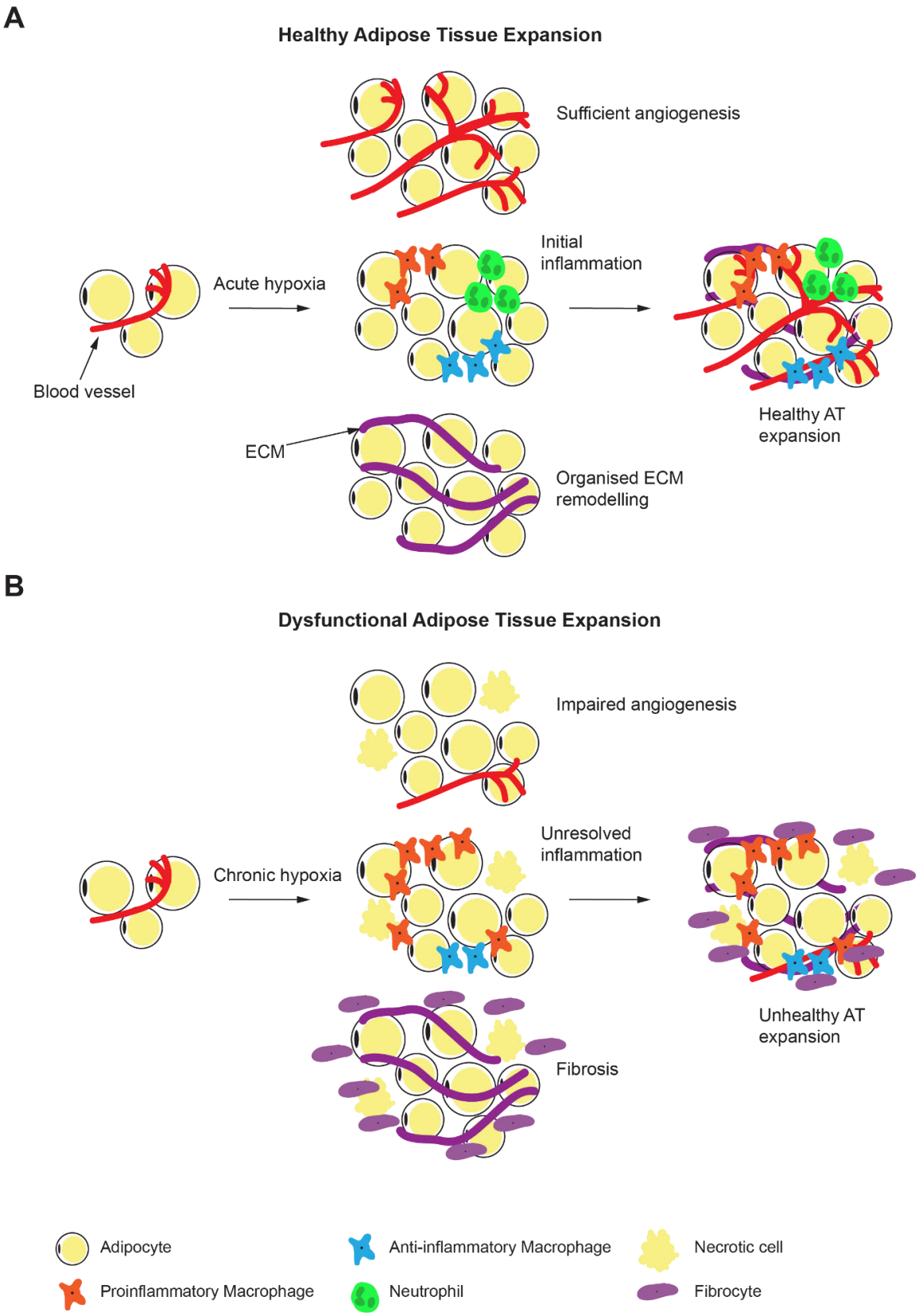

Figure 1.4 – Dysfunctional adipose tissue is characterised by inflammation, fibrosis and impaired angiogenesis

Figure 1.4 – Dysfunctional adipose tissue is characterised by inflammation, fibrosis and impaired angiogenesis. A. Schematic showing healthy adipose tissue expansion. Adapted from (Crewe et al., 2017). **B.** Schematic showing dysfunctional adipose tissue expansion. ECM (Extracellular matrix). Adapted from (Crewe et al., 2017).

1.1.7 – Adipose morphology modulates adipose tissue dysfunction

One factor known to influence adipose tissue dysfunction is adipose morphology. Adipose morphology is defined as the number and size distribution of adipocytes within adipose tissue (Hoffstedt et al., 2010). A hyperplastic adipose morphology is characterised by the presence of many small adipocytes, while a hypertrophic adipose morphology is characterised by the presence of few large adipocytes (Hoffstedt et al., 2010). Inter-individual variation in adipose morphology is present in human populations, with both morphologies being associated with different metabolic parameters (Hoffstedt et al., 2010, Salans et al., 1973, Veilleux et al., 2011). For example, a hypertrophic morphology is associated with adipocyte apoptosis, and increased levels of blood cholesterol and triglycerides (Hoffstedt et al., 2010). Furthermore, larger adipocytes are known to secrete less adiponectin and more inflammatory cytokines such as IL-6 and TNF- α (Skurk et al., 2007). Basal lipolysis is also increased in hypertrophic adipocytes, increasing the release of free fatty acids (Wueest et al., 2009). In contrast a hyperplastic morphology is associated with improved metabolic parameters and therefore with improved, glucose, insulin and lipid profiles (Hoffstedt et al., 2010). Taken together this shows that a hyperplastic adipose morphology is associated with a normal metabolic profile, while a hypertrophic adipose morphology is associated with a dysregulated metabolic profile. Therefore, targeting adipose morphology with an aim to generate a more hyperplastic adipose morphology would be one way to improve obesity associated adipose tissue dysfunction.

Adipose tissue morphology is controlled by changes in adipocyte number or changes in adipocyte size. Changes in adipocyte size are controlled by lipid entering and leaving the cell. Lipids are stored in adipocytes via fatty acid uptake or lipogenesis **(Figure 1.5C)** (Lapid and Graff, 2017). Lipids are stored in adipocytes in the form of triglycerides (Lapid and Graff, 2017). Adipocytes can decrease in size by releasing lipid through lipolysis, in this process triglycerides undergo hydrolysis to release fatty acids **(Figure 1.5D)** (Lapid and Graff, 2017). Both lipolysis and lipid uptake by adipocytes are highly regulated by a number of factors, including a wide range of environmental factors (Spiegelman and Flier, 1996). Adipocytes can increase in number through the proliferation and subsequent differentiation of progenitor cells, in a process known as adipogenesis **(Figure 1.5A)** (Siersbaek and Mandrup, 2011). Adipocytes can also decrease in number via apoptosis **(Figure 1.5B)** (Tsuboyama-

Kasaoka et al., 2000). It is known that adipocyte number remains stable in adults, irrespective of weight loss or gain, with a roughly 10% turnover of adipocytes each year (Spalding et al., 2008). In summary, adipose tissue can expand by increasing adipocyte cell number or size and I will now focus on increases in cell number as a way to promote healthy adipose tissue expansion.

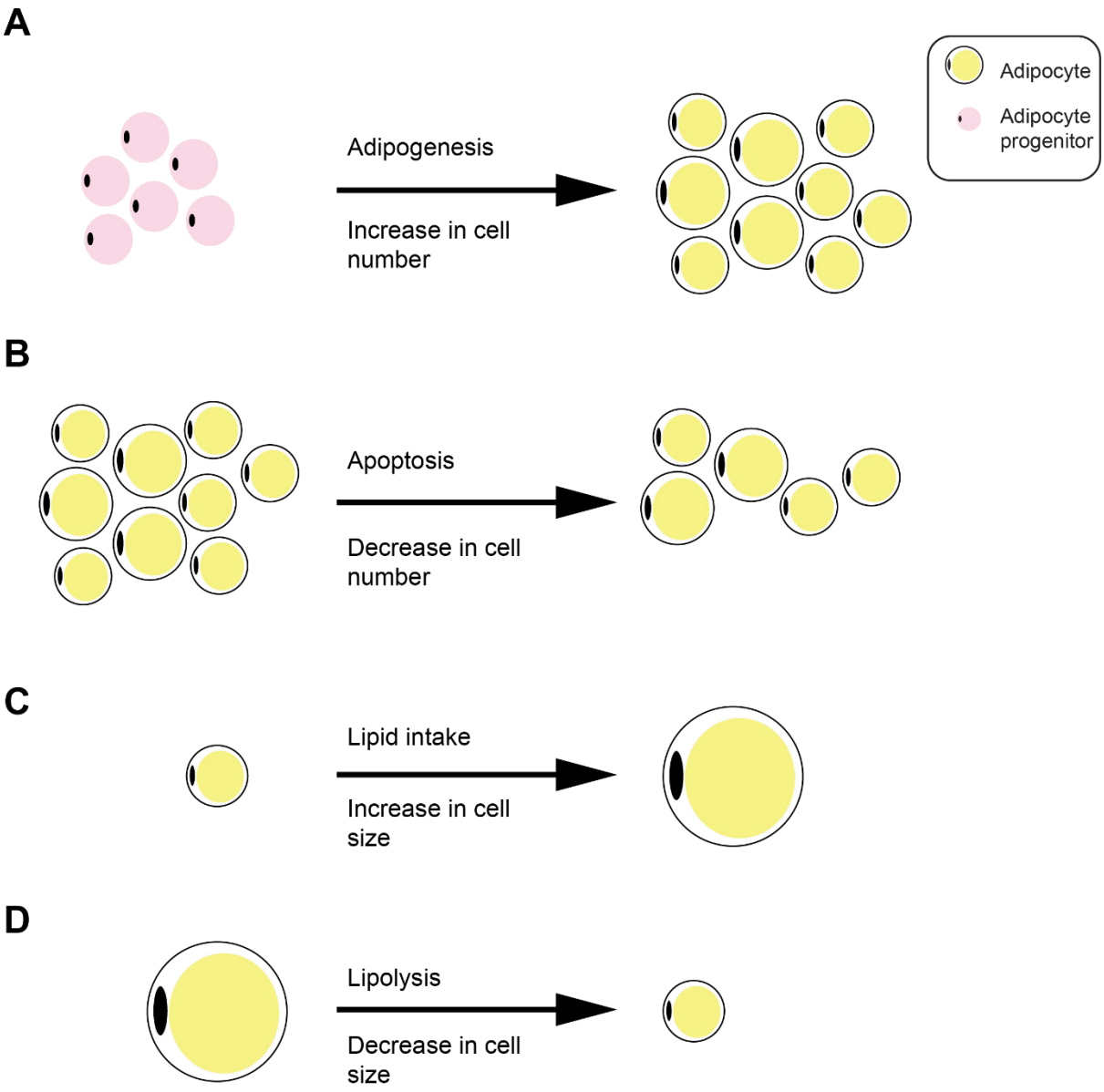

Figure 1.5 – Adipose tissue expands by increases in adipocyte cell number and cell size. A. Schematic showing how adipocytes increase in number. **B.** Schematic showing how adipocytes decrease in number. **C.** Schematic showing how adipocytes increase in size. **D.** Schematic showing how adipocytes decrease in size.

1.1.8 – Healthy adipose tissue expansion can alleviate obesity associated AT dysfunction

The adipose tissue expandability hypothesis suggests a reason for adipose tissue dysfunction (Virtue and Vidal-Puig, 2008). This hypothesis states that the capacity of an individual to expand their fat mass is a more important determinant of obesity associated metabolic dysfunction than the absolute amount of adipose tissue that an individual possesses (Virtue and Vidal-Puig, 2008). To test this hypothesis various mouse models have been employed (Kim et al., 2007, Virtue and Vidal-Puig, 2008). One study limited adipose tissue expansion by generating a mouse with a dominant negative mutation in the proadipogenic factor *Pparg* (Peroxisome proliferator activated receptor gamma) (Virtue and Vidal-Puig, 2008). The *Pparg* mutant mice were then crossed onto the ob/ob background (Virtue and Vidal-Puig, 2008). The ob/ob mouse contains a mutation in the leptin receptor which causes it to eat excessively and become profoundly overweight (Virtue and Vidal-Puig, 2008). The mice generated were found to be much more insulin resistant than ob/ob controls, despite having 14% less adipose tissue (Virtue and Vidal-Puig, 2008). In contrast, a mouse model in which adipose tissue expansion is apparently limitless shows improved metabolic parameters (Kim et al., 2007). Overexpression of adiponectin in ob/ob mice led to a significant increase in adipocyte cell number and overall expansion of adipose tissue mass (Kim et al., 2007). Despite having a body weight 50% greater than ob/ob mice, the adiponectin overexpressing mice had lower glucose, insulin and triglyceride levels in blood plasma (Kim et al., 2007). Overall, data from the two mouse models demonstrates that it is the ability of adipose tissue to expand which determines whether the tissue becomes dysfunctional. Therefore, improving the ability of AT to expand could help to alleviate obesity associated AT dysfunction.

1.2 – The genetic control of adipose tissue expansion and morphology

1.2.1 – Adipogenesis drives AT expansion and is controlled by a network of transcription factors

Adipogenesis is the process by which fibroblast like progenitor cells differentiate to become mature lipid filled adipocytes **(Figure 1.6A)** (Siersbaek et al., 2012). Much is known about adipose progenitor cells themselves and this is discussed further in chapter 4. Adipogenesis is controlled by a tightly regulated transcriptional cascade and much of our knowledge of the molecular mechanisms which control adipocyte differentiation come from *in vitro* studies of preadipocyte cell line models and primary cell cultures (Siersbaek et al., 2012). These cells can be induced to undergo adipogenesis, and differentiate into mature adipocytes, using a standard hormonal cocktail containing, insulin, cAMP elevating agent, glucocorticoids and growth factors **(Figure 1.6A & B)** (Siersbaek et al., 2012). Many studies using these cell line models have revealed the core transcriptional cascade which controls adipogenesis (Siersbaek et al., 2012).

Preadipocyte cell line models undergo synchronous differentiation in response to the addition of a chemical stimulus (Siersbaek et al., 2012). Addition of the hormonal cocktail to preadipocytes leads to the activation of multiple early pro-adipogenic transcription factors and the repression of anti-adipogenic factors (Siersbaek et al., 2012). These early transcription factors have been referred to as the first wave of transcription factors and include the CCAT enhancer binding protein (*Cebp*) family members *Cebpb* and *Cebpd* **(Figure 1.6B)** (Siersbaek et al., 2012, Tang et al., 2003, Tanaka et al., 1997). Other early transcription factors include *Krox20* (early growth response 2, Egr2), *Stat5a* (Signal transducer and activator of transcription 5a) and members of the *Klf* (Kruppel-like factors) family **(Figure 1.6B)** (Siersbaek et al., 2012, Chen et al., 2005, Oishi et al., 2011, Floyd and Stephens, 2003). This first wave of transcription factors then brings about the expression of a second wave of transcription factors (Siersbaek et al., 2012). The most important factors in the second wave are *Cebpa* and *Pparg*, which are considered to be master regulators of adipogenesis **(Figure 1.6B)** (Siersbaek et al., 2012, Rosen et al., 1999). In addition to *Cebpa* and *Pparg*, several other transcription factors including *Srebp-1c* (sterol regulatory element-binding protein-1c) and *Klf15* have been shown to

regulate the late phase of adipogenesis **(Figure 1.6B)** (Siersbaek et al., 2012, Kim and Spiegelman, 1996). These late phase adipogenic factors then induce the gene expression programme which leads to the mature adipocyte phenotype (Siersbaek et al., 2012). Overall, adipogenesis is controlled by a complex network of transcription factors, with *Cebpa* and *Pparg* acting as master regulators.

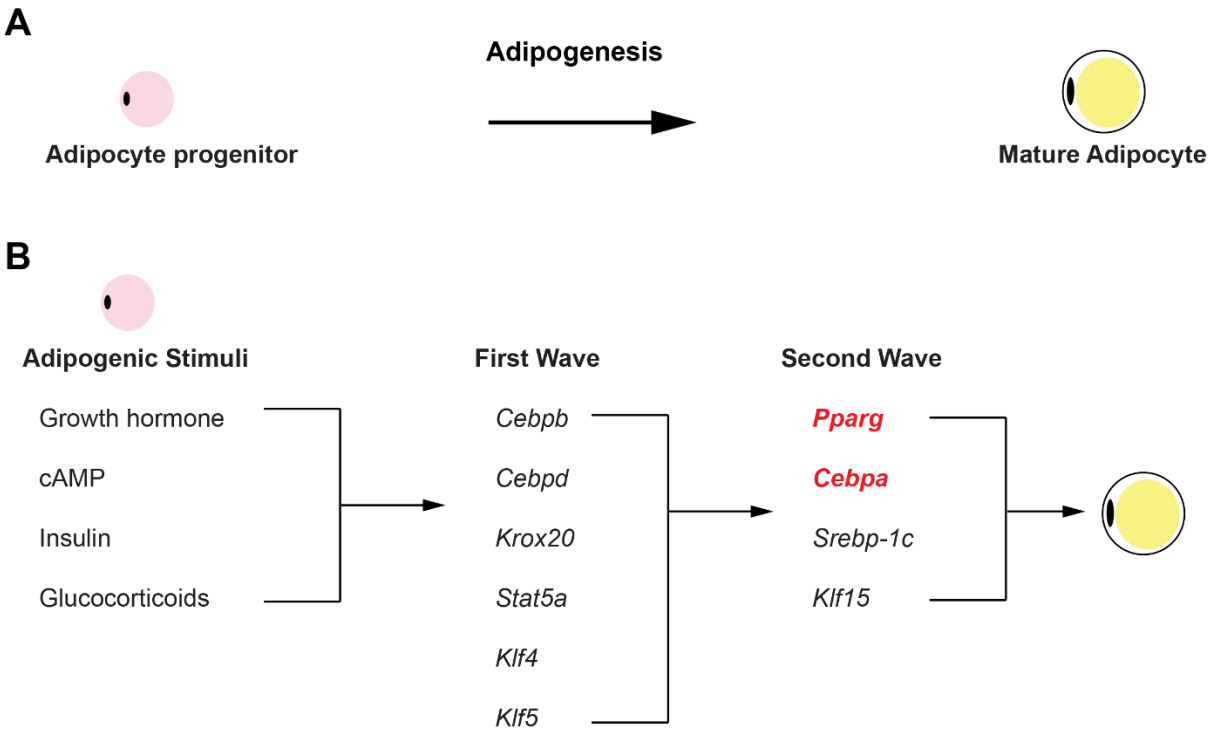

Figure 1.6 – Adipogenesis is controlled by a network of transcription factors. A. Schematic showing adipogenesis. **B.** Schematic showing the transcriptional control of adipogenesis. The master regulators of adipogenesis, *Pparg* and *Cebpa*, are highlighted in red. Adapted from (Siersbaek and Mandrup, 2011).

1.2.2 - Adipogenesis leads to changes in chromatin structure

In addition to gene expression changes, extensive chromatin remodelling also takes place during adipogenic differentiation. Multiple studies have examined genome wide changes in chromatin organisation in response to adipogenic differentiation (Sarusi Portuguez et al., 2017, Siersbaek et al., 2011, Siersbaek et al., 2014, Siersbaek et al., 2017). For example, DNase-Seq has been used to map sites of open chromatin, which are indicative of enhancer regions, during 3T3-L1 adipogenic differentiation (Siersbaek et al., 2011). This revealed extensive chromatin remodelling which could be grouped into four distinct temporal profiles (Siersbaek et al., 2011). These profiles consisted of; sites which are induced early in adipogenesis and remain open, sites transiently induced 4 hours after induction, sites transiently induced 24 hours after induction and sites which open late in adipogenesis (Siersbaek et al., 2011). In addition, multiple transcription factors have been shown to bind cooperatively at transcription factor hotspots during adipogenesis (Siersbaek et al., 2014). Finally, it has been shown that genome reorganisation takes place during adipogenesis and that the factor RXR is central to genome reorganisation at the beginning of adipogenesis (Sarusi Portuguez et al., 2017). In summary, as well as leading to changes in gene expression, the adipogenic pathway also causes extensive changes in chromatin remodelling.

1.2.3 - *Pparg* and *Cebpa* act together as master regulators of adipogenesis

Cebpa and *Pparg* are master regulators of adipogenesis and act cooperatively to bring about adipogenesis (Linhart et al., 2001). *Cepba* and *Pparg* are also the best studied regulators of adipogenesis (Linhart et al., 2001). *Cebpa* is a basic leucine zipper transcription factor which is most abundantly expressed in adipose tissue, the liver and the placenta (Linhart et al., 2001). Cell culture studies have also shown that *Cebpa* expression can trigger the differentiation of preadipocytes into mature adipocytes, though this requires *Pparg* expression (Linhart et al., 2001). PPARG is a nuclear receptor which heterodimerises with RXRA (Retinoid X receptor alpha) and binds DR1 (direct repeat 1) sites in the DNA (Lefterova et al., 2008). The DR1 site is a direct repeat of the AGGTCA element, conserved to various degrees and separated by a single nucleotide (Lefterova et al., 2008). *Pparg* has been found to be both

necessary and sufficient for adipogenesis *in vitro* (Lefterova et al., 2008). PPARG and CEBPA have also been found to bind adjacent sites during adipogenesis (Lefterova et al., 2008). A 2008 study used ChIP followed by DNA hybridisation to whole genome tilling array to determine the PPARG binding sites in the 3T3-L1 preadipocyte cell line (Lefterova et al., 2008). 5299 PPARG binding sites were identified and consensus CEBP binding motifs were found in the vicinity of over 90% of these sites (Lefterova et al., 2008). Furthermore, examination of PPARG and CEBPA binding sites near genes upregulated during differentiation revealed that 60% of genes were bound by both factors, 3% of genes were bound by PPARG only and 25% of genes were bound by CEBPA only (Lefterova et al., 2008). Together this demonstrates that *Pparg* and *Cepba* are key factors required for adipogenesis and that they act cooperatively to drive adipogenic differentiation.

1.2.4 - *Pparg*, a master regulator of adipogenesis, influences adipose morphology and expansion *in vivo*

In addition to regulating adipogenesis *in vitro, Pparg* has also been shown to regulate adipogenesis *in vivo*. Whole body *Pparg* knockout mice are embryonic lethal, due to defects in placental function (Barak et al., 1999). Therefore, adipose tissue specific *Pparg* knockout mice have been generated to investigate the function of *Pparg* in adipose tissue expansion *in vivo* (Wang et al., 2013a). A study by Wang et al (2013) generated adipose specific *Pparg* knockout mice by crossing *Pparg* floxed mice to an Adipoq-Cre line. The Adipoq-Cre line is driven by the regulatory region of adiponectin and so expression is limited to adipocytes (Wang et al., 2013a). The knockout mice were found to have a near complete loss of adipose tissue and the few adipocytes which were present were found to be vastly enlarged **(Figure 1.7A)** (Wang et al., 2013a). In addition, the knockout mice were observed to have enlarged livers, with substantial lipid accumulation and were also found to be insulin resistant (Wang et al., 2013a). These findings are in line with observations from humans, in which dominant negative mutations in *PPARG* have been associated with severe insulin resistance and diabetes (Barroso et al., 1999). In summary, *Pparg* signalling can modulate adipose morphology and thereby impact insulin signalling.

Pparg overexpression has also been shown to impact adipogenesis *in vivo* (Sugii et al., 2009). In order to investigate the role of *Pparg* in adipogenesis, a

transgenic mouse which expressed a dominant active form of *Pparg* was generated (Sugii et al., 2009). The mouse expressed a VP16 PPARG fusion protein, which was created by fusing the activation domain of the herpes simplex virus VP16 protein to PPARG (Saez et al., 2004, Sugii et al., 2009). The resultant protein was capable of regulating *Pparg* target genes independent of ligand and was under the control of an AP2 promoter (Sugii et al., 2009). The AP2 promoter drives expression only in adipocytes and pre-adipocytes and so expression of the dominant active protein was restricted to adipose tissue (Sugii et al., 2009). The transgenic mice were found to exhibit normal growth and AT development but adipocytes in WAT were found to have a more hyperplastic morphology than those of WT mice **(Figure 1.7B)** (Sugii et al., 2009). Furthermore, the transgenic mice had lower fasting glucose levels and enhanced insulin sensitivity, following a high fat diet (Sugii et al., 2009). Taken together this demonstrates that *Pparg* signalling can modulate adipose morphology and improve insulin sensitivity, thereby providing proof of principle that modulation of adipose morphology can improve systemic metabolic health.

1.2.5 - A key regulator of adipogenesis, *Cebpa,* can alter adipose levels *in vivo*

Similarly to *Pparg, Cebpa* can also influence adipogenesis *in vivo.* Whole body *Cebpa* knockout mice die shortly after birth due to severe hypoglycaemia, caused by defects in liver development (Flodby et al., 1996, Wang et al., 1995). To overcome this problem, a study by Linhart et al (2001) generated a transgenic mouse model in which *Cebpa* expression was restricted to the liver. A transgenic line in which *Cebpa* is expressed under the albumin promoter was generated and crossed to the *Cebpa* knockout line (Linhart et al., 2001). This produced a mouse in which *Cebpa* was expressed only in hepatocytes and improved the survival of the *Cebpa* knockout mice almost 3 fold (Linhart et al., 2001). When the knockout mice were examined no WAT was found, demonstrating that *Cebpa* is required for the commitment of preadipocytes to white adipocytes **(Figure 1.7C)** (Linhart et al., 2001). Serum insulin levels were found to be increased, despite normal glucose levels, suggestive of peripheral insulin resistance (Linhart et al., 2001). In summary, *Cebpa* seems to be essential for the development of mature white adipocytes *in vivo* and perturbation of *Cebpa* signalling can impact insulin sensitivity.

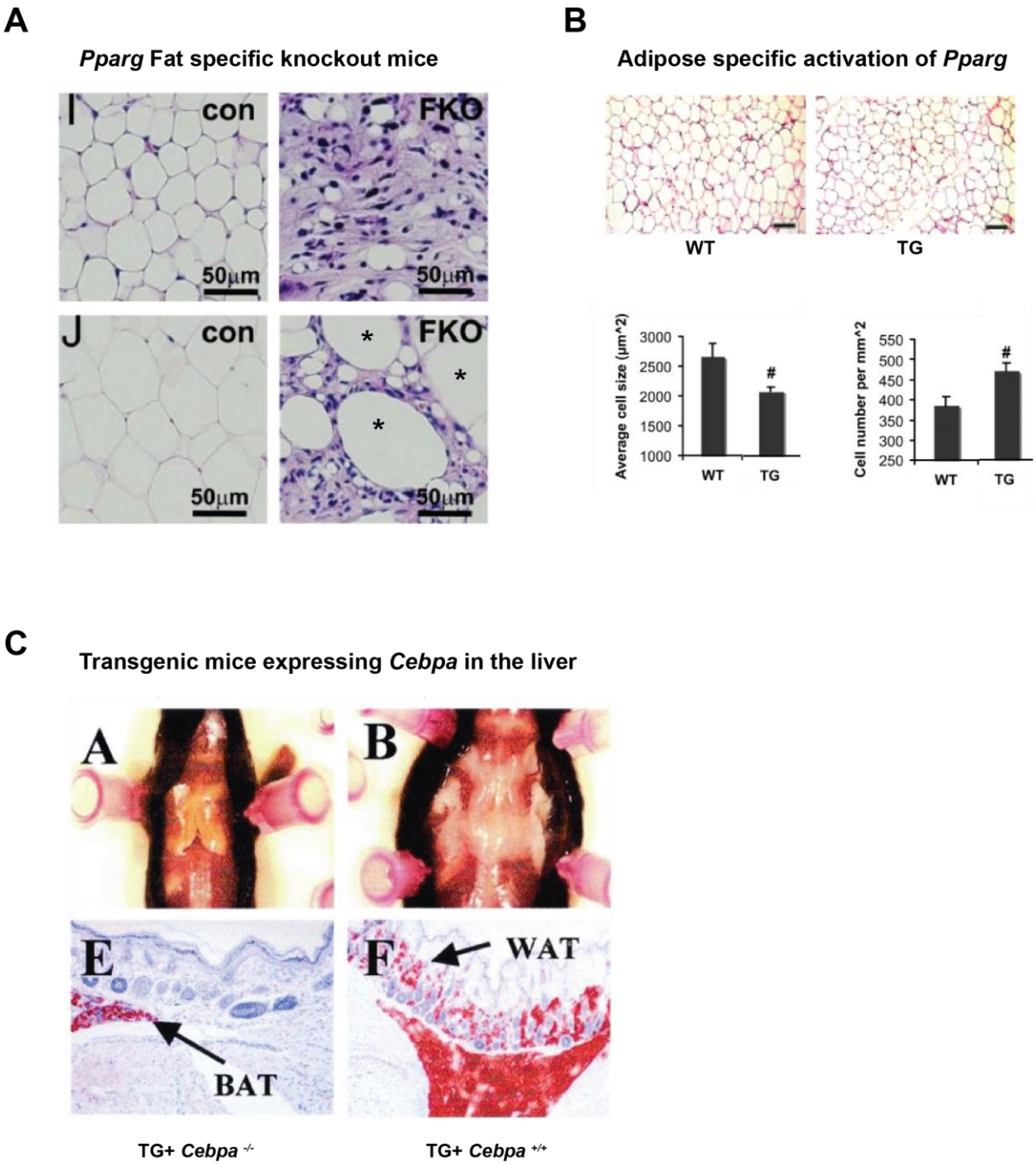

Figure 1.7 – *Pparg* and *Cebpa* influence adipose tissue levels *in vivo*. A. H&E stain of WAT. Con (Control littermates) FKO (AT specific *Pparg* knock out). I shows inguinal WAT. G shows gonadal WAT. Stars show the presence of very large adipocytes. Adapted from (Wang et al., 2013a). **B.** H&E stain of WAT from adipose specific *Pparg* overexpression mice. TG (Transgenic) Adapted from (Sugii et al., 2009). **C.** Macroscopic absence of WAT in the interscapular region of 7 day old transgenic knockout mice and Oil red O staining of WAT in the dermis. Adapted from (Linhart et al., 2001).

1.2.6 – Project Aim - Identification of novel genes which control AT expansion and AT morphology

The network of transcription factors which control adipogenesis in cell line models is well described (Siersbaek et al., 2012). From this work two key regulators of adipogenesis have emerged, *Pparg* and *Cebpa* (Siersbaek et al., 2012). Further *in vivo* studies have shown that both genes are required for adipose tissue expansion and can influence systemic metabolic health (Linhart et al., 2001, Wang et al., 2013a). In addition, *Pparg* overexpression studies have shown *Pparg* to be capable of modulating adipose morphology and improving insulin sensitivity (Sugii et al., 2009). Taken together this provides proof of principle that alterations in adipose expansion and adipose morphology can influence systemic metabolic health. As *Pparg* and *Cebpa* have been well studied in the context of AT expansion the aim of my thesis was to identify novel factors which influence adipose expansion and adipose morphology. In doing this I have identified the gene *Foxp1* (Forkhead box P1) and this gene is the main focus of my thesis.

1.2.7 - Genome wide association studies are used to identify novel genes associated with complex traits and disease

Data from genome wide association studies (GWAS) can be used to identify novel genes which may regulate adipose tissue expansion and morphology. GWAS studies are often used to look for associations between genetic variation and specific traits or diseases (Visscher et al., 2012). GWAS studies use single nucleotide polymorphisms (SNPs) as a marker of a region in which genetic variation is associated with a specific trait or disease (Nica and Dermitzakis, 2013). However, the SNP itself will often not be responsible for the observed association and instead marks a region of the genome which contains many more SNPs, each of which may be responsible for the observed association (Nica and Dermitzakis, 2013). Therefore, further testing is required to identify the causal SNP and any resultant gene expression changes (Nica and Dermitzakis, 2013). Overall GWAS studies have the power to identify novel genes associated with specific traits and diseases.

GWAS studies are particularly useful when looking at the genetic causes of complex diseases and traits such as obesity or BMI (Manolio et al., 2009). Both obesity and BMI are polygenic traits influenced by many genes (Manolio et al., 2009).

For example, many genes are thought to influence body weight, with the total number of genes which have a small effect on body weight predicted to exceed 100 (Hinney et al., 2010). In recent years GWAS studies have identified many loci associated with BMI, with variants often found within non-coding regions (Speakman et al., 2018). One example of this is the *FTO* gene, which was identified by a GWAS study in 2007 as being associated with BMI, and with genetic variation at the *FTO* loci being linked to food intake (Speakman et al., 2018). Therefore, GWAS studies can identify novel candidate genes which may influence adipose tissue expansion.

1.2.8 - Multiple genome wide association studies have found that genetic variation at the *FOXP1* locus is associated with altered body weight

GWAS studies have been used to identify genetic variation associated with BMI (Hoffmann et al., 2018, Kichaev et al., 2019, Speakman et al., 2018). For example, a study in 2019 looked at the genetic variation associated with BMI (Kichaev et al., 2019). This study used data from the UK Biobank to identify novel associations between genotype and complex traits in 459,000 individuals (Kichaev et al., 2019). One association found was between genetic variation at the *FOXP1* locus and BMI **(Figure 1.8B)** (Kichaev et al., 2019). This was not the only study to find that genetic variation at the *FOXP1* locus is associated with adiposity traits, as an earlier study in 2012 found a similar association (Fox et al., 2012). This study looked at the genetic variation associated with levels of subcutaneous and visceral adipose tissue and used a smaller sample size of 5560 women and 4997 men of European ancestry (Fox et al., 2012). Computed tomography was used to measure abdominal adipose depots and an association between variation at the *FOXP1* locus and levels of SAT was found (Fox et al., 2012). Finally, a GWAS study in 2019 looking at the genetic variation associated with Anorexia Nervosa also found an association with the *FOXP1* locus **(Figure 1.8A)** (Watson et al., 2019). Anorexia is characterised primarily by a very low BMI and the 2019 study used 16,992 cases and 55,525 controls, all of European ancestry, to look for associations between genetic variation and anorexia nervosa (Watson et al., 2019). Genetic variation at 8 loci were found to be associated with anorexia, and one of these loci was found within an intron of the *FOXP1* gene **(Figure 1.8A)** (Watson et al., 2019). In summary, three independent GWAS studies have found that variation at the *FOXP1* locus is associated with traits related to body

weight. These studies therefore suggest that *FOXP1* may play a role in controlling body weight and adipose levels.

A

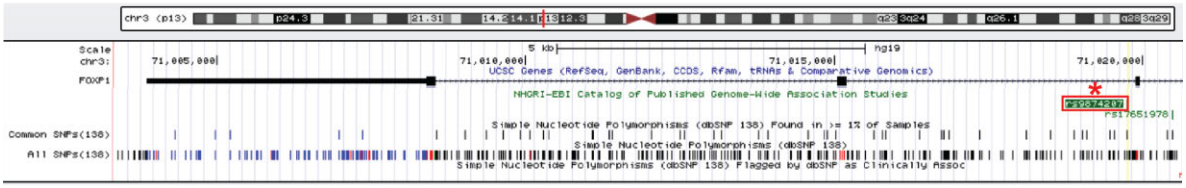

B

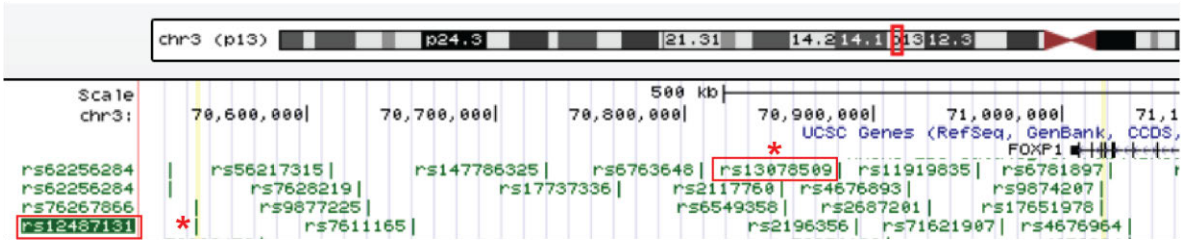

Figure 1.8 – GWAS studies have identified genetic variation at the *FOXP1* locus associated with body weight. A. SNP in intron 2 of the *FOXP1* gene associated with anorexia nervosa, identified (Watson et al., 2019). **B.** SNPs upstream of *FOXP1* associated with BMI, identified by (Kichaev et al., 2019). Figure created using UCSC genome browser.

1.2.9 - *FOXP1* mRNA levels are positively associated with BMI

In addition to GWAS data, data from other studies have implicated *FOXP1* in the control of body weight and adipose levels (Civelek et al., 2017). Data from the 2017 METSIM (Metabolic Syndrome in Men) study found that *FOXP1* mRNA levels in SAT are positively associated with both BMI ($P = 1.20x10^{-10}$) and increased waist-hip ratio ($P = 7.76x10^{-4}$) (Civelek et al., 2017). The study by Civelek et al (2017) took subcutaneous adipose tissue from 770 extensively phenotyped Finish men of the METSIM study and measured mRNA levels. *FOXP1* mRNA levels in SAT were also associated with increased insulin levels ($P = 3.15x10^{-3}$), increased proinsulin levels ($P = 7.27x10^{-3}$), decreased Matsuda insulin sensitivity index ($P = 1.26x10^{-3}$), decreased adiponectin ($P = 7.68x10^{-4}$), decreased HDL cholesterol ($P = 3.13x10^{-5}$) and increased blood triglycerides ($P = 5.15x10^{-4}$) (Civelek et al., 2017). In summary, *FOXP1* expression levels in SAT are associated with increased body weight and adverse metabolic outcomes.

1.2.10 - *Foxp1* is a transcription factor which belongs to the Fox family

Foxp1 or Forkhead Box P1 is a transcription factor which belongs to the *Fox* family of genes **(Figure 1.9A)** (Hannenhalli and Kaestner, 2009). The *Fox* family is an ancient family of genes, which are found in species ranging from yeast to humans (Hannenhalli and Kaestner, 2009). The unifying feature of all FOX proteins is the roughly 100 residue forkhead DNA binding domain, which is highly conserved across all members of the family (Hannenhalli and Kaestner, 2009). The conservation of the DNA binding domain between orthologous family members is striking, with the *drosophila melanogaster* and human FOXA1 DNA binding domains showing 90% similarity (Hannenhalli and Kaestner, 2009). The forkhead domain (FHD) itself is formed of three alpha helices (H), three beta sheets (S) and two wing regions (W) which flank the third beta sheet **(Figure 1.9A)** (Hannenhalli and Kaestner, 2009). The structure of this region when bound to DNA adopts a butterfly like winged shape, and this has led to the FHD to also be termed the winged helix domain (Hannenhalli and Kaestner, 2009). *Foxp1* therefore belongs to a large family of genes, which are grouped together based on their highly conserved FHD DNA binding domain.

1.2.11 - *Foxp1* is expressed throughout the body

The mouse *Foxp1* gene was first identified in 2001 during a screen for new *Fox* family members, performed on a mouse lung cDNA library (Shu et al., 2001). Since then it's expression has been described in multiple tissues during development, including in neural, intestinal and cardiovascular tissues (Shu et al., 2001). *FOXP1* is also widely expressed in adult tissues (Fagerberg et al., 2014). The Genotype-Tissue Expression (GTEx) project, which used RNA Seq to classify tissue specific expression of genes across all major human organs and tissues, found that *FOXP1* is widely expressed across human tissues **(Figure 1.9B)** (Fagerberg et al., 2014). *FOXP1* was found to be expressed in the adrenal gland, bone marrow, brain, colon, adipose, heart, kidney, liver, lung, pancreas, prostate, skin, spleen, stomach, ovary, testis and bladder **(Figure 1.9B)** (Fagerberg et al., 2014). Highest expression was found in the lung, ovary and prostate (Fagerberg et al., 2014). Of note is the expression of *FOXP1* in adipose tissue, which has also been shown in mice **(Figure 1.9C)** (Fagerberg et al., 2014, Liu et al., 2019). In summary, *Foxp1* is widely expressed and is expressed in adipose tissue.

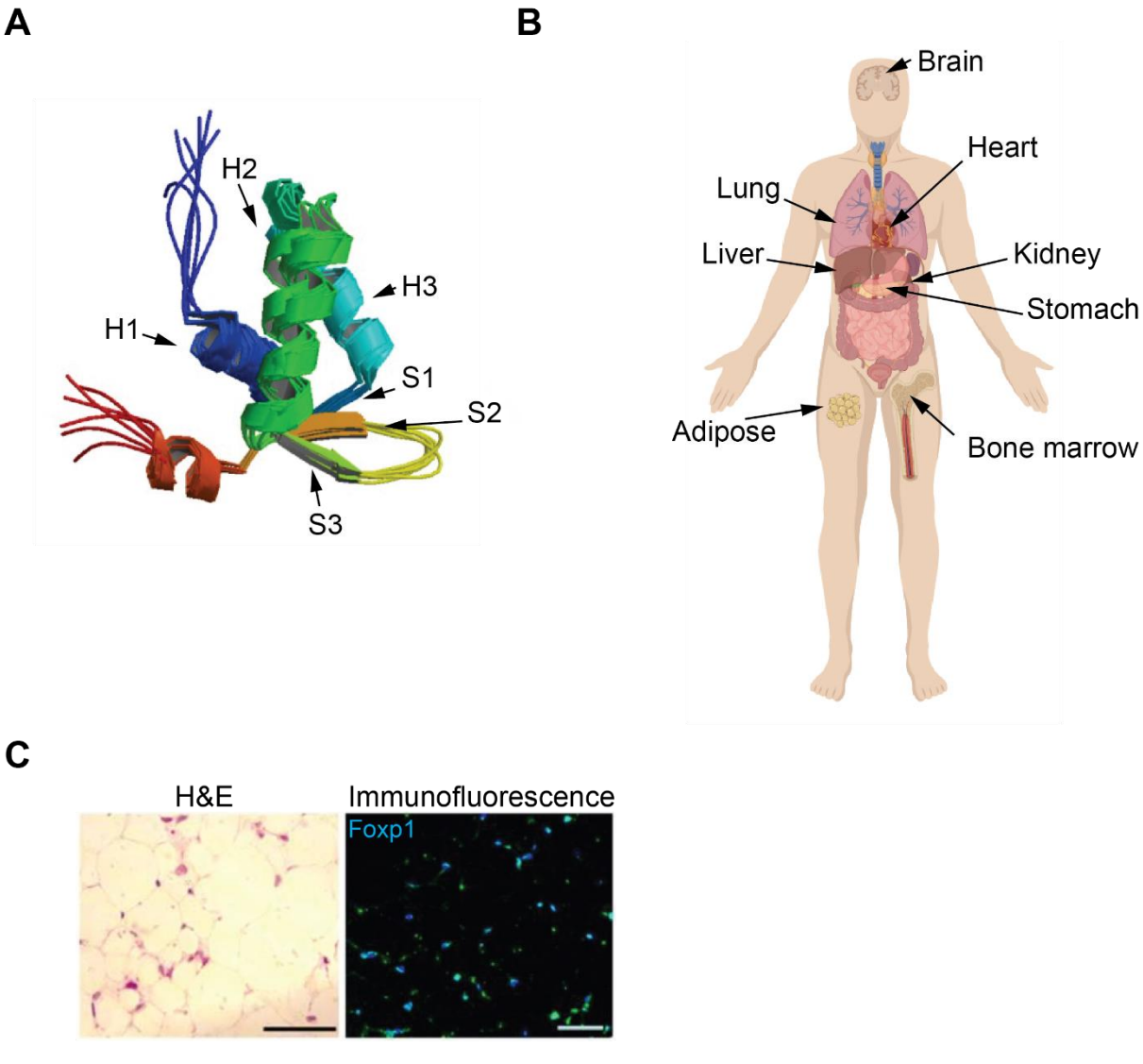

Figure 1.9 – *Foxp1* is a transcription factor which is expressed throughout the body. A. The 3D structure of the FOXP1 DNA binding domain. The alpha helices (H) and Beta sheets (S) are shown. Adapted from (Chu et al., 2011). **B.** Schematic showing the human expression of *FOXP1*. Expression data was taken from GTex (Fagerberg et al., 2014) and the schematic was produced using Biorender. **C.** H&E and immunostaining of SAT from mice. Dapi staining is shown in blue and FOXP1 staining is shown in green. Scale bar is 50 µm. Adapted from (Liu et al., 2019).

1.2.12 - *Foxp1* drives the proliferation and differentiation of progenitor cells

Variation at the *FOXP1* locus has been associated with BMI and body weight, suggesting that *FOXP1* may be a novel gene which influences adipose tissue expansion (Kichaev et al., 2019, Watson et al., 2019). *FOXP1* is a transcription factor which is known to be expressed in adipose tissue (Fagerberg et al., 2014). However, it is unknown if *FOXP1* acts on adipose tissue to bring about transcriptional changes which influence adipose tissue expansion. The known roles of *Foxp1* in other tissues provide insights into how *Foxp1* may influence adipose tissue expansion. For example, *Foxp1* is known to have roles in progenitor cells. Therefore, *Foxp1* may act in progenitor cells to influence adipose tissue expansion.

Foxp1 is known to drive the proliferation and differentiation of progenitor cells in multiple tissues (Fu et al., 2018, Gabut et al., 2011, Hu et al., 2006, Leishman et al., 2013, Li et al., 2017). For example, *Foxp1* has been shown to maintain multipotency in mammary gland stem cells (Fu et al., 2018). Mice with loss of *Foxp1* expression in the mammary gland showed stunted mammary gland development, suggesting that *Foxp1* is required for the differentiation of mammary stem cells into specialised cells types (Fu et al., 2018). *Foxp1* has also been shown maintain the proliferation of embryonic stem cells (ESCs), with an alternative splicing event in *Foxp1* found to be active in ESCs (Gabut et al., 2011). This alternative splicing event was found to stimulate the expression of pluripotency genes and to repress the expression of genes involved in lineage specification and differentiation (Gabut et al., 2011). Finally, *Foxp1* has been shown to drive progenitor cell proliferation and differentiation in bone marrow mesenchymal stem cells (MSCs) (Li et al., 2017). In this study, MSCs were isolated from the bone marrow of *Foxp1* bone marrow MSC specific knockout mouse and were found to have decreased osteogenic differentiation in culture and a reduced ability to expand (Li et al., 2017). This suggests that *Foxp1* is required to maintain the proliferation of bone marrow MSCs. Taken together these data show that *Foxp1* drives the proliferation and differentiation of progenitor cells from multiple tissues and suggests a clear mechanism by which *Foxp1* could influence adipose tissue expansion.

1.2.13 - *Foxp1* influences adipose tissue expansion and controls brown/beige adipocyte differentiation

Whole body *Foxp1* knockout mice could provide additional information on whether *Foxp1* influences adipose tissue expansion. However, when a whole body *Foxp1* mouse knockout was generated in 2004, it was found to be embryonic lethal due to defects in heart development (Wang et al., 2004). Homozygous mutants were found to die at embryonic day E14.5 and displayed several signs of cardiovascular failure, such as oedema, perivascular haemorrhage, and a slower heart rate than WT litter mates (Wang et al., 2004). The homozygous mutants also died before the development of adipose tissue and so leave open the question of whether *Foxp1* is required for adipose tissue expansion. The study also highlights the fact that *Foxp1* is a widely expressed transcription factor and will play many roles in different tissues. In summary whole body *Foxp1* knockout mice die before the development of adipose tissue and so do not provide clues as to whether *Foxp1* is required for adipose tissue expansion.

Evidence exists to suggest that *Foxp1* is important for adipose tissue expansion (Liu et al., 2019). A recent study examining the role of *Foxp1* in brown/beige adipocyte differentiation found that loss of *Foxp1* expression in white adipose tissue led to smaller adipose tissue depots **(Figure 1.10)** (Liu et al., 2019). The study by Liu et al (2019) generated two adipose specific *Foxp1* knockout mice lines. The lines were generated by crossing *Foxp1* floxed mice to aP2 Cre mice, in which Cre is expressed by adipocytes and adipose progenitors, and by crossing to adiponectin Cre mice, in which Cre is expressed by adipocytes (Liu et al., 2019). Both strains of mice were found to have smaller brown and white AT depots and were found to gain less weight in response to an eight week high fat diet **(Figure 1.10A. B. C. & D)** (Liu et al., 2019). Together this suggests that *Foxp1* is required for AT expansion. However, the study focused on brown and beige adipose tissue expansion and how *Foxp1* influenced WAT expansion was not investigated (Liu et al 2019). In summary the study by Liu et al (2019) suggests that *Foxp1* is required for AT expansion, though the question of how *Foxp1* drives adipose tissue expansion remains.

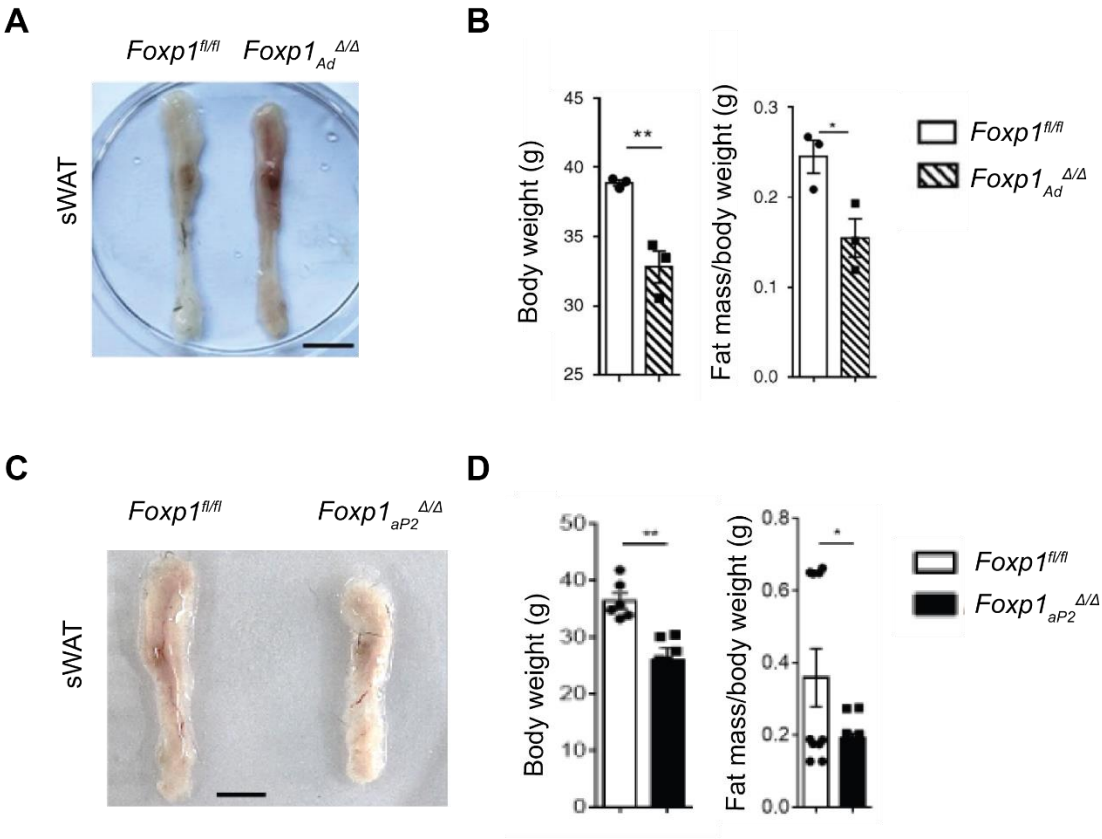

Figure 1.10 – *Foxp1* is required for the expansion of WAT. A. Reduced size of sWAT depot in $Foxp1_{Ad}^{\Delta/\Delta}$ mice. sWAT (subcutaneous WAT). Scale bar is 2 cm. **B.** $Foxp1_{Ad}^{\Delta/\Delta}$ mice gain less weight in response to a high fat diet. **C.** Reduced size of sWAT depot in $Foxp1_{aP2}^{\Delta/\Delta}$ mice. sWAT (subcutaneous WAT). Scale bar is 1 cm **D.** $Foxp1_{aP2}^{\Delta/\Delta}$ mice gain less weight in response to a high fat diet. Figure adapted from Liu et al (2019).

1.2.14 - The *Foxp* subfamily shows divergent DNA binding to the *Fox* family

Foxp1 belongs to the *Fox* gene family, which is comprised of multiple subfamilies **(Figure 1.11A)** (Hannenhalli and Kaestner, 2009). The *Foxp* subfamily has four members, *Foxp1, Foxp2, Foxp3* and *Foxp4*, and is considered one of the most distantly related *Fox* family members **(Figure 1.11A)** (Wang et al., 2003). Like other *Fox* family members, the FHD of FOXP proteins is also made up of three alpha helices (H), three beta sheets (S) and two wing regions (W) **(Figure 1.9A)** (Medina et al., 2016). In most FOX proteins the first wing, which connects Beta-sheets 2 and 3, is a 5-7 amino acid sequence, however this sequence is truncated in the *Foxp* subfamily (Stroud et al., 2006). The sequence of wing 2 is also diverged in the *Foxp* subfamily and the heightened variability of these regions suggests that the wings may have specialised functions within each subfamily (Stroud et al., 2006). The FHD of *Foxp1* may therefore recognise a slightly different DNA sequence than other *Fox* family members. This suggests that the transcriptional changes brought about from FOXP1 binding DNA will differ from those caused by other FOX family members.

The divergent nature of the FHD in the *Foxp* subfamily suggests that FOXP proteins may bind DNA differently to other *Fox* family members. In addition to its FHD domain, FOXP1 also contains a N-terminal zinc finger domain (Wang et al., 2003). Zinc finger domains function as interaction domains and can bind DNA, RNA or proteins (Wang et al., 2003). Consequently, unlike most *Fox* family members which bind DNA as a monomer, *Foxp1* is known to bind DNA as a dimer (Stroud et al., 2006). Although *Foxp1* exists as both a monomer and dimer in solution, dimerization has been found to be essential for DNA binding with *Foxp1* forming both homodimers and heterodimers with other *Foxp* subfamily members (Li et al., 2004). It has been suggested that this manner of dimerization would allow both copies of *Foxp1* to bind DNA simultaneously and that FOXP1 proteins may loop DNA or mediate interchromosomal interactions (Stroud et al., 2006). In summary FOXP1 proteins bind DNA as dimers and therefore it is important to consider the normal binding partners of FOXP1 when interpreting data from *Foxp1* mutants.

1.2.15 - *Foxp1* acts as a transcriptional repressor

Foxp1 is a transcription factor which acts as a transcriptional repressor (Li et al., 2004). A luciferase reporter assay was used to show that *Foxp1* confers transcriptional repression **(Figure 1.11B)** (Li et al., 2004). Expression vectors containing full length *Foxp1, Foxp2,* and *Foxp4* cDNAs were cotransfected into lung epithelial cells with a pCC10.luc reporter (Li et al., 2004). The mouse CC10 promoter contains a FOX protein consensus DNA binding site and is active in lung epithelial cells (Li et al., 2004). On contransfection, activity of the mouse CC10 promoter was significantly repressed **(Figure 1.11B)** (Li et al., 2004). Activity of a CMV promoter, which does not contain a FOX consensus site, was not affected **(Figure 1.11B)** (Li et al., 2004). Together this shows that *Foxp1* acts as a transcriptional repressor.

1.2.16 - *Foxp1* interacts with members of the adipogenic network

Foxp1 is a transcriptional repressor and has been shown to interact with multiple transcription factors in multiple tissues (Li et al., 2004, Li et al., 2017). Of interest, *Foxp1* has been shown to interact with transcription factors known to control adipogenesis (Li et al., 2017). Coimmunoprecipitation assays in the 3T3-L1 cell line have shown that FOXP1 interacts with both CEBPB and CEBPD **(Figure 1.11C)** (Li et al., 2017). *Cebpb* and *Cebpd* are both active early in the adipogenic pathway and activate a master regulator of the process, *Pparg* (Li et al., 2017). It has also been shown that *Foxp1* can repress *Pparg* expression **(Figure 1.11D)** (Li et al., 2017). C3H10T1/T2 cells, which are functionally similar to MSCs, were transfected with plasmids expressing CEBPB and CEBPD and *Pparg-luciferase* activity measured **(Figure 1.11D)** (Li et al., 2017). Coexpression of FOXP1 significantly reduced luciferase activity, showing that *Foxp1* can repress *Cebpb/Cebpd* transactivation of *Pparg* **(Figure 1.11D)** (Li et al., 2017). Furthermore, it has been suggested that *Foxp1* can directly repress *Pparg* (Li et al., 2017). A FOXP1 consensus binding site has been identified upstream of the *Pparg* transcriptional start site and ChIP-PCR has been used to show that there is strong FOXP1 binding at this site (Li et al., 2017). Taken together this suggests that FOXP1 binds to and represses the expression of known drivers of adipogenesis. The binding partners of FOXP1 in adipose tissue and the effect of *Foxp1* on known regulators of adipogenesis should therefore be taken into account when analysing data from *Foxp1* mutants.

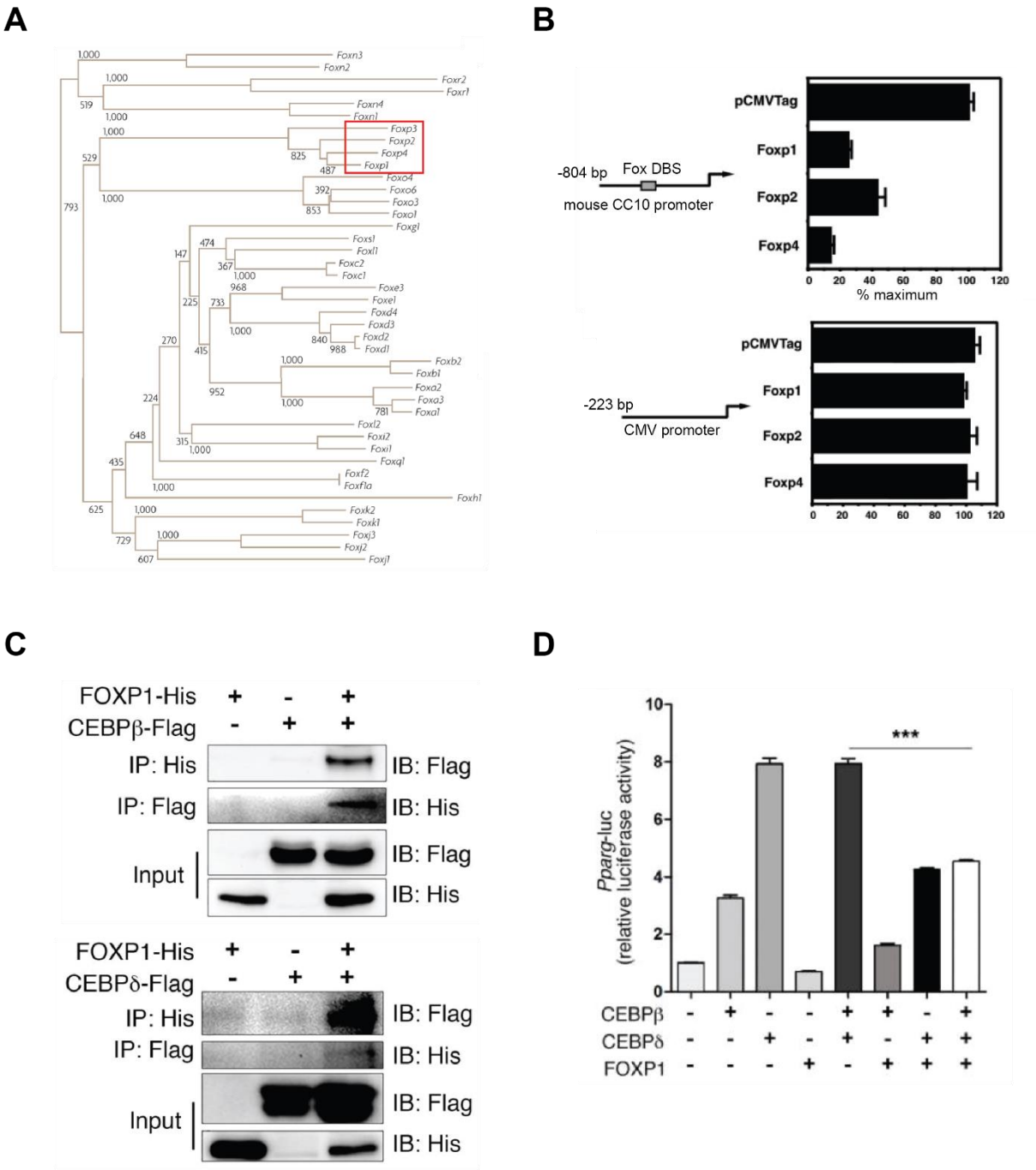

Figure 1.11 - *Foxp1* acts as a transcriptional repressor. A. Phylogenetic tree showing the *Fox* family of transcription factors. The *Foxp* transcription factors are highlighted by the red box. Numbers represent bootstrap values. Adapted from (Hannenhalli and Kaestner, 2009). **B.** Luciferase reporter assay showing *Foxp1* acts as a transcriptional repressor. Adapted from (Li et al., 2004). **C.** Coimmunoprecipitation of FOXP1-His and with CEBPB-Flag or CEBPD Flag, following transfection into 3T3-L1 cells. Adapted from (Li et al., 2017). **D.** Luciferase reporter assay in C3H10T1/T2 cells, n = 3. Adapted from (Li et al., 2017).

1.3 - Zebrafish as a model of adipose tissue expansion

Adipose tissue in zebrafish was first described by Song and Cone in 2007 (Song and Cone, 2007). In the years since then much has been learnt about adipose tissue in zebrafish and zebrafish have emerged as a useful model through which to study adipose tissue. It is now known that zebrafish possess adipose tissue which is anatomically, morphologically, and molecularly homologous to that of mammalian white adipose tissue (Flynn et al., 2009, Imrie and Sadler, 2010, Minchin and Rawls, 2017b). It is the presence of this homologous adipose tissue combined with unique features of the zebrafish, such as the ability to perform *in vivo* imaging, that make zebrafish an exciting model to study adipose tissue. In this section, I outline the current understanding on adipose tissue development and function in zebrafish and provide a rationale for using zebrafish to investigate the hypothesis that *foxp1* maintains progenitor cell populations in AT and is required for AT expansion.

1.3.1 - Zebrafish are a widely used model organism in biomedical research

Zebrafish (*Danio rerio*) are a species of small freshwater fish, native to south Asia. Zebrafish have been used in scientific research since the 1960s but it is in the last 10-15 years that much of the research using zebrafish has taken place (Teame et al., 2019). Some of the main advantages of using zebrafish in research are their high fecundity, external fertilisation, rapid development and transparent embryos (Lieschke and Currie, 2007). Other advantages include, the availability of a fully sequenced zebrafish genome and the relative ease of genetic manipulation (Lieschke and Currie, 2007). Zebrafish are also vertebrates and so contain structures and organ systems important in human disease (Lieschke and Currie, 2007). 70% of zebrafish genes are conserved to humans and 84% of genes known to be associated with human disease have an orthologous gene in zebrafish (Teame et al., 2019). Together these features make zebrafish a useful research tool and zebrafish have been used to study a wide range of topics, including organ development, cancer, and heart regeneration (Drummond and Davidson, 2016, Gonzalez-Rosa et al., 2017, White et al., 2013). In summary zebrafish are a useful model organism and have been used to study a wide range of biomedical questions.

1.3.2 - Adipose tissue in zebrafish is morphologically homologous to mammalian white adipose tissue

An emerging area of zebrafish research is the study of adipose tissue, and adipose tissue in zebrafish is known to be morphologically homologous to mammalian white adipose tissue (Flynn et al., 2009, Imrie and Sadler, 2010). One of the first studies to identify WAT in zebrafish used a combination of histological sectioning, lipid staining with Oil Red O and analysis of cell morphology to identify zebrafish WAT (Imrie and Sadler, 2010). The morphology of mammalian white adipocytes is very distinctive and zebrafish adipocytes appear to share this morphology. Zebrafish adipocytes have been described as cells containing a singular lipid droplet, a small amount of cytoplasm and a peripheral nucleus (Imrie and Sadler, 2010). Although the presence of a singular lipid droplet is a defining characteristic of mature mammalian adipocytes, the presence of multiple small lipid droplets is a hallmark of early terminal differentiation of mammalian adipocytes **(Figure 1.12A)** (Flynn et al., 2009). The presence of multiple lipid droplets has also been observed in zebrafish adipocytes, through the use of electron microscopy **(Figure 1.12A)** (Flynn et al., 2009). Another defining characteristic of mammalian white adipocytes is their large size (Ma et al., 2015). Zebrafish adipocytes are also large in size and have been found to exceed 100 µm in diameter (Flynn et al., 2009). Finally, ultrastructural analysis has shown that zebrafish adipocytes are metabolically active and show enrichment in filamentous mitochondria and caveolae **(Figure 1.12A)** (Flynn et al., 2009). These features are again reminiscent of mammalian adipocytes. Taken together this data demonstrates that zebrafish adipocytes are morphologically homologous to mammalian white adipocytes.

1.3.3 - Adipose tissue in zebrafish is functionally homologous to mammalian white adipose tissue

In addition to being morphologically homologous to mammalian white adipose tissue, zebrafish adipose tissue is also functionally homologous to mammalian white adipose tissue. In mammals adipose tissue acts as a dynamic energy store, storing lipid in times of energy excess and mobilising lipid in times of energy deficit (Ma et al., 2015). Adipose tissue in zebrafish has also been shown to act as an energy store and zebrafish have been shown to mobilise lipid from adipose tissue **(Figure 1.12B)**

(Flynn et al., 2009). A study in 2009 starved zebrafish and monitored adipose tissue levels using Nile Red staining **(Figure 1.12B)** (Flynn et al., 2009). Nile Red stains the neutral lipid within adipose tissue (Flynn et al., 2009). It was found that Nile Red staining decreased on starvation, suggesting that lipid had been mobilised and used as an energy source **(Figure 1.12B)** (Flynn et al., 2009). Conversely, it has also been shown that adipose tissue in zebrafish increases in size in response to energy excess (Oka et al., 2010). Oka et al (2010) placed zebrafish on an eight week high fat diet and monitored their response by measuring body weight **(Figure 1.12C)**. The zebrafish were fed the freshly hatched nauplii of brine shrimp, Artemia, which have a relatively high fat content (Oka et al., 2010). The control diet group was fed enough Artemis to meet their calorie requirements, while the high fat diet group was overfed (Oka et al., 2010). Following the diet, the high fat diet group were found to have a significantly greater BMI than the control diet group, suggesting that these fish had increased levels of AT and were using AT as an energy store **(Figure 1.12C)** (Oka et al., 2010). Other more recent studies, which use Nile Red to measure AT levels directly, have also shown that a high fat diet in zebrafish leads to increased levels of AT (Minchin and Rawls, 2017b). In summary, adipose tissue in zebrafish acts as an energy store and is functionally similar to mammalian white adipose tissue.

1.3.4 - Adipose tissue in zebrafish is molecularly homologous to mammalian white adipose tissue

The genetic regulation of adipose tissue appears to be conserved to zebrafish. For example, many genes known to be expressed in mammalian white adipose tissue are also expressed in zebrafish adipose tissue. The master regulator of mammalian adipogenesis, *pparg*, is known to be expressed in zebrafish (Flynn et al., 2009). *in situ* hybridisations have demonstrated that, like in mammals, *pparg* is expressed by adipocytes in zebrafish **(Figure 1.12D)** (Flynn et al., 2009, Imrie and Sadler, 2010). Unlike *pparg*, which is widely expressed, the gene *fabp4* is known to be expressed exclusively in adipose (Flynn et al., 2009). Zebrafish possess two orthologs of *Fabp4*, *fabp11a* and *fabp11b*, and *in situ* hybridisations have shown that *fabp11a* is expressed in zebrafish adipocytes **(Figure 1.12D)** (Flynn et al., 2009). Transcription factors important for the control of adipogenesis in mammals, such as *cepba* and *cebpb*, have also been found to be expressed in zebrafish adipose tissue (Imrie and Sadler, 2010). Finally, qPCR was used to show that the hormones adiponectin and

adipsin, which are expressed by mammalian AT, are expressed in zebrafish AT (Imrie and Sadler, 2010). Together this suggests that zebrafish AT expresses many of the same genes as mammalian WAT.

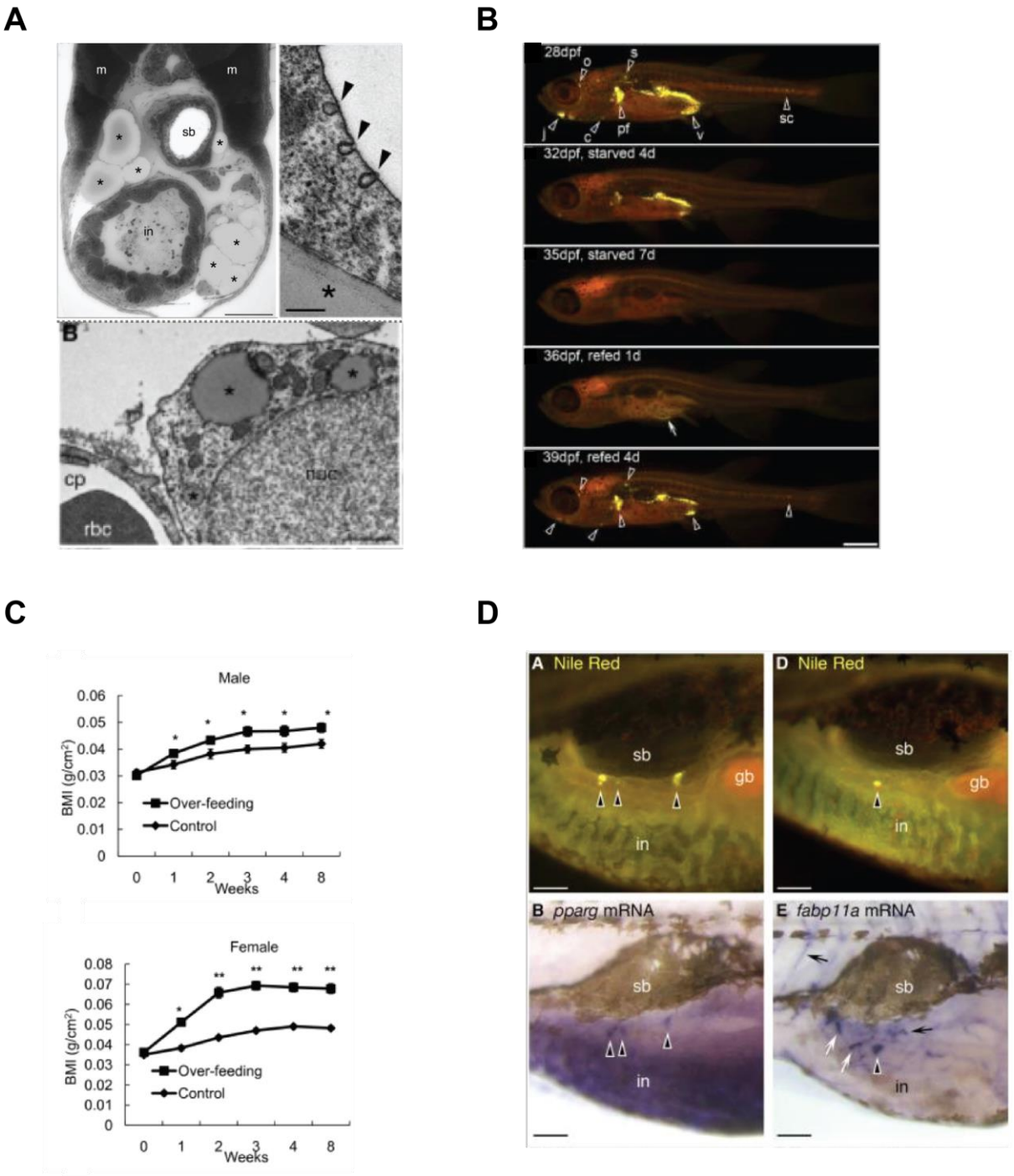

Figure 1.12 – Zebrafish AT is morphologically, functionally and molecularly homologous to mammalian AT

Figure 1.12 – Zebrafish AT is morphologically, functionally and molecularly homologous to mammalian AT. A. Electron microscopy images showing that zebrafish AT is morphologically homologous to mammalian AT. Asterisks show lipid droplets. Arrow heads show caveolae. Sb (swim bladder). In (intestinal tract) Scale bar is 100 µm in top left panel, 200 nm in top right panel and 1 µm in bottom panel. Adapted from (Flynn et al., 2009). **B.** Nile red images showing decreased Nile Red staining in response to starvation. Scale bar is 1 mm. Adapted from (Flynn et al., 2009). **C.** Graphs showing increase in BMI of zebrafish over-fed compared to normally fed fish. Adapted from (Oka et al., 2010). **D.** In situ hybridisations showing expression of *pparg* and *fabp11a* in adipose tissue. Adipose tissue is shown by Nile red staining in the top panels. Scale bar is 100 µm. Adapted from (Flynn et al., 2009).

1.3.5 - Adipose tissue in zebrafish is anatomically homologous to mammalian white adipose tissue and the development of zebrafish adipose tissue has been mapped.

Adipose tissue in zebrafish is found in discrete depots, much like in mammals (Minchin and Rawls, 2017b). A comprehensive classification of zebrafish adipose depots exists and shows zebrafish to possess 34 regionally distinct AT depots **(Figure 1.13A)** (Minchin and Rawls, 2017b). This system classified depots by anatomical location, with depots classified as internal AT and subcutaneous AT **(Figure 1.13A)** (Minchin and Rawls, 2017b). Internal AT was also further broken down into visceral AT and non-visceral AT **(Figure 1.13A)** (Minchin and Rawls, 2017b). Overall adipose tissue in zebrafish is anatomically conserved, with adipose found in discrete depots.

The zebrafish AT depot classification system also provides a list of developmental milestones, detailing when during development AT depots are likely to be present (Minchin and Rawls, 2017b). Imrie and Sadler (2010) first reported that AT development in zebrafish is controlled by both fish size and time. However, more recent work by Minchin and Rawls (2017) has provided a more comprehensive timeline of adipose tissue development in zebrafish. The study used 362 fish between 20 and 39 dpf (days post fertilisation) and created regression models, so that AT size could be predicted across a range of postembryonic fish (Minchin and Rawls, 2017b). The appearance of new AT depots was used to define discrete milestones and 26 milestones were identified (Minchin and Rawls, 2017b). It was found that, while increase in adipose tissue area remained steady throughout the dataset, growth of individual depots showed distinct trajectories (Minchin and Rawls, 2017b). This led to the development of models of growth for each depot and provided a tool through which deviation from normal AT growth could be assessed (Minchin and Rawls, 2017b). In summary, adipose tissue in zebrafish is found in discrete depots and a detailed timeline of normal AT growth exists.

1.3.6 - Lipophilic dyes can be used to stain adipose tissue in zebrafish

Adipose tissue in zebrafish was first identified using histological sectioning and staining (Imrie and Sadler, 2010). These methods are often used when analysing mammalian WAT, however this can lead to incomplete preservation of WAT architecture and provides limited information on cellular dynamics (Xue et al., 2010).

Fortunately, the nature of zebrafish makes them well suited to overcome the challenges of imaging WAT in mammals. A dye commonly used to stain adipose tissue in zebrafish is Nile Red (Flynn et al., 2009). Nile Red stains neutral lipid and so will stain the lipid found within adipocytes but will not stain polarised lipid, such as that found in cell membranes (Flynn et al., 2009). This staining can be used in live zebrafish and the small size of zebrafish means that it can be used to measure whole body adiposity (Flynn et al., 2009). Furthermore, Nile Red staining and measurement of fluorescence area have been shown to be a good proxy for total AT area (Tingaud-Sequeira et al., 2011). Tingaud-Sequeira et al (2011) demonstrated that there is a good correlation between the fluorescence area stained by Nile Red and the total triglyceride content of a fish. In addition to Nile Red other fluorescent dyes can be used to stain AT in zebrafish **(Figure 1.13B)** (Minchin and Rawls, 2011, Minchin and Rawls, 2017a). Detailed methods also exist for the imaging of live zebrafish using both a stereomicrosope and a confocal microscope **(Figure 1.13B)** (Minchin and Rawls, 2011, Minchin and Rawls, 2017a). In summary techniques exist which allow adipose tissue to be imaged and area quantified in live zebrafish.

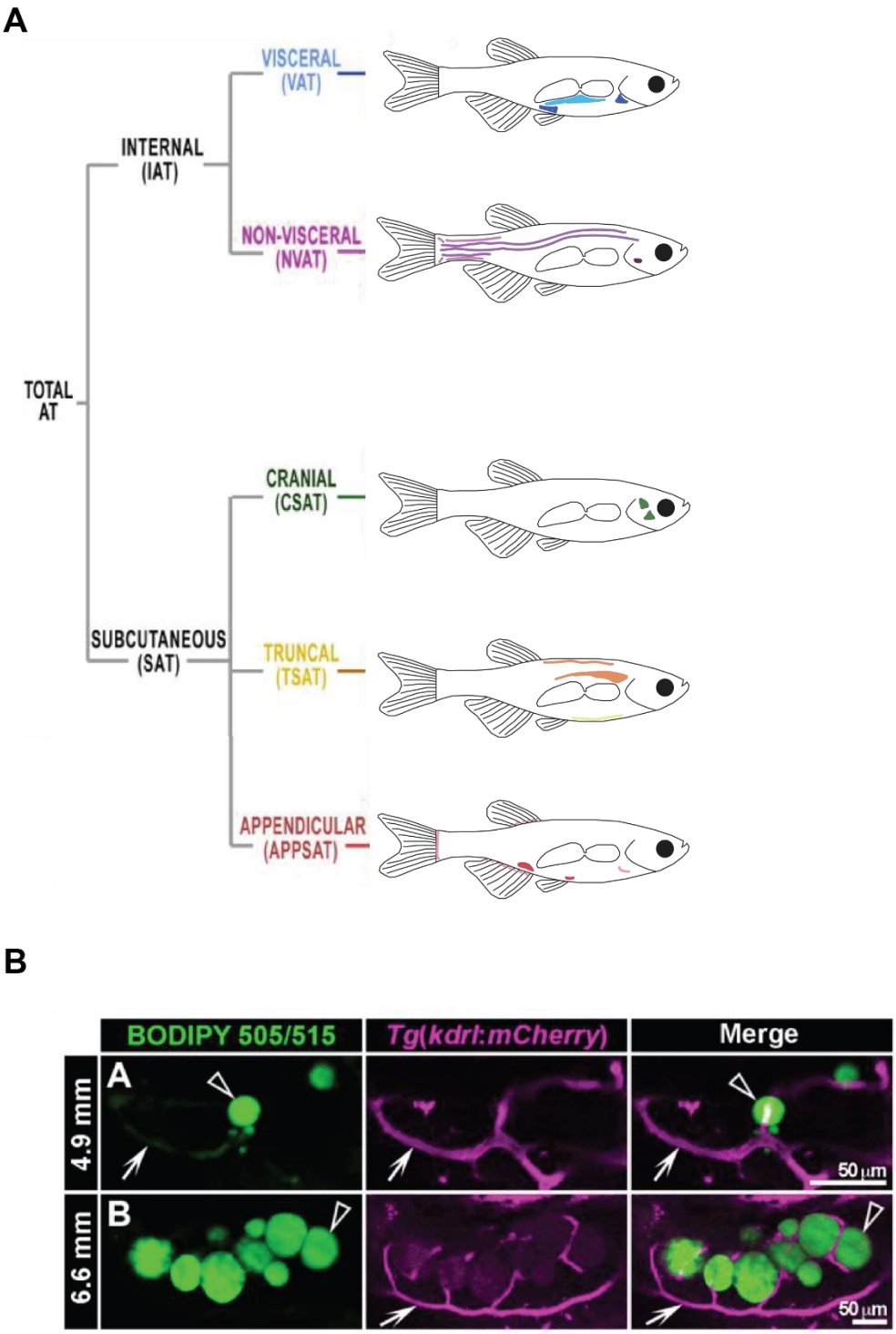

Figure 1.13 – Zebrafish AT is anatomically homologous to mammalian WAT and can be imaged *in vivo*. A. Schematic showing the location of AT depots in zebrafish. Adapted from (Minchin and Rawls, 2017b). **B.** Zebrafish visceral AT stained with lipophilic dyes. The *Tg(kdrl:mCherry)* line expressed mCherry fluorescent protein in the endothelial cells of the vasculature. Adapted from (Minchin and Rawls, 2011).

1.3.7 - The genetic control of adipose tissue development is conserved in zebrafish

In addition to expressing similar genes to mammalian AT, zebrafish AT also appears to be under the same genetic control as mammalian AT. Evidence for this comes from growth hormone mutants. Energy metabolism and somatic growth are known to be closely linked in humans, with childhood obesity being linked to increased linear growth and undernutrition linked to growth retardation (McMenamin et al., 2013). Conversely, altered levels of growth hormones (GH) have also been linked to changes in adiposity in mammals (McMenamin et al., 2013). GH deficient children are short and mildly obese and inactivation of GH in rodents leads to obesity, independent of food intake (McMenamin et al., 2013). This mammalian growth hormone deficient phenotype has also been observed in zebrafish (McMenamin et al., 2013). A study in 2013 found that zebrafish GH mutants show severe growth defects and increased adiposity **(Figure 1.14A & B)** (McMenamin et al., 2013). The zebrafish mutants were also found to have significantly more AT than size matched WT fish and a more hypertrophic adipose morphology **(Figure 1.14A & C)** (McMenamin et al., 2013). The phenotype of GH deficient zebrafish seems to be very similar to that of GH deficient children and rodents and suggests that the genetic control of adipose tissue is conserved to zebrafish.

1.3.8 - Zebrafish can be used as a tool to test if genes identified by human GWAS studies have a role in adipose tissue expansion

Zebrafish can be used to test the role of novel genes involved in the regulation of AT expansion. In this thesis I have used zebrafish to investigate the role of the gene *foxp1* in AT expansion. Zebrafish have previously been used to test if genes identified through human GWAS studies affect measures of adiposity. One example of this is the 2015 study by Minchin et al, which looked at the role of the gene *plxnd1* (Plexin D1) in body fat distribution (Minchin et al., 2015). GWAS studies had implicated *PLXND1* in body fat distribution and type 2 diabetes, however the role of *PLXND1* in adiposity and insulin resistance was unknown (Minchin et al., 2015). The study made use of *plxnd1* zebrafish mutants and found that these mutants had decreased levels of VAT, a more hyperplastic VAT morphology and improved glucose tolerance following a high fat diet **(Figure 1.14D & E)** (Minchin et al., 2015). In humans it was

discovered that there is a positive association between VAT *PLXND1* mRNA levels and a more hypertrophic VAT morphology, and that *PLXND1* mRNA is significantly increased in the VAT of obese patients with type 2 diabetes (Minchin et al., 2015). In conclusion it has been demonstrated that zebrafish can be used to elucidate the role of novel genes in adipose tissue distribution and that these findings can be relevant to human disease. Therefore, zebrafish are a suitable model in which to investigate the hypothesis that *foxp1* maintains progenitor cell populations in AT and is required for AT expansion.

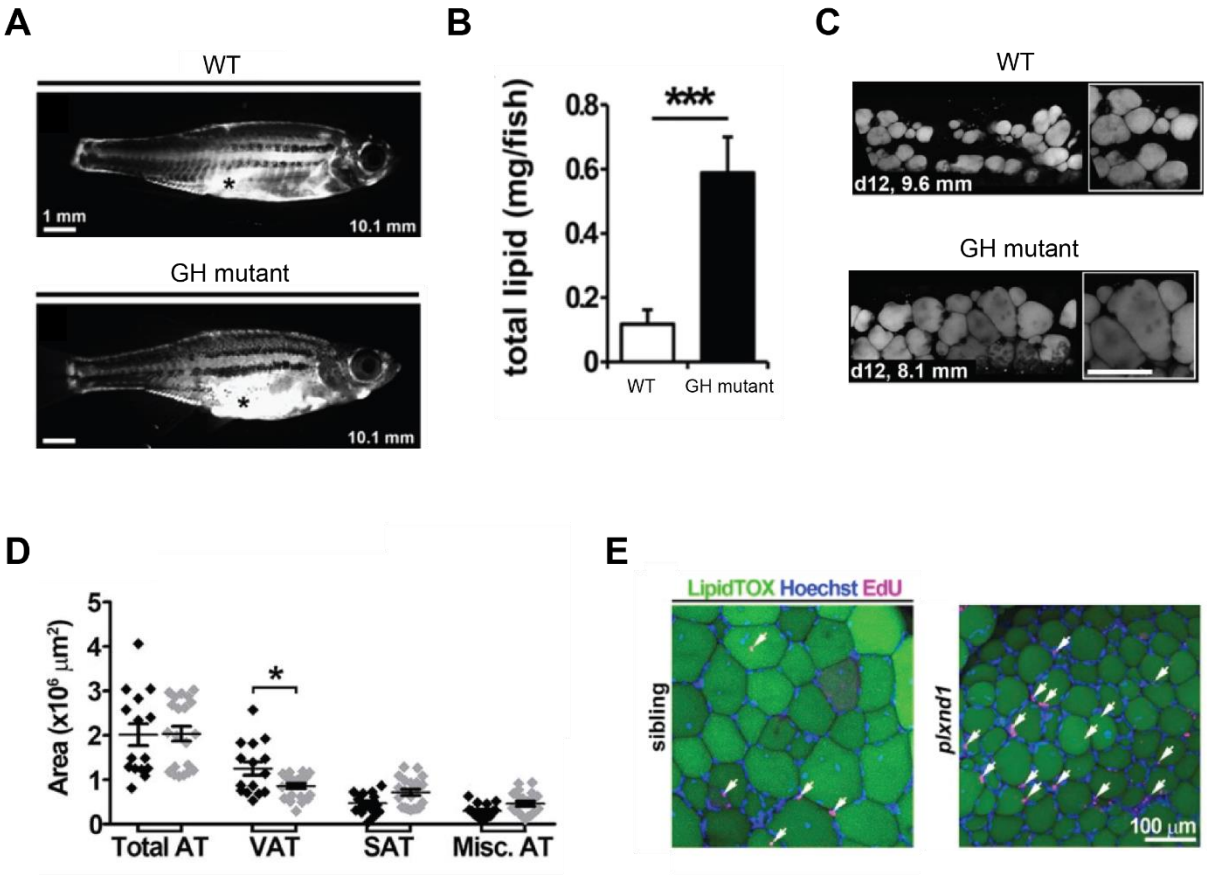

Figure 1.14 – The genetic control of adipose tissue expansion is conserved to zebrafish. A. Nile red images of size matched WT and GH mutant zebrafish. Adapted from (McMenamin et al., 2013). **B.** Graph showing total lipid in WT and GH mutant zebrafish. Adapted from (McMenamin et al., 2013). **C.** Confocal imaging of LipidTOX stained SAT. Imaging from day 12 (d12) shown. Scale bar is 100 µm. Adapted from (McMenamin et al., 2013). **D.** Graph showing AT areas in WT and *plxnd1* mutant zebrafish. Adapted from (Minchin et al., 2015). **E.** Maximum intensity projections of VAT stained with LipidTOX in WT and *plxnd1* mutant zebrafish. Arrows point to EdU positive nuclei. Adapted from (Minchin et al., 2015).

1.4– Hypotheses and Aims

The overall aim of my thesis was to establish whether the genetic control of adipose tissue expansion is conserved between zebrafish and mammals, and to identify and test novel regulators of AT expansion using zebrafish as a model. The first part of this aim, to determine whether the genetic control of AT expansion is conserved between zebrafish and mammals, is addressed in chapter 5 and more specific aims and hypotheses relating to this aim are discussed below. The second part of my overall aim, to identify and test novel regulators of AT expansion, is addressed in chapters 3 and 4 and more specific aims and hypotheses are discussed below.

1.4.1 – Aim 1 - Identification of factors which regulate adipose morphology and expansion

The main driver of obesity associated disease risk is metabolic dysfunction. Metabolic dysfunction is characterised by dysfunctional adipose tissue, which is hypoxic, fibrotic and filled with necrotic adipocytes **(Figure 1.4B)** (Crewe et al., 2017). Dysfunctional adipose tissue is created when adipose reaches its capacity to expand **(Figure 1.4)** (Crewe et al., 2017). Mouse models have demonstrated that improving the ability of adipose tissue to expand can lead to a "healthy" version of obesity in which animals are grossly obese but show normal levels of blood glucose and are not insulin resistant (Kim et al., 2007). Adipose tissue expansion can be driven by increases in cell size or number, with hyperplastic growth improving metabolic parameters, such as levels of fasting glucose (Sugii et al., 2009). Therefore, one aim of my thesis is to identify factors which regulate adipose tissue expansion and adipose tissue morphology, with the aim to improve obesity associated adipose tissue dysfunction.

1.4.2 - Hypothesis - *Foxp1* maintains progenitor cell populations in white adipose tissue and is required for adipose tissue expansion

Foxp1 is a transcription factor which is expressed in multiple tissues, including adipose tissue (Fagerberg et al., 2014). Data from GWAS studies has found an

association between variation at the *FOXP1* locus and measures relating to adiposity, such as BMI and SAT levels (Fox et al., 2012, Kichaev et al., 2019). Further data linking *Foxp1* to changes in adipose levels is provided by a recent study in 2019 which showed that loss of *Foxp1* in adipose tissue leads to reduced levels of AT (Liu et al., 2019). However, a mechanism to explain how *Foxp1* influences adipose tissue levels remains to be uncovered. *Foxp1* is known to drive the proliferation and differentiation of progenitor cells in tissues other than adipose (Fu et al., 2018, Gabut et al., 2011, Hu et al., 2006, Leishman et al., 2013, Li et al., 2017). For example, in embryonic stem cells, *Foxp1* represses the expression of genes required for differentiation and *Foxp1* is also required for the differentiation of MSCs (Gabut et al., 2011, Li et al., 2017). From these known roles of *Foxp1* in progenitor cells it is reasonable to suggest that *Foxp1* may also act on progenitor cells in adipose tissue. This leads me to the hypothesis that *Foxp1* maintains progenitor cell populations in adipose tissue and is required for adipose tissue expansion **(Figure 1.15A & B)**. This hypothesis will be the main focus of my thesis and is addressed in chapters 3 and 4.

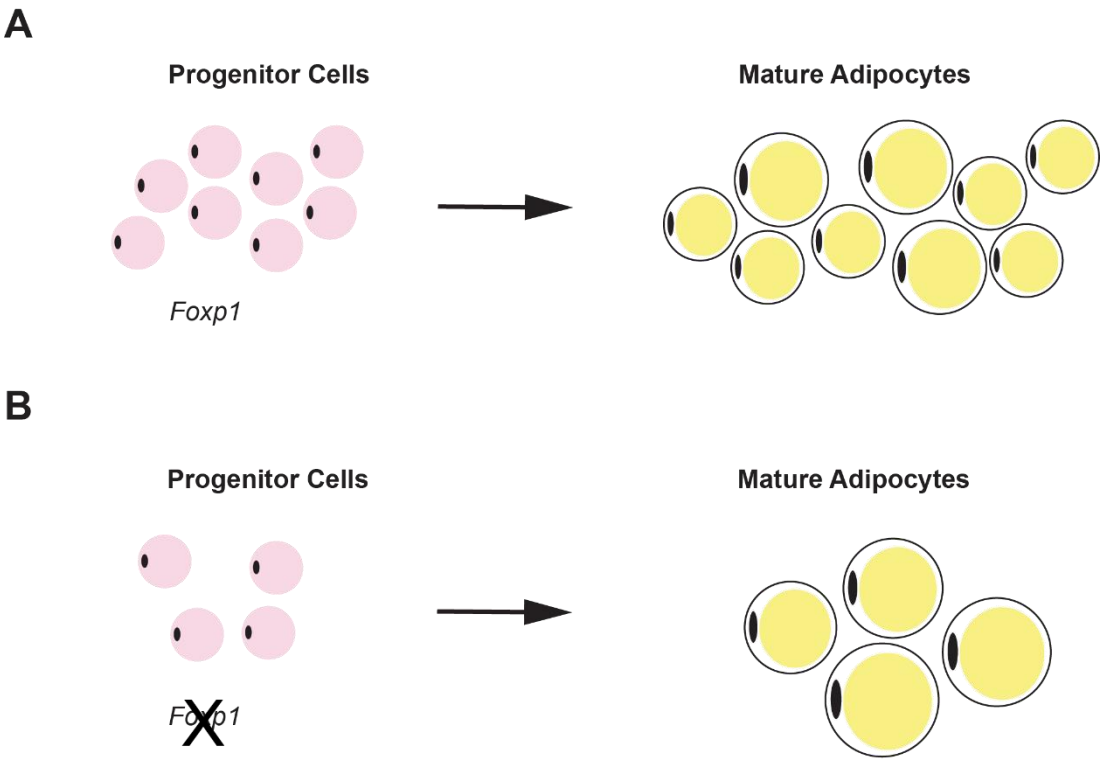

Figure 1.15 – Hypothesis: *Foxp1* maintains progenitor cell populations in adipose tissue and is required for adipose tissue expansion. A. Schematic showing that *Foxp1* maintains progenitor cells in AT and is required for AT expansion. **B.** Schematic showing the hypothesised effect of loss of *Foxp1* in AT. Loss of *Foxp1* leads to improper progenitor cell maintenance and reduced AT expansion.

1.4.3 – Aim 2 – Establishing zebrafish as a model of AT expansion

Zebrafish are an emerging model of AT biology and much is known about AT in zebrafish. For example, zebrafish possess AT which is functionally homologous to mammalian WAT (Flynn et al., 2009). Furthermore, the morphology of zebrafish adipocytes is very similar to that of mammalian white adipocytes, with zebrafish adipocytes sharing their characteristic large cellular size and presence of a singular lipid droplet (Flynn et al., 2009, Imrie and Sadler, 2010). AT in zebrafish is also molecularly homologous to mammalian WAT, with tissues in both species expressing genes such as *pparg, cebpa* and *fapb4* (Flynn et al., 2009, Imrie and Sadler, 2010). However, much of what is known of the molecular regulation of AT expansion in mammals is unknown in zebrafish. Therefore, the second aim of my thesis is to determine whether the genetic control of AT expansion is conserved between zebrafish and mammals and to further establish zebrafish as a model of AT expansion.

1.4.4 – Hypothesis – The role of *cebpa* in AT expansion is conserved between zebrafish and mammals

Cebpa is a master regulator of adipogenesis and is required for AT expansion *in vivo* (Linhart et al., 2001). *Cebpa* expression can trigger the differentiation of preadipocytes into adipocytes *in vitro* and mouse *Cebpa* knockout models show near complete loss of WAT (Linhart et al., 2001). While *cebpa* is expressed by AT in zebrafish, whether *cebpa* is required for AT expansion is unknown (Imrie and Sadler, 2010). As many aspects of AT biology are conserved between zebrafish and mammals, it is reasonable to expect that the genetic control of AT expansion is also conserved. This leads me to the hypothesis that the role of *cebpa* in AT expansion is conserved between zebrafish and mammals. This hypothesis was addressed in chapter 5.

Chapter 2 – Materials and Methods

2.1 - Generation of zebrafish mutants using CRISPR/Cas9

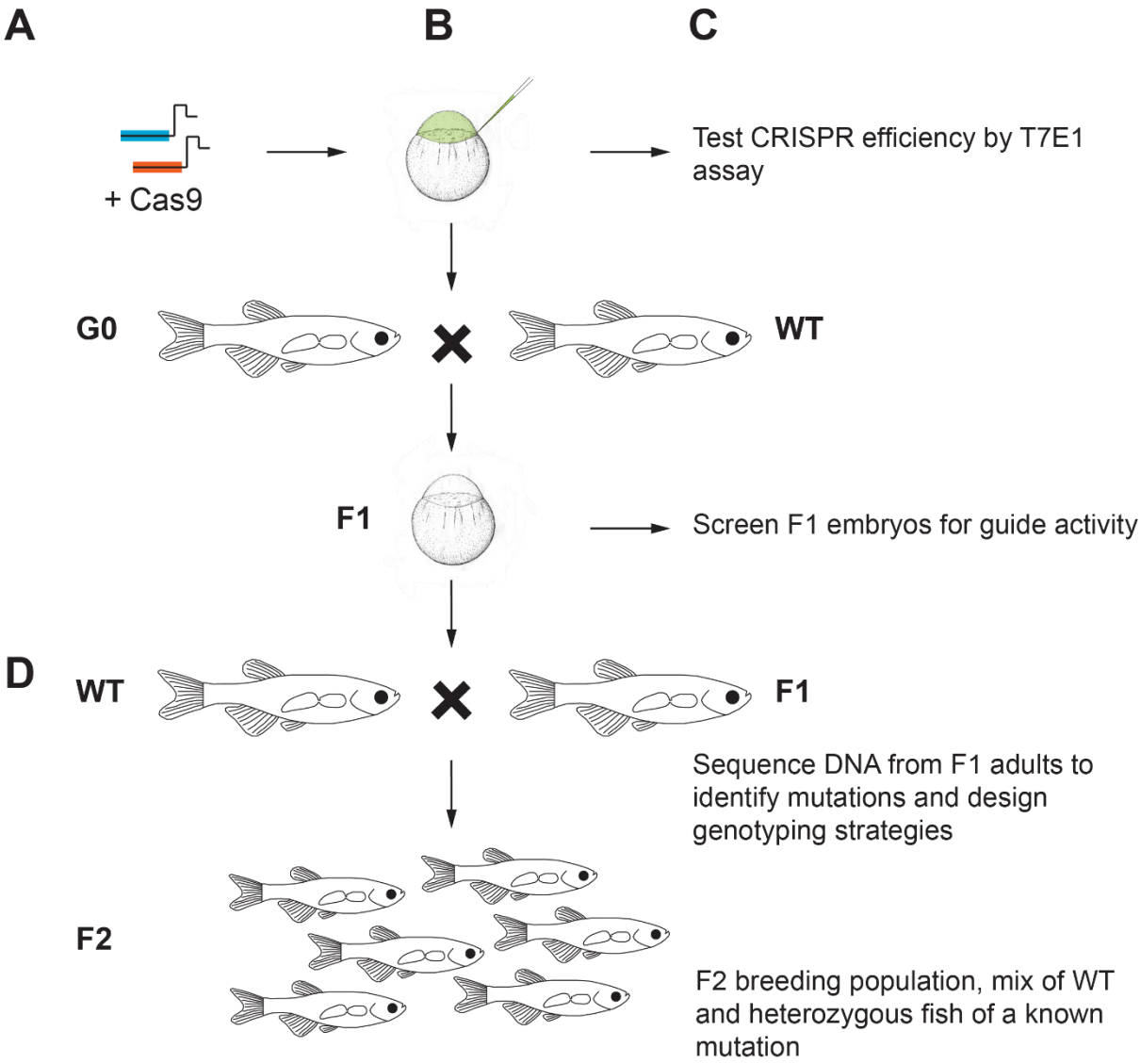

Figure 2.1 – Generation of stable zebrafish mutants. A. Schematic showing gRNAs. **B.** Schematic showing injection of gRNAs into the zebrafish embryo. **C.** Description of the test for guide activity. **D.** Description of stable mutant identification and design of genotyping strategies.

2.1.1 - Creation of gRNAs

The sequence of the genes of interest were identified and guide RNAs created **(Table 2.1)**.

Identification of functional protein domains to be targeted using CRISPR

Protein domains targeted using CRISPR were identified using Ensembl. The protein summary and Domains & Features tabs were utilised to identify the domains of Foxp1a, Foxp1b and Cebpa.

CRISPR Guide Design

sgRNAs (single guide RNA) to target genes of interest were designed using the CHOPCHOP programme (Labun et al., 2016). Guides were selected based on proximity to the region of interest, CHOPCHOP score and a lack of predicted off target effects. The desired oligo was altered so that the first two bases were GA. The Sp6 promoter sequence was then placed in front of the designed oligo and the tracrRNA sequence behind (Sp6-target sequence-tracrRNA). The complete sequence was then ordered from IDT.

Table 2.1- Location and sequence of CRISPR guides

Gene targeted	**Exon/ region targeted**	**Sequence**
foxp1a	Exon 2 – Translational start site	GAATAGCAGTCCGACTGGGC
foxp1a	Exon 8 – zinc finger domain	GACAGAGGATGGCCACTTTG
foxp1a	Exon 14 – fork head domain	GACGAGTGGAGAATGTGAAG
foxp1b	Exon 15 – fork head domain	GATAACGAAGCATACGTGAA
Cebpa	Exon 1	GAACTAGGTACGGGCGTCG

Table 2.2 – Sequence of Sp6 promoter and tracrRNA

Target	**Sequence**
Sp6 Promoter	ATTTAGGTGACACTATA
tracrRNA	GTTTTAGAGCTAGAAATAGC

Annealing of CRISPR guides

The recipe for the guide production is as follows

Table 2.3 – recipe for annealing sgRNA guides	
Reagent	**Amount (µl)**
Q5 buffer	2.5
10 mM DNTPs	0.25
sgRNA Oligo (10 µM)	0.5
Oligo 2 (10 µM)	0.5
Q5 polymerase	0.25
Nuclease free water	8

Q5 polymerase and buffer (NEB, M0491S), DNTPs (NEB, N0447S).

PCR amplification steps were as follows.

1- 98°C for 2 minutes
2- 55°C for 10 minutes
3- 72°C for 10 minutes

Products were then run on an agarose gel to check for bands.

Gel Electrophoresis

Electrophoresis was performed on a 1% agarose gel made in 1XTBE buffer with gel red (5 µl/100ml). PCR reactions were loaded directly onto gels and ran at 100V for 30 minutes. A 10 Kb DNA ladder (NEB, N0469S), was also loaded onto the gels. DNA was visualised using a UV transilluminator (UVIDOC HD6).

The recipe for 10X TBE is as follows

Table 2.4 – recipe for 10X TBE	
Reagent	**Amount (g)**
Tris	108
EDTA	18.6
Boric Acid	55
Water	1000 ml

CRISPR Guide Production

mMessage mMachine SP6 transcription kit (Invitrogen, AM1340) was used to produce capped RNA from the PCR template. The recipe for the transcription reaction is as follows

Table 2.5 – recipe for mMessage mMachine	
Reagent	**Amount (µl)**
NTP Cap	5
Buffer	1
PCR template	1.5
SP6 enzyme	1
Nuclease free water	1.5

The transcription reaction was incubated at 37°C overnight. The next day 1 µl of turbo DNase (mMessage mMachine kit) was added to the reaction mix and the samples incubated at 37°C for 15 minutes.

CRISPR Guide cleaning

Guides were cleaned using the zymo RNA clean and concentrate kit (Zymo Research, D4004). Clean RNA was eluted in 20 µl of nuclease free water.

Measuring concentration of RNA

The concentration of the clean RNA was measured using the NanoDrop 1000 spectrophotometer. 1 µl of nuclease free water was used to calibrate the machine and 1 µl of the eluted RNA was used to check RNA quality and concentration. A 260/280 ratio of around 2 and a 260/230 ratio of around 2 was classified as having a high level of purity.

2.1.2 - Injection of gRNAs

Guide RNAs were injected into zebrafish embryos at the one cell stage **(Figure 2.1B)**.

Microinjection of guide RNAs into zebrafish embryos

Needles for injections were made by pulling borosilicate glass capillaries (World Precision Instruments), using a P-97 Falming/Brown micropipette puller. Microinjections were performed using a picopump microinjector (PV820). All embryos were injected at the one cell stage. All gRNAs were injected into WIK embryos.

The following reaction mixture was used

Table 2.6 – Recipe for sgRNA injections	
Reagent	**Amount (µl)**
Cas9 (800 ng/µl)	1
sgRNA (300 ng/µl)	1
Phenol red	0.5
Nuclease free water	0.5

Cas9 (NEB, M0646T). Phenol Red (Sigma, P0290)

The injection mixture was incubated at 37°C for 5 minutes. 1 nl was injected into each zebrafish embryo.

2.1.3 - Screening for guide activity

A T7E1 assay was used to screen for guide activity **(Figure 2.1C)**.

Genomic DNA isolation

gDNA (genomic DNA) was extracted from pools of 5 embryos before 5 days of age. Embryos were placed in 100 µl of 50 mM NaOH and incubated at 95°C for 20 minutes. 10 µl of 1 M TrisHCl was added and samples were centrifuged at 4000 rpm for 10 minutes. The supernatant was then transferred to a fresh tube.

Design of primers to test if CRISPR guides are cutting

PCR primers for determining if guides were cutting DNA in CRISPR mutated fish were designed using the Primer3Plus programme (Untergasser et al., 2007).

Primers were chosen which amplified regions containing CRISPR guide RNAs. Products were around 500 bp.

Table 2.7 - Primers to amplify locus surrounding target site of CRISPR guide		
CRIPSR guide	**Forward Primer**	**Reverse Primer**
foxp1a (ATG)	ATGCTGGGTTCCACACACTT	GGCACGCATGTTTTGTCAT
foxp1a (ZFD)	CAACCAGGACAAACAGCGTA	CATTGTCCAGTGCAAACCTG
foxp1a (FHD)	GCCAGATTGGACTGGATGTT	TTATTTCCAGGCCATTCTGG
foxp1b (FHD)	TTCAGTTTCAGCTCCTTCCTTC	TGGAAGTCAAGCTACCAGCA
cebpa (ATG)	TTGCTTGGCTGTCGTAGATG	ATCAGCGCCTACATTGATCC

PCR

PCR was used to amplify the locus surrounding the target site of the CRISPR guide. A GoTaq master mix was used (Promega, M783B). The recipe for the PCR is as follows

Table 2.8 – Recipe for PCR reaction	
Reagent	**Volume (µl)**
Go Taq	5
gDNA	2
Primers (10 µM)	1
Nuclease free water	2

The following PCR conditions were then used

1- 94°C for 3 minutes
2- 94°C for 20 seconds
3- 55°C for 30 seconds
4- 72°C for 1 minute

Repeat step 2 to 4, 30 times

5- 72°C for 5 minutes
6- 10°C final hold

Reannealing of PCR products from CRISPR guide injected fish

PCR products were heated and reannealed with the following temperatures and timings. 95°C for 10 minutes. Then cooled to 85°C with 2°C drop in temperature every 10 seconds. Then cooled to 25°C with a 2°C drop in temperature every 10 seconds.

T7 Endonuclease 1 Assay

T7 Endonuclease 1 (T7E1) enzyme (NEB, M0302S) was used to cut DNA and assess levels of mutagenesis. The following reaction mixture was made up

Table 2.9 – Recipe for T7E1 reaction	
Reagent	**Volume (µl)**
PCR product	8
Buffer 2	1
T7E1 enzyme	0.3
Nuclease free water	0.7

The reaction mixture was then incubated at 37°C for 30 minutes. The products were separated by gel electrophoresis and differences in banding patterns assessed. Guides which were found to be active were reinjected into WT embryos and these embryos raised. G0 adult fish were then outcrossed to WT fish and their embryos screened for guide activity. Fish found to produce embryos which contained indels at the CRISPR target site, as shown by T7E1 assay, were crossed again to WT fish and the embryos raised.

2.1.4 - Identifying the nature of mutations created by CRISPR

DNA from F1 fish was sent for Sanger sequencing to determine the nature of the mutation introduced **(Figure 2.1D)**.

Isolating gDNA from adult fish by fin clips

F1 offspring of G0 fish known to produce embryos in which CRISPR guides are active, were fin clipped. Fish were lightly anesthetised using MS-222. The end of the caudal fin rays were then removed, using scissors which had been sterilised with ethanol. The fish was allowed to recover in fresh system water and the fin placed in 100 µl of 50 mM NaOH. gDNA was then extracted and amplified using PCR.

Cloning PCR products into a vector for sequencing by TopoTA Cloning

PCR products created via amplification with GoTaq were cloned into the pCR8 vector (Invitrogen, K4500J10). The following reaction mix was made.

Table 2.10 – Recipe for TopoTA cloning reaction

Reagent	**Volume (µl)**
pCR8 vector	0.25
Salt	0.25
PCR product	0.25
Nuclease free water	0.75

The mixture was then incubated for 15 minutes at 25°C. This was then cooled to 4°C and 20 ul of One Shot Top10 chemically competent E.Coli added (Invitrogen, C404003). The reaction was incubated at 4°C for 30 minutes and then a heat shock was performed at 42°C for 45 seconds. The mixture was cooled to 4°C and 250 µl of SOC (Super Optimal Broth) added. The cells were then allowed to recover at 37°C for 1 hour. 250 µl of the reaction mixture was then spread onto agar plates containing spectinomycin (Sigma, S2647-100MG) at 50 µg/ml. Plates were incubated overnight at 37°C.

Identifying clones which contain the desired insert by colony PCR

The following reaction mixture was made

Table 2.11 – Recipe for colony PCR	
Reagent	**Volume (ul)**
GoTaq	7.5
Primers	1
Nuclease free Water	6.5

The colony of interest was picked, with a pipette tip, re-streaked on a fresh agar plate and then the pipette tip was placed in the PCR reaction mixture. The re-streaked agar plate was incubated at 37°C for 6 hours. The pipette tip was mixed in the reaction mixture and then removed. PCR was then performed and 2 µl of the products ran on an agarose gel to check for insertion into the vector. Insertion was determined by product size.

Colonies where an insertion was thought to have taken place, were then picked from the re-streaked plate and used to inoculate 1.5 ml of LB containing spectinomycin. Samples were incubated shaking overnight at 37°C.

Minipreps to isolate PCR products in the sequencing vector

Minipreps were performed using QIAprep Spin Miniprep Kit (QIAGEN, 27104) and all centrifugations were performed using a standard table-top micro-centrifuge.

Sequencing of unknown CRISPR mutant DNA

Sequencing was performed using a Mix2Seq kit (Eurofins). Reactions were set up according to the manufacturers instructions.

Sequence alignment of potential CRISPR mutant DNA with wild type DNA

Sequence alignment was performed using Clustal Omega software (EMBL-EBI). Sequences of DNA from F1 fish were aligned to the corresponding WT sequence, as found on Ensembl.

Nature of stable mutants generated

The table below lists the stable mutants generated and gives the nature of the mutation in each case. In the results chapters the *foxp1a*$^{(ed16/ed16)}$ and *foxp1b*$^{(ed25/ed25)}$ alleles will be referred to as *foxp1a*$^{(-/-)}$ and *foxp1b*$^{(-/-)}$ respectively for simplicity.

Table 2.12 – Stable mutants generated	
Allele name	**Nature of mutation**
foxp1a$^{(ed14/ed14)}$	7bp indel close to the translational start site of *foxp1a* – results in a frameshift and the introduction of an early stop codon
foxp1a$^{(ed15/ed15)}$	7bp indel in the FHD of *foxp1a* – results in a frameshift and the introduction of an early stop codon
foxp1a$^{(ed16/ed16)}$	13bp indel in the FHD of *foxp1a* – results in a frameshift and the introduction of an early stop codon
foxp1a$^{(ed17/ed17)}$	45bp indel in the ZFD of *foxp1a* – inframe mutation
foxp1a$^{(ed18/ed18)}$	10bp indel in the ZFD of *foxp1a* – results in a frameshift and the introduction of an early stop codon
cebpa$^{(ed19/ed19)}$	38bp deletion close to the translation start site of cebpa - results in a frameshift and the introduction of an early stop codon
cebpa$^{(ed20/ed20)}$	7bp deletion close to the translation start site of cebpa - results in a frameshift and the introduction of an early stop codon
foxp1b$^{(ed23/ed23)}$	5bp deletion in the FHD of *foxp1b* – results in a frameshift and the introduction of an early stop codon
foxp1b$^{(ed24/ed24)}$	3bp deletion in the FHD of *foxp1b* – results in a frameshift and the introduction of an early stop codon
foxp1b$^{(ed25/ed25)}$	4bp indel in the FHD of *foxp1b* – results in a frameshift and the introduction of an early stop codon
foxp1b$^{(ed26/ed26)}$	12bp insertion in the FHD of *foxp1b* – inframe mutation

2.1.5 - Genotyping stable lines

Strategies were devised to genotype stable lines by PCR or restriction digest **(Figure 2.1D)**. Genotyping strategies for Ed14 and Ed15 were unable to be designed.

Ed16

Primers were designed which recognised either the 13bp indel in the ed16 mutants, or the WT sequence. Two PCR reactions were then set up, one containing the forward, reverse and WT primers, and one containing the forward, reverse and mutant primers. The PCR products were then run on an agarose gel and the banding pattern used to determine the genotype of the fish being tested **(Figure 2.2A & B)**. For example, a band for the WT primer reaction and no band for the mutant primer mix would be identified as a WT fish **(Figure 2.2A & B)**. The sequences of the primers used are shown in the table below.

Table 2.13 – *foxp1a*$^{(ed16/ed16)}$ genotyping primers	
Primer	**Sequence**
Forward	GCCAGATTGGACTGGATGTT
Reverse	TTATTTCCAGGCCATTCTGG
WT	ACGAGTGGAGAATGTGAAGG
Mutant	AAACGGCCCCCTCGTACT

Ed17

foxp1a$^{(ed17/ed17)}$ mutants were genotyped using PCR. As the *foxp1a*$^{(ed17/ed17)}$ mutation was caused by a large deletion, a normal PCR was carried out and a band shift looked for. The primers which had previously been used to amplify the region, before the T7E1 assay, were used.

Table 2.14 – *foxp1a*$^{(ed17/ed17)}$ genotyping primers	
Primer	**Sequence**
Forward	CAACCAGGACAAACAGCGTA
Reverse	CATTGTCCAGTGCAAACCTG

Ed18

foxp1a$^{(ed18/ed18)}$ mutants were genotyped using a restriction enzyme. The area spanning the *foxp1a*$^{(ed18/ed18)}$ lesion was amplified by PCR **(Table 2.14)**. The following reaction mixture was then made.

Table 2.15 – Recipe for BslI restriction digest	
Reagents	**Volume (µl)**
Restriction enzyme BslI	0.25
10X buffer	1.25
PCR product	5
Nuclease free water	6

BslI (NEB, R0555S). The mixture was incubated at 55 °C for 15 minutes and ran on a 2% agarose gel **(Figure 2.2C)**. The enzyme only cuts WT DNA.

Ed19

cebpa$^{(ed19/ed19)}$ mutants were genotyped by PCR. As the *cebpa*$^{(ed19/ed19)}$ mutant contains a large deletion, a PCR reaction was set up in which primers spanned the mutation site. A band shift was used to genotype fish **(Figure 2.2D)**. The table below shows the sequence of the primers used.

Table 2.16 – cebpa$^{(ed19/ed19))}$ genotyping primers	
Primer	**Sequence**
Forward	TTGCTTGGCTGTCGTAGATG
Reverse	ATCAGCGCCTACATTGATCC

Ed20

The *cebpa*$^{(ed20/ed20)}$ mutants were genotyped by a restriction digest. The area spanning the *cepba*$^{(ed20/ed20)}$ lesion was amplified by PCR **(Table 2.16)**. The following reaction mixture was then made.

Table 2.17 – Recipe for BtgI restriction digest	
Reagents	**Volume (µl)**
Restriction enzyme BtgI	0.25
10X buffer	1.25
PCR product	5
Nuclease free water	6

BtgI (NEB, R0608S). The mixture was incubated at 37 °C for 15 minutes and ran on a 2% agarose gel **(Figure 2.2E)**. The enzyme cuts WT DNA twice and mutant DNA once.

Ed23, Ed24, Ed25, Ed26

The *foxp1b*$^{(ed23/ed23)}$, *foxp1b*$^{(ed24/ed24)}$, *foxp1b*$^{(ed25/ed25)}$ and *foxp1b*$^{(ed26/ed26)}$ mutants were genotyped by a restriction digest. The area spanning the lesions was amplified by PCR **(Table 2.18)**.

Table 2.18 – *foxp1b*$^{(ed23/ed23)}$, *foxp1b*$^{(ed24/ed24)}$, *foxp1b*$^{(ed25/ed25)}$ and *foxp1b*$^{(ed26/ed26)}$ genotyping primers	
Primer	**Sequence**
Forward	TTCAGTTTCAGCTCCTTCCTTC
Reverse	TGGAAGTCAAGCTACCAGCA

The following reaction mixture was then made.

Table 2.19 – Recipe for HpyCH4IV restriction digest	
Reagents	**Volume (µl)**
Restriction enzyme HpyCH4IV	0.25
10X buffer	1.25
PCR product	5
Nuclease free water	6

HpyCH4IV (NEB, R0619S). The mixture was incubated at 37 °C for 15 minutes and ran on a 2% agarose gel **(Figure 2.2F)**. The enzyme only cuts WT DNA.

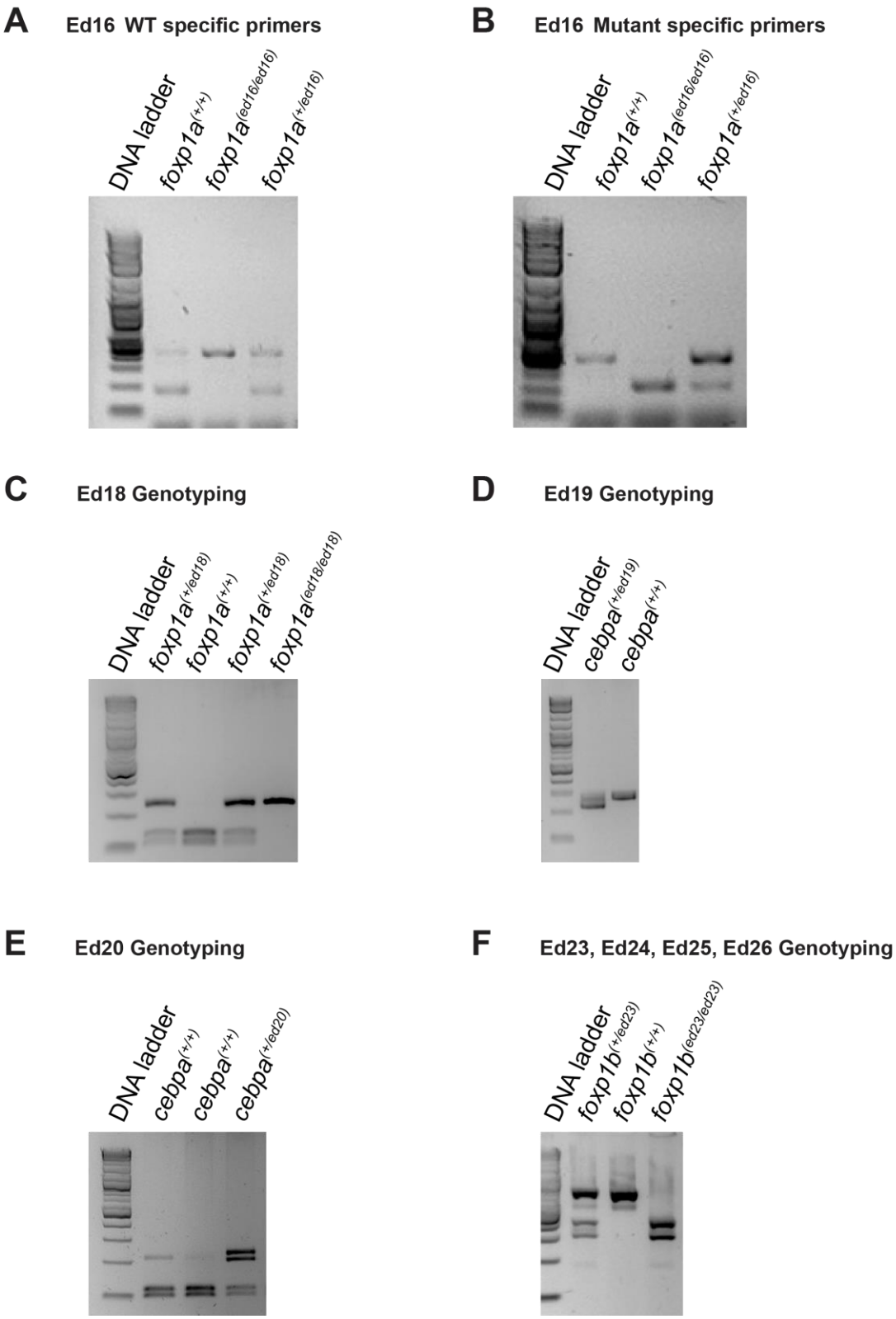

Figure 2.2 – Genotyping stable lines.

Figure 2.2 – Genotyping stable lines. A. Example of banding patterns for *foxp1a*$^{(+/+)}$, *foxp1a*$^{(+/ed16)}$ and *foxp1a*$^{(ed16/ed16)}$ genotypes. **B.** Example of banding patterns for *foxp1a*$^{(+/+)}$, *foxp1a*$^{(+/ed16)}$ and *foxp1a*$^{(ed16/ed16)}$ genotypes. **C.** Example of banding patterns for *foxp1a*$^{(+/+)}$, *foxp1a*$^{(+/ed18)}$ and *foxp1a*$^{(ed18/ed18)}$ genotypes. **D.** Example of banding patterns for *cebpa*$^{(+/+)}$, and *cebpa*$^{(+/ed19)}$ genotypes. **E.** Example of banding patterns for *cebpa*$^{(+/+)}$, and *cebpa*$^{(+/ed20)}$ genotypes. **F.** Example of banding patterns for *foxp1b*$^{(+/+)}$, *foxp1b*$^{(+/ed23)}$ and *foxp1b*$^{(ed23/ed23)}$ genotypes.

High throughput genotyping of *foxp1a*$^{(ed16/ed16)}$ and *foxp1b*$^{(ed25/ed25)}$ fish

Having generated *foxp1a*$^{(ed16/ed16)}$;*foxp1b*$^{(ed25/ed25)}$ double mutants, it became impractical to genotype these fish by PCR and restriction digest. Therefore, KASP genotyping assays were designed. The KASP on demand service was purchased from LGC Biosearch Technologies. Assays were then designed and validated for the genotyping of *foxp1a*$^{(ed16/ed16)}$ and *foxp1b*$^{(ed25/ed25)}$ fish.

gDNA was extracted from fish and added to the following reaction mixture

Table 2.20 – recipe for KASP reaction mix	
Reagent	**Amount (µl)**
KASP master mix (LGC Genomics, KBS-1016-016)	2.5
gDNA	2.5
Primers	0.07

The reaction mixture was placed into a 384 well plate and then placed into a Roche LightCycler 480 machine. The following conditions were used for the ed16 primers.

1- 94°C for 15 minutes
2- 94°C for 20 seconds
3- 61°C for 60 seconds (decreasing by 0.6°C per cycle to achieve a final temperature of 55°C)
4- Repeat steps 2 and 3, 9 times
5- 94°C for 20 seconds
6- 55°C for 60 seconds
7- Repeat steps 5 and 6, 25 times
8- 30°C for 60 seconds

The following conditions were used for the ed25 primers

1- 94°C for 15 minutes
2- 94°C for 20 seconds
3- 68°C for 60 seconds (decreasing by 0.6°C per cycle to achieve a final temperature of 62°C)
4- Repeat steps 2 and 3, 9 times

5- 94°C for 20 seconds
6- 62°C for 60 seconds
7- Repeat steps 5 and 6, 25 times
8- 30°C for 60 seconds

Three recycle steps were then used for each of the genotyping assays. The recycle steps were as follows

1- 94°C for 20 seconds
2- 57°C for 1 minute
3- Repeat steps 1 and 2, twice
4- 37°C for 1 minute

Genotypes were then assigned based on the readout of the Kasp assay. Each sample was assigned to a genotype based on a fluorescent readout.

2.2 - Generation of a transgenic line which labels adipocytes and pre-adipocytes

To generate the transgenic line non-coding elements, identified through DNase Seq during adipogenesis, were used (Siersbaek et al., 2011). Highly conserved non-coding elements (CNEs), which were conserved to zebrafish, were then prioritised by GO term analysis (Hiller et al., 2013). Primers were then designed to the prioritised adipoCNEs and PCR amplified. The PCR products were then cloned into an expression vector and injected into zebrafish embryos at the one cell stage **(Figure 2.3)**. The embryos were screened for GFP expression and GFP positive embryos raised. These fish were then outcrossed to WT fish and offspring with GFP expression in adipose selected for.

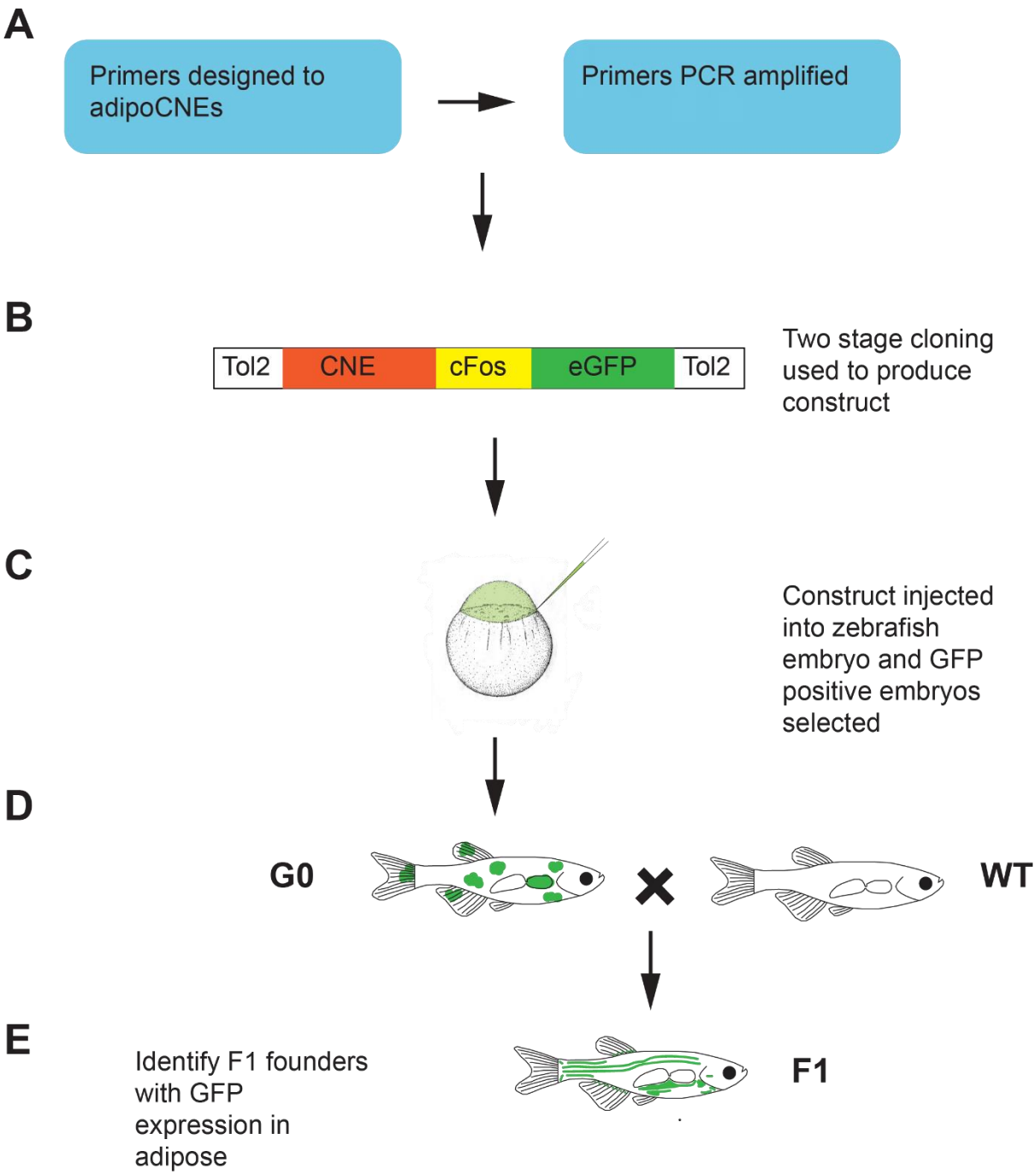

Figure 2.3 – Generation of a transgenic line which labels adipocytes. A. Schematic showing amplification of CNEs. **B.** Schematic of the construct injected. **C.** Injection of transgenic construct. **D.** Outcrossing of G0 fish. Green marks highlight the mosaic expression of GFP in G0 fish. **E.** Identification of F1 founder lines with GFP expression in AT. Green lines show the major adipose depots in zebrafish.

Insertion of adipoCNEs into an expression vector by LR cloning

As described previously PCR primers were designed, and the adipoCNE amplified by PCR. The PCR product was then cleaned and cloned into the pCR8 vector. Cleaned PCR products in the pCR8 vector were cloned into the pGW-cFosEGFP (Fisher et al., 2006) vector **(Figure 2.2B)**. The following reaction mixture was made

Table 2.21 – Recipe for LR cloning	
Regents	**Amount (µl)**
pCR8 vector	0.25
pGW-cFosEGFP	0.25
TE	2
LR clonase (Life Technologies, 11791020)	0.25

The samples were then incubated at 25°C for 3 hours. The samples were cooled to 4°C and 0.4 µl of Proteinase K added. The reaction mixture was then incubated at 37°C for 10 minutes. A heat shock was performed by cooling the samples to 4°C, adding 20 µl of One Shot Top10 chemically competent E.Coli, cooling for another 10 minutes and then heating the samples to 42°C for 45 seconds. This was again cooled to 4°C and 200 µl of LB broth added. The samples were then allowed to recover at 37 °C for 1 hour. 250 µl of the reaction mixture was spread onto agar plates containing ampicillin (Fisher Scientific, 10193433) at 50 µg/ml. Plates were incubated overnight at 37°C.

Colony PCR was then performed, as described previously, to check for insertion of DNA into the vector. Colonies containing the correct insert were then amplified, miniprepped to extract DNA and the DNA cleaned ready for injection.

Injection of transgenic construct

The following reaction mixture was made **(Figure 2.3C)**.

Table 2.22 – recipe for injection mixture	
Reagents	**Amount (µl)**
Tol2 mRNA (50 ng/µl)	1.5
DNA (100 ng/µl)	0.75
Phenol Red	0.75

10 nl of the reaction mixture was injected into WT zebrafish embryos as described previously. GFP positive embryos were selected for and raised. These fish were then outcrossed to WT fish and offspring with GFP expression in AT selected for.

2.3 - Zebrafish protocols

2.3.1 – Zebrafish Husbandry

Raising embryos

Zebrafish embryos were raised in petri dishes containing 50 ml of dilute methylene blue until 5 dpf. Methylene blue was diluted by adding 2 ml of 0.1% methylene blue to 1 litre of water. Any unfertilised or dead embryos were removed from the dish at 24 hpf. The embryos were housed in an incubator at 28.5 °C, on a 14 hour light / 10 hour dark cycle. Embryos were kept at a density of 30 fish per dish.

Maintenance of juvenile and adult fish

At 5 dpf embryos were transferred to a 3 litre tank filled with a small amount of water. Fish were kept at a density of 20 fish per tank. At 21 dpf the tank was filled and connected to flowing water. Fish were maintained at 28.5 °C on a 14 hour light / 10 hour dark cycle.

Feeding

All zebrafish were fed three times a day. Fish were given two dry feeds and one wet feed. Dry feeds were obtained from SDS (Special Diet Services) and Skretting. SDS diets of SDS100, 200 and 300 were given, with increasing number corresponding to increasing fish age. These diets were composed of fish products, cereal grain products and by-products, by-products of oils and fats, vitamins, minerals and antioxidants. Diets are composed of 60% protein and 14.5% lipid. The wet feed was brine shrimp. Fish under the age of 21 dpf were fed paramecia rather than brine shrimp.

2.3.2 - Survival Assay

cepba$^{(+/ed19)}$ and *cebpa*$^{(+/ed20)}$ fish were incrossed and the offspring raised as described above. Every day the fish were counted and dead embryos removed. The

number of fish present each day and the number of dead fish were recorded until 21 dpf.

2.3.3 - Imaging

Nile Red imaging

Nile Red dye (Sigma, 72485) was added to water containing fish at a final concentration of 0.5 µg/ml. The fish were incubated in the dark at room temperature for 30 minutes. Epinephrine (Fisher Scientific, 11926891) was then added to the solution at a final concentration of 5 mg/ml to retract the pigment from the fish. Fish were then lightly anesthetised, and transferred to a petri dish lid containing a 4% methyl cellulose droplet. The fish was then gently positioned and imaged using a stereomicroscope. After imaging the fish were recovered in fresh system water.

Foxp1:eGFP imaging

Deep red Lipid-Tox (Invitrogen, H34350) was added to water containing fish at a 1 in 1000 dilution. The fish were incubated in the dark at room temperature for 1 hour. Epinephrine was then added to the solution at a final concentration of 5 mg/ml to retract the pigment from the fish. The fish were then transferred to a solution of system water and MS-222 at a dilution of 1 in 20 and anesthetised until their gills had stopped moving. The fish was transferred to a petri dish lid containing a 4% methyl cellulose droplet and gently positioned. LSAT was then imaged using a stereomicroscope and the fish recovered.

2.3.4 - High Fat Diet

A high fat diet was set up with fish of around 1 month of age. Fish to be placed on the diet were stained with Nile red, imaged and recovered individually in 12 well dishes. The SL of the fish was then measured and fish separated into two groups with equal average SL. Fish were then randomly paired up and placed as two fish per mesh insert **(Figure 2.4B)**. This allowed pairs of fish to be tracked through the diet.

The mesh inserts were placed into 10 litre tanks fitted with lids which accommodated 4 inserts. The location of the inserts in the tanks was rotated daily to account for any differences in feeding **(Figure 2.4C)**. A random schedule detailing the location of each insert, for the duration of the diet, was drawn up before the diet began.

Fish assigned to the HFD group were immersed in a 5% egg yolk solution (Carten et al., 2011, Semova et al.,2012, Walters et al., 2012) for 2 hours each day for a period of two weeks **(Figure 2.4D)**. Control diet fish were also removed from the 10 litre tanks and placed into fresh water. Both the control diet and high fat diet groups received an additional 2 feeds throughout the day.

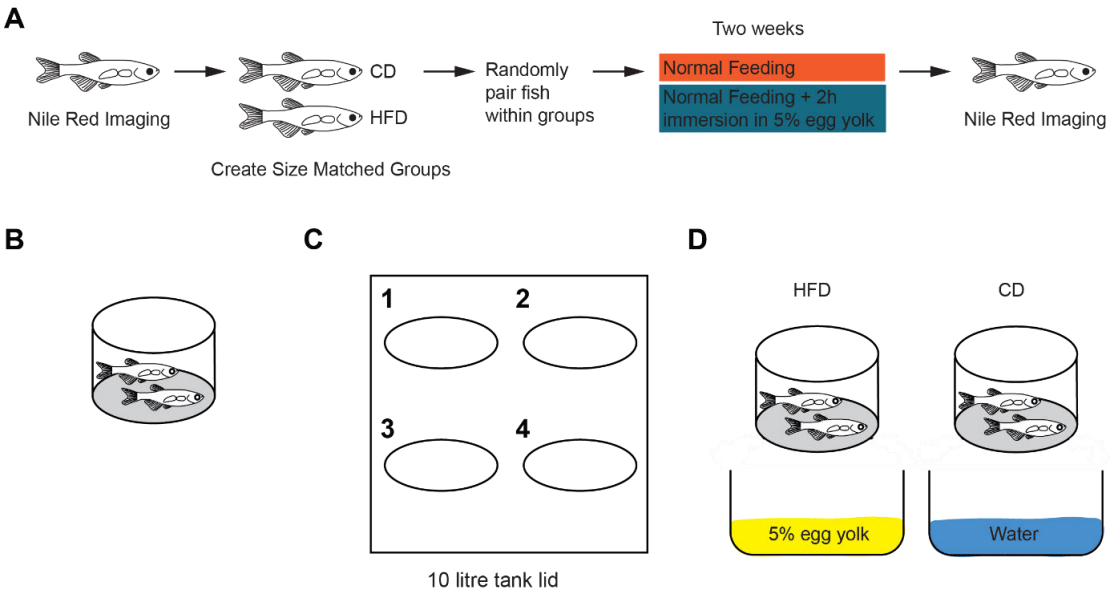

Figure 2.4 – HFD schematic. A. Schematic of the HFD. **B.** Schematic showing the mesh insert fish are housed in for the duration of the experiment. **C.** Schematic showing the lids for 10 litre tanks, into which the mesh inserts are placed. The position of inserts is randomly changed each day to minimise variation due to differences in feeding. **D.** Schematic showing immersion of fish into either HFD or CD.

2.3.5 – Dissections

PVAT dissection

Fish were culled by schedule 1. Briefly fish were killed by an anaesthetic overdose and the heart was then destroyed. Fish were then placed under a microscope with their stomach on the right. An incision was made below the gills, through the transverse plane of the fish **(Figure 2.5A)**. A second incision was then made, perpendicular to the first incision, towards the caudal fin of the fish. The GI tract, and the attached PVAT was then gently removed from the fish. The whole GI tract and PVAT was fixed in 4% PFA overnight at 4°C.

LSAT dissection

Fish were culled by schedule 1. The heads of the fish were then removed, and an incision made down the ventral side of the fish, towards the caudal fin **(Figure 2.5B)**. The GI tract and the caudal fin were also removed. The skin along the flank of the fish was then peeled away and the trunk of the fish fixed in 4% PFA overnight at 4°C

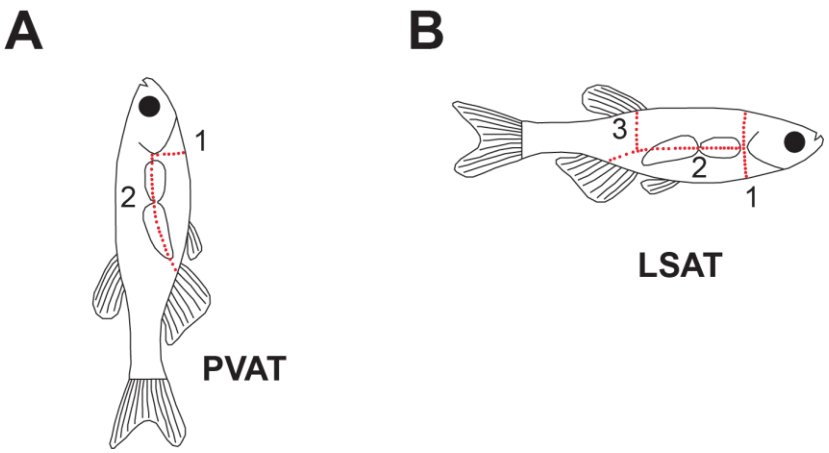

Figure 2.5 – Schematics of PVAT and LSAT dissections. A. Incisions made during PVAT dissections. Red dotted lines show position of incisions. **B.** Incisions made during LSAT dissection. Red dotted lines show position of incisions.

2.3.6 - Blood collection

Fish were fasted overnight and then killed by anaesthetic overdose. Fish were removed from the MS-222 and their gills blotted dry with tissue. The fish was turned onto its back and an incision was made, with dissection scissors, below the gills and through the heart. A pipette was then used to extract blood, and this was stored on dry ice. The blood was centrifuged at 2400 rpm for 10 minutes at 4°C. The top layer of serum was then removed, placed in a fresh tube and stored at -80°C.

2.4 - Molecular biology protocols

2.4.1 - Measuring RNA levels

SVF isolation

PVAT was dissected from multiple adult fish and the dissected tissue was placed in 1 ml of 0.5 mg/ml collagenase solution (Roche, 11088807001). The recipe of the collagenase solution is shown below.

Table 2.23 – Recipe for collagenase solution

Reagent	Volume
Collagenase B	5 mg
Bovine Serum Albumin (Sigma-Aldrich, A3294-50G)	40 mg
Pen/Strep (Life Technologies, 15140148)	20 µl
PBS	10ml

Samples were then incubated at 28.5°C for 1 hour 30 minutes, with agitation. The digested samples were passed through a 0.22 µm filter and the remaining mixture centrifuged at 300g for 5 minutes. The resulting cell pellet was then used for RNA extraction.

RNA isolation for measurement of transcript levels by qPCR

RNA was collected using the RNeasy mini kit (Qiagen 74104). 350 µl of RLT buffer was added to SVF isolated cells and homogenised by pipetting. 350 µl of RLT buffer was also added to PVAT and the tissue homogenised using a micropestle (Eppendorf, 0030120.973). RNA extraction was then carried out as per the instructions of the kit. The optional DNase digestion step was performed (Qiagen, 79254). RNA was eluted into 25 µl of nuclease free water.

cDNA synthesis

cDNA was synthesised using superscript IV reverse transcriptase (Invitrogen, 18090010). All RNA samples to be reverse transcribed were first diluted to the

concentration of the sample with the lowest RNA concentration. The following mixture was made up.

Table 2.24 – Recipe for reverse transcription	
Reagent	**Volume (µl)**
Random Primers (Invitrogen, SO142)	0.5
dNTP (10mM) (NEB, N0447S)	1
Oligo (dT) primers (Invitrogen, AM5730G)	0.5
RNA	10

The mixture was incubated at 65°C for 5 minutes. The mixture was then cooled to 4°C and the following mixture added.

Table 2.25 – Recipe for reverse transcription, part 2	
Reagent	**Volume (µl)**
5X buffer	4
0.1M DTT	2
RNase inhibitor (Promega, N2511)	1

This mixture was then incubated for 2 minutes at 42°C. This was then cooled to 4°C and 2 µl of superscript added. The mixture was heated to 42°C for 60 minutes and then 70°C for 15 minutes. 1 µl of RNase was added and the mixture incubated at 37°C for 20 minutes. cDNA was then diluted to a concentration of 5 ng/µl.

qPCR

qPCR was performed on a Roche LightCycler 480 machine. Luna qPCR master mix (NEB, M3003L) was used to perform qPCR. The following recipe was used.

Table 2.26 - Recipe for qPCR	
Reagent	**Volume (µl)**
Primers	1
Luna	5
cDNA	1
Nuclease free water	3

Reactions were loaded onto a 384 well plate. The qPCR steps were as follows; 95°C for 10 minutes, 45 cycles of 95°C for 15 seconds, 60°C for 30 seconds and 72°C for 30 seconds. Then 95°C for 5 seconds, 65°C for 60 seconds and finally 40°C for 30 seconds.

Table 2.27 - Zebrafish qPCR primers		
Gene Targeted	**Forward Primer**	**Reverse Primer**
Pparg	TGCCGCATACACAAGAAGAG	ATGTGGTTCACGTCACTGGA
Cebpa	ATCAGCGCCTACATTGATCC	TTGCTTGGCTGTCGTCGTAGATG
Cebpa (ed19 and ed20 transcript levels)	ACCCATCTACGACAGCCAAG	GAGTCGCCAAGCTCATCTTC
Bactin	GCCTCCGATCCAGACAGAGT	TGACAGGATGCAGAAGGAGA
foxp1a	GGCCACTTTGAGGATGACTC	CCTCGCCACCTAAAACTCAG
foxp1b	CATTGGCTCCTCTTTTACGC	ACAGCAACGGTAGTGACAGC

2.4.2 - Measuring protein levels

Making protein lysate

The caudal fin rays were removed from juvenile zebrafish and placed on dry ice. 500 µl of RIPA buffer (Thermo, 8990), containing 1x protease inhibitor (Thermo, A32953), was added to a pool of 7 fins. This was then homogenised using a TissueRuptor. The tissue was homogenised by 3, 10 second bursts of the TissueRuptor. The samples were then centrifuged at top speed for 15 minutes, at 4°C. 300 µl of the clean lysate was removed and added to 75 µl of LDS blue (Novex, B0008) and 30 µl of reducing agent (Novex, B0009). This was heated to 95°C for 10 minutes and then centrifuged for 1 minute at 10,000 rpm.

Western blot

500 ml of 1x MOPs (Novex, B0001) buffer was made by diluting 20x stock solution with DI water. The loading buffer was then poured into the gel container. A precast 8% Bis-Tris gel (Invitrogen, NW00082BOX) was placed into the buffer. 25 µl of protein lysate was loaded onto the gel, alongside 8 µl of protein ladder (Thermo Scientific, 26619). The gel was run at 110 V for 45 minutes. The gel was then removed from the casing and a wet transfer performed. The gel, and the membrane it was transferred onto, were soaked in running buffer. The recipe for the running buffer is shown in the table below.

Table 2.28 - Recipe for running buffer	
Reagent	**Volume**
Glycine	15 g
Tris-Base	3.5 g
Methanol	200 ml
DI Water	800 ml

The gel and membrane were soaked in the running buffer, and sandwiched between blotting paper and sponges in the transfer unit. The sponges and filter paper were also soaked in running buffer. The transfer cassette was then placed into the gel tank and filled with the running buffer. The transfer was performed at room temperature, at 20 V for 60 minutes. After this the membrane was removed and placed in a 5% milk solution, consisting of milk powder and 1x TBSTx. TBSTx was made by adding 500 µl of Tween-20 (Biotium, 22002) to 500 ml of 1x TBST. The recipe for TBST can be found in the table below.

Table 2.29 - Recipe 10X TBSTx	
Reagent	**Volume**
Tris-Base	24.4 g
NaCl	87.7 g
DI Water	1 L

The membrane was incubated in the 5% milk solution for 1 hour at room temperature, while rocking. The membrane was then transferred to a 5% milk solution containing FOXP1 antibody (PA5-26848) at a 1 in 1000 dilution and β-actin antibody

(Sigma, A2228) at a 1 in 25,000 dilution. The membrane was incubated in the primary antibody solution overnight at 4°C while rocking. The following day the membrane was washed 4 times in 1X TBSTx. Each wash lasted 15 minutes and all washes were performed while rocking. The membrane was then transferred to a 5% milk solution, containing HRP anti mouse (Invitrogen, 31430) and HRP anti rabbit (Invitrogen, 31460) antibodies to recognise the β-actin and FOXP1 antibodies respectively. The HRP anti mouse antibody was used at a concentration of 1 in 3000, and the HRP anti rabbit antibody at 1 in 5000. The membrane was then incubated for 1 hour at room temperature while rocking. The secondary antibodies were washed from the membrane with 4x 15 minute washes in 1x TBSTx at room temperature while rocking.

Western blot development

Excess TBSTx was tapped off the membrane onto tissue paper. The membrane was then placed into a light cassette. 500 µl of ECL developing solution reagent A (Thermo scientific, 32209) was added to 500 µl of solution B in 1 ml tube and mixed by pipetting. 1 ml of the ECL solution was then pipetted onto the membrane and the cassette closed. The ECL solution was left on the membrane in the dark for 1 minute. The membrane was then removed and placed into a film cassette. Clingfilm was used to cover the membrane and the cassette closed. The cassette was taken to a dark room with a red light. X-ray film was then placed over the membrane and the cassette closed for 20 minutes. The film was passed through an x-ray developing machine.

2.4.3 - Lipid stains

Fixed adipose depots were incubated with Lipid-Tox (Life Technologies, H34477) at a 1 in 300 dilution, overnight at 4°C, protected from light.

2.4.4 - Confocal imaging

Confocal imaging of fixed tissue

Fixed PVAT and LSAT depots were placed in 8 well slides (Ibidi, 80821) and mounted in 1% LMP agarose. All imaging was performed using a Zeiss 710 microscope.

Confocal imaging of euthanised fish

Culled fish were placed in 8 well slides and mounted in 1% LMP agarose, containing MS-222 diluted by 1 in 20. All imaging was performed using a Zeiss 710 microscope.

2.4.5 - Blood assays

Glucose (BioVision, K606-100), triglyceride (BioVision, K622-100) and cholesterol (BioVision, K623-100) assays were performed as per the manufacturers instructions. 1 µl of blood was used to perform the glucose and cholesterol assays and 0.2 µl used for the triglyceride assays. The fluorometric assays were used for the glucose and triglyceride measurements and the colorimetric assay used for the cholesterol measurements.

2.5 - Image analysis

2.5.1 - Nile Red image analysis

Total adipose area measurements

Image J was used to analyse all images. The threshold tool was used to mark the total fluorescence area and the image converted to a binary image. The total marked area was then measured.

VAT and SAT measurements

Image J was used to analyse all the images. Individual adipose depots were drawn around and their area measured.

2.5.2 - Adipose morphology measurements

Image J was used to analyse the stacks generated. The line tool was used to measure each lipid droplet at its widest point, and this gave a measure of the lipid droplet diameter. The line tool was also use to draw across each lipid droplet as a mark of which lipid droplets had been measured.

2.5.3 - *Foxp1:eGFP* time course image analysis

Image Processing

Images taken on the stereomicroscope were broken out into green, magenta and composite images and saved as TIF files. For each fish, images from the same location within SAT but in different focal planes were then stacked into one image using Zerene Stacker software. Image J was then used to stitch adjacent images together. Stitching was performed using the pairwise stitching tool (Preibisch et al., 2009). Images which couldn't be stitched in Image J were manually aligned in Photoshop and the autoblend tool used to merge the two images. This produced one image of the entire SAT depot of each fish imaged.

Image analysis

Image J was used to analyse the images generated. Progenitor cells were defined as GFP positive, lipid negative cells. Adipocytes were defined as GFP positive cells with a single lipid droplet. Each GFP positive cell was numbered and tracked throughout the time-course imaging. The number of progenitor cells and adipocytes were recorded. The area of each lipid droplet was also recorded. The number of branching events per LSAT was measured and branching events were defined as a chain of 3 or more adipocytes which branch away from the main line of the LSAT at a roughly 45° angle. Finally, the location of new cells within LSAT was measured. Dorsal and ventral cells were defined as cells separated by more than 2 adipocytes vertically from the main horizontal line of LSAT.

2.5.4 - Liver area image analysis

Image J was used to analyse the images. Each liver was drawn around and the area measured.

Chapter 3 – *foxp1* regulates adiposity levels in zebrafish

3.1 - Introduction

Obesity is a global health problem (WHO). The World Health Organisation has estimated that 13% of the adult population worldwide were obese in 2016 and that globally more people are now obese than underweight (WHO). Obesity is characterised by excess adipose tissue accumulation and is defined clinically by a Body Mass Index (BMI) of over 30 kg/m^2 (WHO). The classification of obesity as a health problem is due to the increased disease risk it confers, with obesity being linked to an increased risk of cardiovascular disease and diabetes (Martin et al., 2015). However, the mechanisms through which increased levels of adipose tissue (AT) lead to an increased risk of disease are not yet fully understood.

Multiple theories exist to explain why obesity is associated with increased disease risk. One of these theories is the adipose expandability hypothesis (Virtue and Vidal-Puig, 2008). The adipose expandability hypothesis states that adipose tissue has a limited capacity to expand and that when this is reached, for example during obesity, the adipose tissue becomes dysfunctional (Virtue and Vidal-Puig, 2008). Adipose tissue expands via hyperplastic growth, an increase in adipocyte cell number, and hypertrophic growth, an increase in adipocyte cell size (Spiegelman and Flier, 1996). Dysfunctional adipose tissue is associated with hypertrophic growth and increased adipocyte cell size (Crewe et al., 2017). It is further characterised by hypoxia, cellular senescence and necrotic adipocyte death (Crewe et al., 2017). Dysfunctional adipose tissue also loses its ability to store lipid, which results in ectopic deposition of lipid in the liver and insulin resistance (Lafontan, 2014). Therefore, a better understanding of how adipose tissue function can be maintained during obesity could lead to the development of treatments to alleviate obesity associated disease.

Obesity and body weight are known to be partly genetically regulated (Maes et al., 1997). For example, data from monozygotic twin studies have estimated the heritability of BMI to be between 50-90% (Maes et al., 1997). In some cases, the causes of obesity can be attributed to the large effect of a single monogenic mutation (Khera et al., 2019). However, in the vast majority of cases the genetic causes of obesity are thought to result from the cumulative effect of many genes, with each gene having a modest effect (Khera et al., 2019). Therefore, although some genes which confer a large effect on body weight have been identified, the genetic regulation of body weight is still poorly understood. Consequently, the overall goal of this project is

to identify genetic factors which influence adipose levels, and to understand the molecular mechanisms by which they exert this influence.

Genome wide association studies (GWAS) have been used to identify novel genetic factors underpinning obesity and body weight. GWAS studies take large human populations and look for SNPs (Single Nucleotide Polymorphisms) which appear more frequently in one condition than another (Visscher et al., 2012). For example, a GWAS study may look for SNPs which occur more frequently in obese subjects than in lean subjects (Speakman et al., 2018). A recent GWAS found that variation at the *FOXP1* locus (encoding Forkhead Box P1) was associated with BMI (Kichaev et al., 2019). A second GWAS study identified variation at eight novel loci associated with anorexia nervosa, characterised by decreased body fat levels, including variation at the *FOXP1* locus (Watson et al., 2019). Finally, a GWAS study in 2012 found that variation at the *FOXP1* locus was associated with levels of subcutaneous adipose tissue (SAT) (Fox et al., 2012). Aditionally, that *FOXP1* mRNA levels in SAT have been shown to be positively associated with BMI, insulin levels, an increased blood triglycerides (Civelek et al., 2017). Altogether, multiple GWAS studies have implicated *FOXP1* in the regulation of body weight and increased *FOXP1* expression levels in SAT are associated with increased body weight and adverse metabolic outcomes.

The data described above suggest that *FOXP1* may play a role in regulating body weight, adiposity levels and metabolic health; however, the role of *FOXP1* in adipose tissue is largely unknown. *FOXP1* or Forkhead box P1 is a transcription factor and is part of the Fox family of proteins, which contain a winged helix DNA binding domain (Hannenhalli and Kaestner, 2009). *FOXP1* is expressed in multiple tissues, including adipose tissue (Fagerberg et al., 2014). Data from GTex (Genotype-Tissue expression portal), which catalogues the results of RNA-Seq experiments in human tissues, has shown that *FOXP1* mRNA is more abundant in human subcutaneous adipose tissue than in visceral (Fagerberg et al., 2014). This is also true in mice, with microarray data from adipocytes showing that *Foxp1* mRNA is more highly expressed in SAT (Gesta et al., 2006). In addition to expression data, there is also data available relating to the function of *Foxp1* in adipose tissue (Liu et al., 2019). A recent study found that mutant mice, which lack *Foxp1* expression in adipose tissue, have slightly reduced levels of white AT on a control diet and gain less white AT in response to a high fat diet (Liu et al., 2019). However, the study primarily focused on the role of

Foxp1 in thermogenic brown and beige AT and the role of *Foxp1* within white AT was largely unaddressed (Liu et al., 2019). Therefore, *Foxp1* is known to influence adipose tissue levels, however the mechanism by which it does this is unknown.

One known function of *Foxp1* is to promote the renewal of stem and progenitor cells (Gabut et al., 2011, Li et al., 2017). For example, *Foxp1* is known to stimulate the expression of genes required for pluripotency and to repress the expression of genes required for the differentiation of embryonic stem cells (Gabut et al., 2011). Furthermore, *Foxp1* has been shown to be essential for the proliferation and self-renewal of mesenchymal stem cells (Li et al., 2017). Overall, this suggests that *Foxp1* may regulate adiposity levels by influencing adipose progenitor cell proliferation and differentiation. My hypothesis is therefore that *Foxp1* maintains progenitor cell populations in adipose tissue and is required for adipose tissue expansion.

In this chapter I use zebrafish as a model to investigate the hypothesis that *foxp1* maintains adipose progenitor cell number and is required for adipose tissue expansion. To address this hypothesis, I have generated novel *foxp1* zebrafish mutants using CRISPR mutagenesis. I have then used these mutants to test my hypothesis by measuring adipose levels in response to both a control and high fat diet (HFD). I found that *foxp1* mutant fish showed reduced AT expansion in response to a HFD and that mutants had a more hypertrophic AT morphology, characterised by fewer but larger lipid droplets. Overall, I have found novel experimental evidence that *foxp1* is required for AT expansion. This is the first data to suggest that *foxp1* has an *in vivo* role in AT expansion and suggests that *foxp1* may be a therapeutic target for controlling body weight and associated disease.

3.2 - Results

3.2.1 - *foxp1* is duplicated in zebrafish, with the *foxp1b* gene showing the highest level of conservation of mammalian *Foxp1*

In order to investigate if *foxp1* influences adiposity levels, I have chosen to use zebrafish as a model system. It is well known that many genes in zebrafish and other teleost fish have undergone a gene duplication and to check whether this was the case for *foxp1* I made use of the Gene-tree function on Ensembl (ENSGT00900000140822) (Wafer et al., 2017). Briefly, gene tree shows the maximum likelihood phylogenetic tree for a given gene and represents the evolutionary history of that gene (TreeBeST). Using gene tree, I was able to trace the human ortholog of *FOXP1* to determine which gene or genes are present in zebrafish. Zebrafish have two orthologs of *FOXP1, foxp1a* and *foxp1b* **(Figure 3.1)**. I then wished to determine which zebrafish *foxp1* paralog is most closely related to mammalian *Foxp1*. To do this I compared the sequences of human, mouse and *Xenopus Foxp1* to that of the zebrafish *foxp1a* and *foxp1b* **(Figure 3.1A & B)**. I made use of Clustal Omega sequence alignment software to compare the cDNA and protein sequences from the previously mentioned species and found that *foxp1b* shows greater sequence homology to mammalian orthologs than *foxp1a* **(Figure 3.1B & C)**. Foxp1a was found to show 62.05% amino acid conservation to human FOXP1, while Foxp1b showed a greater level of conservation at 77.59% **(Figure 3.1C)**. The greater level of conservation in *foxp1b* suggests that this gene has been under greater selective pressure than *foxp1a* and implies that *foxp1b* may be more likely to have retained the ancestral function of *Foxp1*.

3.2.2 - The functional domains of zebrafish Foxp1 proteins are highly conserved to mammalian FOXP1

At a whole gene level, both Foxp1a and Foxp1b show only moderate levels of conservation to human FOXP1. Therefore, I also wanted to determine how well the functional domains of FOXP1 were conserved between zebrafish and mammals. *foxp1* is named for the presence of a forkhead DNA binding domain (FHD) and as a transcription factor one of its main roles is to bind DNA (Hannenhalli and Kaestner, 2009). In addition to it's DNA binding domain, FOXP1 also contains a zinc finger

domain which mediates protein-protein interactions and is thought to be important in the dimerization of FOXP1 (Li et al., 2004). I therefore wished to determine to what extent the forkhead and zinc finger domains (ZFD) of FOXP1 are conserved to zebrafish. Using the protein summary feature on Ensembl (ENSDARP00000107924.2 & ENSDARP00000064937.3), and the Pfam and Smart databases (El-Gebali et al., 2019, Letunic and Bork, 2018), I was able to confirm that both *foxp1a* and *foxp1b* contained both a forkhead DNA binding domain and a zinc finger protein-protein interaction domain **(Figure 3.1C & D)**. With this information, and information on the mouse sequences of the FHD and ZFD, I was able to identify the protein sequences of the functional domains in *foxp1a* and *foxp1b* (Li et al., 2004, Stroud et al., 2006). By comparing these sequences to that of their human ortholog, I found that the protein sequences of the Foxp1a and Foxp1b FHD and ZFD are well conserved. The Foxp1a FHD shows 95.4% similarity to the human FOXP1 FHD and the Foxp1b FHD shows 98.85% similarity **(Figure 3.1E)**. The Foxp1a ZFD shows 87.50% similarity and the Foxp1b ZFD shows 91.67% similarity to the human FOXP1 ZFD sequence **(Figure 3.1E)**. The protein alignments of the ZFD and the FHD can be found in the appendix **(Figure 7.1A & B)**. In summary both Foxp1a and Foxp1b show high levels of conservation in functional protein domains and Foxp1b appears to be more conserved than Foxp1a.

A

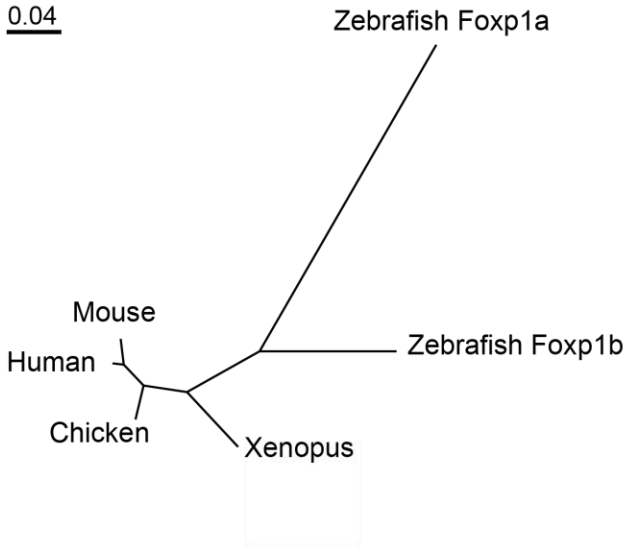

B

cDNA sequence	Zebrafish *foxp1a* (202)	Zebrafish *foxp1b* (202)
Zebrafish *foxp1a* (202)	100%	59.28%
Zebrafish *foxp1b* (202)	59.28%	100%
Xenopus foxp1 (201)	55.57%	68.34%
Mouse *Foxp1* (204)	57.37%	53.67%
Human *FOXP1* (202)	57.17%	54.51%

C

Protein sequence	Zebrafish Foxp1a (202)	Zebrafish Foxp1b (202)
Zebrafish Foxp1a (202)	100%	63.46%
Zebrafish Foxp1b (202)	63.46%	100%
Xenopus Foxp1 (201)	57.27%	70.28%
Mouse FOXP1 (204)	61.20%	76.79%
Human FOXP1 (202)	62.05%	77.59%

D

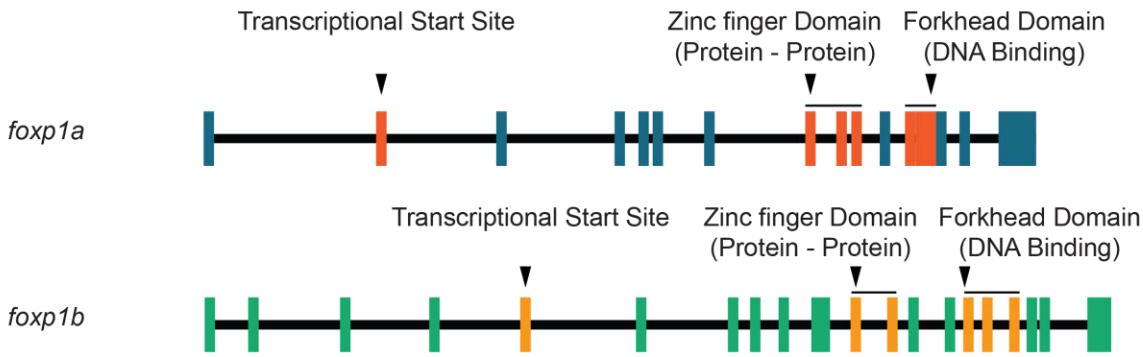

E

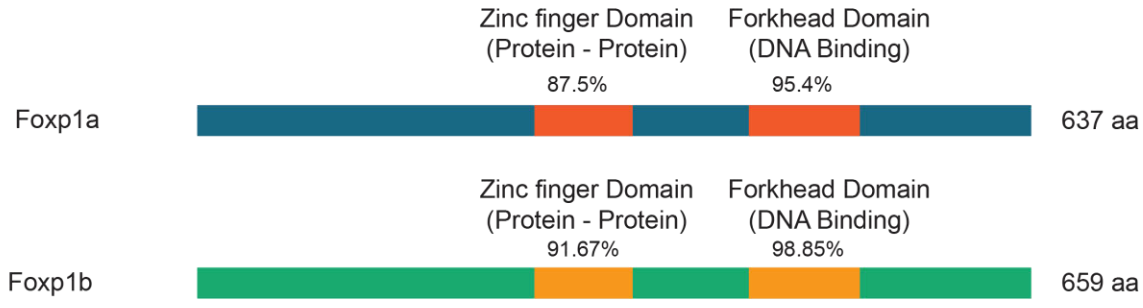

Figure 3.1 – The *foxp1* gene is duplicated in zebrafish, with the foxp1b gene showing the highest level of conservation to mammalian *Foxp1*.

Figure 3.1 – The *foxp1* gene is duplicated in zebrafish, with the foxp1b gene showing the highest level of conservation to mammalian *Foxp1*. A. Unrooted phylogenetic tree showing conservation between amino acid sequences. Amino acid sequences were aligned using Clustal Omega. Unrooted was used to generate the tree (Pole Bioinformatique Lyonnais). Scale bar shows amino acid changes per site. **B.** Comparison of *Foxp1* isoforms homologous to the human isoform 202. Numbers correspond to isoforms as identified on Ensembl. Sequences were aligned using Clustal Omega. **C.** Comparison of FOXP1 protein sequences homologous to the human isoform 202. Numbers correspond to isoforms as identified on Ensemble. Sequences were aligned using Clustal Omega. **D.** Schematic of *foxp1a* and *foxp1b* transcripts. Orange marks functional domains. **E.** Schematic of Foxp1a and Foxp1b proteins. Both proteins contain a zinc finger domain (Pfam) and a forkhead DNA binding domain (El-Gebali et al.). Domains shown in orange. Percentages show conservation between the sequence of the zebrafish and human functional domains. Amino acid length of proteins is shown.

3.2.3 - *foxp1* is expressed in adipose tissue in zebrafish

I next wanted to determine whether *foxp1* is expressed in zebrafish adipose tissue. In mammals *FOXP1* is known to be expressed in AT, however it is not known if *foxp1a* or *foxp1b* are expressed in zebrafish AT (Fagerberg et al., 2014, Gerin et al., 2009). To examine whether *foxp1* is expressed in zebrafish AT, RNA was extracted from pancreatic visceral adipose tissue (PVAT) and *foxp1* transcript levels measured by RT-qPCR **(Figure 3.2A & B)**. I found that both *foxp1a* and *foxp1b* were expressed in PVAT, as were the known regulators of adipogenesis *pparg* and *cebpa* **(Figure 3.2B)**. *foxp1a* was found to be more highly expressed than *foxp1b* and both were expressed to a lesser extent than *pparg* or *cebpa* **(Figure 3.2B)**. *cepba* was expressed more highly than any other gene tested **(Figure 3.2B)**. Together this demonstrates that both *foxp1a* and *foxp1b* are expressed in AT in zebrafish.

3.2.4 - *foxp1* is expressed in the SVF in zebrafish

To test whether *foxp1a* and *foxp1b* are expressed exclusively in adipocytes, I next measured mRNA levels in the stromal vascular fraction (SVF). To do this I dissected PVAT from wild type (Cawthorn et al.) fish and digested the tissue using collagenase **(Figure 3.2A)**. The adipocytes were then separated from the other cell types in AT by centrifuging the digested tissue **(Figure 3.2A)**. The adipocytes were discarded, leaving behind the SVF **(Figure 3.2A)**. The SVF consists of multiple cell types including adipocyte progenitor cells, vascular cells, haematopoietic cells and fibroblasts **(Figure 3.2A)**. RNA was extracted from the SVF and mRNA levels measured by RT-qPCR **(Figure 3.2A)**. Both *foxp1a* and *foxp1b* were found to be expressed in the SVF **(Figure 3.2C)**. The dynamics of expression in the SVF were very similar to that of the whole PVAT, with *cebpa* again being the most highly expressed **(Figure 3.2B & C)**. *pparg* showed the lowest expression in the SVF and had very similar levels of expression to both *foxp1a* and *foxp1b* **(Figure 3.2C)**. Together these data show that the expression of *foxp1* in the adipose depot is not due to expression of *foxp1* exclusively in adipocytes and demonstrates that *foxp1* is expressed in cells of the SVF.

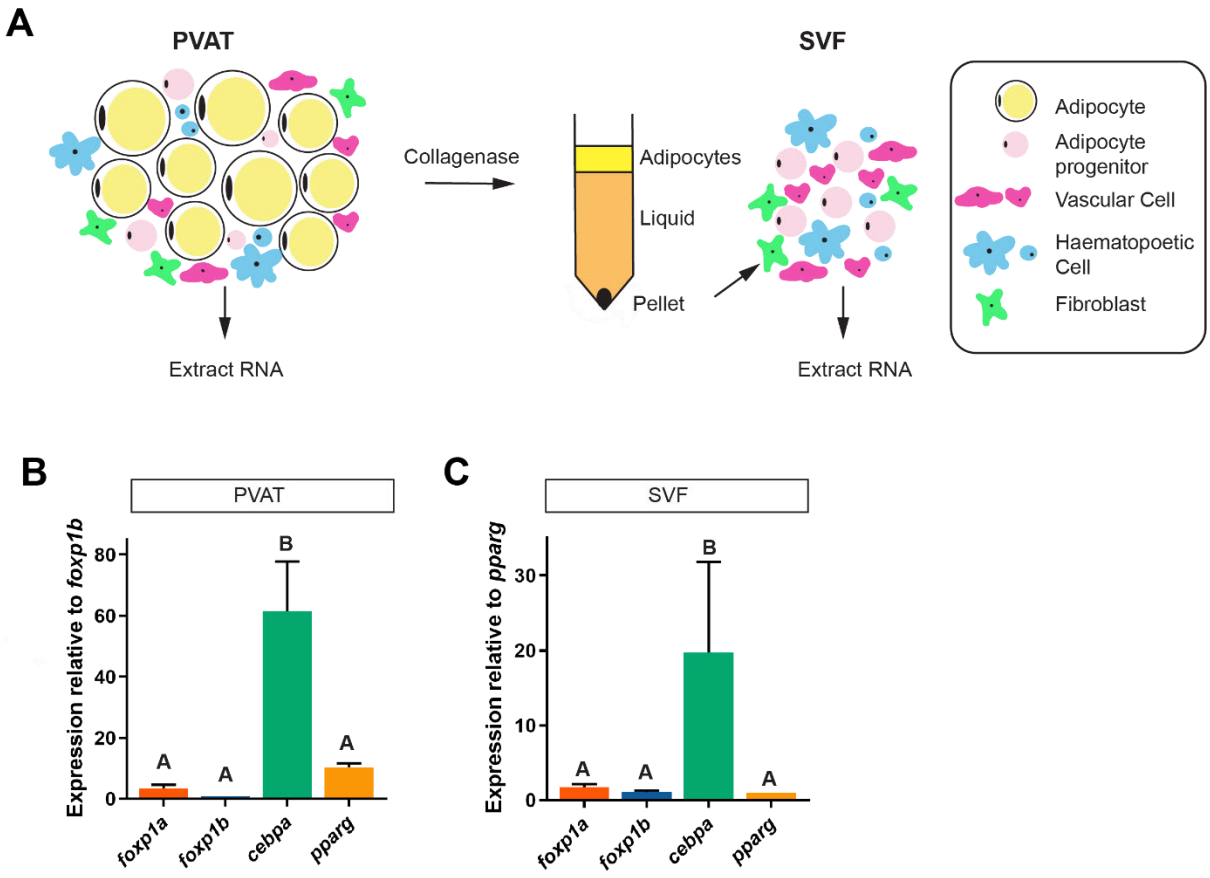

Figure 3.2 – *foxp1a* and *foxp1b* are expressed in the adipose tissue compartment and in the stromal vascular fraction. A. Schematic showing which cell types RNA was extracted from. **B.** n = 2-3. Error bars show standard deviation. A one-way ANOVA was performed, $F_{3,6}$ = 39.71 p = 0.0002. Letters indicate differences between groups, different letters indicate significant differences between groups and the same letters indicate no difference. **C.** n = 3. Error bars show standard deviation. A one-way ANOVA was performed, $F_{3,8}$ = 6.972 p = 0.0127. Letters indicate differences between groups, different letters indicate significant differences between groups and the same letters indicate no difference.

3.2.5 - CRISPR/Cas9 was used to generate zebrafish with heritable mutations in *foxp1a* and *foxp1b*

To test the role of *foxp1* in adipose tissue expansion, I next generated loss of function *foxp1a* and *foxp1b* alleles. To achieve this, I made use of the CRISPR/Cas9 system. CRISPR/Cas9 is a system which has been adapted from bacteria and allows site specific double stranded DNA breaks to be created through the use of a Cas9 enzyme (Hwang et al., 2013). I first designed a series of guide RNAs (gRNAs) targeting the different functional domains of *foxp1a* and *foxp1b* **(Figure 3.3A)**. I targeted close to the translational start site to try and disrupt as much protein function as possible, the zinc finger domain was targeted to stop the proteins from dimerising and the forkhead domain was targeted to prevent DNA binding **(Figure 3.3A)**. The gRNAs were then synthesised and injected into WT zebrafish embryos at the one cell stage, along with the Cas9 nuclease protein **(Figure 3.3A).** The mutagenic activity of each of the guides was then assessed using a T7 endonuclease 1 (T7E1) assay **(Stage 1 Figure 3.3A & Figure 3.4A)**. gRNAs which produced a different banding pattern to that of uninjected fish were deemed to be active and inducing mutations **(Stage 1 - Figure 3.4A)**. The active gRNAs were then reinjected into WT embryos, in order to generate stable lines **(Stage 1 - Figure 3.3A)**. These embryos were raised until adulthood and became the G0 generation **(Stage 2 - Figure 3.3A & B)**. In order to generate stable mutant lines, G0 fish with germline mutations were identified. Adult G0 fish were outcrossed to WT fish and their progeny screened by T7E1 assay for lesions at the CRISPR target locus **(Stage 2 - Figure 3.3B & Figure 3.4B)**. G0 fish found to have germline mutations were again crossed to WT fish and their offspring raised to adulthood, to generate F1 fish with germline *foxp1* mutations **(Figure 3.3B)**. In summary this strategy generated a F1 generation of fish with heritable mutations in either *foxp1a* or *foxp1b*.

3.2.6 - The nature of the mutations generated by CRISPR/Cas9 were identified and mutations predicted to have a severe effect on protein function were selected

The CRISPR/Cas9 system does not induce mutations in all F1 fish and the effect of the mutations induced is also not likely to be the same. To determine if a mutation had occurred and the nature of the mutation, DNA from F1 fish was sent for

sequencing **(Stage 3 - Figure 3.3C)**. Tissue from the caudal fin of adult F1 fish was taken and gDNA extracted **(Stage 3 - Figure 3.3C)**. This gDNA was then sent for sequencing. Predicted frameshift mutations in all domains were selected for, as these were predicted to severely disrupt protein function **(Stage 3 – Figure 3.3C)**. In frame mutations at the ZFD and FHD were also selected for, as these were predicted to disrupt the function of individual domains without affecting overall protein function. The selected F1 mutants were then outcrossed to WT fish **(Figure 3.3D)**. This then produced a breeding stock, 50% of which were WT and 50% of which were heterozygous for a known mutation **(Figure 3.D)**. Overall I was able to generate a series of mutant alleles (described in the next section) which were predicted to have a severe effect on the function of Foxp1a or Foxp1b.

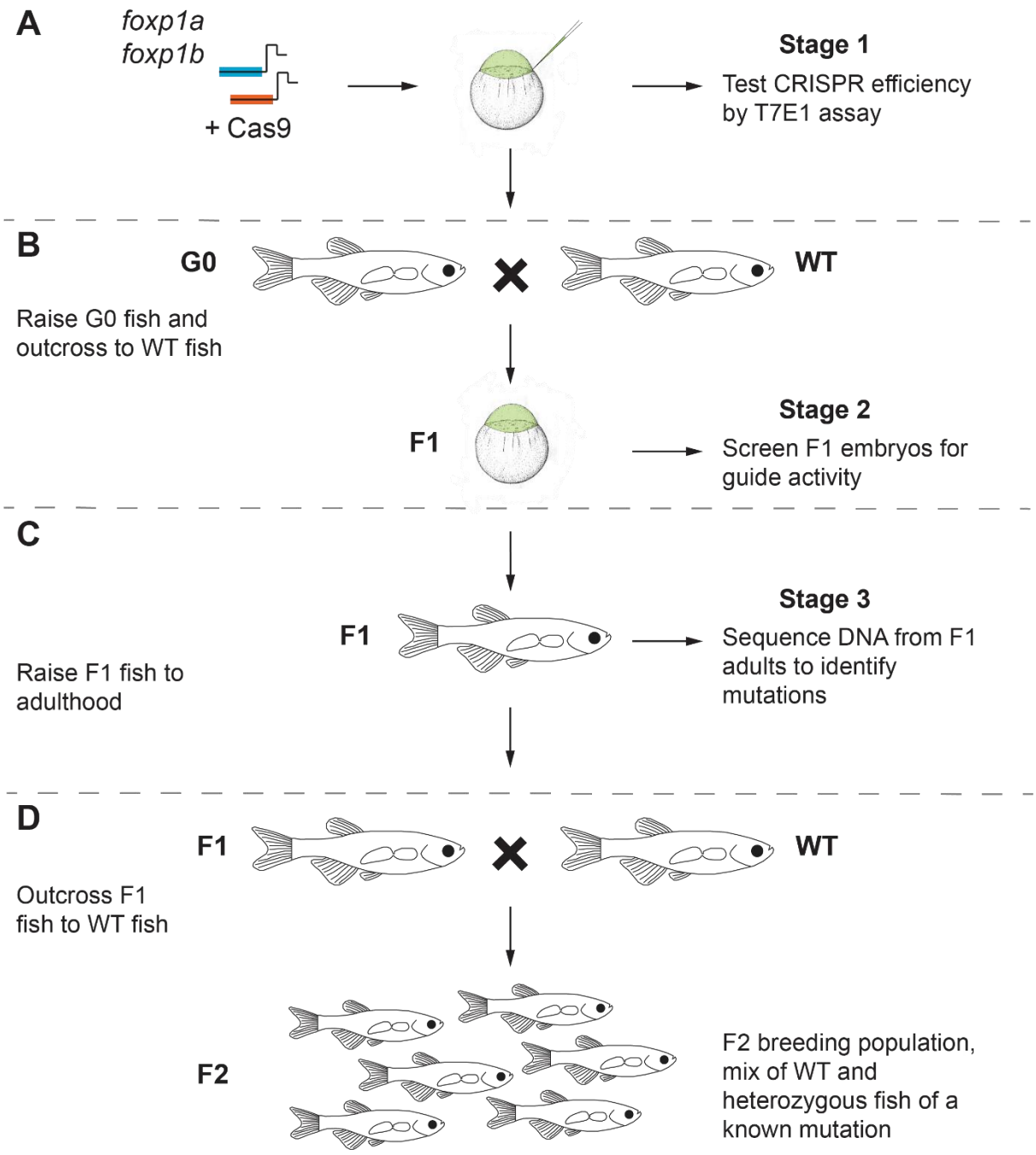

Figure 3.3 – Injection of CRISPR guides targeting *foxp1* leads to mutations in *foxp1a* and *foxp1b*. Schematic showing strategy for creating stable mutants. **A.** Schematic showing generation of guide RNAs, injection into zebrafish embryos and testing of CRISPR efficiency. **B.** Schematic showing the outcrossing of GO fish and the testing of CRISPR guide efficiency in F1 embryos. **C.** Schematic showing the identification of mutations in F1 adults. **D.** Schematic showing outcrossing of F1 fish to create an F2 breeding stock.

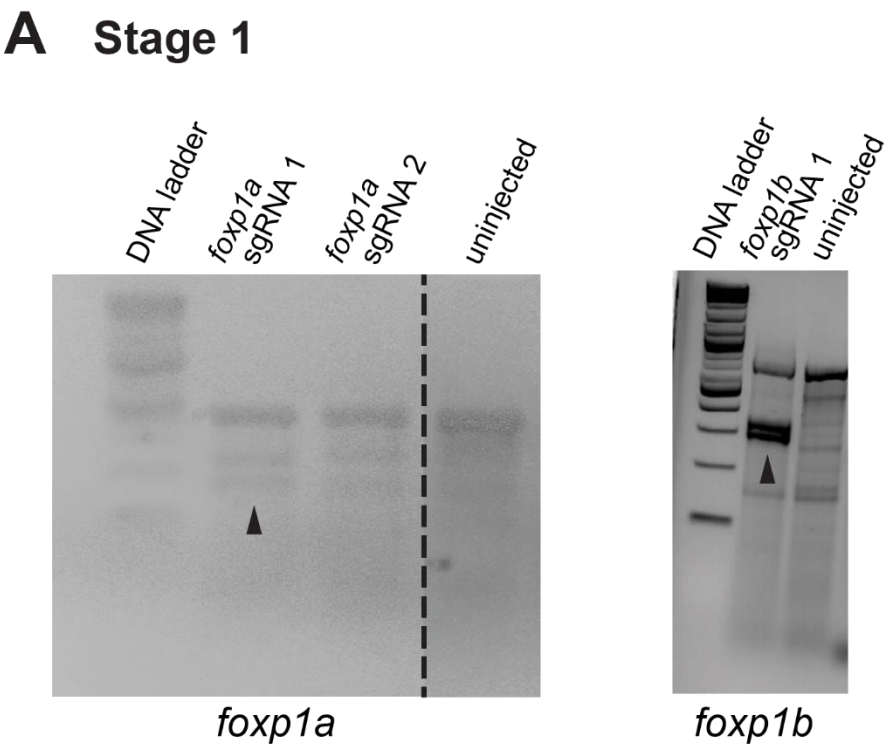

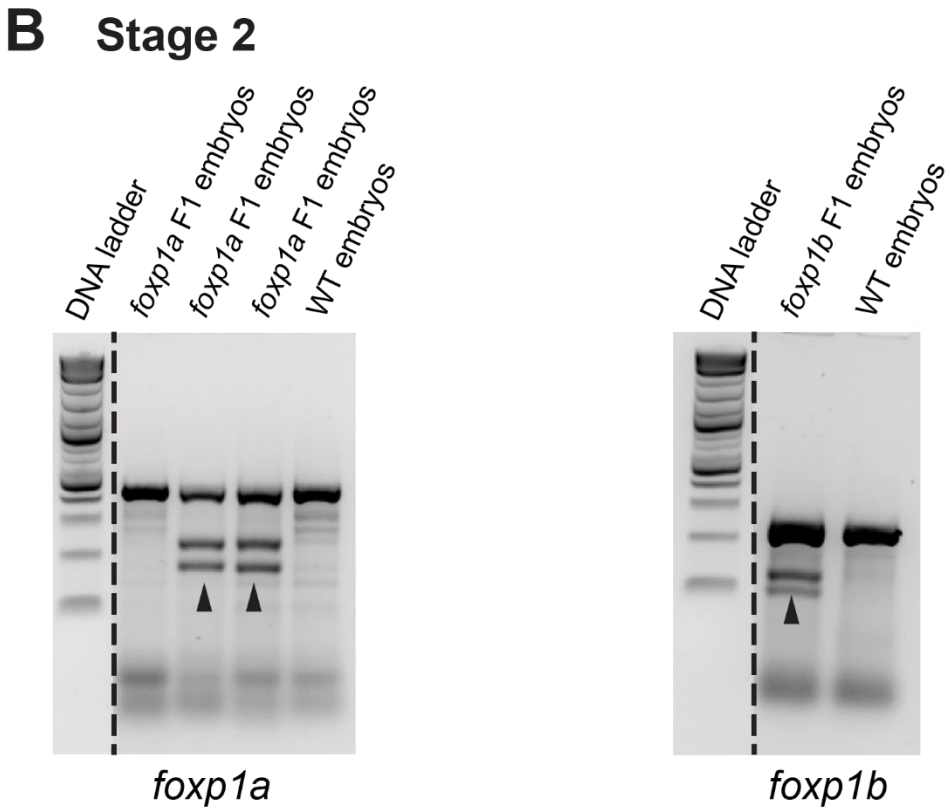

Figure 3.4 – CRISPR/Cas9 induces mutations at the *foxp1a* and *foxp1b* loci.

Figure 3.4 – CRISPR/Cas9 induces mutations at the *foxp1a* and *foxp1b* loci. A. T7E1 assay gels used to test CRISPR guide efficiency. See stage 1 of Figure 3.3. Guides are cutting if the banding pattern in the injected lane is different to that of the uninjected lane. Arrowheads highlight changes in the banding patterns in the injected fish. Pools of 10 embryos were tested. The dotted line indicates that some lanes of the gel have been removed. The complete gel image can be found in the appendix. **B.** T7E1 assay gels used to test CRISPR activity in F1 embryos. See stage 2 of Figure 3.3. Guides are cutting if the banding pattern in the injected lane is different to that of the uninjected lane. Arrowheads highlight changes in the banding patterns in the injected fish. Pools of 10 embryos were tested. The dotted line indicates that some lanes of the gel have been removed. The complete gel image can be found in the appendix **(Figure 7.1)**.

3.2.7 - A series of nine mutant alleles, predicted to have severe effects on Foxp1 protein function, were generated using CRISPR/Cas9

Using CRISPR/Cas9 and the strategy outlined above, I was able to generate nine *foxp1* mutant alleles. I generated one frameshift mutation close to the transcriptional start site of *foxp1a*, which is predicted to introduce an early stop codon and cause the protein to be non-functional **(Figure 3.5A & B)**. I also generated a frameshift mutation at the ZFD of *foxp1a* and this again is predicted to introduce an early stop codon and result in a non-functional protein **(Figure 3.5A & C)**. An inframe mutation targeting the ZFD of *foxp1a* was also selected and this mutant protein is predicted to be unable to dimerise but able to bind DNA **(Figure 3.5A & C)**. The final *foxp1a* mutant alleles generated are two frameshift mutations targeting the FHD and both are predicted to be loss of function mutations due to the lack of a DNA binding domain **(Figure 3.5A & D)**. In addition to the *foxp1a* mutants, I generated 4 *foxp1b* mutants **(Figure 3.5E & F)**. Three of the *foxp1b* mutant alleles are the result of frameshifts at the FHD and one is the result of an inframe mutation at the FHD **(Figure 3.5E & F)**. All of the *foxp1b* mutants are predicted to be unable to bind DNA. In summary, using CRISPR/Cas9 I effectively induced mutations in both *foxp1a* and *foxp1b* and generated a series of novel zebrafish mutants.

3.2.8 - Mutations targeting the forkhead domain of *foxp1a* and *foxp1b* show high levels of transcript degradation

Having generated a series of *foxp1a* and *foxp1b* mutant alleles, I next wanted to identify the alleles most likely to have the strongest loss of function. It was hypothesised that the alleles with the greatest levels of transcript degradation would also show the greatest levels of protein reduction and therefore the most severe phenotypes. I therefore assessed the alleles generated for transcript degradation. From the sequencing of F1 fish I was able to identify alleles which resulted in a predicted frameshift across all the functional domains of *foxp1a* **(Figure 3.5A, B, C & D)**. I was also able to identify an inframe mutation and frameshift mutations at the forkhead domain of *foxp1b* **(Figure 3.5E & F)**. Of the nine alleles identified, I was able to use PCR and restriction digests to genotype seven alleles. The remaining two alleles, *foxp1a*$^{(ed14/ed14)}$ and *foxp1a*$^{(ed15/ed15)}$, were unable to be genotyped due to the repetitive nature of the sequences surrounding the mutations **(Figure 3.5B & D)**. For

the alleles I was able to genotype, I extracted RNA from pools of WT and mutant embryos at 5 dpf. Levels of *foxp1a* and *foxp1b* transcripts were then measured by RT-qPCR and the fold change calculated **(Figure 3.5G)**. High levels of transcript degradation were observed for all frameshift alleles, with *foxp1a*$^{(ed18/ed18)}$ showing the highest levels with a 38.6 fold reduction in *foxp1a* mRNA. **(Figure 3.5C & G)**. The only allele not to show high levels of transcript degradation was the *foxp1b*$^{(ed26/ed26)}$ allele, which does not result in a frameshift and shows only a 1.3 fold reduction in *foxp1b* mRNA levels **(Figure 3.5F & G)**. In summary 5 out of the 6 alleles tested showed high levels of transcript degradation.

3.2.9 - Alleles targeting the forkhead domain of *foxp1a* and *foxp1b* were selected for further functional studies

Of the nine mutant alleles generated, I chose to use FHD mutants to test my hypothesis. I chose these mutants as they were predicted to disrupt the ability of Foxp1a and Foxp1b to bind DNA, which is the central function of Foxp1. I chose the *foxp1a*$^{(ed16/ed16)}$ allele, as it showed high levels of transcript degradation with a 3.3 fold reduction, and the *foxp1b*$^{(ed25/ed25)}$ allele, which showed similar levels of transcript degradation with a 2.8 fold reduction **(Figure 3.5G)**. For the remainder of this thesis, I will focus on these two alleles to test the role of *foxp1a* and *foxp1b* in AT expansion. For simplicity these alleles will now be referred to as *foxp1a*$^{(-/-)}$ and *foxp1b*$^{(-/-)}$. I have used both of these alleles individually to test my hypothesis and I have also generated *foxp1a*$^{(-/-)}$;*foxp1b*$^{(-/-)}$ double mutants to help test my hypothesis. Overall, I chose to make use of the *foxp1a* and *foxp1b* alleles which target the FHD and show high levels of transcript degradation.

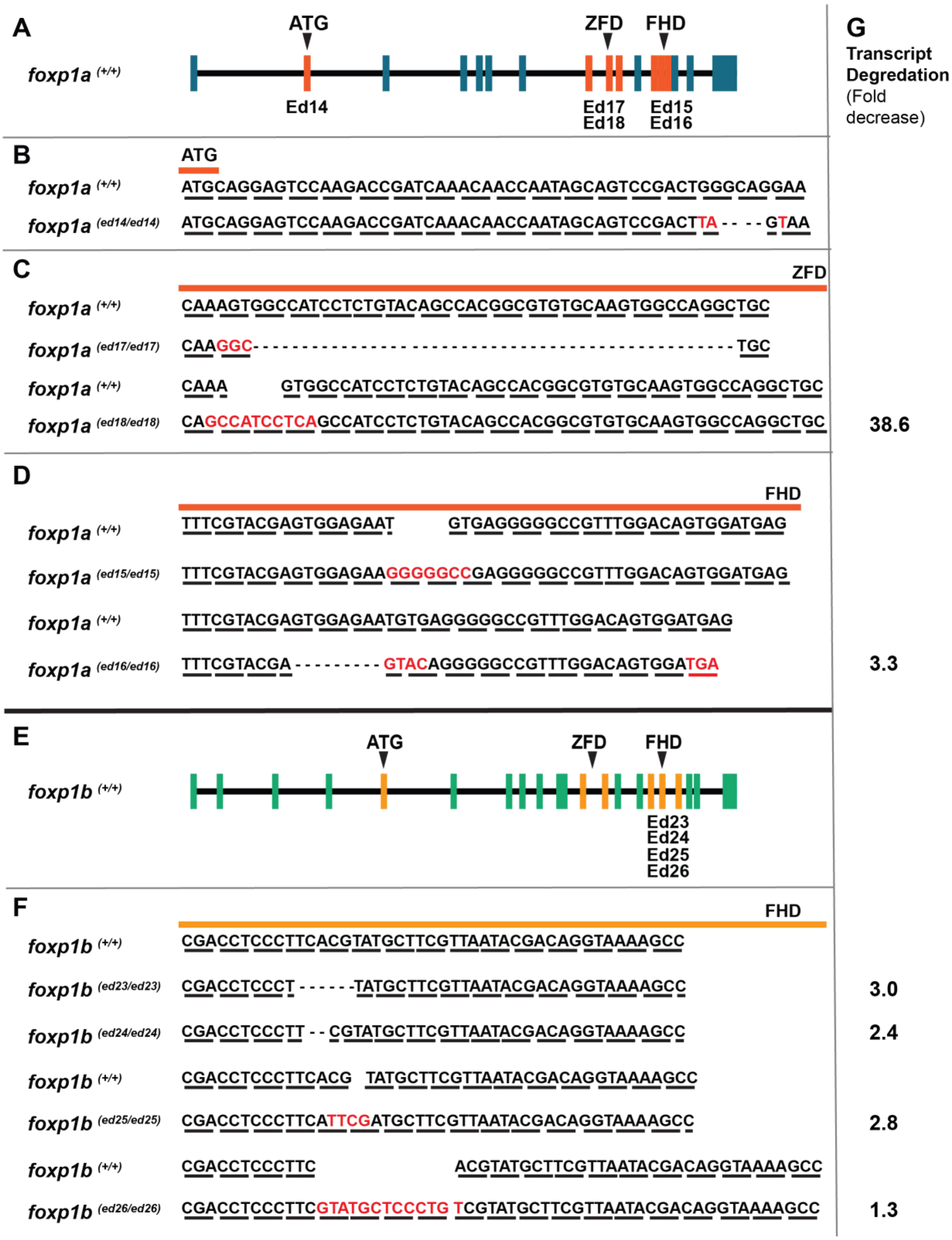

Figure 3.5 – Frameshift mutations in *foxp1* lead to transcript degradation.

Figure 3.5 – Frameshift mutations in *foxp1* lead to transcript degradation. A. Schematic of the *foxp1a* exon structure. **B.** *foxp1a*$^{(ed14/ed14)}$ mutant shows a 7bp indel resulting in a frameshift. **C.** *foxp1a*$^{(ed17/ed17)}$ allele shows a 45bp indel which does not change in the reading frame. *foxp1a*$^{(ed18/ed18)}$ allele shows a 10bp indel, resulting in a frameshift. **D.** *foxp1a*$^{(ed15/ed15)}$ allele shows a 7bp indel resulting in a frameshift. *foxp1a*$^{(ed16/ed16)}$ allele shows a 13bp indel resulting in a frameshift. **E.** Schematic of the *foxp1b* exon structure. **F.** *foxp1b*$^{(ed23/ed23)}$ allele shows a 5bp deletion resulting in a frameshift. *foxp1b*$^{(ed24/ed24)}$ allele shows a 2bp deletion resulting in a frameshift. *foxp1b*$^{(ed25/ed25)}$ allele shows a 4bp indel resulting in a frameshift. *foxp1b*$^{(ed26/ed26)}$ allele shows a 12bp insertion, which doesn't alter the reading frame. **B.C.D. & F.** Letters represent DNA bases. Red letters show changed based in the mutants. Thick dashed lines under the bases represent codons. Small dashes lines show deletions in the mutants. **G.** mRNA fold decrease in homozygous mutants.

3.2.10 - The *foxp1a*$^{(-/-)}$ allele is predicted to have a reduced ability to bind DNA

To test the hypothesis that *foxp1* is required for adipose tissue expansion, I first examined the role of *foxp1a*. The *foxp1a* allele I chose to use is *foxp1*$^{(-/-)}$, which is caused by a 13bp indel in the FHD **(Figure 3.6A & B)**. This mutation consisted of an 8bp deletion and a 4bp change and is predicted to lead to a frameshift and the introduction of an early stop codon within the FHD **(Figure 3.6A & B)**. I first wanted to predict the likely effect of this mutation on the FHD of *foxp1a* and therefore on the ability of *foxp1a* to bind DNA. As the mutation in *foxp1a*$^{(-/-)}$ is towards the 3' end of the FHD the function of this domain could be retained in the mutant **(Figure 3.6A)**. To determine whether this was likely I identified the sequence of the FHD in zebrafish. In mouse the FHD of Foxp1 is made up of 90 highly conserved amino acids, and these residues are well conserved to zebrafish (Stroud et al., 2006). In the *foxp1a*$^{(-/-)}$ mutants 8 residues of the FHD were predicted to be changed and 16 were predicted to be absent **(Figure 3.6C & D)**. Furthermore, 4 amino acids known to be involved in DNA binding were absent or altered in the *foxp1a*$^{(-/-)}$ mutant **(Figure3.6D)**. The altered or absent residues include a tryptophan residue, which interacts extensively with the sugar phosphate backbone of DNA and stabilises the DNA protein complex (Stroud et al., 2006) **(Figure 3.6D)**. Two arginine residues, which also stabilise the Foxp1 DNA complex are also absent in the *foxp1a*$^{(-/-)}$ mutants (Stroud et al., 2006) **(Figure 3.6D)**. Taken together this suggests that the *foxp1a*$^{(-/-)}$ mutants will be unable to bind DNA.

3.2.11 - *foxp1a*$^{(-/-)}$ mutants do not show genetic compensation

foxp1a$^{(-/-)}$ mutants were selected based on the fact that these mutants show high levels of transcript degradation. However, a recent paper has shown that mutant mRNA degradation is linked to increased expression of related genes (El-Brolosy et al., 2019). I therefore wished to measure the mRNA levels of genes closely related to *foxp1a* and determine whether they are altered in the *foxp1a*$^{(-/-)}$ mutants. To do this, 5 dpf fish were genotyped and RNA extracted from pools of 3 embryos. I then used RT-qPCR to measure the levels of all of the *foxp* genes in *foxp1*$^{(-/-)}$ mutants and WT siblings **(Figure 3.6F)**. I found that levels of *foxp1b, foxp2, foxp3a, foxp3b* and *foxp4* were not significantly increased in *foxp1a*$^{(-/-)}$ mutants **(Figure 3.6F)**. Together these

data suggest that it is reduced levels of *foxp1a* and not increased levels of other *foxp* transcripts that are responsible for any phenotypes observed in *foxp1a*$^{(-/-)}$ mutants.

3.2.12 - *foxp1a*$^{(-/-)}$ mutants show a large reduction in Foxp1 proteins levels

To determine the severity of the *foxp1a*$^{(-/-)}$ *allele*, I next wanted to assess Foxp1 protein levels. Protein lysate was extracted from the caudal fins of pools of 7 juvenile fish, and a Western blot was then performed using antibodies against FOXP1 and ACTB (Beta-Actin), with ACTB acting as a loading control **(Figure 3.6G)**. Zebrafish Foxp1a protein is predicted to be 72 kDa and Foxp1b is predicted to be 78 kDa. Based on this and previous studies in mouse the zebrafish Foxp1 protein is expected to be between 70 and 80 kDa (Rao et al., 2010). Western blotting using a FOXP1 antibody revealed a band in the WT sample at around 65 kDa **(Figure 3.6G)**. Foxp1 protein levels were found to be severely reduced in *foxp1a*$^{(-/-)}$ mutants **(Figure 3.6G)**. Whole mount antibody staining was also attempted in adipose tissue, though this did not work (data not shown). The staining also did not appear to work in non-adipose tissues, such as the heart and brain (data not shown). In summary *foxp1a*$^{(-/-)}$ mutants are likely to be loss of function mutants, as evidenced by reduced levels of *foxp1a* transcript and Foxp1 protein.

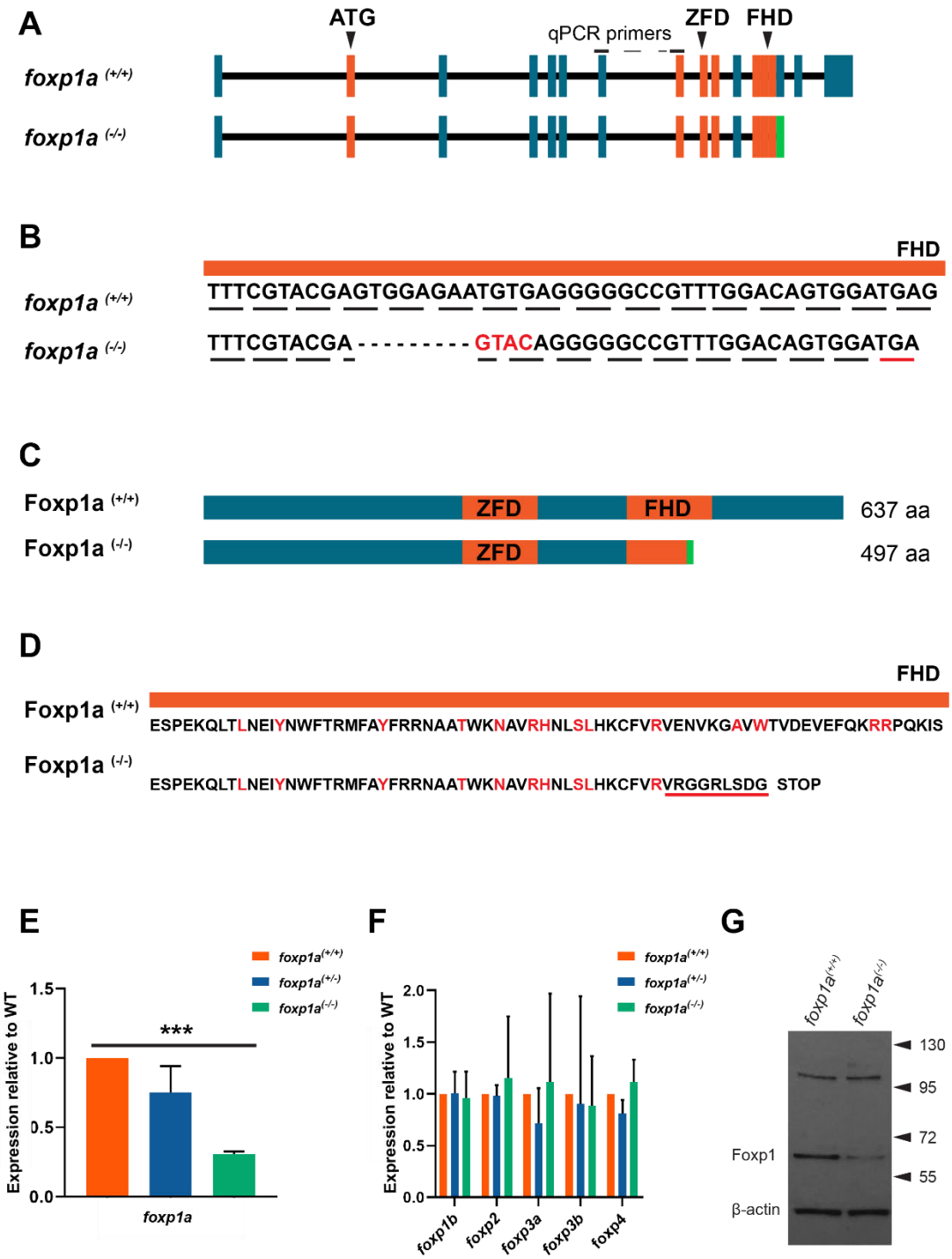

Figure 3.6 – A 13bp indel in *foxp1a* leads to a predicted frameshift mutation.

Figure 3.6 – A 13bp indel in *foxp1a* leads to a predicted frameshift mutation. A. Schematic showing the exon structure of *foxp1a*$^{(+/+)}$ and *foxp1a*$^{(-/-)}$. Orange bars show exons coding for functional domains (Pfam and Smart). ATG (ATG transcriptional start site). ZFD (zinc finger domain). FHD (forkhead domain). Dotted line shows where qPCR primers target **B.** Schematic showing changes to DNA in *foxp1a*$^{(-/-)}$ mutants. Letters indicate DNA bases. Small dashed lines show where a deletion has taken place. Red letters show changed bases. Dashed lines under the bases show the reading frame. The red line shows the presence of an early stop codon. **C.** Schematic showing the protein structure of Foxp1a$^{(+/+)}$ and Foxp1a$^{(-/-)}$. Orange bars show functional domains. The green bar shows changes to the protein sequence in the mutant. Numbers show predicted amino acid protein lengths. **D.** Schematic showing the changes to the amino acid sequence of the forkhead domain in the Foxp1a$^{(-/-)}$ mutant. Letters represent amino acids and red letters show amino acids known to be involved in DNA binding. The red line highlights the changed amino acids in the Foxp1a$^{(-/-)}$ mutants. **E.** n = 3 pools of 3 fish. A two tailed t-test was performed $p < 0.001$. Error bars show standard deviation **F.** n = 3 pools of 3 fish. Error bars show standard deviation. Two tailed t-tests were performed. *foxp1b, foxp2, foxp3a, foxp3b* and *foxp4* mRNA levels were not found to be significantly different in *foxp1a*$^{(+/-)}$ or *foxp1a*$^{(-/-)}$ mutants when compared to WT siblings. **G.** 20 minute exposure. Each lane contains protein from a pool of 7 fish.

3.2.13 - *foxp1a*$^{(-/-)}$ mutants have unaltered levels of AT during normal development

To test if *foxp1* is required for AT expansion, I first examined adiposity levels in the *foxp1a*$^{(-/-)}$ mutants. To achieve this, I incrossed *foxp1a*$^{(+/-)}$ fish and raised the resultant offspring until 4 weeks of age. The fish were then genotyped and *foxp1a*$^{(-/-)}$ mutant fish and *foxp1a*$^{(+/+)}$ siblings were stained with Nile red at 5 weeks of age. The fish were then imaged using a fluorescence stereomicroscope **(Figure 3.7A)**. Image J was used to measure the standard length (SL) of the fish and this was compared to the total fluorescence area, which acts as a proxy for total AT area (Tingaud-Sequeira et al., 2011). Under normal fed conditions, *foxp1a*$^{(-/-)}$ mutant fish were found to show no differences in levels of AT relative to SL when compared to *foxp1a*$^{(+/+)}$ siblings **(Figure 3.7C)**. *foxp1a*$^{(-/-)}$ fish were also found to develop normally and had an unaltered SL when compared to WT siblings **(Figure 3.7B)**. In summary, *foxp1a*$^{(-/-)}$ fish have unaltered levels of AT during normal development.

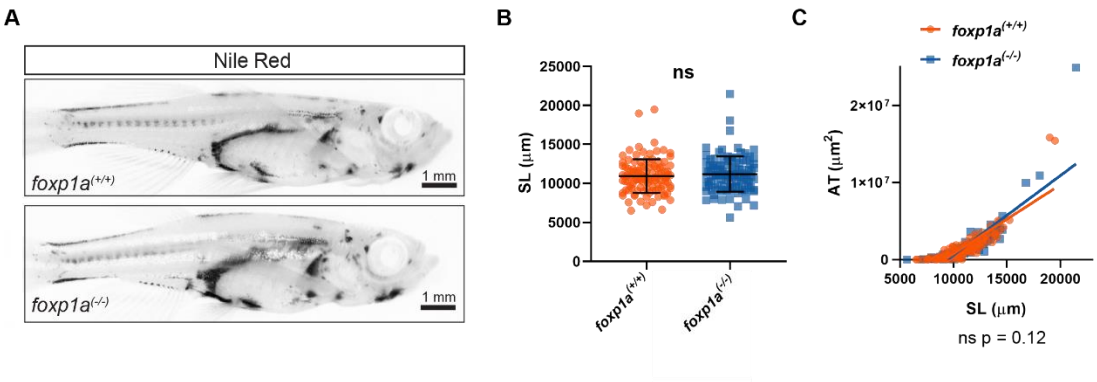

Figure 3.7 – *foxp1a*$^{(-/-)}$ mutants have unaltered levels of AT during normal development. A. Representative Nile Red images. Nile Red staining shown in black. Fish are 5 weeks of age. **B.** n = 106-111. Data from 6 experiments. Error bars show mean and standard deviation. A two tailed t-test was performed, p = 0.39 **C.** n = 106-111. Data from 6 experiments. An Ancova analysis was performed, and the slope of the lines were not found to be significantly different $F_{1,213}$ = 2.413 p = 0.12

3.2.14 - *foxp1a*$^{(-/-)}$ mutants gain less AT in response to a HFD

I next placed *foxp1a*$^{(-/-)}$ fish on a HFD to see if adipose tissue expansion in the mutant fish was altered in response to this dietary stimulus. I incrossed *foxp1a*$^{(+/-)}$ fish and raised the offspring until 4 weeks of age **(Figure 3.8A)**. At this point the fish were genotyped and separated into *foxp1a*$^{(+/+)}$ and *foxp1a*$^{(-/-)}$ groups **(Figure 3.8A)**. The fish were then stained with Nile Red and divided into 2 size matched groups, one HFD and one control diet group **(Figure 3.8A)**. Fish within these groups were randomly paired **(Figure 3.8A)**. The pairing of fish within groups minimised variation due to differences in fish size and allowed adipose measurements to be taken from the same fish before and after the diet. Fish then were subjected to a 2 week HFD, consisting of a 2 hour daily immersion in a 5% egg yolk solution (Carten et al., 2011, Semova et al., 2012, Walters et al., 2012,) **(Figure 3.8A)**. Finally, fish were stained with Nile Red and imaged at the end of the diet **(Figure 3.8A)**. Analysis of the Nile Red measurements following the HFD revealed that the *foxp1a*$^{(+/+)}$ HFD fish had significantly more AT than *foxp1a*$^{(+/+)}$ control diet (CD) siblings, demonstrating that the HFD induces increased adiposity **(Figure 3.8C & D)**. However *foxp1a*$^{(-/-)}$ HFD mutant fish were found to have significantly less total AT than *foxp1a*$^{(+/+)}$ HFD siblings **(Figure 3.8B & C)**. Nile Red measurements taken before and after the HFD also allowed me to measure changes in AT levels in response to the diet. *foxp1a*$^{(-/-)}$ mutants gained less AT in response to the HFD, though this difference was just short of significance **(Figure 3.8D)**. Taken together this shows that while *foxp1a*$^{(-/-)}$ mutant fish have normal levels of AT on a control diet, they gain less AT than WT fish when fed a HFD.

3.2.15 - *foxp1a*$^{(-/-)}$ mutants gain less SAT in response to a HFD

As visceral and subcutaneous adipose tissue (SAT) are known to have different properties in mammals, I also wanted to see if there were any differences in the response of VAT and SAT to the HFD in the *foxp1a*$^{(-/-)}$ mutants (Ibrahim, 2010). AT depots in zebrafish can be classified into visceral and subcutaneous depots and so measurements were taken of VAT and SAT depots from the Nile Red images **(Figure 3.8B)**. These measurements showed that the effect of the diet was significant in WT fish for both VAT and SAT **(Figure 3.8E & F)**. However, while *foxp1a*$^{(-/-)}$ mutant fish gained normal levels of VAT they gained significantly less SAT than WT siblings

(Figure 3.8E & F). These data suggest that *foxp1a* may play a greater role in subcutaneous adipose tissue expansion than in visceral adipose tissue expansion.

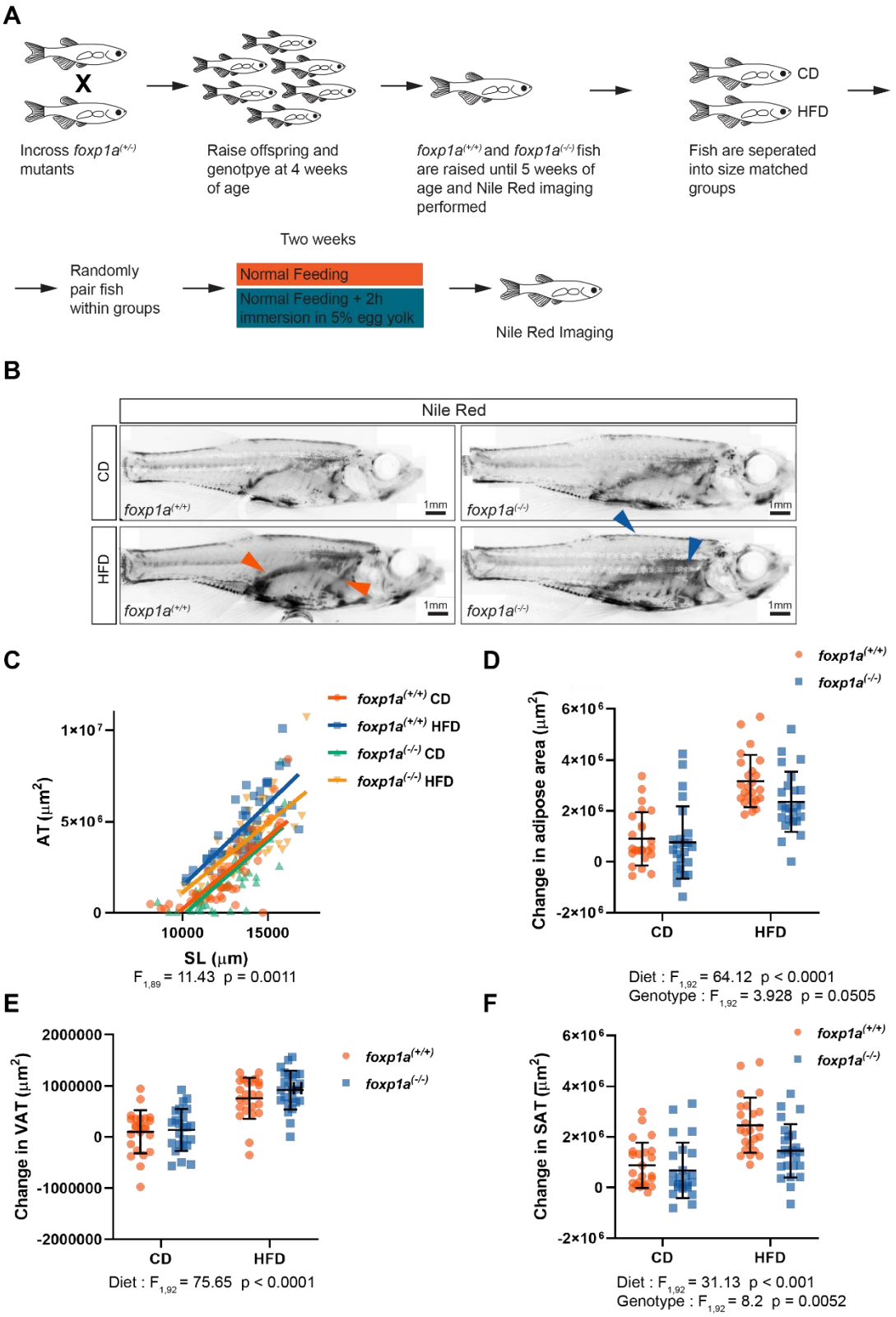

Figure 3.8 - *foxp1a*$^{(-/-)}$ mutants gain less AT in response to a HFD.

Figure 3.8 - *foxp1a*$^{(-/-)}$ mutants gain less AT in response to a HFD. A. Schematic showing how the HFD was conducted. **B.** Representative Nile Red images. Orange arrow heads show the locations of major VAT depots, PVAT (pancreatic VAT) and RVAT (Renal VAT). Blue arrow heads show the locations of major SAT depots, LSAT (lateral SAT) and aDSAT (anterior dorsal SAT) **C.** n = 47. Data from 4 experiments. An Ancova analysis was performed and the slope of the *foxp1a*$^{(+/+)}$ HFD and *foxp1a*$^{(-/-)}$ HFD lines were found to be significantly different $F_{1,89} = 11.43$, $p = 0.0011$. **D.** n = 24. Data from 4 experiments. A two-way ANOVA was performed and the effect of diet was found to be significant $F_{1,92} = 64.12$, $p < 0.0001$. Genotype, $F_{1.92} = 3.928$, $p = 0.0505$. **E.** n = 24. Data from 4 experiments. A two-way ANOVA was performed and the effect of diet was found to be significant $F_{1,92} = 75.65$, $p < 0.0001$. **F.** n = 24. Data from 4 experiments. A two-way ANOVA was performed and the effects of both diet and genotype were found to be significant. Diet, $F_{1,92} = 31.13$, $p < 0.0001$. Genotype, $F_{1,92} = 8.2$, $p = 0.0052$. **D.E.F.** Error bars show mean and standard deviation.

3.2.16 - *foxp1a*$^{(-/-)}$ mutants have a more hypertrophic lipid droplet morphology

I next examined the morphology of the lipid droplets within adipose tissue, as the reduced expansion of AT in the *foxp1a*$^{(-/-)}$ mutants may be due to reduced hyperplastic or hypertrophic growth. To assess AT lipid droplet morphology *foxp1a*$^{(-/-)}$ mutant fish and WT siblings were placed on a 2 week HFD, following the same protocol as described previously **(Figure 3.7A)**. Following the HFD fish were stained with LipidTOX and the lateral SAT (LSAT) depot imaged through the skin of euthanised fish, using confocal microscopy **(3.9E & F)**. Once this imaging was complete the PVAT depot was dissected from the fish and the whole depot imaged by confocal microscopy **(3.9A & B)**. Both the number and diameter of the lipid droplets present in each depot were measured. The effect of the HFD was apparent when looking at the morphology of both the visceral and subcutaneous depot in WT fish, with the average diameter of the lipid droplets being significantly increased in both **(Figure 3.9D & H)**. No changes in lipid droplet number in response to the HFD were observed in WT fish **(Figure 3.9C & G)**. *foxp1a*$^{(-/-)}$ mutants showed a genotype specific effect in LSAT only and had a significantly greater average lipid droplet diameter than their WT siblings **(Figure 3.9H)**. No differences were observed between *foxp1a*$^{(-/-)}$ mutant fish and WT siblings in lipid droplet number in either the PVAT or LSAT depot **(Figure 3.9C & G)**. Taken together these data suggest that the SAT of *foxp1a*$^{(-/-)}$ mutants expands via hypertrophic growth to a greater extent than the SAT of WT fish.

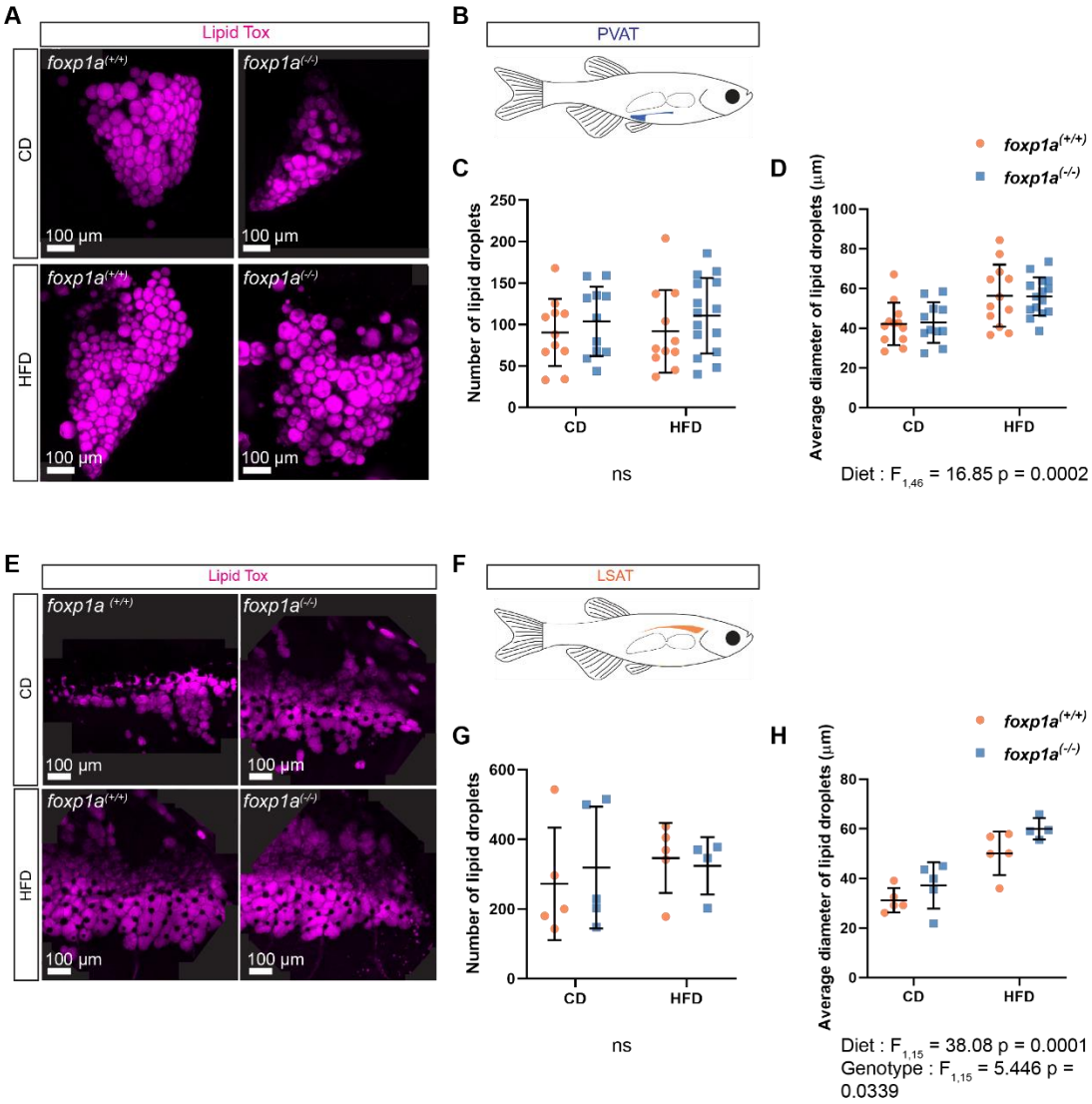

Figure 3.9 – *foxp1a*$^{(-/-)}$ mutants have a more hypertrophic LSAT lipid droplet morphology

Figure 3.9 – *foxp1a*$^{(-/-)}$ mutants have a more hypertrophic LSAT lipid droplet morphology. A. Representative maximum intensity projections of PVAT (Pancreatic VAT). The anterior end of the depot is to the right of the image and the posterior to the left. **B.** Schematic showing the location of PVAT. **C.** Number of lipid droplets per PVAT. N = 12 **D.** Average diameter of lipid droplets per PVAT. A two way ANOVA was performed and the effect of diet was found to be significant $F_{1,46}$ = 16.85 p = 0.0002. n = 12. **E.** Representative maximum intensity projections of LSAT (Lateral SAT). The anterior end of the depot is to the right. **F.** Schematic showing the location of LSAT. **G.** Number of lipid droplets per LSAT. N = 4-5. **H.** Average diameter of lipid droplets per LSAT. A two way ANOVA was performed and the effect of both diet and genotype were found to be significant. Diet, $F_{1,15}$ = 38.08 p = 0.0001. Genotype, $F_{1,15}$ = 5.446 p = 0.0339.

3.2.17 - *foxp1a*$^{(-/-)}$ mutants have normal levels of blood metabolites

As *foxp1a*$^{(-/-)}$ mutants show a defect in adipose tissue expansion in response to a HFD, I next wanted to determine if the metabolic health of *foxp1a*$^{(-/-)}$ mutants was affected. A severe defect in AT expansion would mean that a reduced amount of lipid would be able to be stored in AT and this would lead to increased levels of blood fatty acids and triglycerides (Lafontan, 2014). This could also potentially lead to increased levels of blood glucose and cholesterol (Lafontan, 2014). To determine the severity of the AT expansion defect observed in the *foxp1a*$^{(-/-)}$ mutants, levels of lipid metabolites in the blood were measured following a 1 week HFD **(Figure 3.10A)**. *foxp1a*$^{(+/-)}$ fish were incrossed and their offspring genotyped at 4 weeks of age **(Figure 3.10A)**. *foxp1a*$^{(-/-)}$ fish and WT siblings were then raised at equal stocking densities until 2 months of age, at which point they were placed on a 1 week HFD **(Figure 3.10A)**. Following the diet, fish were fasted overnight, euthanised and blood extracted from the fish **(Figure 3.10A)**. The blood was then used to measure levels of glucose, triglyceride and cholesterol **(Figure 3.10B. C. & D)**. No differences were observed in the levels of glucose, triglyceride or cholesterol in the *foxp1a*$^{(-/-)}$ mutants when compared to WT siblings **(Figure 3.10B. C. & D)**. However the effect of the HFD could be observed with both *foxp1a*$^{(-/-)}$ and *foxp1a*$^{(+/+)}$ fish on the HFD having significantly higher levels of blood triglycerides than fish on the control diet **(Figure 3.10C)**. Taken together this suggests that AT expansion in response to a HFD is not so severely impaired as to lead to ectopic lipid deposition in the *foxp1a*$^{(-/-)}$ mutants.

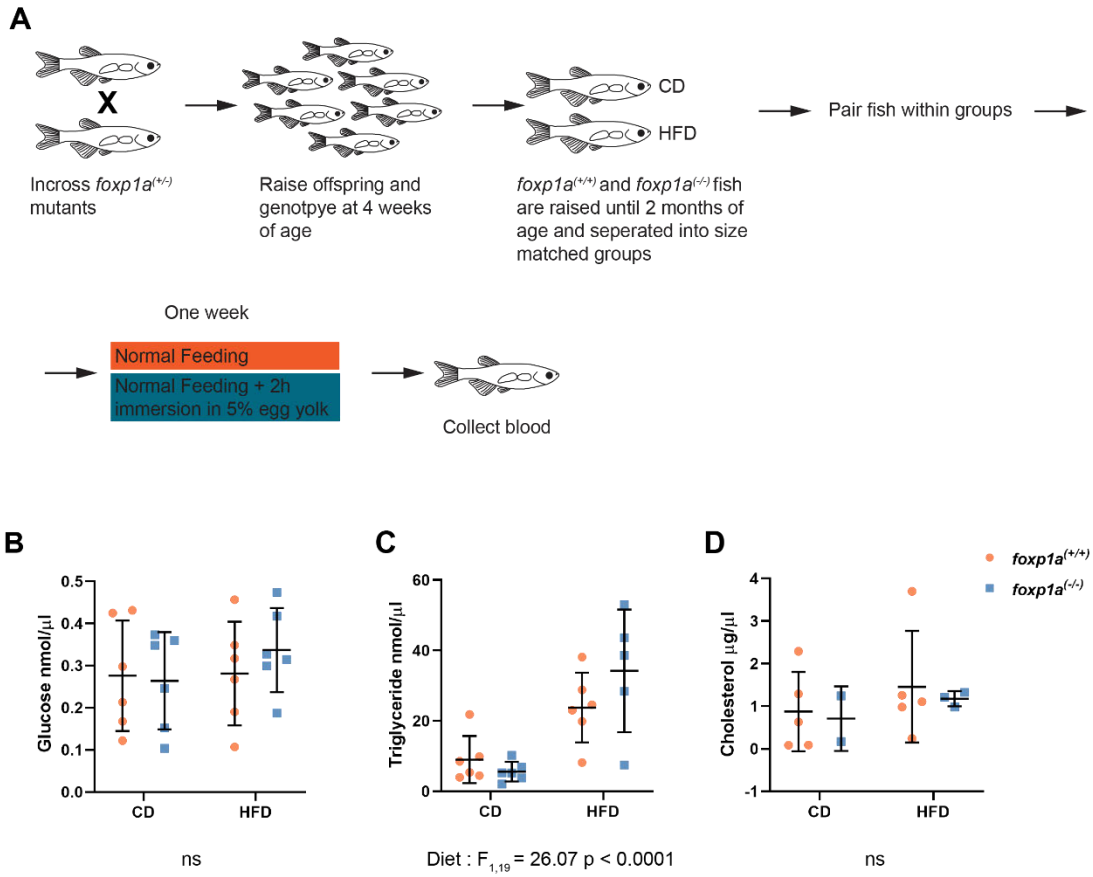

Figure 3.10 – *foxp1a*$^{(-/-)}$ mutants have normal levels of blood metabolites. A. Schematic showing HFD protocol. **B.** n = 5-6. **C.** n = 5-6. A two way ANOVA was performed and the effect of diet was found to be significant. $F_{1,19} = 26.07$ $p < 0.0001$. **D.** n = 2-5. **B.C.D.** Error bars show mean and standard deviation.

3.2.18 - The *foxp1a*$^{(-/-)}$ mutant phenotype suggests that *foxp1a* plays an important role in AT expansion

The most notable phenotype of the *foxp1a*$^{(-/-)}$ mutants is a reduction in adipose tissue expansion following a HFD **(Figure 3.11A)**. Following a HFD, *foxp1a*$^{(-/-)}$ mutants gain less AT, specifically they gain less SAT and they have a more hypertrophic SAT morphology **(Figure 3.11A)**. Taken together these data support the hypothesis that *foxp1* is required for AT expansion and point to a role for *foxp1a* specifically within SAT **(Figure 3.11B & C)**.

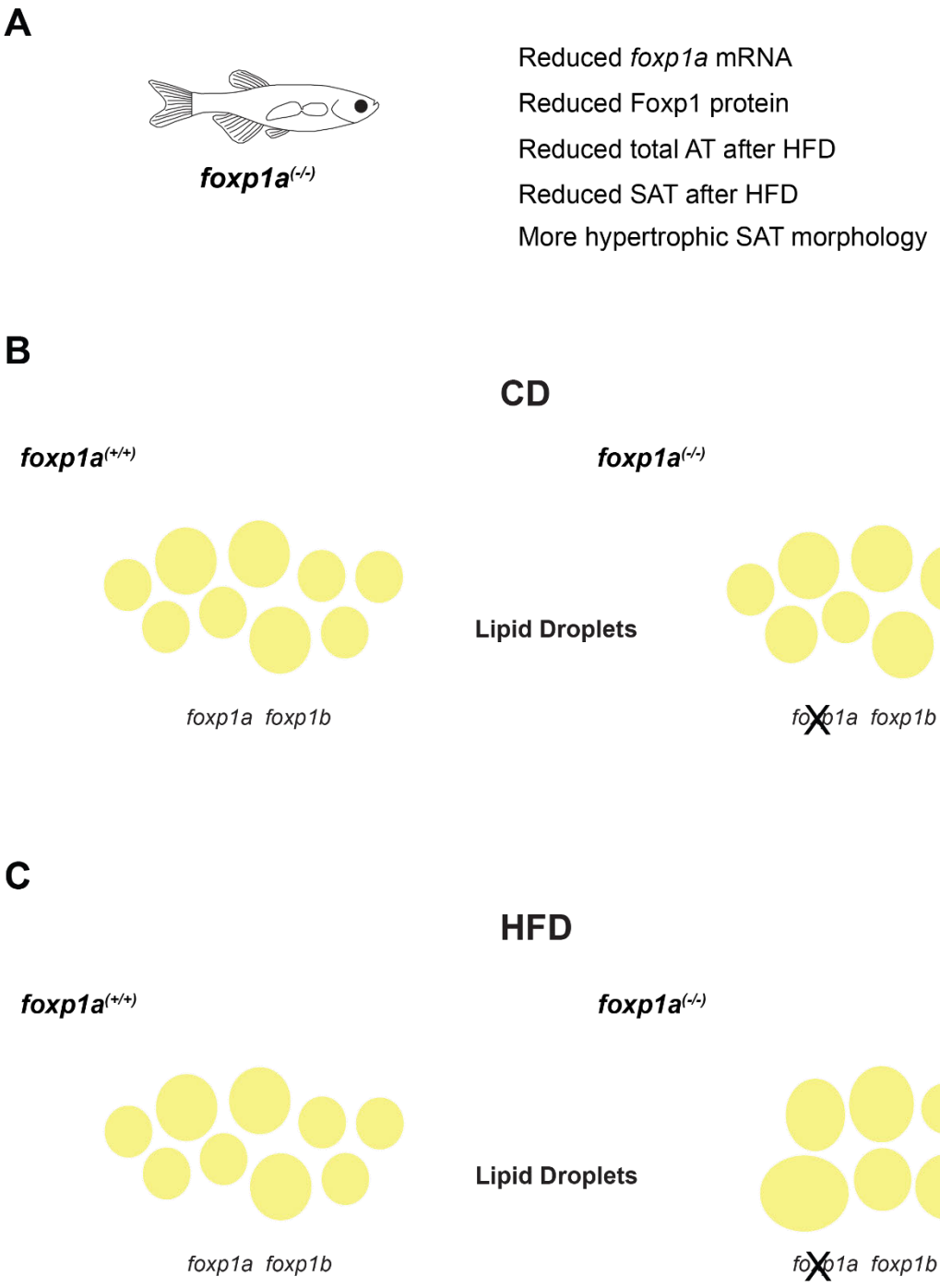

Figure 3.11 - *foxp1a* is required for SAT expansion in response to a HFD. A. Summary of the phenotype of the *foxp1a*$^{(-/-)}$ mutants. **B.** Schematic showing lipid droplet morphology in *foxp1a*$^{(-/-)}$ fish on a control diet. **C.** Schematic showing lipid droplet morphology in *foxp1a*$^{(-/-)}$ mutants on a HFD.

3.2.19 - The *foxp1b*$^{(-/-)}$ allele is predicted to have a reduced ability to bind DNA

Having examined the role of *foxp1a* in AT expansion (section 3.2.10 - 3.2.18), I next wanted to examine the role of *foxp1b*. As stated previously, I have made use of the *foxp1b*$^{(-/-)}$ allele to test my hypothesis. The *foxp1b*$^{(-/-)}$ allele is characterised by a 4bp indel at the FHD of *foxp1b* **(Figure 3.12)**. The 4bp indel is comprised of a 3bp change and a 1bp insertion, which leads to a frameshift and the introduction of an early stop codon **(Figure 3.12A & B)**. As the mutation in *foxp1b*$^{(-/-)}$ occurs at the start of the FHD it was thought that it would be likely to disrupt the ability of the FHD to bind DNA **(Figure 3.12A)**. To check if this was the case, I translated the predicted base changes in the mutant to predicted amino acid changes and then aligned this sequence with that of WT Foxp1b **(Figure 3.12C & D)**. The *foxp1b*$^{(-/-)}$ mutant was found to retain the first 5 amino acids of the FHD but all other residues had been changed to nonsense sequence or were absent **(Figure 3.12D)**. Therefore, it was concluded that the mutant Foxp1b protein would be unlikely to be able to bind DNA.

3.2.20 - *foxp1b*$^{(-/-)}$ mutants do not show genetic compensation

As with the *foxp1a*$^{(-/-)}$ allele, I also wanted to determine whether the *foxp1b*$^{(-/-)}$ mutants showed genetic compensation. To do this 5 dpf embryos were fin clipped, genotyped and RNA extracted from pools of 3 embryos. I then used RT-qPCR to measure levels of *foxp1a, foxp2, foxp3a, foxp3b* and *foxp4* in the *foxp1b*$^{(-/-)}$ mutants and WT siblings **(Figure 3.12F)**. None of the genes tested were found to be significantly upregulated in the *foxp1b*$^{(-/-)}$ mutants **(Figure 3.12F)**. Interestingly levels of *foxp3a* and *foxp3b* were significantly downregulated in *foxp1b*$^{(+/-)}$ mutants compared to WT siblings **(Figure 3.12F)**. This finding is at odds with the results from the *foxp1b*$^{(-/-)}$ mutants and further experiments are needed to interpret this result. Overall, a reduction in levels of *foxp1b* transcripts and no apparent compensation in the *foxp1b*$^{(-/-)}$ mutants gives confidence to the idea that the *foxp1b*$^{(-/-)}$ allele is a loss of function allele.

3.2.21 - *foxp1b*$^{(-/-)}$ mutants have a large reduction in Foxp1 protein levels

To assess the severity of the *foxp1b*$^{(-/-)}$ allele, I next measured Foxp1 protein levels. Protein was extracted from the caudal fin of pools of 7 mutant and WT juvenile fish and a western blot was performed as described previously in section 3.2.12 **(Figure 3.12G)**. I found that levels of Foxp1 were severely reduced in the *foxp1b*$^{(-/-)}$ mutants **(Figure 3.12G)**. This suggests that the *foxp1b*$^{(-/-)}$ allele is a loss of function allele and will be useful for further experiments looking at the function of *foxp1b*.

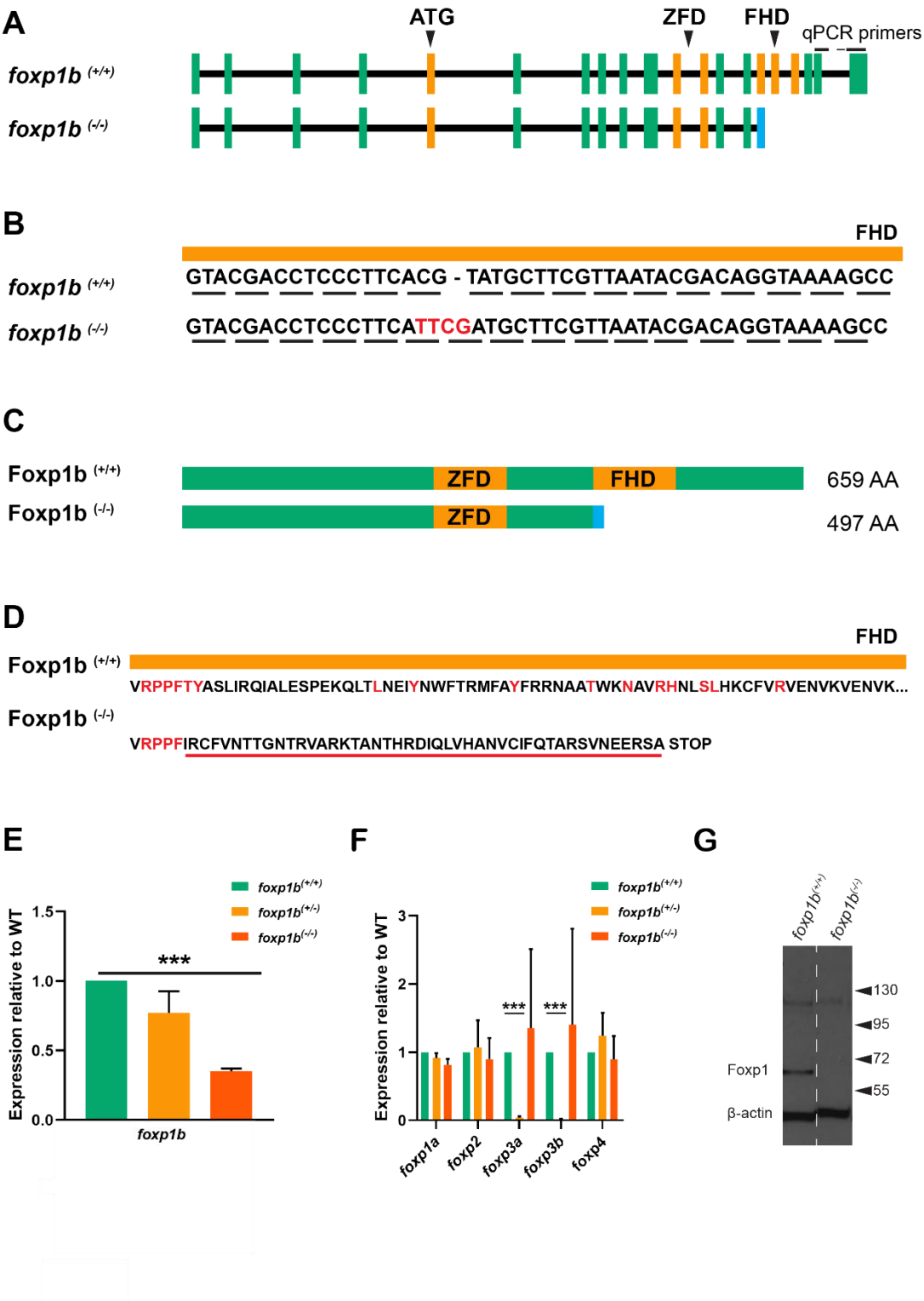

Figure 3.12 – The *foxp1b*$^{(-/-)}$ mutants have reduced *foxp1b* mRNA levels, reduced Foxp1 protein levels and do not show genetic compensation.

Figure 3.12 – The *foxp1b*$^{(-/-)}$ mutants have reduced *foxp1b* mRNA levels, reduced Foxp1 protein levels and do not show genetic compensation. A. Schematic showing the exon structure of *foxp1b*$^{(+/+)}$ and *foxp1b*$^{(-/-)}$. Orange bars show exons coding for functional domains (Pfam and Smart). ATG (ATG transcriptional start site). ZFD (zinc finger domain). FHD (forkhead domain). Dashed line shows the exons targeted by the qPCR primers. **B.** Schematic showing changes to the DNA sequence in *foxp1b*$^{(-/-)}$ mutants. Letters indicate DNA bases. Small dashed lines show where an insertion has taken place. Red letters show changed bases. Dashed lines under the bases show the reading frame. **C.** Schematic showing the protein structure of *foxp1b*$^{(+/+)}$ and *foxp1b*$^{(-/-)}$. Orange bars show functional domains. The blue bar shows changes to the protein sequence in the mutant. Numbers show predicted amino acid lengths of proteins. **D.** Schematic showing the changes to the amino acid sequence of the forkhead domain in the *foxp1b*$^{(-/-)}$ mutant. Letters represent amino acids and red letters show amino acids known to be involved in DNA binding. The red line highlights the changed amino acids in the *foxp1b*$^{(-/-)}$ mutants. **E.** n = 3 pools of 3 fish. A two tailed t-test was performed $p < 0.001$. Error bars show standard deviation **F.** n = 3 pools of 3 fish. Error bars show standard deviation. Two tailed t-tests were performed. **G.** 20 minute exposure. Each lane contains protein from a pool of 7 fish. Dashed white line shows where a lane has been spliced out of the gel.

3.2.22 - *foxp1b*$^{(-/-)}$ mutants are smaller than WT siblings but have unaltered levels of AT during normal development

I next wanted to begin to test my hypothesis, that foxp1 is required for AT expansion, by assessing the effect of a reduction in *foxp1b* on AT levels. To achieve this, I incrossed *foxp1b*$^{(+/-)}$ fish and raised their offspring until 30 dpf. The fish were then genotyped and stained with Nile Red. As described previously, the fish were imaged using a fluorescence stereomicroscope and total AT area was measured and compared to SL **(Figure 3.13A)**. *foxp1b*$^{(-/-)}$ mutant fish were found to be significantly smaller than WT siblings but were found to have normal levels of AT relative to their size **(Figure 3.13B & C)**. These data suggest that *foxp1b*$^{(-/-)}$ mutants have reduced somatic growth but that AT development is normal in this context.

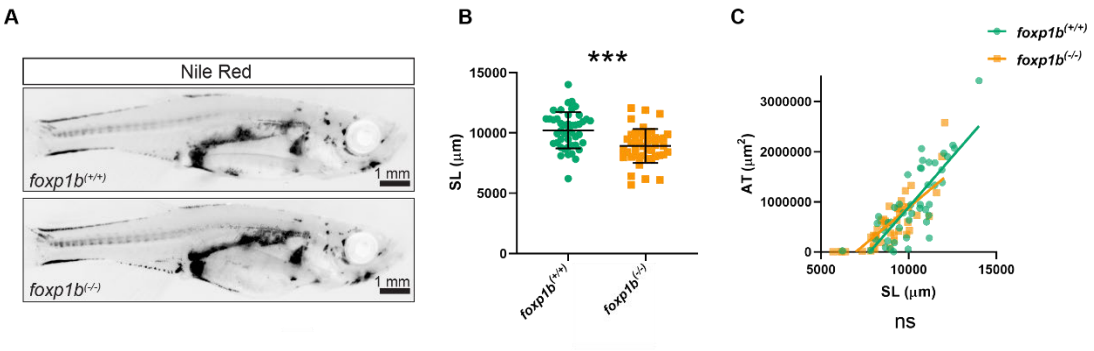

Figure 3.13 – *foxp1b*$^{(-/-)}$ mutants are smaller than WT siblings and have unaltered levels of AT during normal development. A. A. Representative Nile Red images. Nile Red staining shown in black. **B.** n = 45. Data from 4 experiments. A two tailed t-test was performed, $p < 0.0001$. **C.** n = 45. Data from 4 experiments. An Ancova analysis was performed and the lines were not found to be significantly different $F_{1,86} = 3.646$, $p < 0.0595$. ns (Not Significant).

3.2.23 - *foxp1b*$^{(-/-)}$ mutants gain less AT in response to a HFD

To further test my hypothesis, that *foxp1b* is required for AT expansion, I next placed *foxp1b*$^{(-/-)}$ fish on a 2 week HFD. The purpose of the HFD was to stimulate AT expansion and the same HFD method described previously in section 3.2.14 was used. Briefly *foxp1b*$^{(+/-)}$ fish were incrossed and their offspring raised until 4 weeks of age **(Figure 3.14A)**. The fish were then genotyped and at 5 weeks of age the *foxp1b*$^{(+/+)}$ and *foxp1b*$^{(-/-)}$ fish were stained with Nile Red **(Figure 3.14A)**. The fish were then separated into size matched groups and placed on a 2 week HFD **(Figure 3.14A)**. Fish were also stained with Nile Red at the end of the diet **(Figure 3.14A)**. Nile Red staining following the HFD showed that *foxp1b*$^{(+/+)}$ HFD fish had significantly more AT than *foxp1b*$^{(+/+)}$ CD fish, demonstrating that the HFD is capable of inducing significant adipose tissue accumulation **(Figure 3.14B & C)**. *foxp1b*$^{(-/-)}$ HFD fish were found to have less total AT following the diet than *foxp1b*$^{(+/+)}$ HFD fish, though this difference was not significant **(Figure 3.14B & C)**. However, when the change in total AT area was measured, comparing AT area before and after the diet, the effect of genotype was found to be significant **(Figure 3.14D)**. Therefore, these data suggest that *foxp1b* is required for AT expansion in response to a HFD.

3.2.24 - *foxp1b*$^{(-/-)}$ mutants gain less VAT in response to a HFD

As *foxp1a*$^{(-/-)}$ mutants were found to have a specific defect in SAT expansion, I next wished to determine if this was also true of *foxp1b*$^{(-/-)}$ mutants. To do this I again used Nile Red images to measure the levels of VAT and SAT **(Figure 3.14E & F)**. The effect of diet was found to be significant in both VAT and SAT, suggesting that the HFD induces both AT subtypes to expand **(Figure 3.14E & F)**. However, unlike *foxp1a*$^{(-/-)}$ mutants, *foxp1b*$^{(-/-)}$ mutants gained significantly less VAT in response to the HFD and showed normal levels of SAT expansion **(Figure 3.14E & F)**. This difference in phenotypes between the two mutants suggests that the *foxp1a* and *foxp1b* paralogues may have undergone subfunctionalisation and that the paralogues may play distinct roles in VAT and SAT expansion. In summary *foxp1b*$^{(-/-)}$ mutants gain less VAT in response to a HFD, suggesting that *foxp1b* may play a greater role in VAT expansion.

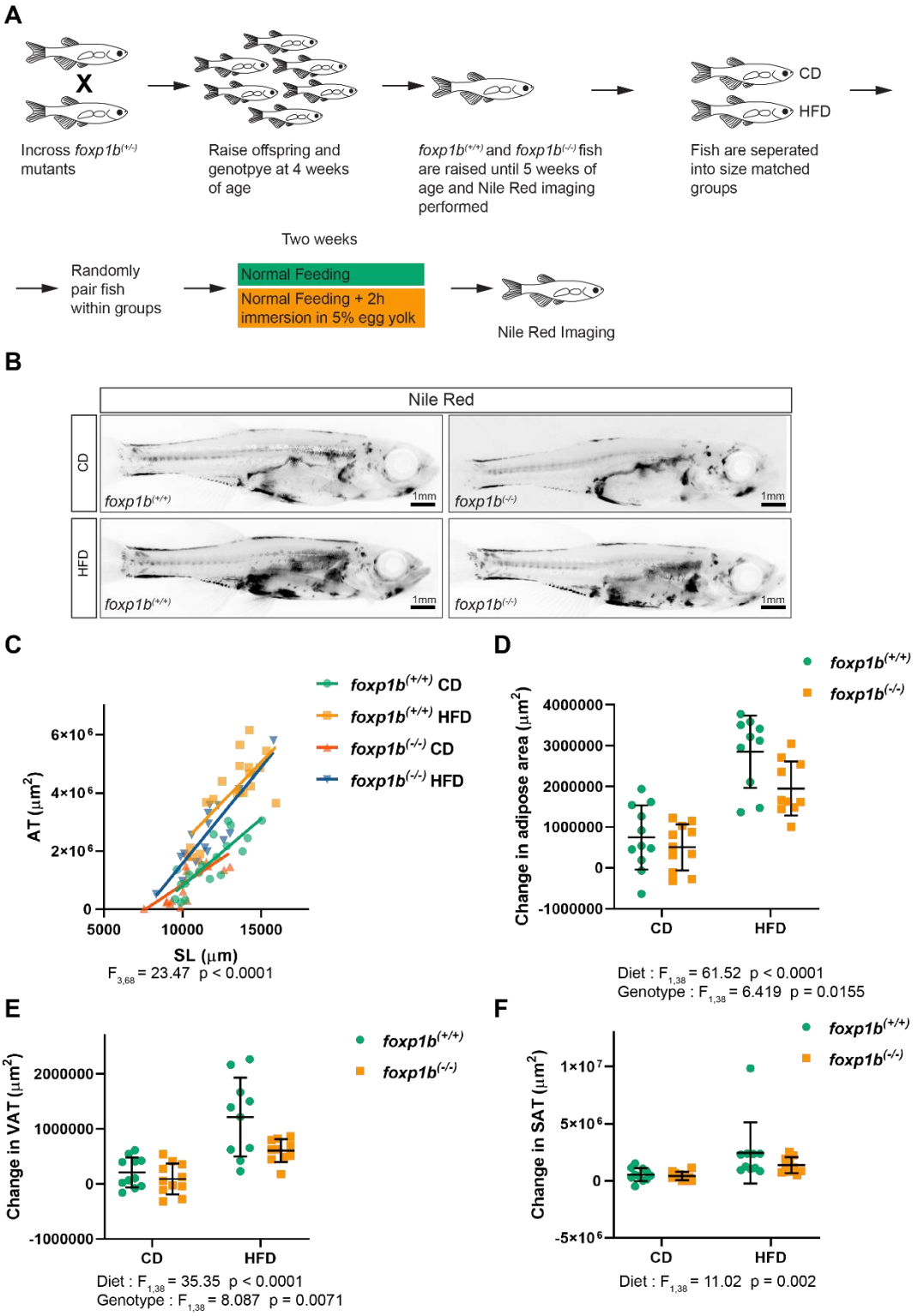

Figure 3.14 – *foxp1b*$^{(-/-)}$ mutants gain less visceral adipose tissue in response to a HFD

Figure 3.14 – *foxp1b*$^{(-/-)}$ mutants gain less visceral adipose tissue in response to a HFD. A. Schematic showing how the HFD was conducted. **B.** Representative Nile Red images. **C.** n = 29. Data from 3 experiments. **D.** n = 10-11. Data from 3 experiments. A two-way ANOVA was performed and the effect of both diet and genotype were found to be significant. Diet, $F_{1,38} = 61.52$, $p < 0.0001$. Genotype, $F_{1,38} = 6.419$, $p = 0.0155$. **E.** n = 10-11. A two-way ANOVA was performed and the effect of both diet and genotype were found to be significant. Diet, $F_{1,38} = 35.35$, $p < 0.0001$. Genotype, $F_{1,38} = 8.087$, $p = 0.0071$. **F.** n = 10-11. A two-way ANOVA was performed and the effect of diet was found to be significant, $F_{1,38} = 11.02$, $p = 0.002$. **D.E.F.** Error bars show mean and standard deviation.

3.2.25 - *foxp1b*$^{(-/-)}$ mutants do not show changes in lipid droplet morphology

As *foxp1b*$^{(-/-)}$ mutants show reduced levels of AT expansion in response to a HFD, I next wanted to determine whether this reduced expansion had an impact on adipose morphology. Adipose tissue can expand via hyperplastic or hypertrophic growth and so I wanted to determine whether the balance between these two modes of growth was altered in the *foxp1b*$^{(-/-)}$ mutants. To test this, *foxp1b*$^{(-/-)}$ fish were placed on a 2 week HFD, as described previously **(Figure 3.14A)**. Following the HFD fish were stained with lipidTOX and LSAT imaged through the skin of euthanised fish **(Figure 3.15E & F)**. PVAT was then dissected from the fish and the whole depot imaged **(Figure 3.15A & B)**. Adipose morphology was assessed by measuring lipid droplet number and diameter. The effect of the HFD was apparent in both the PVAT and LSAT depots with a significantly greater average lipid droplet diameter in the HFD groups compared to the control diet groups **(Figure 3.15D & H)**. No changes in lipid droplet number were observed in response to the HFD **(Figure 3.15C & G)**. Similarly, no differences were observed between *foxp1b*$^{(-/-)}$ and *foxp1b*$^{(+/+)}$ fish in either the PVAT or LSAT depot **(Figure 3.15C. D. G. & H)**. The lack of phenotype in the *foxp1b*$^{(-/-)}$ mutants suggests that the experiment is underpowered or that the reduced VAT expansion in the *foxp1b*$^{(-/-)}$ mutants does not alter the balance between hypertrophic and hyperplastic growth.

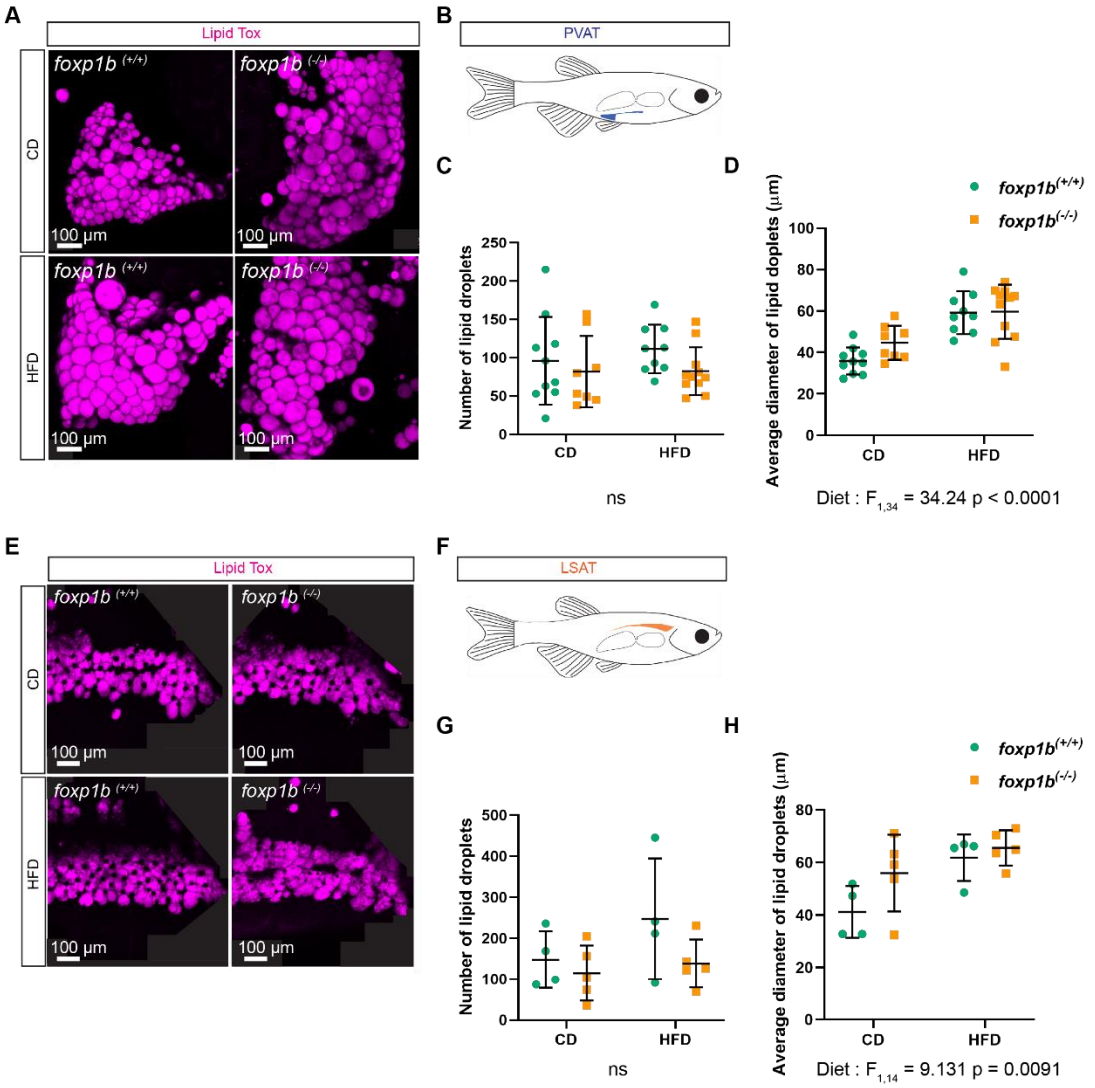

Figure 3.15 – *foxp1b*$^{(-/-)}$ mutants show no changes in adipose morphology following a HFD. A. Representative maximum intensity projections of PVAT depots. The anterior end of the depot is to the right of the image and the posterior to the left. **B.** Schematic showing the location of the PVAT depot. **C.** n = 9-11 **D.** n = 9-11. A two way ANOVA was performed and the effect of diet was found to be significant $F_{1,34}$ = 34.24 p < 0.0001. **E.** Representative maximum intensity projections of sections of the LSAT depot. The anterior of the depot is to the right of the image. **F.** Schematic showing the location of the LSAT depot. **G.** n = 4-5. **H.** n = 4-5. A two way ANOVA was performed and the effect of diet was found to be significant $F_{1,14}$ = 9.131 p = 0.0091. **C.D.G & H.** Error bars show mean and standard deviation.

3.2.26 - *foxp1b*$^{(-/-)}$ mutants do not have altered levels of blood metabolites

Finally, I wanted to determine how severe the defect in AT expansion was in the *foxp1b*$^{(-/-)}$ mutants. As a readout of defective AT expansion, I looked at levels of blood metabolites. Long term exposure to a HFD can lead to improper lipid storage and altered levels of blood metabolites. In mutants which already have impaired AT expansion altered levels of lipid metabolites may be observed after shorter periods of exposure. I therefore examined levels of lipid metabolites in the blood of *foxp1b*$^{(-/-)}$ mutants, and I again made use of a HFD. *foxp1b*$^{(-/-)}$ fish were raised until 2 months of age and then placed on a 1 week HFD **(Figure 3.16A)**. Following the HFD fish were euthanised and blood collected **(Figure 3.16A)**. Levels of glucose, cholesterol and triglycerides were measured **(Figure 3.16B. C. & D)**. No differences were observed between *foxp1b*$^{(-/-)}$ mutant fish and WT siblings, though the effect of the diet on triglyceride levels could be observed **(Figure 3.16B. C. & D)**. Together these data suggest that AT expansion in *foxp1b*$^{(-/-)}$ mutants is not impaired to the extent as to cause an altered blood metabolite profile.

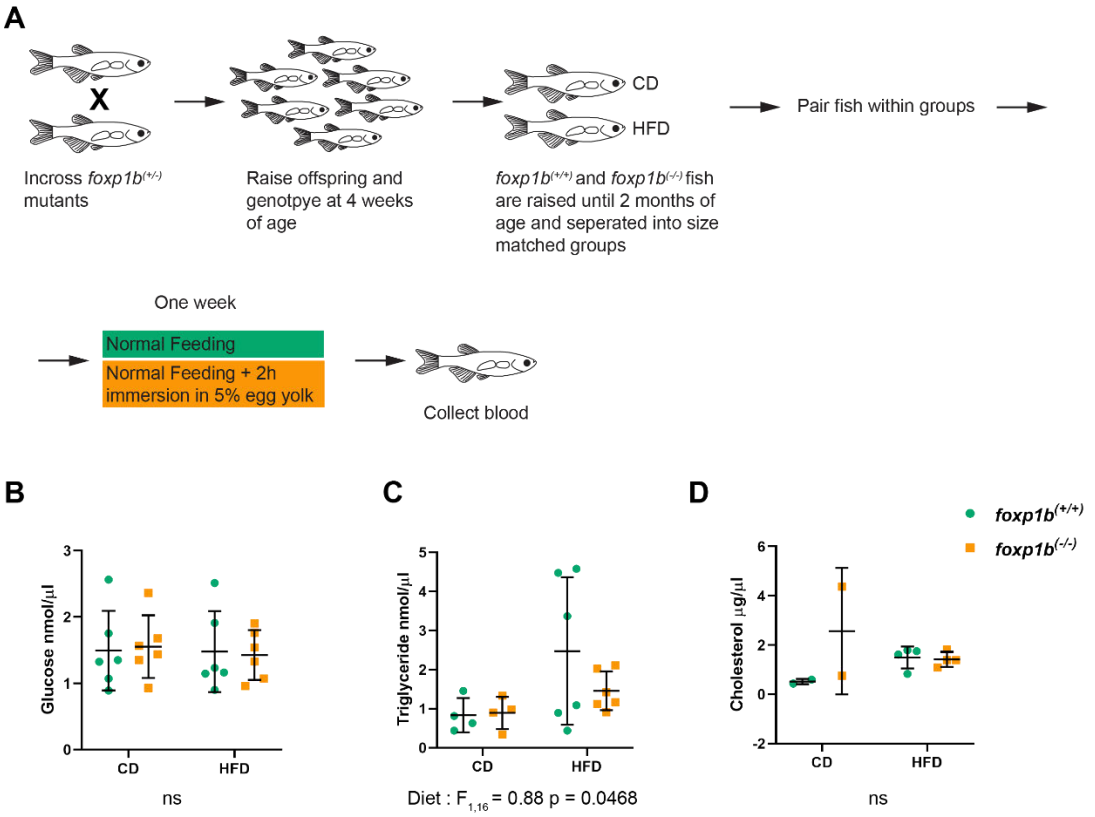

Figure 3.16 – *foxp1b*$^{(-/-)}$ mutants do not have altered levels of blood metabolites. **A.** Schematic showing HFD protocol. CD (Control Diet). HFD (High Fat Diet). **C.** A two way ANOVA was performed and the effect of diet was found to be significant. $F_{1,16}$ = 0.88 p = 0.0468. **B. C & D.** n = 2-6. Error bars show mean and standard deviation.

3.2.27 - The *foxp1b*$^{(-/-)}$ mutant phenotype suggests that *foxp1b* is required for visceral AT expansion in response to a HFD

In summary, I have found evidence to support the hypothesis that *foxp1* is required for AT expansion. *foxp1b*$^{(-/-)}$ mutants have reduced levels of *foxp1b* mRNA, reduced levels of Foxp1 protein and show no signs of genetic compensation **(Figure 3.17A)**. *foxp1b*$^{(-/-)}$ mutants are also significantly smaller than WT siblings but have normal levels of AT relative to their size **(Figure 3.17A)**. Following a HFD *foxp1b*$^{(-/-)}$ mutants gain less AT and specifically they gain less VAT **(Figure 3.17A)**. Therefore, loss of *foxp1b* seems not to effect AT expansion during a control diet, but is sufficient to cause impaired VAT expansion during a HFD **(Figure 3.17B & C)**. Together these data support my hypothesis about the role of *foxp1b* in AT expansion. It also allows me to refine my hypothesis with regards to *foxp1b* and to hypothesise that *foxp1b* is important for VAT expansion in response to a HFD **(Figure 3.17C)**.

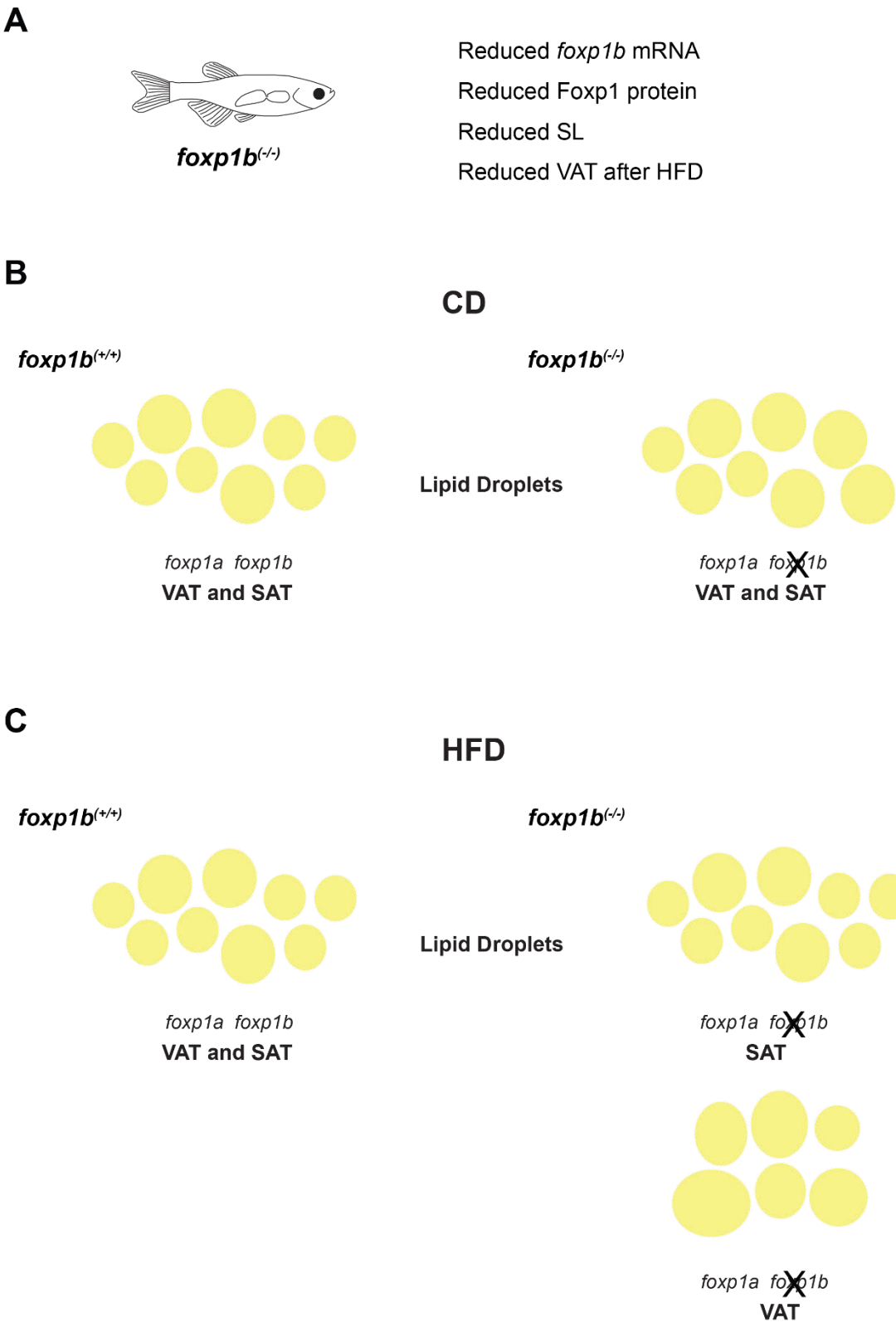

Figure 3.17 – *foxp1b* is required for VAT expansion in response to a HFD

Figure 3.17 – *foxp1b* is required for VAT expansion in response to a HFD. A. Summary of the main phenotypes of the *foxp1b*$^{(-/-)}$ mutants. **B.** Schematic illustrating what is hypothesised to occur during AT expansion on a control diet. **C.** Schematic illustrating what is hypothesised to occur during AT expansion on a HFD.

3.2.28 - *foxp1a*$^{(-/-)}$*;foxp1b*$^{(-/-)}$ mutants have reduced levels of *foxp1a* and *foxp1b* mRNA

To test the hypothesis that *foxp1* is required for AT expansion I have also made use of *foxp1a*$^{(-/-)}$*;foxp1b*$^{(-/-)}$ double mutants. These mutants were generated by crossing *foxp1a*$^{(-/-)}$ *and foxp1b*$^{(-/-)}$ mutants. *foxp1* transcript levels are known to be reduced in the single mutants, however I also wanted to check whether *foxp1* levels were reduced in the double mutants. To achieve this, 5 dpf fish were fin clipped, genotyped and RNA extracted from pools of 2-3 embryos. RT-qPCR was then used to determine the levels of *foxp1a* and *foxp1b* mRNA **(Figure 3.18A & B)**. Levels of *foxp1a* and *foxp1b* were found to be reduced by 3.56 fold and 2.9 fold respectively in the *foxp1a*$^{(-/-)}$*;foxp1b*$^{(-/-)}$ mutants **(Figure 3.18B)**. This demonstrates that the *foxp1a*$^{(-/-)}$*;foxp1b*$^{(-/-)}$ double mutants show similar levels of transcript degradation to the single mutants.

3.2.29 - *foxp1a*$^{(-/-)}$*;foxp1b*$^{(-/-)}$ mutants do not show genetic compensation

As reduction in levels of *foxp1a* and *foxp1b* could lead to genetic compensation, I also measured the levels of other *foxp* genes in the *foxp1a*$^{(-/-)}$*;foxp1b*$^{(-/-)}$ mutants. Using the RNA collected from the 5dpf embryos, levels of *foxp2, foxp3a, foxp3b* and *foxp4* were measured by RT-qPCR **(Figure 3.18C)**. It was found that none of the other *foxp* genes were upregulated in the *foxp1a*$^{(-/-)}$*;foxp1b*$^{(-/-)}$ mutants **(Figure 3.18C)**. This suggests that any phenotypes observed in the *foxp1a*$^{(-/-)}$*;foxp1b*$^{(-/-)}$ mutants will be due to a reduction in the levels of *foxp1a* and *foxp1b*, and not due to increased expression of other *foxp* genes.

3.2.30 - *foxp1a*$^{(-/-)}$*;foxp1b*$^{(-/-)}$ mutants have reduced levels of Foxp1 protein

To determine the likely severity of the *foxp1a*$^{(-/-)}$*;foxp1b*$^{(-/-)}$ mutants, I also checked to see if levels of Foxp1 protein were decreased in the mutants. To do this protein was extracted from the caudal fins of pools of 7 juvenile fish. The protein lysate was then run on a western blot and probed with antibodies against FOXP1 and ACTB **(Figure 3.18D)**. A strong band was found for Foxp1 at around 65 kDa in the *foxp1a*$^{(+/+)}$*;foxp1b*$^{(+/+)}$ sample. A much weaker band was found in the same position in the *foxp1a*$^{(-/-)}$*;foxp1b*$^{(-/-)}$ mutant sample, and levels of Foxp1 were found to be severely

reduced **(Figure 3.18D)**. This suggests that any phenotypes observed in the *foxp1a*$^{(-/-)}$;*foxp1b*$^{(-/-)}$ mutants are due to a reduction in Foxp1 protein levels.

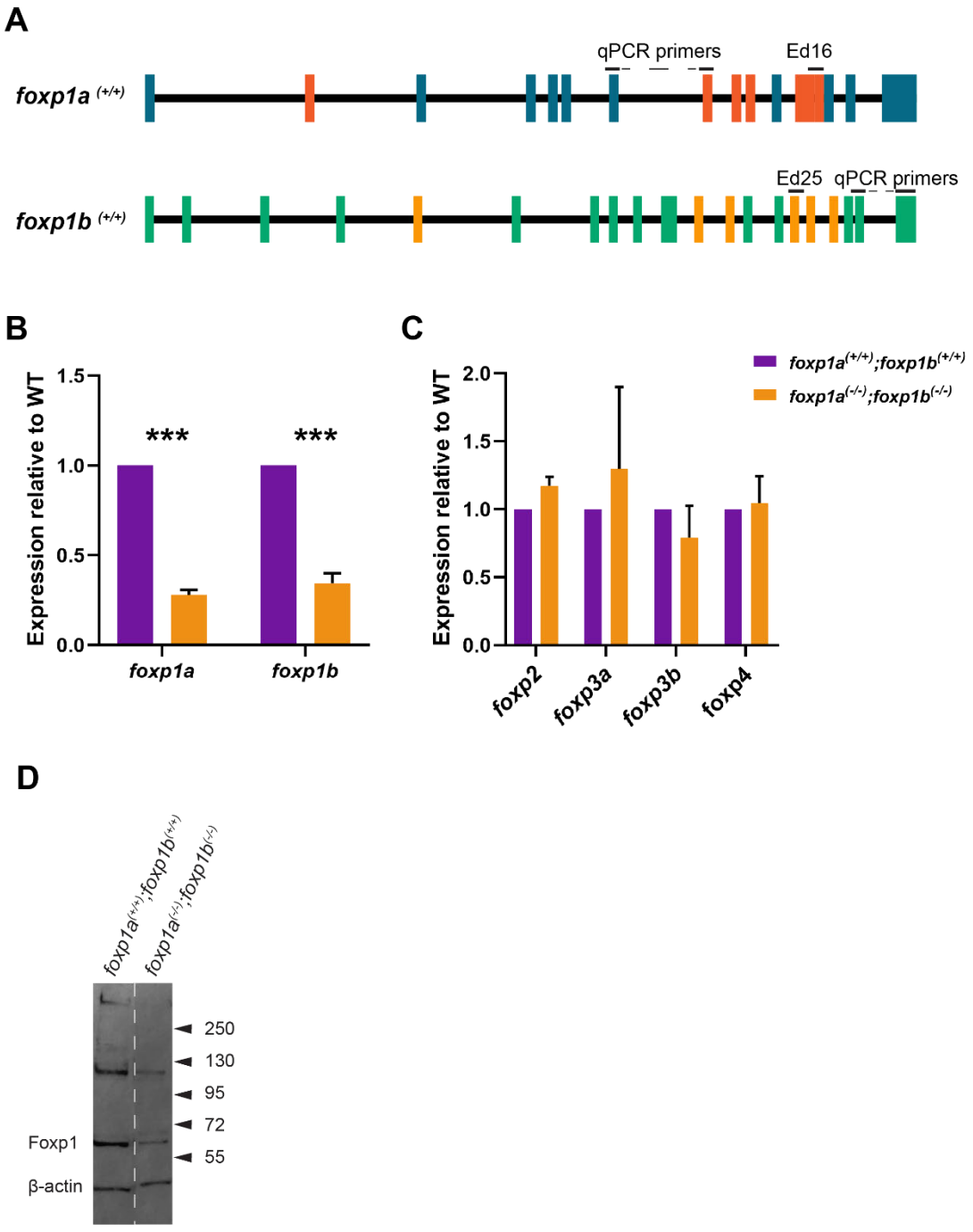

Figure 3.18 – levels of *foxp1* mRNA and Foxp1 protein are reduced in *foxp1a*$^{(-/-)}$*;foxp1b*$^{(-/-)}$ mutants and no genetic compensation is observed.

Figure 3.18 – levels of *foxp1* mRNA and Foxp1 protein are reduced in *foxp1a*$^{(-/-)}$*;foxp1b*$^{(-/-)}$ mutants and no genetic compensation is observed. A. Schematic showing the location of qPCR primers. The location of the ed16 and ed25 mutations are marked. Functional domains are shown in orange. **B.** n = 3 pools of 1-2 fish. Two tailed t-tests were performed, $p < 0.001$. Error bars show standard deviation. **C.** n = 2 pools of 1-2 fish. Two tailed t-tests were performed, no differences were significant. **D.** 20 minute exposure. Each lane contains protein from 7 fish. Dotted line shows where lanes have been removed.

3.2.31 - *foxp1a*$^{(-/-)}$*;foxp1b*$^{(-/-)}$ mutants have reduced levels of AT

To investigate my hypothesis with regards to the *foxp1a*$^{(-/-)}$*;foxp1b*$^{(-/-)}$ mutants, I first looked at levels of AT in the mutant fish. *foxp1a*$^{(-/-)}$*;foxp1b*$^{(-/-)}$ fish were raised until 30 dpf and then stained with Nile Red. Total AT area was then quantified and plotted relative to fish length. Similarly to the *foxp1b*$^{(-/-)}$ mutants *foxp1a*$^{(-/-)}$*;foxp1b*$^{(-/-)}$ mutants were found to be significantly smaller than their WT siblings **(Figure 3.19A & B)**. *foxp1a*$^{(-/-)}$*;foxp1b*$^{(-/-)}$ mutants were also found to have less AT relative to SL than their WT siblings **(Figure 3.19C)**. *foxp1a*$^{(-/-)}$*;foxp1b*$^{(-/-)}$ mutants were found to have reduced levels of AT when compared to *foxp1a*$^{(-/-)}$ and *foxp1b*$^{(-/-)}$ single mutants **(Figure 3.19D)**. These data support the hypothesis that *foxp1* is required for AT expansion.

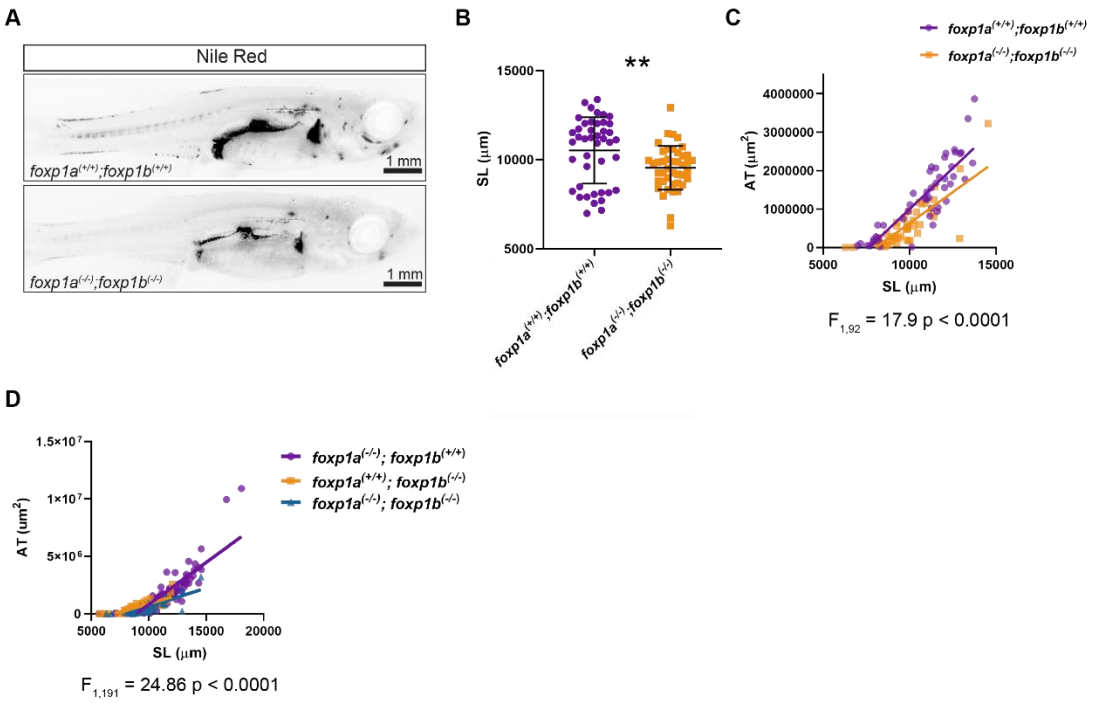

Figure 3.19 – *foxp1a*$^{(-/-)}$*;foxp1b*$^{(-/-)}$ mutants have reduced levels of AT. A. Representative Nile Red images. Nile Red staining shown in black. **B.** n = 43. Data from 3 experiments. Error bars show mean and standard deviation. A two tailed t-test was performed, p = 0.007. **C.** n = 43. Data from 3 experiments. An Ancova analysis was performed and the slope of the lines found to be significantly different, $F_{1,92} = 17.9$ $p < 0.0001$. **D.** n = 45-105. Data from 3 experiments. An Ancova analysis was performed and the slope of the lines found to be significantly different, $F_{2,191} = 24.86$ $p < 0.0001$.

3.2.32 - *foxp1a*$^{(-/-)}$*;foxp1b*$^{(-/-)}$ mutants have reduced levels of AT following a HFD

To further test my hypothesis, I placed the *foxp1a*$^{(-/-)}$*;foxp1b*$^{(-/-)}$ mutants on a HFD to stimulate adipose tissue expansion **(Figure 3.20A)**. *foxp1a*$^{(-/-)}$*;foxp1b*$^{(-/-)}$ mutant fish and WT siblings were raised until 5 weeks of age and then placed on a 2 week HFD, as described previously **(Figure 3.20A)**. Following the HFD, *foxp1a*$^{(+/+)}$*;foxp1b*$^{(+/+)}$ HFD fish were found to have significantly more AT than *foxp1a*$^{(+/+)}$*;foxp1b*$^{(+/+)}$ CD fish and this demonstrated that the HFD could induce significant AT expansion **(Figure 3.20B & C)**. *foxp1a*$^{(-/-)}$*;foxp1b*$^{(-/-)}$ HFD mutant fish were found to have slightly less total adipose tissue than WT siblings, though this difference was not significant **(Figure 3.20B & C)**. Similarly, when change in AT was calculated *foxp1a*$^{(-/-)}$*;foxp1b*$^{(-/-)}$ mutants were found to gain less AT than WT fish but again this was not significant **(Figure 3.20D)**. No significant differences were found between levels of VAT or SAT when comparing *foxp1a*$^{(-/-)}$*;foxp1b*$^{(-/-)}$ mutants to WT siblings **(Figure 3.20 E & F)**. In summary *foxp1a*$^{(-/-)}$*;foxp1b*$^{(-/-)}$ mutants seem to have a reduced response to a HFD, which supports the hypothesis that *foxp1* is required for AT expansion. The fact that the reduced response of the *foxp1a*$^{(-/-)}$*;foxp1b*$^{(-/-)}$ mutants to the HFD was not significant, could be explained by variations in the SL of fish of different genotypes and the implications of this will be expanded upon in the discussion.

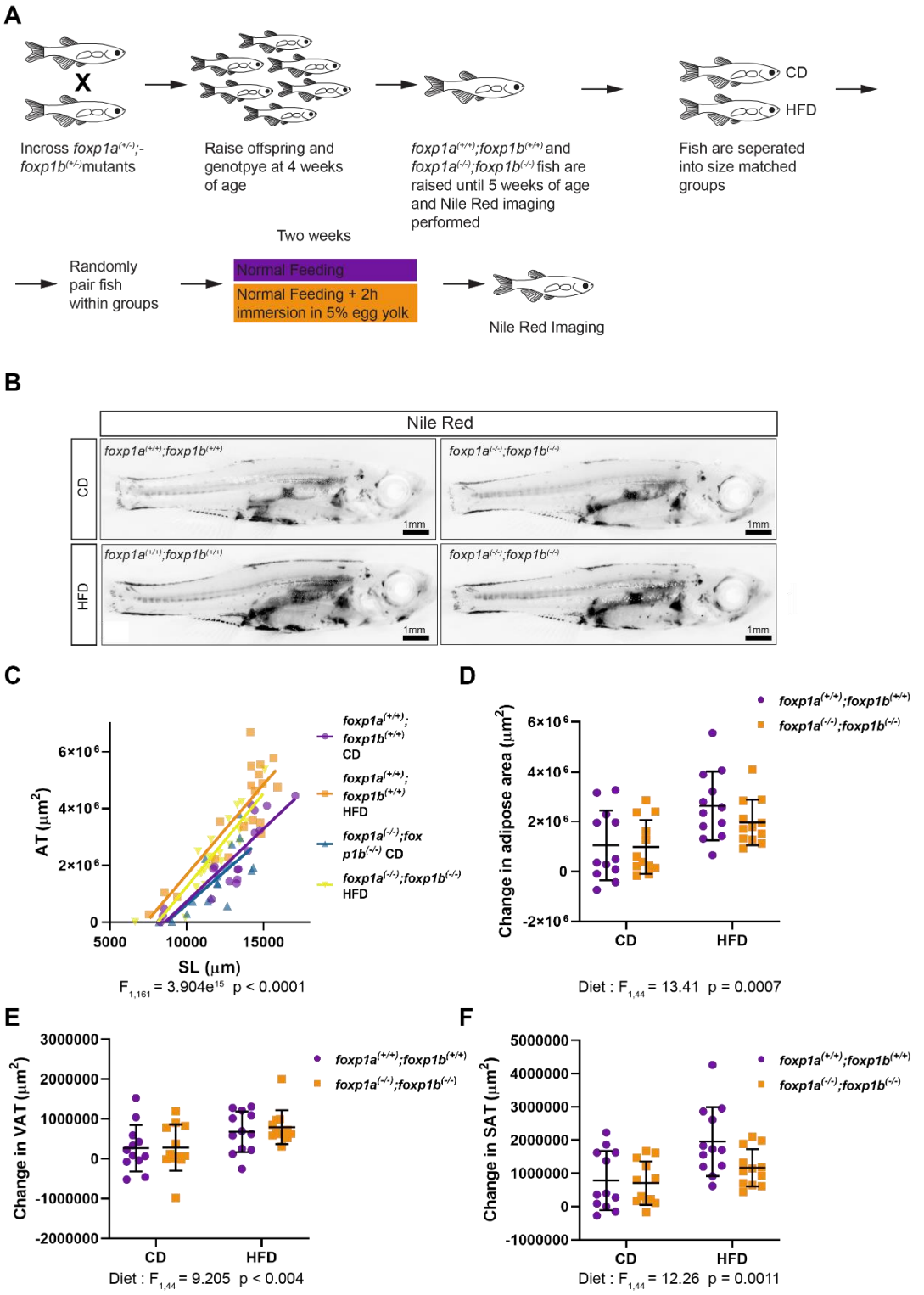

Figure 3.20 – *foxp1a*$^{(-/-)}$;*foxp1b*$^{(-/-)}$ mutants gain less AT in response to a HFD.

Figure 3.20 – *foxp1a*$^{(-/-)}$*;foxp1b*$^{(-/-)}$ mutants gain less AT in response to a HFD. A. Schematic of the HFD protocol. CD (Control Diet). HFD (High Fat Diet). **B.** Representative Nile Red images. Nile Red staining shown in black. **C.** n = 19-20 per group. Data from 3 experiments. An Ancova analysis was performed between *foxp1a*$^{(+/+)}$*;foxp1b*$^{(+/+)}$ CD and *foxp1a*$^{(+/+)}$*;foxp1b*$^{(+/+)}$ HFD groups, $F_{1,161} = 3.904e^{15}$ $p < 0.0001$. **D.** A two-way ANOVA was performed and the effect of diet was found to be significant, $F_{1,44} = 13.41$ $p = 0.0007$. **E.** A two-way ANOVA was performed and the effect of diet was found to be significant, $F_{1,44} = 9.205$ $p = 0.004$. **F.** A two-way ANOVA was performed and the effect of diet was found to be significant, $F_{1,44} = 12.26$ $p = 0.0011$. **D.E.F.** n = 12. Data from 3 experiments. Error bars show mean and standard deviation.

3.2.33 - *foxp1a*$^{(-/-)}$*;foxp1b*$^{(-/-)}$ mutants have a more hypertrophic adipose lipid droplet morphology

To determine whether the reduced AT expansion observed in *foxp1a*$^{(-/-)}$*;foxp1b*$^{(-/-)}$ mutants is accompanied by an altered mode of AT expansion, I next examined AT morphology. The PVAT depot was dissected from *foxp1a*$^{(-/-)}$*;foxp1b*$^{(-/-)}$ mutant and WT adult fish. The depot was then stained with lipidTOX and the whole depot imaged using confocal microscopy **(Figure 3.21A & B)**. Analysis of the lipid droplets showed that *foxp1a*$^{(-/-)}$*;foxp1b*$^{(-/-)}$ mutants had a more hypertrophic adipose morphology than WT siblings **(Figure 3.21C & D)**. The PVAT depot of *foxp1a*$^{(-/-)}$*;foxp1b*$^{(-/-)}$ mutants was found to have fewer lipid droplets, with greater average diameter **(Figure 3.21C & D)**. Due to the low sample size of this experiment statistical testing was not performed. These data suggest that adipose tissue expands by hypertrophic growth in *foxp1a*$^{(-/-)}$*;foxp1b*$^{(-/-)}$ mutants to a larger extent than in WT siblings.

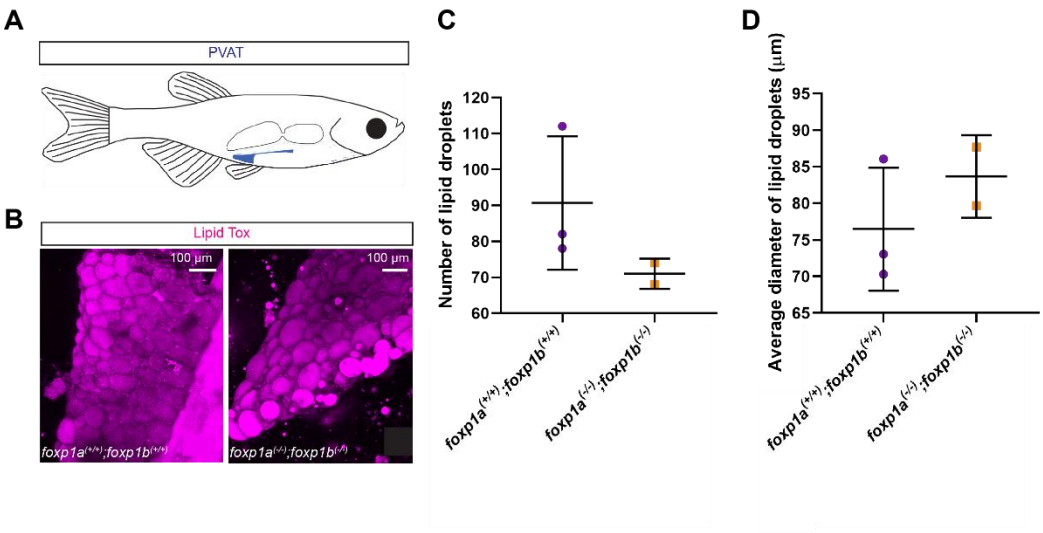

Figure 3.21 – *foxp1a*$^{(-/-)}$*;foxp1b*$^{(-/-)}$ mutants have a more hypertrophic adipose morphology. A. Schematic showing the location of the PVAT depot. **B.** Representative maximum intensity projections. The anterior end of the depot is to the right of the image **C.** n = 2-3. Error bars show mean and standard deviation. **D.** n = 2-3. Error bars show mean and standard deviation.

3.2.34 - *foxp1a*$^{(-/-)}$*;foxp1b*$^{(-/-)}$ mutants have increased levels of blood glucose

An inability of adipose tissue to expand can lead to ectopic lipid deposition and increased levels of lipid metabolites in the blood (Bluher, 2010). To test if the *foxp1a*$^{(-/-)}$*;foxp1b*$^{(-/-)}$ mutants have adipose tissue which is impaired in its ability to store lipid, I measured levels of blood metabolites. Adult fish were euthanised, blood extracted and levels of blood glucose, triglyceride and cholesterol were measured **(Figure 3.22A. B. & C)**. Levels of blood glucose were found to be increased in the *foxp1a*$^{(-/-)}$*;foxp1b*$^{(-/-)}$ mutants when compared to WT siblings, while levels of triglyceride and cholesterol were unchanged **(Figure 3.22A. B. & C)**. Due to the low sample size of the experiment no statistical tests were performed and further data is needed to determine if the observed increase in blood glucose is statistically significant. Overall the data suggests that metabolic health is decreased in *foxp1a*$^{(-/-)}$*;foxp1b*$^{(-/-)}$ mutants.

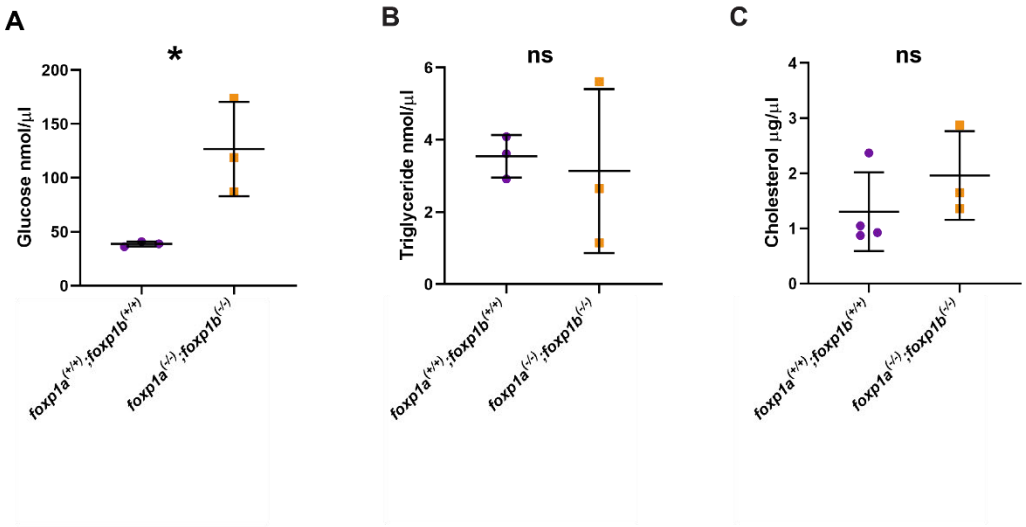

Figure 3.22 – *foxp1a*$^{(-/-)}$*;foxp1b*$^{(-/-)}$ mutants have increased levels of blood glucose. A. n = 3. A two tailed t-test was performed, p = 0.0255. **B.** n = 3. **C.** n = 3-4. **A.B. & C.** Error bars show mean and standard deviation.

3.3 - Discussion

To summarise, I have presented data which supports the hypothesis that *foxp1* is required for AT expansion **(Figure 3.23A)**. These data have allowed me to build models of how AT expansion is affected in each of the mutants described. For example, *foxp1a*$^{(-/-)}$ mutants have reduced levels of *foxp1a*, which results in normal levels of AT on a control diet but reduced AT expansion in response to a HFD **(Figure 3.23B)**. *foxp1a*$^{(-/-)}$ mutants specifically gain less SAT in response to a HFD and this depot was found to have a more hypertrophic morphology **(Figure 3.23B)**. In contrast *foxp1b*$^{(-/-)}$ mutants had reduced levels of *foxp1b*, which resulted in normal levels of AT on a control diet but reduced visceral AT expansion in response to a HFD **(Figure 3.23C)**. Overall data from *foxp1a*$^{(-/-)}$ and *foxp1b*$^{(-/-)}$ mutants support the proposed hypothesis that *foxp1* is required for AT expansion and suggest adipose tissue depot specific roles for *foxp1a* and *foxp1b*.

Data from the *foxp1a*$^{(-/-)}$*;foxp1b*$^{(-/-)}$ mutants is also supportive of a role for *foxp1* in adipose tissue expansion. *foxp1a*$^{(-/-)}$*;foxp1b*$^{(-/-)}$ mutants have reduced levels of *foxp1*, reduced levels of AT on a control diet and reduced AT expansion in response to a HFD **(Figure 3.23D)**. Furthermore, *foxp1a*$^{(-/-)}$*;foxp1b*$^{(-/-)}$ mutants also show signs of dysfunctional AT, with a more hypertrophic AT morphology and increased levels of blood glucose **(Figure 3.23D)**. Some of the data presented from the *foxp1a*$^{(-/-)}$*;foxp1b*$^{(-/-)}$ mutants, such as the response to the HFD, does not fully fit with the data presented from the single mutants. This is due to the fact that data from the *foxp1a*$^{(-/-)}$*;foxp1b*$^{(-/-)}$ mutants is preliminary and needs to be expanded upon. Increasing the sample sizes of the *foxp1a*$^{(-/-)}$*;foxp1b*$^{(-/-)}$ experiments will hopefully reduce the variation observed.

In this chapter I have identified *FOXP1* as a novel regulator of adipose levels. I have generated novel zebrafish *foxp1* mutants to investigate the hypothesis that *foxp1* is required for AT expansion. Using these mutants, I have found data consistent with my hypothesis and shown that loss of *foxp1* leads to reduced AT accumulation, a more hypertrophic adipose morphology and increased levels of blood glucose. In this section I will discuss the limitations of the data I have presented. A broader discussion detailing how this work fits into the existing literature and expanding on future directions can be found in the general discussion section (Chapter 6).

foxp1 was found to be expressed in the PVAT depot. However, due to the nature of the experiment performed more precise expression patterns could not be

determined. It is currently unclear if *foxp1* is expressed either in mature adipocytes or in adipocyte progenitors, as predicted. This is a major limitation as my hypothesis is that *foxp1* directly influences adipose progenitor behaviour. The role of *foxp1* in adipose progenitors is the major focus of chapter 4. Briefly I have generated a transgenic zebrafish line in which GFP is expressed exclusively in adipocytes and pre-adipocytes. The SVF of fish on the transgenic background could be isolated and GFP positive cells selected. *foxp1* expression in adipose progenitor cells could then be assessed.

Another limitation of the data presented is that all of the data comes from whole body *foxp1* mutants. *FOXP1* is known to be widely expressed in humans and therefore any phenotypes observed in the *foxp1* mutants may not be due to the effect of *foxp1* on adipose exclusively. For example, *Foxp1* is known to play a role in the liver and is involved in the regulation of glucose homeostasis (Zou et al., 2015). *Foxp1* inhibits gluconeogenesis in the liver and therefore loss of *foxp1* in the zebrafish mutants could result in increased glucose production and directly impact adipose phenotypes (Zou et al., 2015). One way to overcome this problem would be to create adipose tissue specific mutants. However, a simpler way to show that the phenotype of the *foxp1* mutants was caused by defects in adipose progenitor behaviour would be to grow those cells in culture. Comparing the proliferation and differentiation of adipose progenitor cells from *foxp1* mutants with those from WT siblings, would allow me to determine if there were any adipose autonomous effects of *foxp1* in the mutants.

Finally, the *foxp1* mutants I generated targeted the FHD of the Foxp1 protein rather than the translational start site. Although levels of Foxp1 are reduced in the zebrafish mutants some protein does still remain, and this leaves open the possibility that the mutant protein may have a function in the mutants. The Foxp1 protein contains a forkhead DNA binding domain, and a zinc finger protein-protein interaction domain. The presence of this protein-protein interaction domain allows FOXP1 to form heterodimers with other members of the FOXP family (Li et al., 2004). Therefore, the *foxp1a*$^{(-/-)}$ and *foxp1b*$^{(-/-)}$ mutants described may produce mutant Foxp1 proteins which are able to form heterodimers with other members of the Foxp family and alter the activity of these genes. Comparing the phenotype of *foxp1* mutants lacking a ZFD with those already examined could determine whether the phenotypes observed in

the *foxp1a*$^{(-/-)}$;*foxp1b*$^{(-/-)}$ mutants are the result of loss of *foxp1* function or due to the altered activity of other *foxp* family members.

In summary I have presented results which broadly agree with the hypothesis that *foxp1* maintains progenitor populations in adipose and is required for adipose tissue expansion. Here I have detailed the major limitations of the data I have presented, and a fuller discussion can be found in chapter 6. The results I have presented have not fully addressed the role of *foxp1* in progenitor cell maintenance and that is the focus of chapter 4.

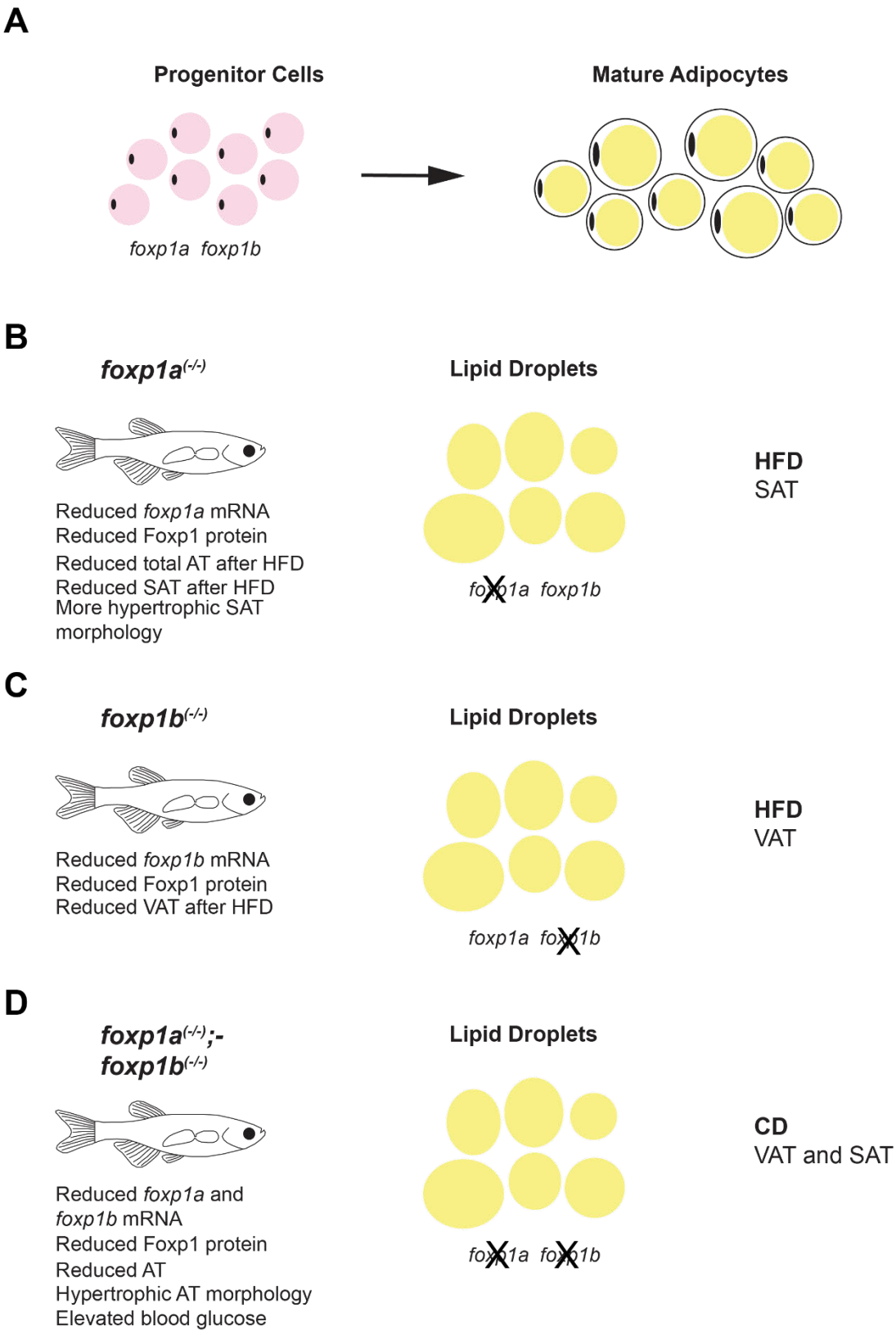

Figure 3.23 – *foxp1* is important in AT expansion.

Figure 3.23 – *foxp1* is important in AT expansion. A. Schematic showing how *foxp1* is hypothesised to maintain progenitor cells in AT. **B.** Summary of the *foxp1a*$^{(-/-)}$ mutant phenotype and a model of the effect loss of *foxp1a* is thought to have on AT. **C.** Summary of the *foxp1b*$^{(-/-)}$ mutant phenotype and a model of the effect loss of *foxp1b* is thought to have on AT. **D.** Summary of the *foxp1a*$^{(-/-)}$;*foxp1b*$^{(-/-)}$ mutant phenotype and a model of the effect loss of *foxp1a* and *foxp1b* has on AT expansion. CD (Control Diet). HFD (High Fat Diet).

Chapter 4 – *foxp1*a plays role in the control of the spatial expansion of LSAT

4.1 - Introduction

Obesity is known to be partially genetically regulated (Maes et al., 1997). However, the genetic regulation of obesity is poorly understood and a better understanding of how genes influence adipose tissue expansion is needed. One gene thought to play a role in adipose tissue expansion is *Foxp1*. *Foxp1* is a transcription factor which is known to promote the renewal of stem and progenitor cells from multiple compartments (Gabut et al., 2011, Li et al., 2017). For example, *Foxp1* has been shown to stimulate the expression of genes required for pluripotency and to repress the expression of genes required for the differentiation of embryonic stem cells (Gabut et al., 2011). Based on *Foxp1's* roles in proliferation and differentiation the hypothesis set out earlier in this thesis was that *Foxp1* maintains progenitor cell populations in adipose tissue and is required for adipose tissue expansion. Accordingly, genetic variation at the *FOXP1* locus is associated with BMI (Kichaev et al., 2019). In chapter 3 I have shown that loss of function *foxp1* mutant zebrafish have less AT than WT siblings, a more hypertrophic lipid droplet morphology within adipose and increased levels of blood glucose (Chapter 3.2). These data suggest that *foxp1* is required for AT expansion and specifically for hyperplastic AT expansion. However, my data in chapter 3 do not address the role of *foxp1* within adipose progenitor cells. Therefore, the aim of this chapter was to investigate the role of *foxp1* within adipose progenitor cells and to further understand the cellular and molecular mechanisms by which *foxp1* promotes adipose formation.

White adipose progenitor cells are fibroblast like cells which are capable of giving rise to mature lipid filled adipocytes (Hepler et al., 2017). Adipose progenitor cells were first described in 1969 by Hollenberg and Vost. The study used tritiated thymidine to measure DNA synthesis in WAT and found a progression of radioactivity from the SVF to mature adipocytes over time, therefore suggesting that adipocyte precursor cells in the SVF were differentiating into mature adipocytes (Hollenberg and Vost, 1969). Later experiments in the 1970's found that cells derived from the SVF of adipose tissue, and which initially resembled fibroblasts, were capable of accumulating triglycerides (Poznanski et al., 1973). Further studies went on to show that these fibroblast like cells go on to display the morphology of mature white adipocytes (Van et al., 1976). However, the fibroblast like cell population extracted from the SVF is heterogeneous and can also be induced to differentiate into osteoblasts, myoblasts and chondrocytes (Brzoska et al., 2005). Furthermore, cells

taken from the SVF can also show variable rates of adipogenesis (Cawthorn et al., 2012). The establishment of clonal preadipocyte cell lines has produced cells which show very high rates of adipogenesis, with the murine 3T3-L1 cell line being the most widely used (Green and Kehinde, 1976). The 3T3-L1 cell line is a preadipocyte cell line which undergoes synchronous differentiation in response to a hormonal cocktail (Green and Kehinde, 1976). The use of lines such as the 3T3-L1 line has allowed much of the molecular control of adipocyte differentiation to be uncovered (Lefterova and Lazar, 2009, Lowe et al., 2011). However, while facilitating the discovery of many aspects of adipogenesis, preadipocyte cell lines do not allow for the *in vivo* study of adipose progenitors.

Study of adipose progenitor cells *in vivo* is important as freshly isolated adipose progenitor cells have been shown to express different cell surface markers than cells in culture (Varma et al., 2007). This suggests that adipose progenitor cells *in vitro* may not behave in the same manner as those *in vivo* and highlights the importance of *in vivo* studies. Much work has been done to determine the *in vivo* origins and nature of adipocyte progenitor cells. For example, Rodeheffer et al (2008) used FACS (Fluorescence activated cell sorting) sorting to sort cells from adipose SVF and determined the nature of cells which give rise to mature adipocytes. It was found that CD29 (integrin beta 1) and CD34 positive cells had high adipogenic potential, with CD29 and CD34 both being expressed by several stem cell populations (Rodeheffer et al., 2008). The adipose progenitor cell population was further refined and a CD31 (Platelet endothelial cell adhesion molecule), CD45 (Protein tyrosine phosphatase receptor type C) and Ter119 negative population and CD29, CD34, Sca1 (Ataxin 1), CD24 positive population was found to have a high adipogenic potential (Rodeheffer et al., 2008). The adipose progenitor cells isolated by FACS were also found to be capable of differentiating into adipocytes *in vivo* (Berry and Rodeheffer, 2013). As the FACS based method of defining the adipose progenitor cell population requires multiple markers, multiple studies have employed lineage tracing methods to identify adipose progenitor cells *in vivo* (Jiang et al., 2017, Tang et al., 2008, Vishvanath et al., 2016). Using lineage tracing *Pdgrfa* (Platelet derived growth factor receptor alpha) was found to be expressed by preadipocytes but not adipocytes (Berry and Rodeheffer, 2013). Preadipocytes have also been shown to express *Pdgfrb, Pparg* and *Zfp423* (Zinc finger protein 423) (Tang et al, 2008, Vishvanath et al., 2016). Further lineage tracing suggested that endothelial cells may give rise to adipocytes (Tran et al., 2012). However, a later study found that the expression

reported by Tran et al (2012) was likely to come from blood vessels closely associated with adipocytes and not from adipocytes themselves (Berry and Rodeheffer, 2013). Tang et al (2008) used genetically marked mice to determine that adipose progenitors reside in the mural compartment of the adipose vasculature. Later work also showed that these cells reside in a niche, initially located distal to the blood vessel and occupying a mural perivascular position later in adipose depot development (Jiang et al., 2014). Finally, it was shown that both *Pdgfrb* and *Vegf* (Vascular endothelial growth factor) are required for the maintenance of adipose progenitor cells within the perivascular niche (Jiang et al., 2017). Overall adipose progenitor cells can be identified *in vivo* through the use of multiple markers however the nature of the *in vivo* models employed means that adipose progenitors cannot be imaged in live animals.

As adipose progenitor cells have been increasingly studied it has become apparent that heterogeneity within this population exists. Jiang et al (2014) used lineage tracing in mice to report that two populations of adipose progenitor cells exist, developmental progenitors which are required for adipose organogenesis and adult progenitors which are required for adipose homeostasis. More recent work has used single cell RNA-Seq to divide adipose progenitors into even more populations (Schwalie et al.,2018, Hepler et al., 2018, Sempere et al,2014). Schwalie et al (2018) used single cell RNA-Seq to identify multiple populations of adipose progenitor cells and found one population to be capable of inhibiting adipocyte differentiation. Meanwhile another study used the same method to identify three adipose progenitor cell populations which gave rise to adipocytes with differing rates of lipolysis (Raajendiran et al., 2019). Finally, Hepler et al (2018) also used single cell RNA-Seq to identify multiple adipose progenitor cell populations, one of which showed pro-inflammatory characteristics. Together this highlights the heterogeneity of adipose progenitor cells. However, nearly all of these studies have relied on the culturing of adipose progenitor cells *in vitro* and do not allow for the imaging of adipose progenitor cells *in vivo* in live animals.

Zebrafish are a useful model organism and are especially well suited to *in vivo* imaging. Zebrafish are optically transparent from fertilization however pigment in the skin develops soon after (Flynn et al., 2009). Mutant zebrafish which lack pigment exist and this allows for the imaging of developmental processes, including adipose tissue formation and growth (Flynn et al., 2009). Lipid dyes can be used to stain adipose tissue in zebrafish and real time imaging of adipose tissues is also possible

(Flynn et al., 2009). However adipose progenitor cells, which lack any lipid, cannot currently be visualised. Many transgenic reporter zebrafish lines exist, including those which mark the vasculature and immune cells (Rafferty and Quinn, 2018). However, a transgenic line which marks adipocytes or adipose progenitor cells does not exist in zebrafish. Therefore, the aim of this chapter is to develop a method for imaging adipose progenitor cells in zebrafish to further investigate the hypothesis that *foxp1* maintains progenitor cell populations in adipose tissue and is required for adipose tissue expansion.

In this chapter I have generated a new transgenic line that enables, for the first time, zebrafish adipocytes and adipose progenitors to be visualised. I use this new transgenic line to map adipose tissue expansion in zebrafish and show that LSAT (Lateral subcutaneous adipose tissue) expands via steady hypertrophic growth with bursts of hyperplastic growth. I have also built a model of spatial LSAT expansion and have shown that LSAT expands first by adding new adipocytes to the centre of the depot and then by forming chains of adipocytes which branch away from the main LSAT body. I then show that rates of hyperplastic and hypertrophic LSAT expansion are unaltered in *foxp1a*$^{(-/-)}$ and *foxp1b*$^{(-/-)}$ mutants during normal development. However, *foxp1a*$^{(-/-)}$ mutants do show an altered spatial expansion of LSAT. Overall, I have compiled novel data on LSAT expansion in zebrafish and have found data which suggests that *foxp1a* is required for normal LSAT expansion.

4.2 - Results

4.2.1 – A candidate enhancer, thought to be active during adipogenesis, was identified using published DNase-Seq data

In order to generate a transgenic line which marks adipocytes and adipocyte progenitors, I first identified putative enhancer elements which might be capable of driving GFP expression in adipose. Zebrafish transgenic lines can be created through the use of enhancers linked to minimal promoters, which are then inserted into the zebrafish genome through the use of the Tol2 transposase (Rafferty and Quinn, 2018). To identify potential enhancers, I used data from a study by Siersbaek et al (2011). Siersbaek et al (2011) induced adipogenesis in the murine 3T3-L1 cell line and then performed DNase-Seq at four different timepoints. 34,269 DNase hypersensitive sites were identified, which were then divided into four profiles (Siersbaek et al., 2011). The first profile was characterised by sites which opened early in adipogenesis and remained open (Siersbaek et al., 2011). The second and third profiles were characterised by sites which opened and closed transiently during adipogenesis, at 4 hours and 24 hours respectively (Siersbaek et al., 2011). The fourth profile was characterised by sites which opened late in adipogenesis and remained open (Siersbaek et al., 2011). As *foxp1* was shown in Chapter 3 to be required for AT expansion, I looked around the *Foxp1* locus for DNase hypersensitive sites (DHS). Two DHS sites were found at the mouse *Foxp1* locus **(Figure 4.1A)**.

As the DHS sites identified by Siersbaek et al (2011) were discovered in a mouse cell line, conservation to zebrafish was next examined. Zebrafish conserved non-coding elements (CNEs), which were conserved to mouse, have been described by Hiller et al **(Figure 4.1A)** (Hiller et al., 2013). The study designed a comparative genomics framework to align isolated genomes, such as the zebrafish genome, with the mouse and human genome and identify CNEs (Hiller et al., 2013). When the two mouse DNase hypersensitive sites were examined only one was found to be conserved to zebrafish **(Figure 4.1A).** This site, which is located within intron 1 of *Foxp1,* is potentially active due to its DNase hypersensitivity and is conserved to zebrafish. This site is now referred to as CNE450. Therefore, CNE450 within intron 1 of *Foxp1* was focused on.

4.2.2 – The CNE in intron 1 of *Foxp1* has activity in adipocytes and adipose progenitors

CNE450 within intron 1 of *Foxp1* is found on chromosome 6 at position 99,466,614-99-747-342 **(Figure 4.1A)**. The CNE is a 385bp element and contains multiple predicted transcription factor binding sites **(Figure 4.1A & B)**. Using MatInspector it was found that the 385bp element contains predicted transcription factor binding sites for five different factors, including the known regulators of adipogenesis *Cebpa*, *Cebpb*, and *Cebpd* **(Figure 4.1B)**. Predicted binding sites for *Hoxa5* (Homeobox A5) and *Nr3c1* (Nuclear Receptor subfamily 3 Group C member 1) were also found **(Figure 4.1B)**. Two zebrafish CNEs are found at CNE450, a 40bp CNE and a 130bp CNE, and both contain predicted transcription factor binding sites **(Figure 4.1B)**. The zebrafish 40bp region contains six predicted binding sites, including for *cebpa, cebpb* and *cebpd* and the 130bp region contains 30 predicted binding sites, again including sites for *cebpa, cebpb* and *cebpd* **(Figure 4.1B)**.

To determine if CNE450 could drive GFP expression in adipose a reporter construct was generated. The CNE was PCR amplified from mouse genomic DNA and cloned into an expression vector. The expression vector contained the CNE, a cFOS minimal promoter and eGFP, flanked by two Tol2 sites. This construct was then injected, along with Tol2 mRNA, into the zebrafish embryo at the one cell stage. Following outcrossing, F2 fish were identified with GFP expression exclusively in adipose tissue. Together this demonstrates that the CNE element at *Foxp1* can drive GFP expression in adipose tissue. The zebrafish elements were also tested for enhancer activity but neither element was capable of driving GFP activity in adipose (data not shown). A combination of both zebrafish elements was also not able to drive GFP activity in adipose (data not shown). In summary, CNE450 can drive GFP expression in adipose.

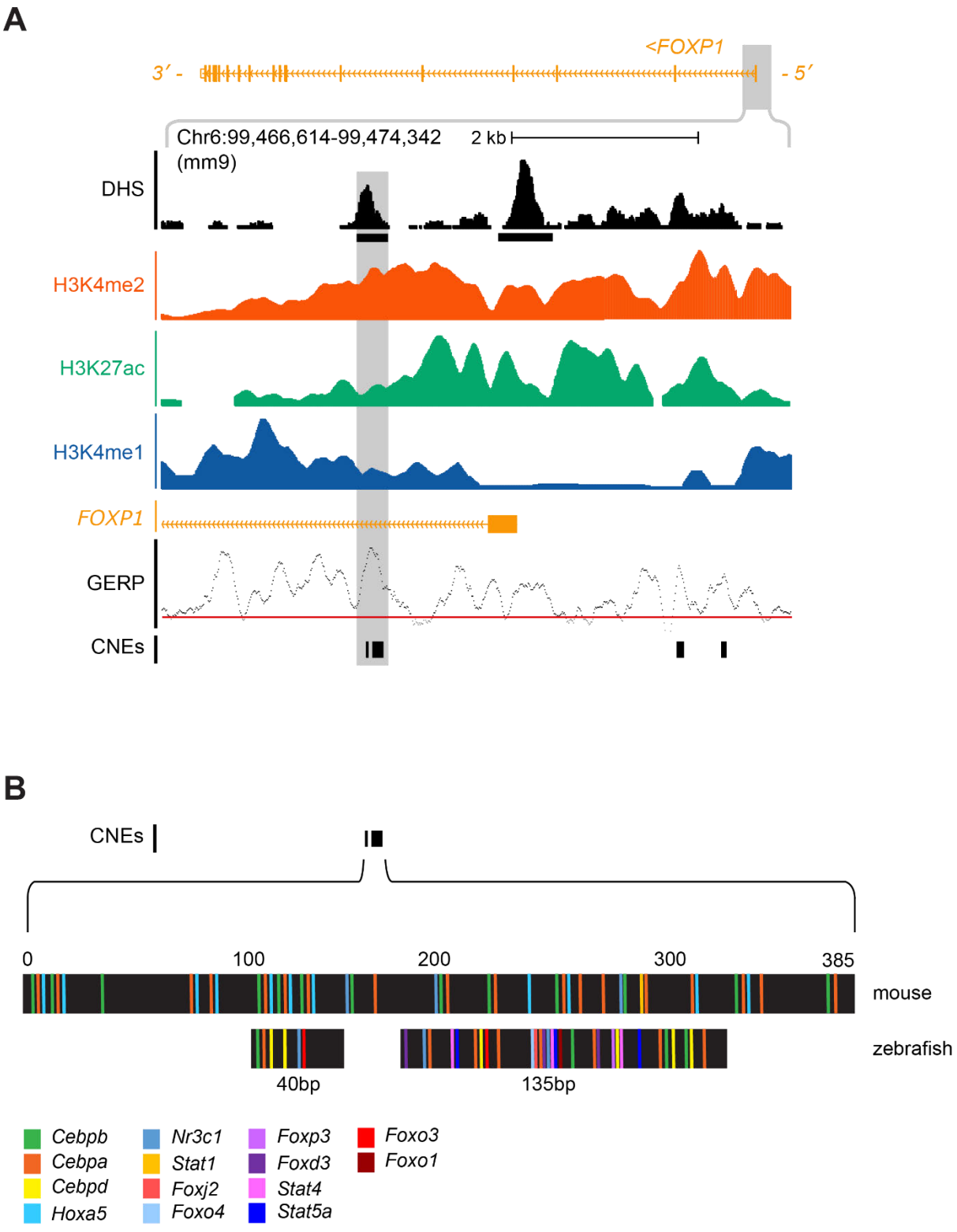

Figure 4.1 – A conserved enhancer element is present at the *Foxp1* locus.

Figure 4.1 – A conserved enhancer element is present at the *Foxp1* locus. A. Schematic showing the enhancer found in intron 1 of the mouse *Foxp1* gene. DHS (DNase hypersensitive sites), and histone modifications are shown. GERP (Genome evolutionary rate profiling) identifies conserved regions of the genome, with a peak indicating conservation. **B.** Schematic showing the enhancer within intron 1 of *Foxp1*. The two regions conserved to zebrafish are also shown. The numbers show the size of the enhancer in base pairs. The coloured lines show the predicted transcription factor binding sites (MatInspector).

4.2.3 – GFP expression in the *Foxp1:eGFP* transgenic line is restricted to regions in which AT depots are known to form and the timing of GFP expression coincides with AT development.

The expression pattern of CNE450, now referred to as *Foxp1:eGFP*, was next examined. *Foxp1:eGFP* fish were imaged under a stereomicroscope and whole body GFP expression was assessed in fish of different stages **(Figure 4.2A)**. Adipose development has been fully mapped in zebrafish, with 34 regionally distinct adipose depots described in the adult fish (Minchin and Rawls, 2017). The first depot known to form is the PVAT depot (Pancreatic visceral AT) at around 4.2 mm SL, and this depot is found close to the pancreas (Minchin and Rawls, 2017). GFP expression in the *Foxp1:eGFP* line was therefore examined in fish larger than 4.2 mm SL. GFP expression in fish of over 4.2 mm SL was found localised to the PVAT depot, with this group of cells going on to show the same saucepan like morphology as has been described of the PVAT depot in older fish **(Figure 4.2A)** (Minchin and Rawls, 2017). The appearance of GFP expression at the anatomical location of previously described adipose depots and at the developmental stage described was observed for all adipose depots in the *Foxp1:eGFP* line (Minchin and Rawls, 2017). Examples of this include GFP expression in the adipose depots found in the head of zebrafish **(Figure 4.2B)**. Minchin and Rawls (2017) have described three adipose depots in the head, which are visible from around 6.6 mm SL. These adipose depots are found close to the operculum (OPC), the eye (OCU) and the hyoid apparatus (HYD) and GFP expression in the *Foxp1:eGFP* line was found in all these locations **(Figure 4.2B)** (Minchin and Rawls, 2017). Another example concerns the LSAT depot, with GFP expression observed at the location of this depot in *Foxp1:eGFP* fish **(Figure 4.2B)**. The LSAT depot has been shown to appear at 8.2 mm SL and runs laterally along the trunk of the zebrafish at the horizontal myoseptum, with expansion primarily along the anterior posterior axis (Minchin and Rawls, 2017). The LSAT depot also appears to be constrained by somite boundaries (Minchin and Rawls, 2017). The first GFP expression at the LSAT depot in the *Foxp1:eGFP* line occurs at around 8.2 mm SL and matches the previously described stage of LSAT development **(Figure 4.2B)**. Furthermore, the group of cells marked by GFP in the *Foxp1:eGFP* line also have the same morphology as described of the LSAT depot **(Figure 4.2B)**. As a final example, AT depots described in the caudal fin show corresponding GFP expression in the *Foxp1:eGFP* line **(Figure 4.2A & B)**. Three AT depots are found in the caudal fin, the DSAT (dorsal SAT), VSAT (ventral SAT) and CFRSAT (caudal fin ray SAT) depots

(Minchin and Rawls, 2017). DSAT is the first depot to form at around 9.5 mm SL and is found in a long thin streak along the dorsal trunk **(Figure 4.2A & B)** (Minchin and Rawls, 2017). VSAT is found from 9.8 mm SL and is found in a long thin streak between the anal fin and caudal fin **(Figure 4.2B)** (Minchin and Rawls, 2017). CFRSAT is formed at 10.8 mm SL and extends across the dorsal ventral axis connecting the DSAT to the VSAT **(Figure 4.2B)** (Minchin and Rawls, 2017). The presence of these depots close to the caudal fin is marked by GFP expression in the *Foxp1:eGFP* line and the appearance of GFP matches the timing of the appearance of these depots **(Figure 4.2B)**. Overall the *Foxp1:eGFP* line appears to have expression exclusively within adipose tissue and appears to mark all AT depots in zebrafish.

4.2.4 – The *Foxp1:eGFP* transgenic line labels both adipocytes and adipose progenitor cells

In order to determine which cell types within adipose tissue showed GFP expression in the *Foxp1:eGFP* line, further imaging at higher magnification was performed **(Figure 4.2B)**. When adipose depots in the tail, head and along the flank of the fish were imaged it became apparent that GFP was being expressed by cells which resembled adipocytes **(Figure 4.2B)**. The cells labelled by GFP were generally found to be large, spherical, and with a large space in the centre unlabelled by GFP **(Figure 4.2B)**. The large space is suggestive of the lipid droplet found within adipocytes and this morphology is the classic morphology of a white adipocyte **(Figure 4.2B)**. To determine if these cells were indeed adipocytes, *Foxp1:eGFP* fish were incubated with LipidTOX which marks the neutral lipid found within adipocytes **(Figure 4.2C)**. The LSAT depot was then imaged using confocal microscopy **(Figure 4.2C)**. The LSAT depot was chosen for its location just below the surface of the skin, which allows this depot to be imaged through the skin of live fish **(Figure 4.2C)**. Nearly all GFP positive cells were stained by LipidTOX, indicating that the cells are indeed adipocytes **(Figure 4.2C)**. The only exceptions were a few GFP positive cells which remained unstained and which were much smaller than those stained by LipidTOX **(Figure 4.2C)**. These GFP positive, LipidTOX negative cells were much more fibroblast like in shape and were long and thin **(Figure 4.2C)**. These cells were hypothesised to be adipose progenitor cells **(Figure 4.2C)**. Later time course imaging, which followed the same fish over multiple consecutive days, has suggested that the

hypothesised adipose progenitors do go on to become mature lipid filled adipocytes and are in fact adipose progenitor cells **(Figure 4.5B)**. Taken together this imaging shows that the *Foxp1:eGFP* line marks adipocytes and adipose progenitor cells, and can be used to image both in the LSAT of live fish.

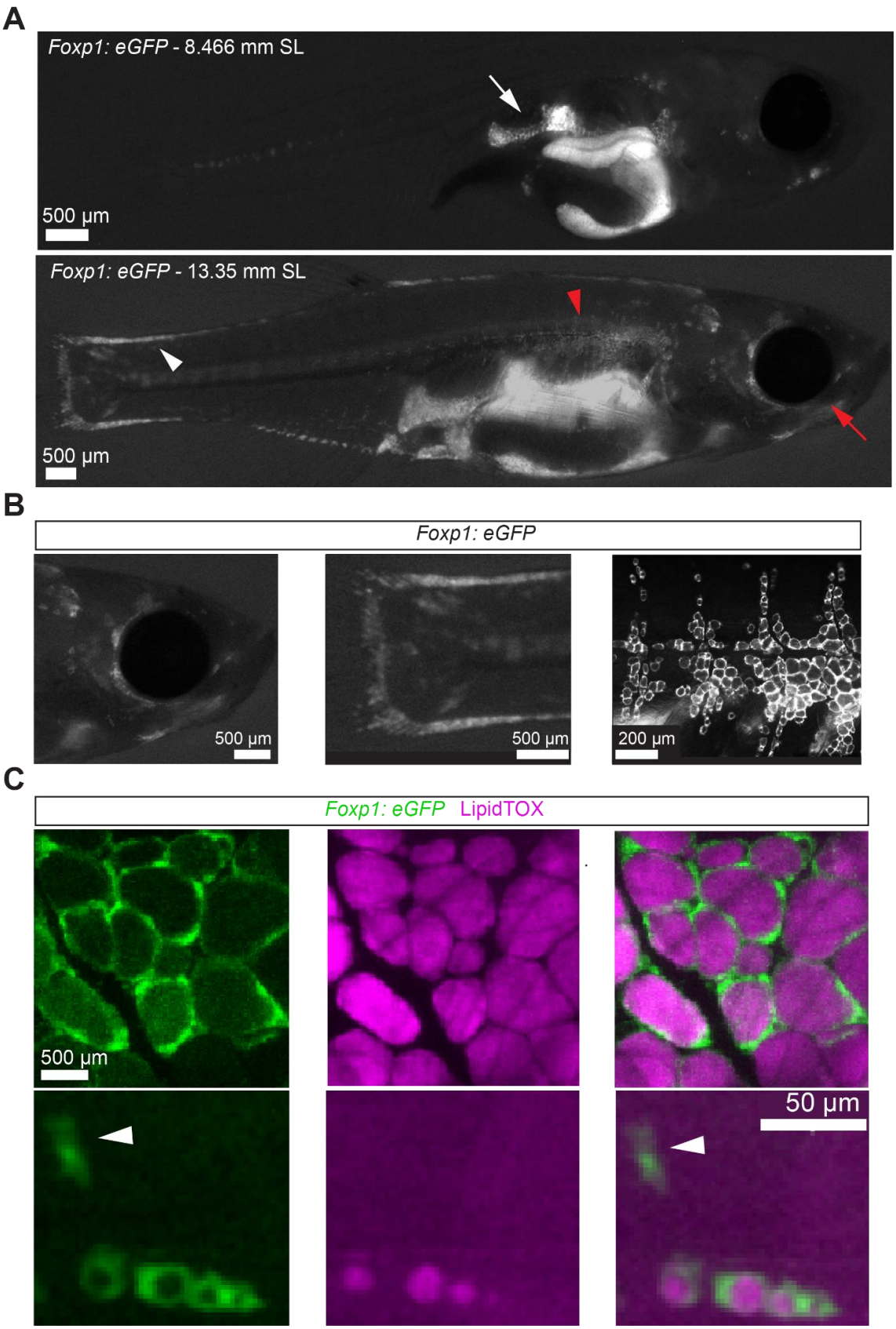

Figure 4.2 – *The Foxp1:eGFP* line has activity in both adipocytes and adipose progenitor cells.

Figure 4.2 – *The Foxp1:eGFP* line has activity in both adipocytes and adipose progenitor cells. A. Fluorescence stereomicroscope images showing GFP expression in the whole fish. GFP expression appears to be confined to adipose tissue and appears to be expressed by all adipose depots. Increased GFP expression and increased levels of adipose tissue can be observed in the larger fish, in the lower panel. The white arrow shows the PVAT depot. Arrows and arrow heads show the locations of the adipose depots highlighted in section B. The white arrow head shows AT depots in the caudal fin. The red arrow head shows the LSAT depot and the red arrow shows AT depots in the head. **B.** Fluorescence stereomicroscope images. GFP expression is found at the location of known adipose depots and in large cells resembling adipocytes. From left to right, GFP expression in the head, tail and body of the fish. **C.** Confocal Z stacks presented as maximum intensity projections showing that GFP is expressed by adipocytes and preadipocytes. The large GFP positive cells are stained by LipidTOX and are shown to contain neutral lipid. GFP positive, lipid negative cells are highlighted by the arrow heads in the lower panel and are believed to be adipose progenitor cells. The adipose progenitor cells have a more fibroblast like morphology than the mature adipocytes. The LSAT depot is shown in both images and the anterior end of the LSAT is found to the right of the images.

4.2.5 - Adipocyte number, adipocyte progenitor number and average lipid droplet area all show a positive correlation with standard length

Having determined that the *Foxp1:eGFP* line can be used to image LSAT growth in live fish, I next wanted to examine the cellular dynamics of LSAT expansion. In order to do this I imaged LSAT at different timepoints during zebrafish development **(Figure 4.3A)**. LSAT first develops at 8.2 mm SL (Minchin and Rawls, 2017). I therefore raised a clutch of *Foxp1:eGFP* fish to approximately 8.2 mm SL, removed 5 fish, stained the fish with LipidTOX and imaged the LSAT of each fish **(Figure 4.3A)**. I then removed an additional 5 fish every 8 days and repeated the imaging process, in order to obtain fish at a range of sizes **(Figure 4.3A)**. At each timepoint I measured the SL of each fish and this was shown to increase across the timepoints, demonstrating that the fish were growing between each timepoint **(Figure 4.3B & C)**. In addition I measured the number of adipocytes, defined as cells which are both GFP positive and LipidTOX positive, and the number of adipose progenitor cells, defined as cells which are GFP positive but LipidTOX negative. The lipid droplet area of each cell was also quantified. I found that the number of adipocytes per LSAT showed a strong positive correlation to SL, therefore adipocyte number increases as zebrafish grow **(Figure 4.3D & E)**. I also found adipose progenitor number to be positively correlated with SL, demonstrating that the number of adipose progenitors increases as fish grow **(Figure 4.3F & G)**. Finally, I found that average lipid droplet area is positively correlated with SL and this shows that LSAT expands by hypertrophic growth as the fish grows **(Figure 4.3H & I)**. Overall, these data demonstrate that as zebrafish grow the number of adipocytes and adipose progenitor cells within LSAT increases and so does the average lipid droplet area of adipocytes.

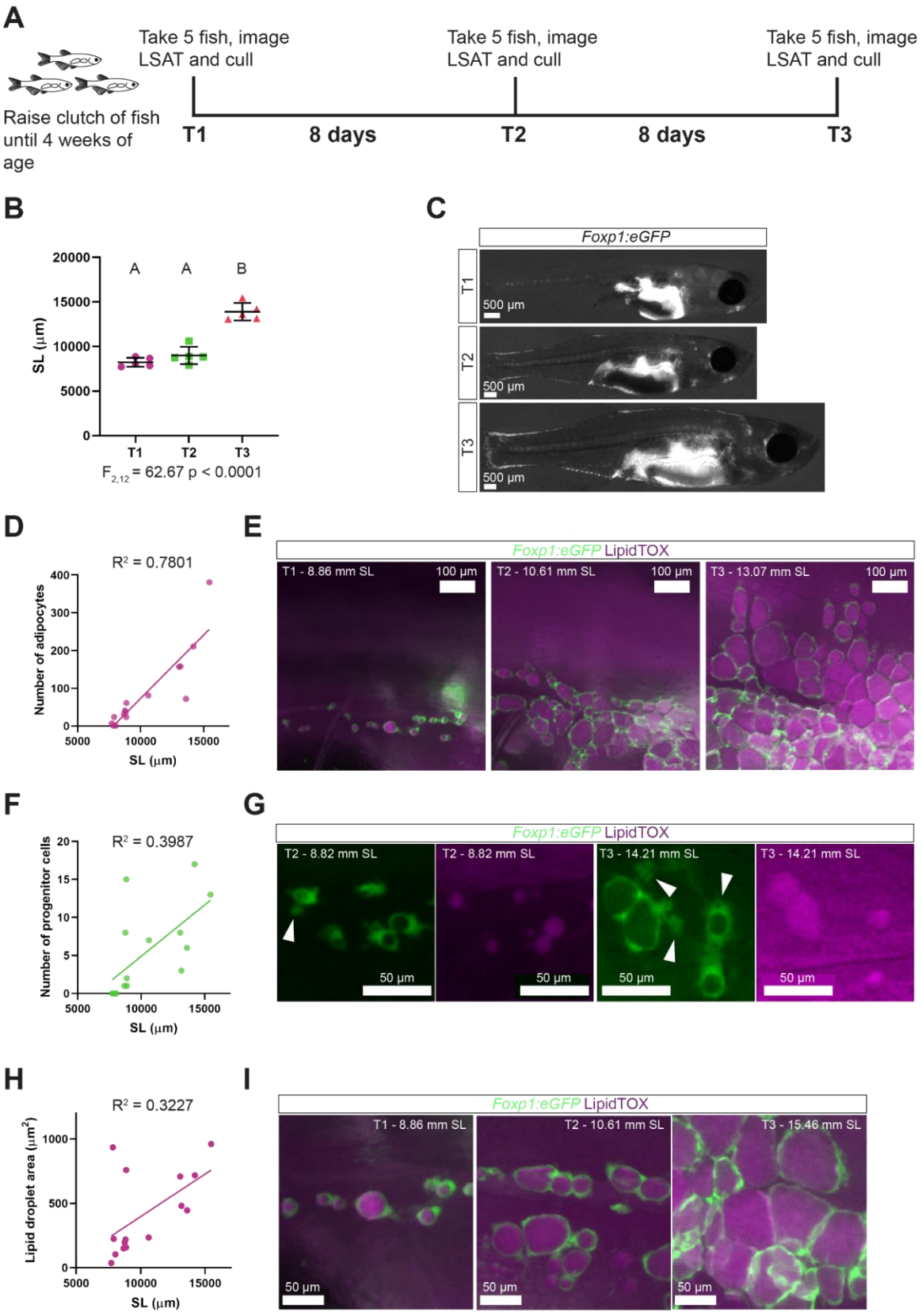

Figure 4.3 - Adipocyte number, adipocyte progenitor number and average lipid droplet area all show a positive correlation with standard length.

Figure 4.3 - Adipocyte number, adipocyte progenitor number and average lipid droplet area all show a positive correlation with standard length. A. Schematic showing the experimental protocol. T1 (Timepoint 1). **B.** Graph showing SL of fish across the experimental timepoints. n = 15. Error bars show mean and standard deviation. A one way ANOVA was performed and the difference between the groups was found to be significant $F_{2,12} = 62.67$ $p < 0.0001$. A post hoc Tukey's multiple comparison was performed, T1 vs T2 $p = 0.3626$. T1 vs T3 $p < 0.0001$. T2 vs T3 $p < 0.0001$. Letters signify differences between groups, different letters indicate significant differences between groups and the same letters indicate no difference. **C.** Fluorescence stereoscopic images of whole fish, showing increased SL across the timepoints. T1 (Timepoint 1). **D.** Scatter graph showing relationship between SL and number of adipocytes. $R^2 = 0.7801$. n = 15. The slope of the line is significantly non zero $F_{1,13} = 46.11$ $p < 0.0001$. **E.** Representative maximum intensity projections of LSAT from each timepoint. All images were taken from the anterior end of the LSAT. The anterior end of the LSAT is to the right of the image. T1 (Timepoint 1). **F.** Scatter graph showing relationship between SL and number of adipose progenitor cells. $R^2 = 0.3987$. n = 15. The slope of the line is significantly non zero $F_{1,13} = 8.619$ $p = 0.0116$. **G.** Representative maximum intensity projections of LSAT showing the presence of adipose progenitor cells. Adipose progenitor cells are defined as GFP positive, lipid negative cells. White arrow heads highlight progenitor cells. Images were taken from the posterior end of the LSAT, the anterior end of the LSAT is to the right of the images. **H.** Scatter graph showing relationship between SL and average lipid droplet area. $R^2 = 0.3227$. n = 15. The slope of the line is significantly non zero $F_{1,13} = 6.192$ $p = 0.0272$. **I.** Representative maximum intensity projections showing increased area of lipid droplets across the timepoints. Images were taken from the anterior end of LSAT, the anterior end of the LSAT is to the right of the images.

4.2.6 - New cells appear most often at the centre of the LSAT depot

In addition to examining the cellular dynamics of LSAT expansion, I also wanted to examine the spatial expansion of LSAT. The LSAT depot is a long thin adipose depot which runs horizontally along the zebrafish at the horizontal myoseptum (Minchin and Rawls, 2017). Expansion occurs primarily along the anterior-posterior axis however expansion also occurs along the dorsal-ventral axis to produce a long thin depot (Minchin and Rawls, 2017). In order to better understand the spatial expansion of LSAT, I wanted to determine how expansion across these axes occurred. To do this I performed two timecourse experiments and measured the locations in which new cells were added to LSAT. *Foxp1:eGFP* fish were raised until approximately 15 mm SL for experiment 1 and 11 mm SL for experiment 2 **(Figure 4.4A)**. The fish were then stained with lipidTOX, and the LSAT depot imaged under a stereomicroscope **(Figure 4.4A)**. The fish were recovered and the imaging repeated every 24 hours, over the course of 3 or 5 days **(Figure 4.4A)**. This allowed LSAT expansion in individual fish to be tracked. To examine LSAT expansion along the anterior-posterior axis I divided the LSAT of each fish into 3 equally sized sections along this axis **(Figure 4.4 B.C. & D)**. I then quantified the number of new cells added to each section of LSAT between each timepoint **(Figure 4.4B. C. & D)**. I found that cells were most often added to the middle of the LSAT depot, suggesting the LSAT first grows by adding cells to the centre of the depot **(Figure 4.4B.C. & D)**. I also examined LSAT expansion along the dorsal-ventral axis **(Figure 4.4E & F)**. The middle region of LSAT was defined as a region which extended two adipocytes dorsal of the horizontal midline of the LSAT and two adipocytes ventral **(Figure 4.4E & F)**. The dorsal region was found above the middle region and the ventral region below **(Figure 4.4E & F)**. When the appearance of new cells was quantified, it was found that most cells were added to the middle region **(Figure 4.4E & F)**. Taken together these data suggest that LSAT first expands by adding new adipocytes to the centre of the depot **(Figure 4.4L)**.

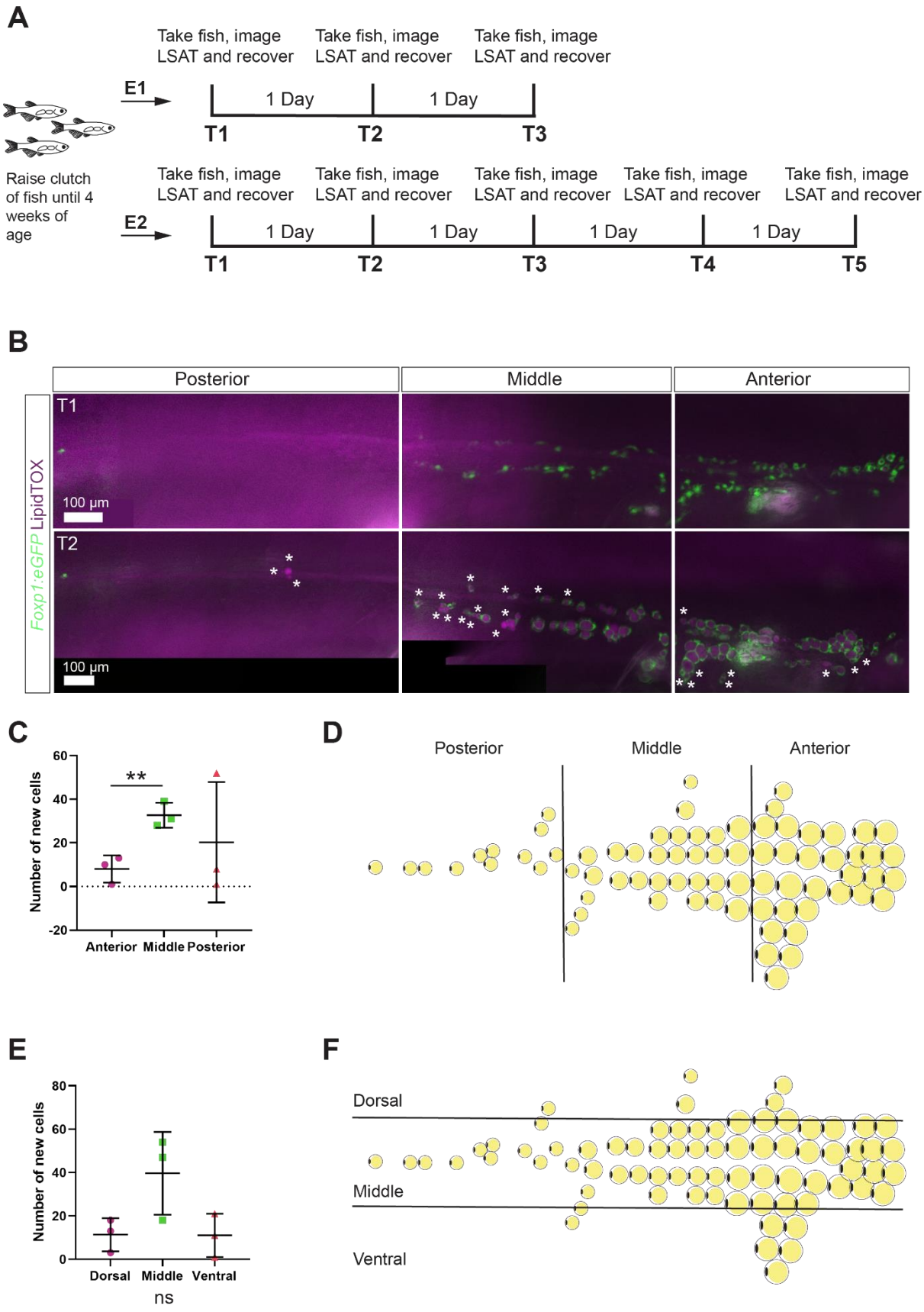

Figure 4.4 – LSAT expands by adding new adipocytes to the centre of the depot.

Figure 4.4 – LSAT expands by adding new adipocytes to the centre of the depot. **A.** Schematic showing the experimental protocol. Data is taken from two experiments, one with 3 timepoints and one with 5 timepoints. E1/E2 (experiment 1/2). Data from experiment 2 takes WT data from a *foxp1a*$^{(+/+)}$ and *foxp1a*$^{(-/-)}$ experiment. **B.** Maximum intensity projection of whole LSAT at T1 and T2. The black boxes on the lower panel are the result of an image processing technique used to stitch multiple images together. The unprocessed images can be found in the appendix. Asterisks highlight the appearance of new cells in the lower panel. **C.** Scatter dot plot showing the location of new cells within the LSAT depot. n = 3. Each point shows the number of new cells which appear in the LSAT of one fish across the 5 timepoints measured. Two tailed t-tests were performed. The difference between the anterior and middle groups were found to be significant, p = 0.0072. The difference between the middle and posterior groups was not found to be significant, p = 0.4913. The difference between the anterior and posterior groups was not found to be significant, p = 0.4930. Error bars show mean and standard deviation. **D.** Schematic showing how the anterior, middle and posterior regions of LSAT were defined. LSAT was divided into three equally sized regions along the anterior-posterior axis. **E.** Scatter dot plot showing the location of new cells within the LSAT depot. n = 3. Each point shows the number of new cells which appear in the LSAT of one fish across the 5 timepoints measured. Two tailed t-tests were performed and the difference between the groups was not found to be significant. Dorsal v middle, p = 0.0754. Ventral v middle, p = 0.0826. Dorsal v ventral, p = 0.9656. Error bars show mean and standard deviation. **F.** Schematic showing how the dorsal, middle and ventral regions were defined. The boundary between the dorsal and middle region was set two adipocytes above the midline of the LSAT. The boundary between the ventral and middle region was set two adipocytes below the middle of the LSAT.

4.2.7 - LSAT branching and branch length is correlated with standard length

To further examine the spatial expansion of LSAT I also wanted to examine adipocytes which branch away from the main LSAT body. I noticed that in fish taken from T1 of the timecourse experiment, with an average SL of 11 mm, LSAT appeared to be formed of one horizontal line of adipocytes **(Figure 4.5A)**. However, the LSAT of fish taken from T5, with an average SL of 12 mm, showed lines of adipocytes branching away from the main horizontal body of the LSAT **(Figure 4.5A)** These lines of adipocytes were found to branch away from the main LSAT body at a roughly 45° angle, both dorsally and ventrally, and appear to be found close to somite boundaries **(Figure 4.5A)**. To determine if the presence of these branches of adipocytes was associated with LSAT expansion, I counted the number of branching events in each LSAT **(Figure 4.5B & C)**. A branching event was defined as a chain of 3 or more adipocytes which branch away from the main LSAT body at a roughly 45° angle. I found that the number of branching events was positively correlated with SL suggesting that branching events increase as the fish grows **(Figure 4.5B)**. However, change in SL was not correlated with change in the number of branching events **(Figure 4.5C)**. This suggests that there is a nonlinear relationship between increases in SL and increases in branching events. In addition to counting the number of branching events per LSAT, I also measured the length of each branch which was defined as the number of cells per branch **(Figure 4.5D & E)**. Similarly to branch number, I found that branch length was positively correlated with SL but that change in SL was not correlated with change in branch length **(Figure 4.5D & E)**. Overall, this suggests that LSAT branching is a key feature of LSAT growth and that both branch number and branch length increase as zebrafish grow. This also allows a model of spatial LSAT expansion to be proposed **(Figure 4.5F)**. In this model LSAT first expands by adding new adipocytes to the centre of the depot and then further expands by forming chains of adipocytes which branch away from the main LSAT body **(Figure 4.5F)**.

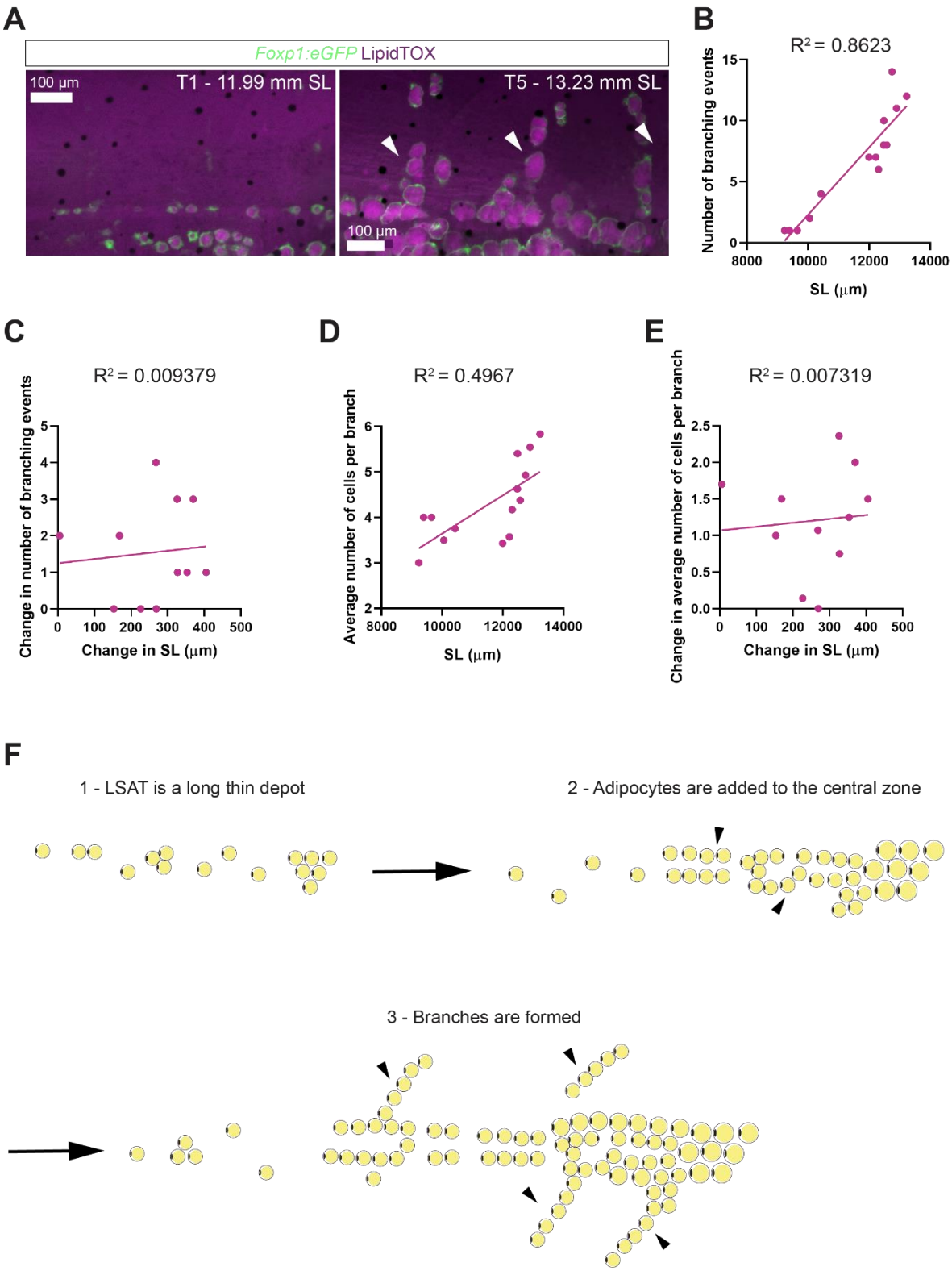

Figure 4.5 - LSAT branching and branch length is correlated with SL.

Figure 4.5 - LSAT branching and branch length is correlated with SL. A. Maximum intensity projections showing the increase in branching events at an increased SL. White arrow heads highlight branches. A branch was defined as 3 or more adipocytes which form a line branching away from the main LSAT body at a roughly 45° angle. The anterior end of the LSAT is to the right of the image **B.** Scatter graph comparing the number of branching events to SL. N = 3. R^2 = 0.8623. The slope of the line is significantly non zero $F_{1,12}$ = 75.13 p < 0.0001. **C.** Scatter graph comparing the change in the number of branching events between timepoints to change in SL. N = 3. R^2 = 0.009379. The slope of the line is not significantly non zero $F_{1,9}$ = 0.08521 p = 0.777. **D.** Scatter graph comparing the average number of cells per branch to SL. N = 3. R^2 = 0.4967. The slope of the line is significantly non zero $F_{1,12}$ = 11.84 p = 0.0049. **E.** Scatter graph comparing the average change in the number of cells per branch to change in SL. N = 3. R^2 = 0.007319. The slope of the line is not significantly non zero $F_{1,9}$ = 0.06636 p = 0.8025. **F.** Schematic showing the proposed model of LSAT growth. Arrow heads at stage 2 highlight adipocytes added to the central zone. Arrow heads at stage 3 highlight the formation of branches.

4.2.8 - LSAT undergoes steady hypertrophic expansion with bursts of hyperplastic expansion

Having examined the spatial expansion of LSAT, I next wanted to look at rates of hypertrophic and hyperplastic growth within LSAT. To do this I used the images taken from the previously described timecourse imaging, in which fish were imaged every 24 hours for either 3 or 5 days **(Figure 4.6A)**. The SL of each fish was measured at each timepoint, and as individual fish could be tracked, the change in SL across each 24 hour period could be calculated **(Figure 4.6B)**. Fish were found to increase in SL between all timepoints, except for two fish between T2 and T3 **(Figure 4.6B & C)**. On average SL increased across the timepoints, with the average increase in SL being 227 µm **(Figure 4.6D)**. The number of adipocytes, the number of adipose progenitor cells and the area of adipocyte lipid droplets was also measured at each timepoint **(Figure 4.6B.E. & G)**. The change in both cell number and cell area were calculated and different growth dynamics were observed at different timepoints **(Figure 4.6B & E)**. Hyperplastic growth was observed between T1 (average 13.9 mm SL) and T2 (average 14.1 mm SL), with a large increase in the number of mature adipocytes present and a decrease in the number of progenitor cells present **(Figure 4.6B & E)**. Cell numbers then remained steady between T2-T3 and T3-T4 **(Figure 4.6B & E)**. A second burst of hyperplastic growth was observed between T4-T5, with an increase in the number of adipocytes **(Figure 4.6B & E)**. On average the number of adipocytes increased between timepoints, with an average increase of 44 adipocytes, and the number of progenitors decreased, with an average decrease of 24 progenitors **(Figure 4.6F)**. In contrast to the bursts of hyperplastic growth, hypertrophic growth remained relatively steady across the experiment, with a slight increase between T4-T5 **(Figure 4.6B & G)**. Change in lipid droplet area was calculated by measuring the change in the lipid droplet area of each cell and the calculating the average of this value. A positive increase in average lipid droplet area was observed between each timepoint and the average increase in area was 347 μm^2 **(Figure 4.6B.G. & H)**. In summary LSAT expands by steady hypertrophic growth with bursts of hyperplastic growth.

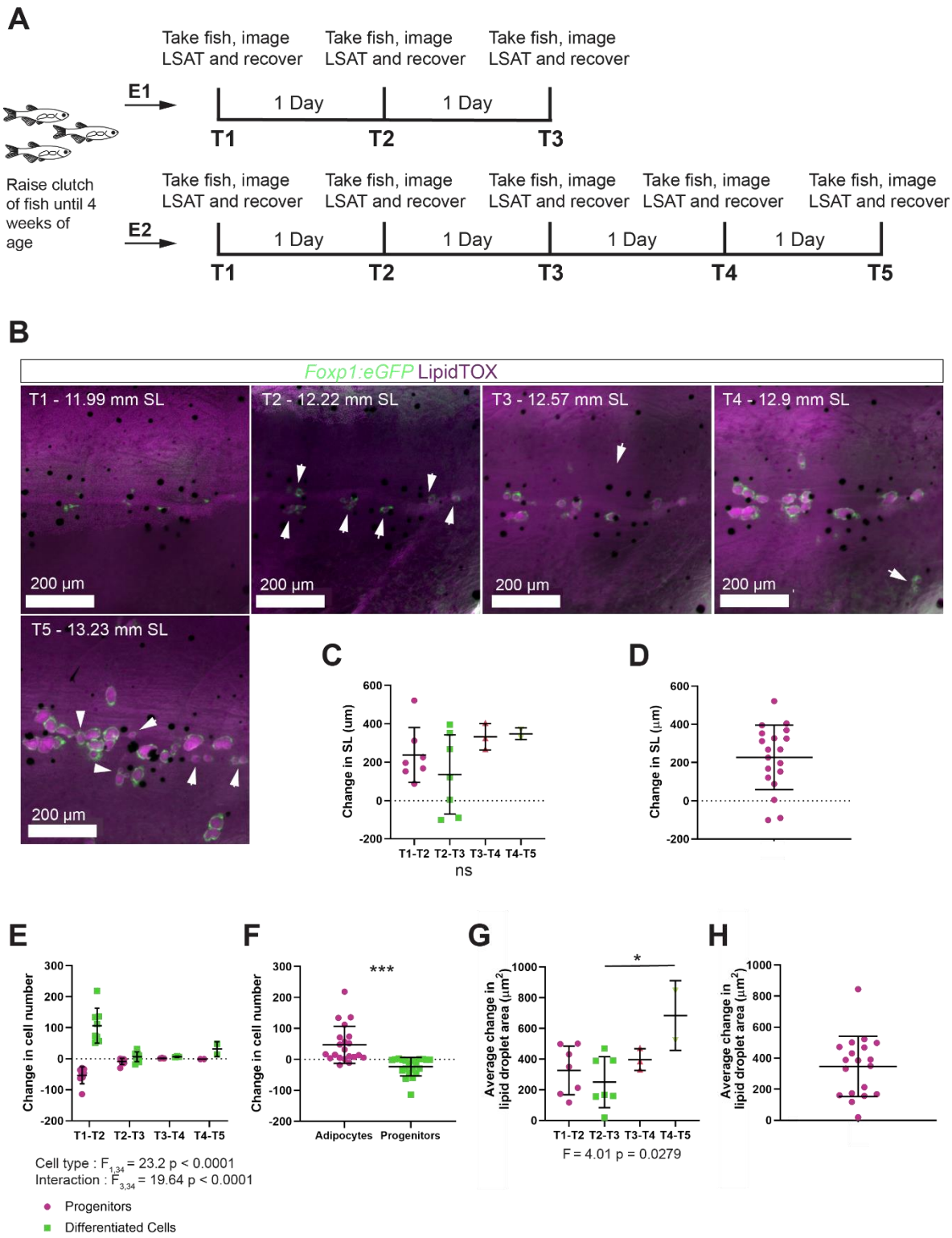

Figure 4.6 – LSAT shows steady hypertrophic growth and bursts of hyperplastic growth.

Figure 4.6 – LSAT shows steady hypertrophic growth and bursts of hyperplastic growth. A. Schematic showing the experimental protocols. Data is taken from two experiments, one with 3 timepoints and one with 5 timepoints. E1/E2 (experiment 1/2). **B.** Representative maximum intensity projections of a section of LSAT in the same fish across 5 timepoints. White arrowheads highlight the appearance of new cells. Images are taken from the posterior end of the LSAT, the anterior end of the LSAT is found to the right of the images. **C.** Scatter dot plot showing change in SL across each experimental timepoint. n = 2-7. Each point shows the change in the SL of one fish across two timepoints. A one way ANOVA was performed and the difference between the groups was not found to be significant $F_{3,15} = 1.564$ $p = 0.2394$. **D.** Scatter dot plot showing change in SL for all fish across all timepoints. n = 2-7. Each point shows the change in the SL of one fish across two timepoints. **E.** Scatter dot plot showing change in cell number across each experimental timepoint. n = 2-7. Each point shows the change in the number of cells present in the LSAT of one fish across 2 timepoints. A two way ANOVA was performed and the difference between the cell types and the interaction between the cell types and the timepoints were found to be significant. Cell types, $F_{1,34} = 23.2$ $p < 0.0001$. Interaction, $F_{3,34} = 19.64$ $p < 0.0001$. **F.** Scatter dot plot showing change in cell number for all fish across all timepoints. Each point shows the change in the number of cells of one fish across two timepoints. A two tailed t-test was performed and the groups were found to be significantly different $p < 0.0001$. **G.** Scatter dot plot showing the average change in lipid droplet area across each experimental timepoint. n = 2-7. Each point shows the average change in the lipid droplet of each cell of one fish across two timepoints. A one way ANOVA was performed and the difference between the groups was found to be significant $F_{3,17} = 4.01$ $p = 0.0279$. A post-hoc Tukey's multiple comparisons test was performed and the difference between T2-T3 and T4-T5 was found to be significant $p = 0.0182$. **H.** Scatter dot plot showing change average lipid droplet area for all fish across all timepoints. Each point shows the change in the average lipid droplet area of one fish across two timepoints. **C-H.** Error bars show mean and standard deviation.

4.2.9 – Changes in average lipid droplet area but not changes in adipocyte number or progenitor number are correlated with changes in SL

I next wanted to examine the relationship between somatic fish growth and changes in cell number and lipid droplet area within LSAT. To do this I plotted change in SL against both change in adipocyte number and change in progenitor number **(Figure 4.7A & B)**. I found that neither change in adipocyte number nor change in progenitor number are correlated with change in SL **(Figure 4.7A & B)**. This suggests that increases in SL do not result in a linear increase in cell number. I also plotted change in average lipid droplet area against change in SL and found a positive correlation between the two variables **(Figure 4.7C)**. The lack of relationship between change in SL and change in cell number, and the relationship between change in lipid droplet area and change in SL is highlighted by Figure 4.7F. No real changes can be seen in cell number between T2-T3 or between T3-T4 **(Figure 4.7F)**. However, while SL remains constant at 12.48 mm between T2-T3, it does increase by 270 µm to 12.75 mm between T3-T4 **(Figure 4.7F)**. This demonstrates the same change in cell number can be observed in both fish which are increasing in SL and fish which are not **(Figure 4.7A & F)**. In contrast no change in lipid droplet area can be seen between T2-T3 when SL does not change, but an increase in lipid droplet area can be observed between T3-T4 when SL increases **(Figure 4.7F)**. Change in adipocyte number was also plotted against change in average lipid droplet area but no correlation was found **(Figure 4.7D)**. Finally, the change in adipocyte number was plotted against the change in progenitor number and a strong negative correlation was found **(Figure 4.7E)**. However, this is not surprising as progenitor cells go on to form adipocytes. In conclusion, change in adipocyte number and change in progenitor number are not correlated with changes in SL, while change in average lipid droplet area is positively correlated with changes in SL. This suggests that while there is not a linear relationship between increased SL and increased cell number, there is a linear relationship between increased lipid droplet area and increased SL.

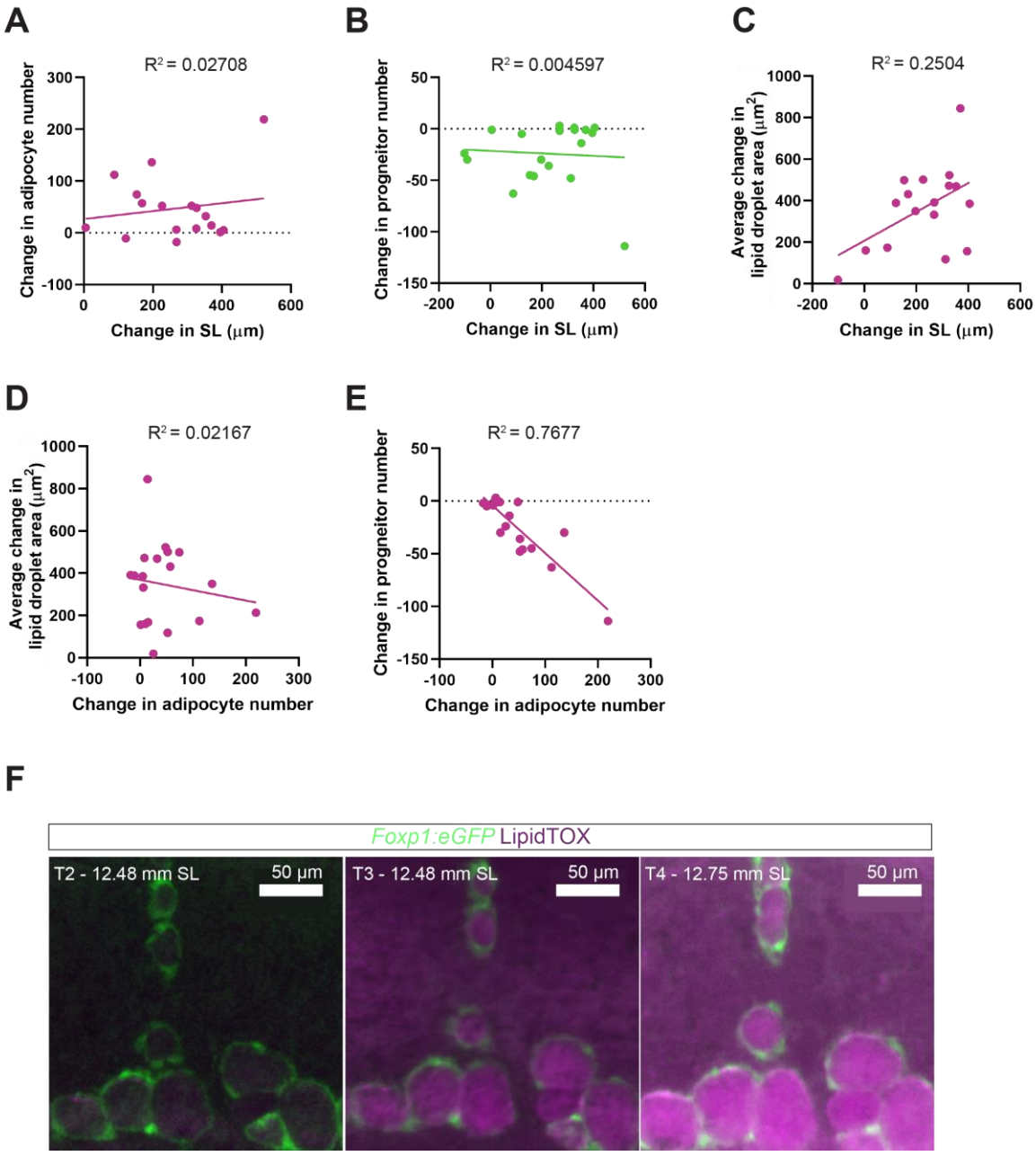

Figure 4.7 – Changes in average lipid droplet area are correlated with changes in SL.

Figure 4.7 – Changes in average lipid droplet area are correlated with changes in SL. A. Scatter graph comparing change in SL to change in adipocyte number. n = 7. Each point shows the change in adipocyte number vs the change in SL for 1 fish between 2 timepoints. R^2 = 0.02708. The slope of the line is not significantly non-zero $F_{1,15}$ = 0.4176 p = 0.5279. **B**. Scatter graph comparing change in SL to change in progenitor number. n = 7. Each point shows the change in progenitor number vs the change in SL for 1 fish between 2 timepoints. R^2 = 0.004597. The slope of the line is not significantly non-zero $F_{1,17}$ = 0.0785 p = 0.7827. **C.** Scatter graph comparing change in SL to change in area lipid droplet area. n = 7. Each point shows the change in average lipid droplet area vs the change in SL for 1 fish between 2 timepoints. R^2 = 0.2507. The slope of the line is significantly non-zero $F_{1,15}$ = 5.01 p = 0.0408. **D.** Scatter plot comparing change in adipocyte number to change in average lipid droplet area. n = 7. Each point shows the change in adipocyte number vs the change in average lipid droplet area for 1 fish between 2 timepoints. R^2 = 0.02167. The slope of the line is not significantly non-zero $F_{1,17}$ = 0.3766 p = 0.5476. **E.** Scatter plot comparing change in adipocyte number to change in progenitor number. n = 7. Each point shows the change in adipocyte number vs the change progenitor number for 1 fish between 2 timepoints. R^2 = 0.7677. The slope of the line is significantly non-zero $F_{1,17}$ = 56.18 p < 0.0001. **F.** Representative maximum intensity projections showing lack of correlation between change in SL and change in cell number and the correlation between change in average lipid droplet area and change in SL. Note that cell number remains constant despite no change in SL between T2-T3 and an increase in SL between T3-T4. Lipid droplet area is unchanged between T2-T3 where no change in SL is observed and increases between T3-T4 when SL also increases. Images are taken from the anterior end of the LSAT, the anterior end of the LSAT is found to the right of the images.

4.2.10 – New cells do not appear most often at the centre of the LSAT depot in *foxp1a*$^{(-/-)}$ mutants

Having built a model of how LSAT expands in WT fish, I next wanted to examine the role of *foxp1* in LSAT expansion. To do this I first looked at the role of *foxp1a* and began by examining its role in the spatial expansion of LSAT. I performed a five day timecourse experiment using both *foxp1a*$^{(-/-)}$ mutant fish and WT siblings **(Figure 4.8A)**. *Foxp1:eGFP:foxp1a*$^{(+/-)}$ fish were incrossed, raised until approximately 12.6 mm SL and genotyped. WT fish and *foxp1a*$^{(-/-)}$ mutants were then incubated with LipidTOX and LSAT was imaged using a stereomicroscope **(Figure 4.8A)**. The fish were recovered and the imaging was repeated every 24 hours for a period of 5 days **(Figure 4.8A)**. This allowed LSAT expansion in individual WT and *foxp1a*$^{(-/-)}$ mutant fish to be tracked. To examine the spatial expansion of LSAT, I examined the location of new cells added to LSAT along the anterior-posterior axis and along the dorsal-ventral axis. I began by looking at expansion across the anterior-posterior axis. To do this I divided the LSAT of each fish into 3 equally sized sections along the anterior-posterior axis and quantified the number of new cells added to each section between each timepoint **(Figure 4.8B & C)**. I found that, as shown previously, new cells were most often added to the middle of the depot in WT fish **(Figure 4.8B & C)**. However, this preference was not found in mutant fish with an equal number of cells being added to the anterior, middle and posterior sections **(Figure 4.8B & C)**. I also examined LSAT expansion along the dorsal-ventral axis, with LSAT being divided into three sections along this axis **(Figure 4.8B & D)**. When the appearance of new cells was quantified, most cells were again added to the middle region in WT fish **(Figure 4.8B & D)**. This was not true of *foxp1a*$^{(-/-)}$ fish with equal numbers of cells being added to each region **(Figure 4.8B &D)**. Taken together this suggests that the spatial expansion of LSAT is altered in *foxp1a*$^{(-/-)}$ mutants and that LSAT in these mutants does not expand by adding new adipocytes to the centre of the depot.

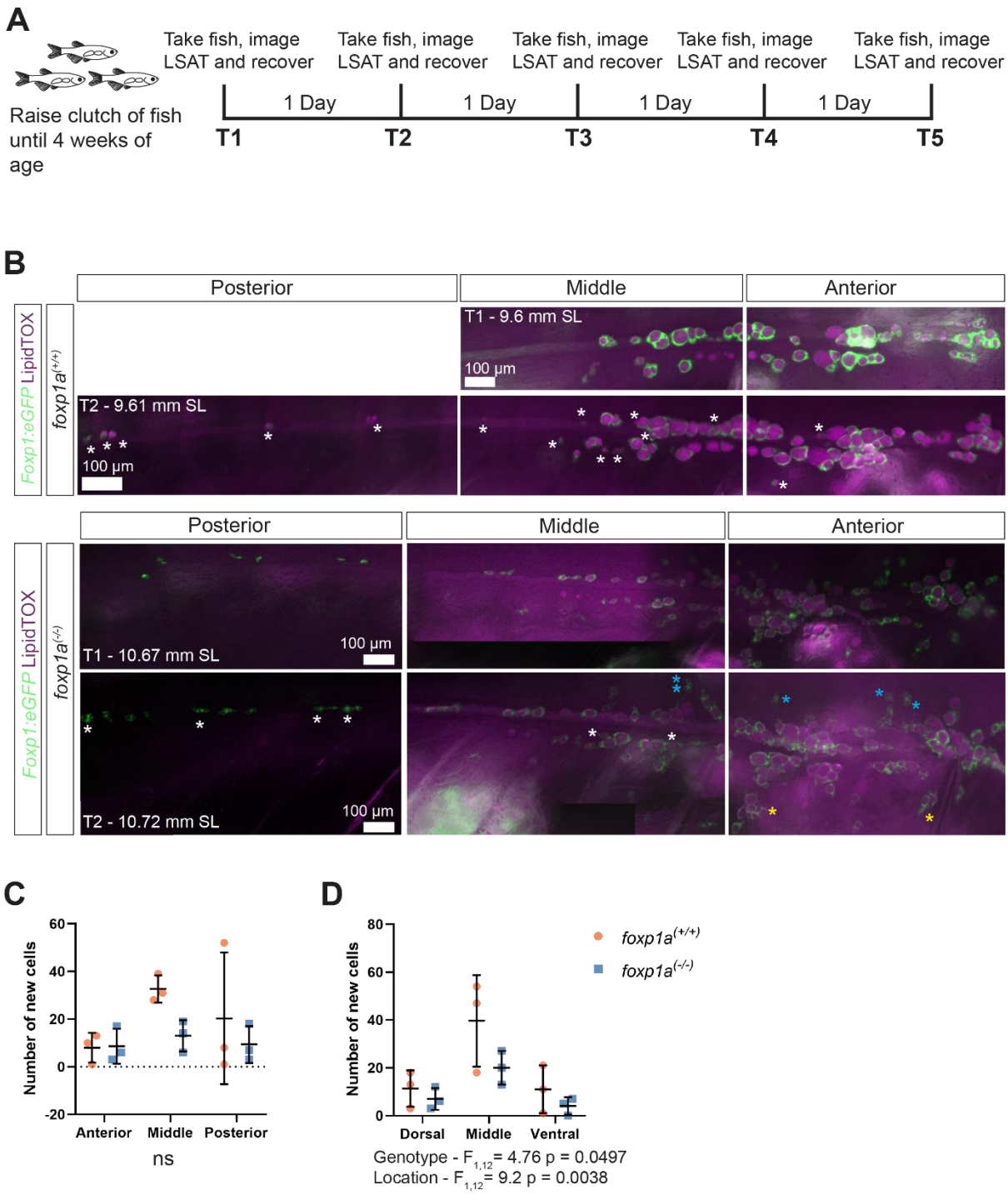

Figure 4.8 – *foxp1a*$^{(-/-)}$ mutants show an altered spatial pattern of LSAT growth.

Figure 4.8 – *foxp1a*$^{(-/-)}$ mutants show an altered spatial pattern of LSAT growth. **A.** Schematic showing the experimental protocol. **B.** Representative maximum intensity projections of the whole LSAT of *foxp1a*$^{(+/+)}$ and *foxp1a*$^{(-/-)}$ fish at two timepoints. Dorsal and ventral cells were defined as cells separated by more than 2 adipocytes vertically from the main horizontal line of LSAT. Asterisks highlight the appearance of new cells. White asterisks show cells considered to be added to the middle of the LSAT. Yellow asterisks show cells added ventrally and blue asterisks show cells added dorsally. Black boxes on the *foxp1a*$^{(-/-)}$ mutant images are created by the image processing software used to stitch the images together. Unprocessed images can be found in the appendix. **C.** Scatter dot plot showing the location of new cells within the LSAT depot. n = 3. Each point shows the number of new cells which appear in the LSAT of one fish across the 5 timepoints measured. A two way ANOVA was performed and the difference between the groups was not found to be significant. **D.** Scatter dot plot showing the location of new cells within the LSAT depot. n = 3. Each point shows the number of new cells which appear in the LSAT of one fish across the 5 timepoints measured. A two way ANOVA was performed and the difference between the genotypes and the location of the new cells were found to be significant. Genotype – $F_{1,12} = 4.76$ $p = 0.0497$. Location of new cells – $F_{2,12} = 9.2$ $p = 0.0038$. **C-D.** Error bars show mean and standard deviation.

4.2.11 – The average number of cells per LSAT branch is greater in *foxp1a*$^{(-/-)}$ mutants

I next wanted to examine LSAT branching, which is the second key feature of my model of spatial LSAT expansion. To do this I first measured the number of branching events in each LSAT. A branch was defined as a chain of three or more cells which branch away from the main LSAT body at a roughly 45° angle **(Figure 4.9A)**. I found that the number of branches was positively correlated with SL in both *foxp1a*$^{(-/-)}$ mutant and WT fish **(Figure 4.9A & B)**. Furthermore I found that the number of branching events relative to SL was not significantly different in WT and *foxp1a*$^{(-/-)}$ mutant fish **(Figure 4.9A & B)**. I also found that change in SL was not correlated with change in branch number in WT or *foxp1a*$^{(-/-)}$ mutant fish **(Figure 4.9C)**. I next examined branch length by counting the number of cells per branch. I found that, similar to branch number, the average number of cells per branch was positively correlated with SL in both *foxp1a*$^{(-/-)}$ mutant and WT fish **(Figure 4.9A & D)**. However, the average number of cells per branch was significantly greater in *foxp1a*$^{(-/-)}$ mutant fish **(Figure 4.9A & D)**. This suggests that the spatial expansion of LSAT is altered in *foxp1a*$^{(-/-)}$ mutant fish. Finally I found that there was no correlation between the change in the average number of cells per branch and the change in SL in either *foxp1a*$^{(-/-)}$ mutant or WT fish **(Figure 4.9E)**. Overall this suggests that spatial LSAT expansion is altered in *foxp1a*$^{(-/-)}$ mutant fish. In the WT model of LSAT expansion, LSAT first expands by adding new cells to the centre of the depot and then further expands by forming chains of adipocytes which branch away from the main LSAT body. LSAT in *foxp1a*$^{(-/-)}$ mutants does not expand by adding cells to the centre of the depot and although branches are formed, they contain significantly more cells than those of WT fish. In summary LSAT expansion is altered in *foxp1a*$^{(-/-)}$ mutants.

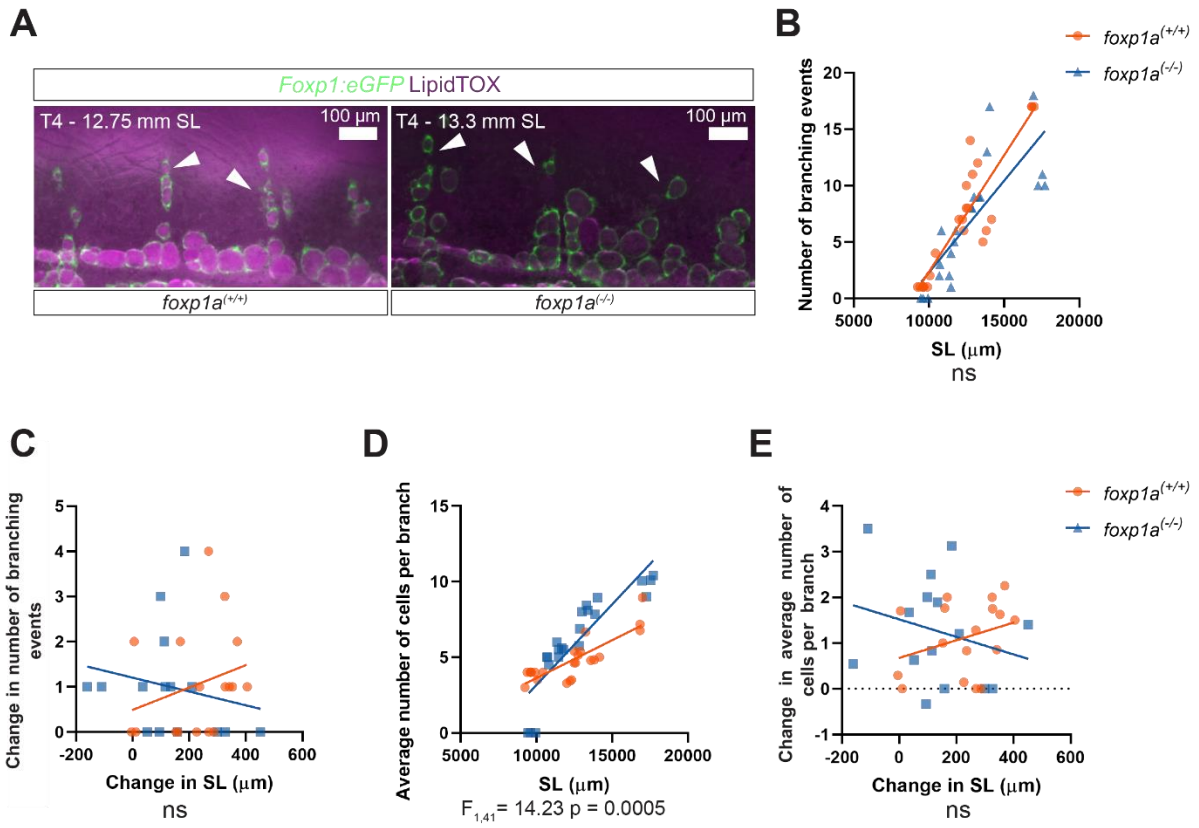

Figure 4.9 - LSAT branching is altered in *foxp1a*$^{(-/-)}$ mutants.

Figure 4.9 - LSAT branching is altered in *foxp1a*$^{(-/-)}$ mutants. A. Maximum intensity projections showing the branching events in WT fish and foxp1a$^{(-/-)}$ mutants. White arrow heads highlight branches. A branch was defined as 3 or more adipocytes which form a line branching away from the main LSAT body at a roughly 45° angle. The anterior end of the LSAT is to the right of the image **B.** Scatter graph comparing the number of branching events to SL. N = 6. *foxp1a*$^{(+/+)}$, R^2 = 0.8182. The slope of the line is significantly non zero $F_{1,21}$ = 94.48 p < 0.0001. *foxp1a*$^{(-/-)}$, R^2 = 0.639. The slope of the line is significantly non zero $F_{1,20}$ = 35.4 p < 0.0001. An ancova analysis was performed and the slopes of the lines were not significantly different $F_{1,41}$ = 1.594 p = 0.214. **C.** Scatter graph comparing the change in the number of branching events between timepoints to change in SL. N = 6. *foxp1a*$^{(+/+)}$, R^2 = 0.07213. The slope of the line is not significantly non zero $F_{1,15}$ = 1.166 p = 0.2973. *foxp1a*$^{(-/-)}$, R^2 = 0.03992. The slope of the line is not significantly non zero $F_{1,13}$ = 0.5406 p = 0.4752. **D.** Scatter graph comparing the average number of cells per branch to SL. N = 6. *foxp1a*$^{(+/+)}$, R^2 = 0.6895. The slope of the line is significantly non zero $F_{1,21}$ = 46.63 p < 0.0001. *foxp1a*$^{(-/-)}$, R^2 = 0.7708. The slope of the line is significantly non zero $F_{1,20}$ = 67.25 p < 0.0001. An ancova analysis was performed and the slopes of the lines were found to be significantly different $F_{1,41}$ = 14.23 p = 0.0005. **E.** Scatter graph comparing the average change in the number of cells per branch to change in SL. N = 6. *foxp1a*$^{(+/+)}$, R^2 = 0.1013. The slope of the line is not significantly non zero $F_{1,15}$ = 1.691 p = 0.2131. *foxp1a*$^{(-/-)}$, R^2 = 0.064. The slope of the line is not significantly non zero $F_{1,13}$ = 0.8889 p = 0.363.

4.2.12 – Hyperplastic and hypertrophic LSAT expansion is unaltered in *foxp1a*$^{(-/-)}$ mutants

Having determined that the spatial expansion of LSAT is altered in *foxp1a*$^{(-/-)}$ mutants, I next wanted to examine rates of hypertrophic and hyperplastic growth. To do this I used images taken in the previously described *foxp1a*$^{(-/-)}$ timecourse experiment, in which fish were imaged every 24 hours over a period of 5 days **(Figure 4.10A)**. The SL of each fish was measured at each timepoint and the change in SL across each 24 hour period calculated **(Figure 4.10B & C)**. SL was found to increase across all of the timepoints, with the exception of one *foxp1a*$^{(-/-)}$ mutant fish which shrinks slightly between T1-T2 **(Figure 4.10B & C**). On average the SL of both WT and *foxp1a*$^{(-/-)}$ mutant fish increased across the timepoints, with average increases in SL of 230 µm and 133 µm respectively **(Figure 4.10B & D)**. The number of adipocytes, the number of adipose progenitor cells and the area of every lipid droplet was also measured at each timepoint **(Figure 4.10E.F. & H)**. When changes in cell number were calculated, similar dynamics were observed to that of previous WT data. Bursts of hyperplastic growth were observed in WT fish between T1-T2 and T4-T5 with increased numbers of adipocytes and decreased numbers of progenitors **(Figure 4.10B.E & F)**. Adipocyte numbers remained steady in WT fish between T2-T3 and T3-T4 and this was accompanied by a fall in progenitor cells between T3-T4 **(Figure 4.10B.E. & F)**. Changes in adipocyte and progenitor numbers in *foxp1a*$^{(-/-)}$ mutant fish followed much the same pattern as those of WT fish, however there was no burst of hyperplastic growth between T1-T2 (**Figure 4.10B & E)**. On average the number of adipocytes increased between timepoints in both WT and *foxp1a*$^{(-/-)}$ mutant fish, with average increases of 17 and 15 adipocytes respectively **(Figure 4.10B & G)**. In contrast the number of progenitor cells decreased on average, with an average decrease of 7 cells in WT fish and 5 cells in *foxp1a*$^{(-/-)}$ mutant fish across the timepoints **(Figure 4.10B & G)**. The change in the average area of lipid droplets per cell was also calculated and steady hypertrophic growth was observed across the experiment for both WT and *foxp1a*$^{(-/-)}$ fish **(Figure 4.10B & H)**. On average lipid droplet area was found to increase by 336 µm^2 in WT fish and 305 µm^2 in *foxp1a*$^{(-/-)}$ fish **(Figure 4.10I)**. In summary LSAT in WT fish follows the same patterns of expansion as previously described, namely steady hypertrophic expansion and bursts of hyperplastic expansion. No differences were observed in hypertrophic and hyperplastic expansion in *foxp1a*$^{(-/-)}$ mutant fish.

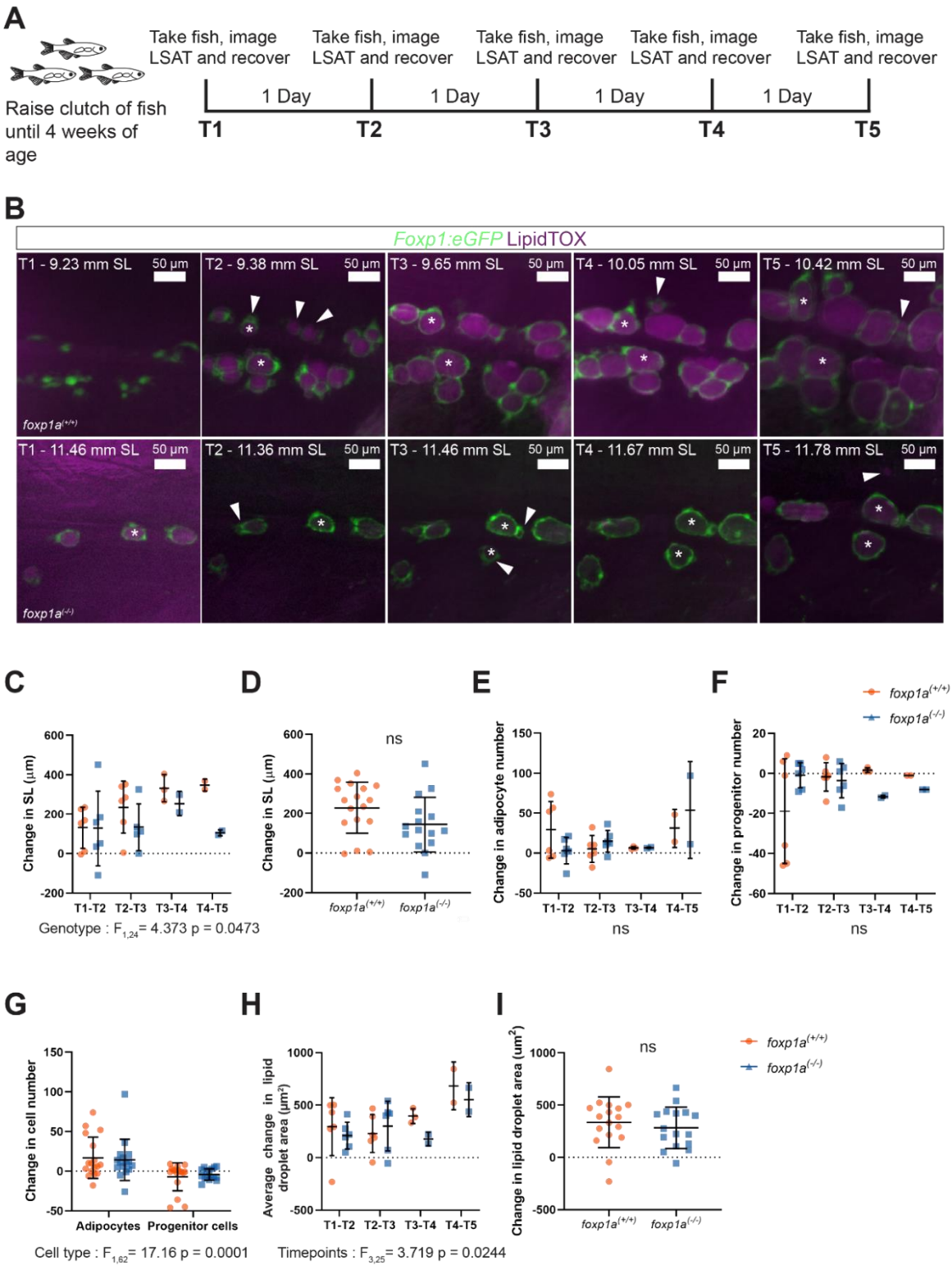

Figure 4.10 – *foxp1a*$^{(-/-)}$ mutants do not show altered rates of hyperplastic and hypertrophic LSAT expansion during normal development.

Figure 4.10 – *foxp1a*$^{(-/-)}$ mutants do not show altered rates of hyperplastic and hypertrophic LSAT expansion during normal development. A. Schematic showing the experimental protocol. **B.** Representative maximum intensity projections of a section of LSAT in the same WT and *foxp1a*$^{(-/-)}$ fish across 5 timepoints. White arrowheads highlight the appearance of new cells. Images are taken from the posterior end of the LSAT, the anterior end of the LSAT is found to the right of the images. **C.** Scatter dot plot showing change in SL across each experimental timepoint. n = 2-7. Each point shows the change in the SL of one fish across two timepoints. A one way ANOVA was performed and the difference between the genotypes was found to be significant $F_{1,24} = 4.373$ p = 0.0473. **D.** Scatter dot plot showing change in SL for all fish across all timepoints. n = 2-7. Each point shows the change in the SL of one fish across two timepoints. A two tailed t-test was performed and the difference between the groups was not found to be significant, p = 0.0831. **E.** Scatter dot plot showing change in adipocyte number across each experimental timepoint. n = 2-7. Each point shows the change in the number of cells present in the LSAT of one fish across 2 timepoints. A two way ANOVA was performed and the difference between the groups was not found to be significant. **F.** Scatter dot plot showing change in progenitor number across each experimental timepoint. n = 2-7. Each point shows the change in the number of cells present in the LSAT of one fish across 2 timepoints. A two way ANOVA was performed and the difference between the groups was not found to be significant. **G.** Scatter dot plot showing change in cell number for all fish across all timepoints. Each point shows the change in the number of cells of one fish across two timepoints. A two way ANOVA was performed and the difference between cell types was found to be significant $F_{1,62} = 17.15$ p = 0.0001. **H.** Scatter dot plot showing the average change in lipid droplet area per cell across each experimental timepoint. n = 2-7. Each point shows the change in the average area of the lipid droplets present in the LSAT of one fish across two timepoints. A two way ANOVA was performed and the difference between the timepoints was found to be significant $F_{3,25} = 3.719$ p = 0.0244. **I.** Scatter dot plot showing change average lipid droplet area for all fish across all timepoints. Each point shows the change in the average lipid droplet area of one fish across two timepoints. A two tailed t-test was performed and the difference between the groups was not found to be significant. **C-I.** Error bars show mean and standard deviation.

4.2.13 – Changes in average lipid droplet area are not correlated with changes in SL in *foxp1a*$^{(-/-)}$ mutants

As a final measure of LSAT expansion in the *foxp1a*$^{(-/-)}$ mutants, I examined the relationship between changes in cell number and lipid droplet area within LSAT and somatic growth. To do this I first plotted change in cell number against change in SL **(Figure 4.11A & B)**. I found no correlation between changes in adipocyte number and changes in SL or between changes in progenitor cell number and changes in SL for either WT or *foxp1a*$^{(-/-)}$ fish **(Figure 4.11A & B)**. This is in keeping with previous WT data and suggests that increases in SL do not result in a linear increase in cell number. I also plotted change in the average lipid droplet area per cell against SL and found a positive correlation for WT fish but not for *foxp1a*$^{(-/-)}$ mutant fish **(Figure 4.11C)**. In contrast when change in adipocyte number was plotted against change in average lipid droplet area no correlation was found for WT fish but a positive correlation was found for *foxp1a*$^{(-/-)}$ fish **(Figure 4.11D)**. Finally change in adipocyte number was plotted against change in progenitor number and while a negative correlation was found for WT fish, no correlation was present for *foxp1a*$^{(-/-)}$ mutant fish **(Figure 4.11E)**. Taken together these data suggest that the relationship between LSAT expansion and somatic growth is altered in *foxp1a*$^{(-/-)}$ mutant fish. The lack of correlation between change in lipid droplet area and change in SL suggests that increased SL doesn't result in increased hypertrophic growth in *foxp1a*$^{(-/-)}$ mutant fish. Furthermore the lack of relationship between change in adipocyte number and change in progenitor number suggests altered adipose progenitor behaviour in *foxp1a*$^{(-/-)}$ mutants. Overall *foxp1a*$^{(-/-)}$ mutants show altered LSAT expansion.

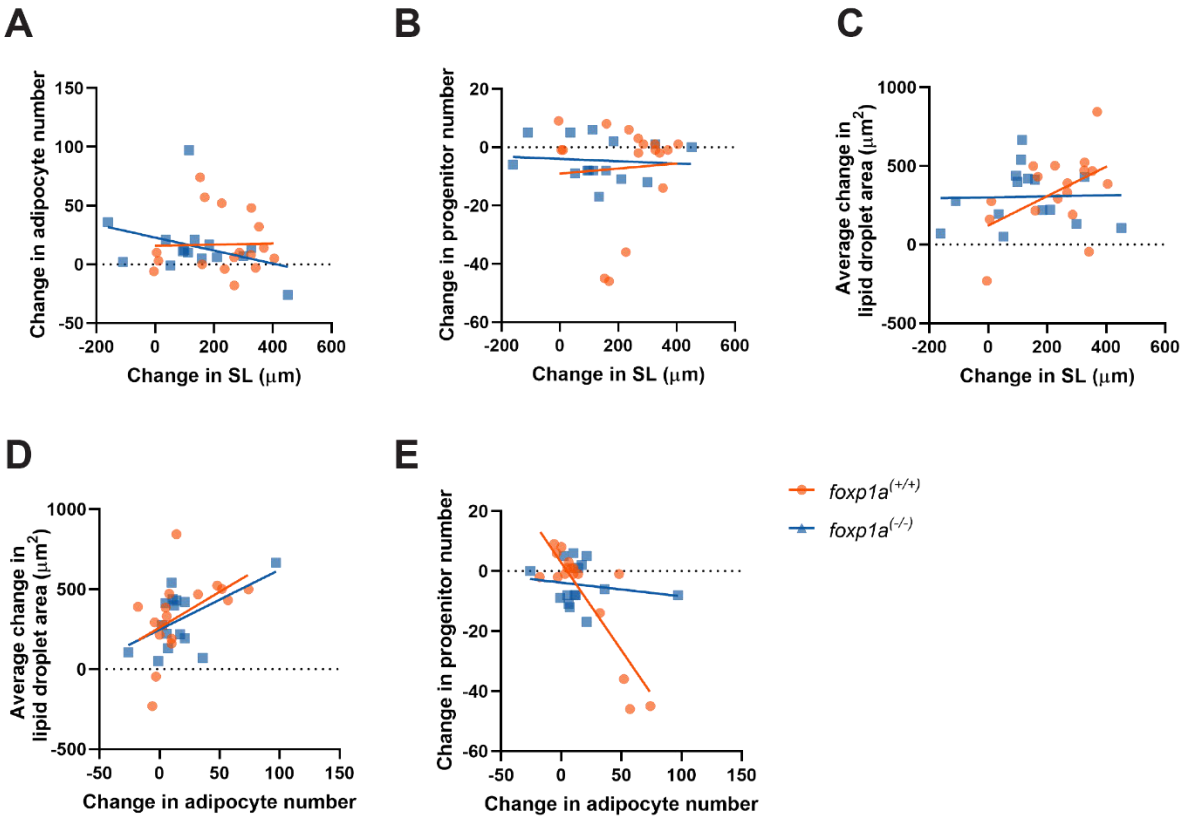

Figure 4.11 – Changes in lipid droplet area are not correlated with changes in SL in *foxp1a*$^{(-/-)}$ mutants.

Figure 4.11 – Changes in lipid droplet area are not correlated with changes in SL in *foxp1a*$^{(-/-)}$ mutants. A. Scatter graph comparing change in SL to change in adipocyte number. n = 6. Each point shows the change in adipocyte number vs the change in SL for 1 fish between 2 timepoints. *foxp1a*$^{(+/+)}$, $R^2 = 0.005$. The slope of the line is not significantly non zero $F_{1,15} = 0.0075$ p = 0.9323. *foxp1a*$^{(-/-)}$, $R^2 = 0.1084$. The slope of the line is not significantly non zero $F_{1,13} = 1.58$ p = 0.2309. **B**. Scatter graph comparing change in SL to change in progenitor number. n = 6. Each point shows the change in progenitor number vs the change in SL for 1 fish between 2 timepoints. *foxp1a*$^{(+/+)}$, $R^2 = 0.004$. The slope of the line is not significantly non zero $F_{1,15} = 0.0609$ p = 0.8084. *foxp1a*$^{(-/-)}$, $R^2 = 0.0076$. The slope of the line is not significantly non zero $F_{1,13} = 0.9896$ p = 0.7581. **C.** Scatter graph comparing change in SL to change in area lipid droplet area. n = 6. Each point shows the change in average lipid droplet area vs the change in SL for 1 fish between 2 timepoints. *foxp1a*$^{(+/+)}$, $R^2 = 0.2527$. The slope of the line is significantly non zero $F_{1,15} = 5.071$ p = 0.0397. *foxp1a*$^{(-/-)}$, $R^2 = 0.00079$. The slope of the line is not significantly non zero $F_{1,13} = 0.01031$ p = 0.9207. **D.** Scatter plot comparing change in adipocyte number to change in average lipid droplet area. n = 6. Each point shows the change in adipocyte number vs the change in average lipid droplet area for 1 fish between 2 timepoints. *foxp1a*$^{(+/+)}$, $R^2 = 0.2294$. The slope of the line is not significantly non zero $F_{1,15} = 4.465$ p = 0.0518. *foxp1a*$^{(-/-)}$, $R^2 = 0.2877$. The slope of the line is significantly non zero $F_{1,13} = 5.251$ p = 0.0391. **E.** Scatter plot comparing change in adipocyte number to change in progenitor number. n = 6. Each point shows the change in adipocyte number vs the change progenitor number for 1 fish between 2 timepoints. *foxp1a*$^{(+/+)}$, $R^2 = 0.7389$. The slope of the line is significantly non zero $F_{1,15} = 42.46$ p < 0.0001. *foxp1a*$^{(-/-)}$, $R^2 = 0.0282$. The slope of the line is not significantly non zero $F_{1,13} = 0.3772$ p = 0.5497.

4.2.14 – New cells are added to the centre of LSAT in *foxp1b*$^{(-/-)}$ mutants

Having determined that LSAT expansion is altered in *foxp1a*$^{(-/-)}$ mutants I next wanted to examine LSAT expansion in *foxp1b*$^{(-/-)}$ mutants. To do this I first examined the spatial expansion of LSAT along the anterior-posterior and dorsal-ventral axes **(Figure 4.12B)**. I incrossed *Foxp1:eGFP:foxp1b*$^{(+/-)}$ fish and raised their offspring until approximately 10 mm SL. Fish were then genotyped and *foxp1b*$^{(-/-)}$ mutants and WT siblings were incubated with LipiTOX and imaged using a stereomicroscope **(Figure 4.12A)**. Fish were recovered and the imaging repeated every 24 hours over a 3 day period **(Figure 4.12A)**. To examine LSAT expansion along the anterior-posterior axis, LSAT was divided into three sections along this axis and the number of new cells in each section recorded **(Figure 4.12B & C)**. In contrast to previous WT data, no difference was observed between the number of cells present in each section **(Figure 4.12B & C)**. This may be due to a small sample size. The same number of cells were also found across all three locations in *foxp1b*$^{(-/-)}$ mutant fish **(Figure 4.12B & C)**. LSAT expansion was next measured along the dorsal-ventral axis, with LSAT being divided into three sections along this axis **(Figure 4.12B & D)**. Here new cells were found most often in the middle region in both WT and *foxp1b*$^{(-/-)}$ mutant fish **(Figure 4.12B & D)**. In summary, the spatial expansion of LSAT appears to be unaltered in *foxp1b*$^{(-/-)}$ mutants.

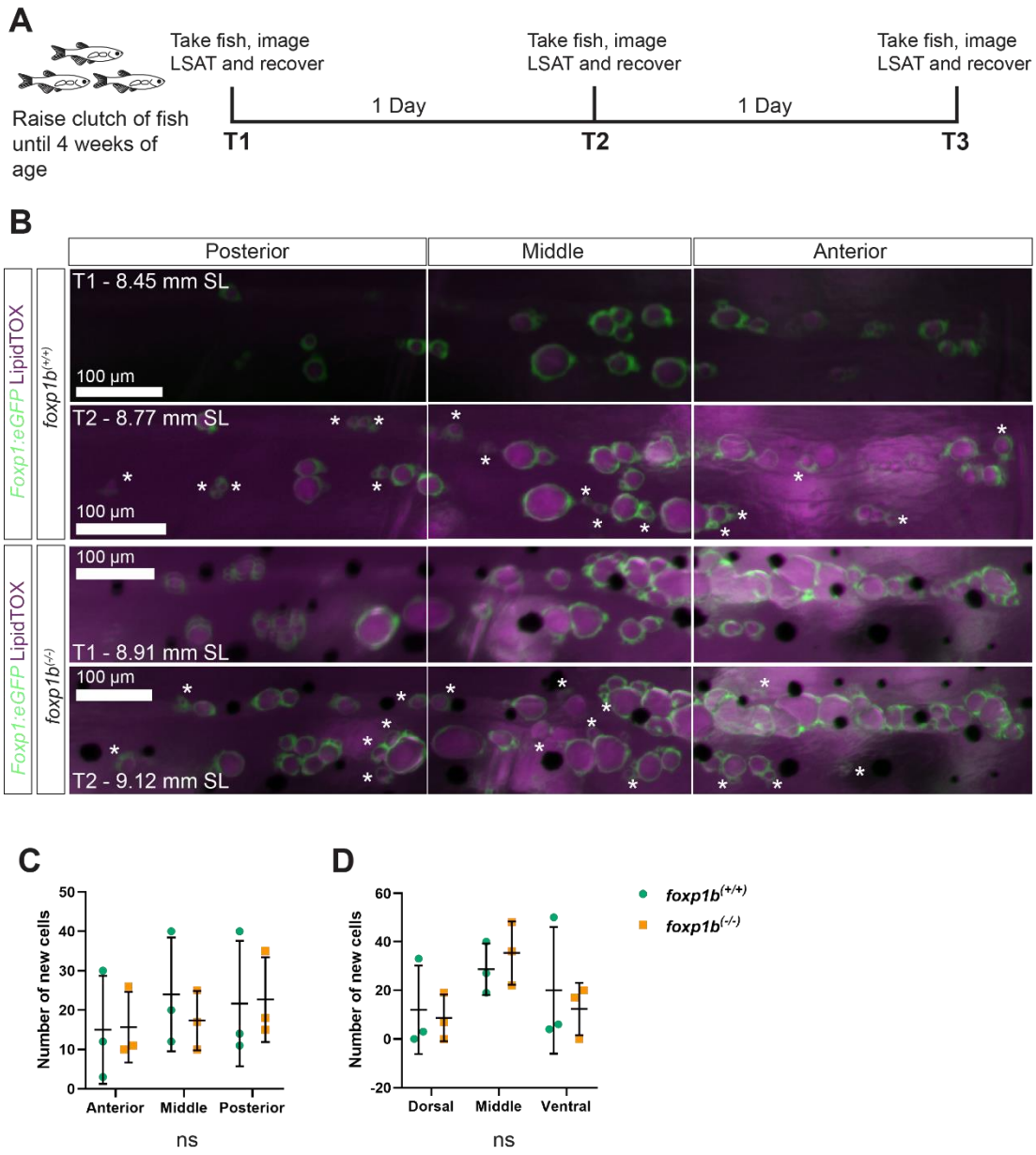

Figure 4.12 – *foxp1b*$^{(-/-)}$ mutants do not show altered spatial LSAT expansion.

Figure 4.12 – *foxp1b*$^{(-/-)}$ mutants do not show altered spatial LSAT expansion. A. Schematic showing the experimental protocol. **B.** Representative maximum intensity projections of the whole LSAT of *foxp1b*$^{(+/+)}$ and *foxp1b*$^{(-/-)}$ fish at two timepoints. Dorsal and ventral cells were defined as cells separated by more than 2 adipocytes vertically from the main horizontal line of LSAT. Asterisks highlight the appearance of new cells **C.** Scatter dot plot showing the location of new cells within LSAT. n = 3. Each point shows the number of new cells which appear in the LSAT of one fish across the 5 timepoints measured. A two way ANOVA was performed and the difference between the groups was not found to be significant. **D.** Scatter dot plot showing the location of new cells within LSAT. n = 3. Each point shows the number of new cells which appear in the LSAT of one fish across the 5 timepoints measured. A two way ANOVA was performed and the difference between the groups was not found to be significant. **C-D.** Error bars show mean and standard deviation.

4.2.15 – The number of branching events per LSAT is not correlated with SL in *foxp1b*$^{(-/-)}$ mutant fish

As *foxp1b*$^{(-/-)}$ mutants show unaltered LSAT expansion along the anterior-posterior and dorsal-ventral axes, I next examined LSAT branching. I first measured the number of branches per LSAT in both WT and *foxp1b*$^{(-/-)}$ mutant fish **(Figure 4.13A & B)**. A branch was defined as a chain of three or more cells which branch away from the main LSAT body at a roughly 45° angle **(Figure 4.13A)**. I found that while branch number is positively correlated with SL in WT fish no such relationship exists in *foxp1b*$^{(-/-)}$ mutant fish **(Figure 4.13A & B)**. I also plotted the change in the number of branching events against the change in SL and found no correlation between the two variables for either WT or *foxp1b*$^{(-/-)}$ fish **(Figure 4.13C)**. I next measured the number of cells per branch and plotted the average number of cells per branch against SL **(Figure 4.13A & D)**. I found a positive correlation between average branch length and SL for both WT and *foxp1b*$^{(-/-)}$ fish, and no significant difference in branch length was found between the two groups **(Figure 4.13D)**. Finally, I plotted change in average branch length against change in SL and found no correlation between the variables in either WT or *foxp1b*$^{(-/-)}$ mutant fish **(Figure 4.13E)**. Taken together this suggests that LSAT branching in *foxp1b*$^{(-/-)}$ mutants is largely unaltered, though the number of branches per LSAT does not show a positive correlation to SL in the *foxp1b*$^{(-/-)}$ mutants. Overall *foxp1b*$^{(-/-)}$ mutants seem to follow the proposed spatial model of LSAT expansion with cells first added to the centre of the LSAT depot and LSAT further expanding by forming branches.

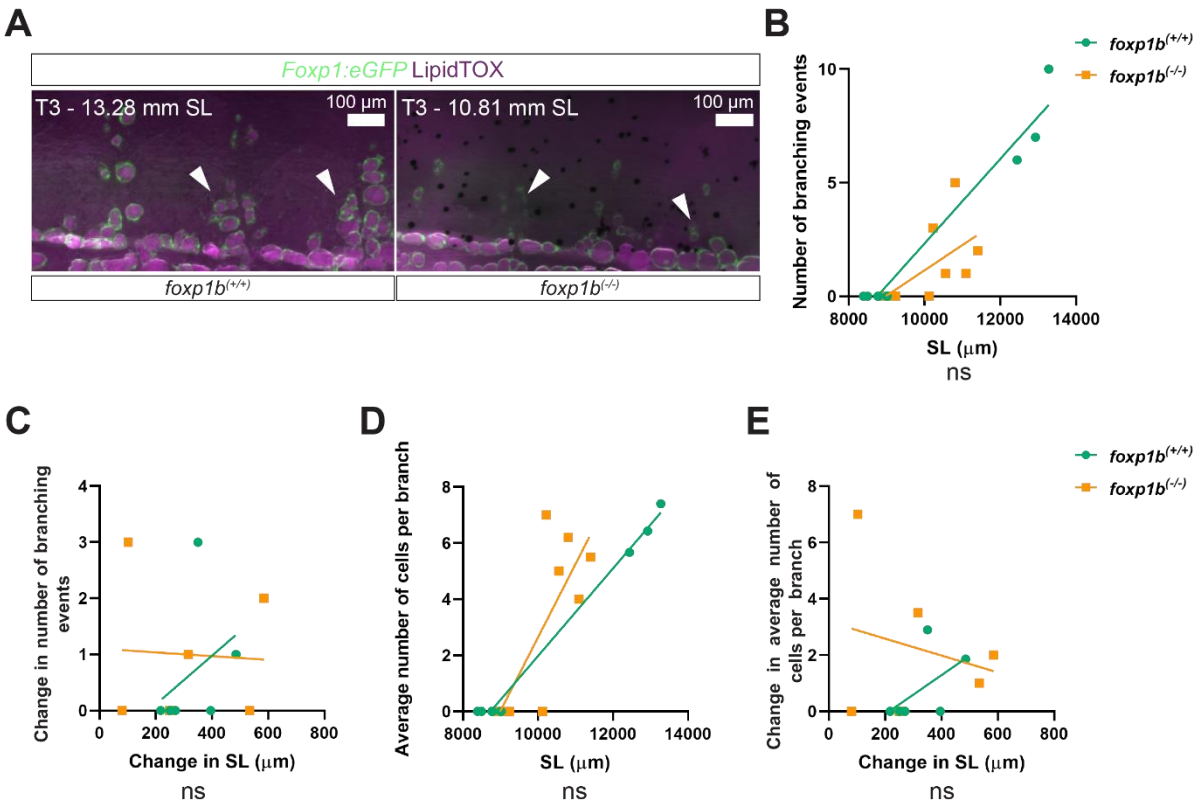

Figure 4.13 – The number of branching events per LSAT in *foxp1b*$^{(-/-)}$ mutants is not correlated with SL

Figure 4.13 – The number of branching events per LSAT in *foxp1b*$^{(-/-)}$ mutants is not correlated with SL. A. Representative maximum intensity projections showing unaltered number of branching events in *foxp1b*$^{(-/-)}$ mutants and WT fish at one timepoint. White arrowheads highlight branching events. Branches are defined as a chain of 3 or more adipocytes which branch away from the main line of the LSAT at a roughly 45° angle. The anterior end of LSAT is found to the right of the images. **B.** Scatter graph comparing the number of branching events to SL. n = 3. *foxp1b*$^{(+/+)}$, R^2 = 0.9605. The slope of the line is significantly non zero $F_{1,7}$ = 170.3 p < 0.0001. *foxp1b*$^{(-/-)}$, R^2 = 0.3318. The slope of the line is not significantly non zero $F_{1,7}$ = 3.477 p = 0.1045. **C.** Scatter graph comparing the change in the number of branching events between timepoints to change in SL. N = 3. *foxp1b*$^{(+/+)}$, R^2 = 0.132. The slope of the line is not significantly non zero $F_{1,4}$ = 0.6081 p = 0.4791. *foxp1b*$^{(-/-)}$, R^2 = 0.003135. The slope of the line is not significantly non zero $F_{1,4}$ = 0.01258 p = 0.9161. **D.** Scatter graph comparing the average number of cells per branch to SL. N = 3. *foxp1b*$^{(+/+)}$, R^2 = 0.9892. The slope of the line is significantly non zero $F_{1,7}$ = 639.4 p < 0.0001. *foxp1b*$^{(-/-)}$, R^2 = 0.5986. The slope of the line is significantly non zero $F_{1,7}$ = 10.44 p = 0.0144. An ancova analysis was performed and the slopes of the lines were not found to be significantly different $F_{1,14}$ = 2.776 p = 0.1179. **E.** Scatter graph comparing the average change in the number of cells per branch to change in SL. N = 3. *foxp1b*$^{(+/+)}$, R^2 = 0.3045. The slope of the line is not significantly non zero $F_{1,4}$ = 1.751 p = 0.2563. *foxp1b*$^{(-/-)}$, R^2 = 0.05662. The slope of the line is not significantly non zero $F_{1,4}$ = 0.2401 p = 0.6498.

4.2.16 - *foxp1b*$^{(-/-)}$ mutants do not show altered hyperplastic or hypertrophic LSAT expansion

I next wanted to examine hypertrophic and hyperplastic LSAT expansion in the *foxp1b*$^{(-/-)}$ mutants. To do this I used images from the *foxp1b*$^{(-/-)}$ timecourse experiment described previously in which fish were imaged every 24 hours over a period of 3 days **(Figure 4.14A)**. The SL of each fish was measured at each timepoint and the change in SL between each timepoint calculated **(Figure 4.14B & C)**. SL was found to increase between each timepoint in both WT and *foxp1b*$^{(-/-)}$ mutant fish with an average increase in SL across all timepoints of 328 µm and 311 µm respectively **(Figure 4.14D)**. The change in the number of adipocytes and progenitor cells between each timepoint was also measured **(Figure 4.14B.E. & F)**. Hyperplastic growth, i.e. increases in adipocyte number, has previously been shown to occur in bursts. Bursts of hypertrophic growth are hard to see in this experiment as it was made up of only three timepoints **(Figure 4.14E)**. Adipocyte number is found to increase between T1-T2 and T2-T3 for both WT and mutant fish, though with only three timepoints and three fish per genotype it is hard to call any of these changes bursts of hyperplastic growth **(Figure 4.14E)**. Progenitor number was found to generally fall between T1-T2 and T2-T3 for WT fish, though it appeared to remain steady in *foxp1b*$^{(-/-)}$ mutant fish **(Figure 4.14F)**. When the change in cell number across all timepoints was plotted it became clear that WT and *foxp1b*$^{(-/-)}$ mutant fish were showing the same patterns of growth, with increases in adipocyte number and little change in progenitor number **(Figure 4.14G)**. WT fish showed an average increase of 19 adipocytes and an average increase of 1 progenitor cell **(Figure 4.14G)**. Meanwhile, *foxp1b*$^{(-/-)}$ mutant fish showed similar changes, with an average increase of 19 adipocytes and an average increase of 3 progenitor cells **(Figure 4.14G)**. The average change in lipid droplet area per cell was also calculated and a steady increase in lipid droplet area was observed across all timepoints for both WT and *foxp1b*$^{(-/-)}$ mutant fish **(Figure 4.14B & H)**. *foxp1b*$^{(-/-)}$ mutant fish showed a slightly lower increase in lipid droplet area than WT fish, with an average increase of 237 µm^2 **(Figure 4.14I)**. The average increase in lipid droplet area in WT fish was 324 µm^2 and the difference in the increase in lipid droplet area between the two genotypes was not found to be significant **(Figure 4.14I)**. In summary although bursts of hyperplastic growth in WT fish were not observed in this experiment no differences in hypertrophic or hyperplastic growth were observed between WT fish and *foxp1b*$^{(-/-)}$ mutants. Therefore, hyperplastic and hypertrophic growth is unaltered in *foxp1b*$^{(-/-)}$ mutants.

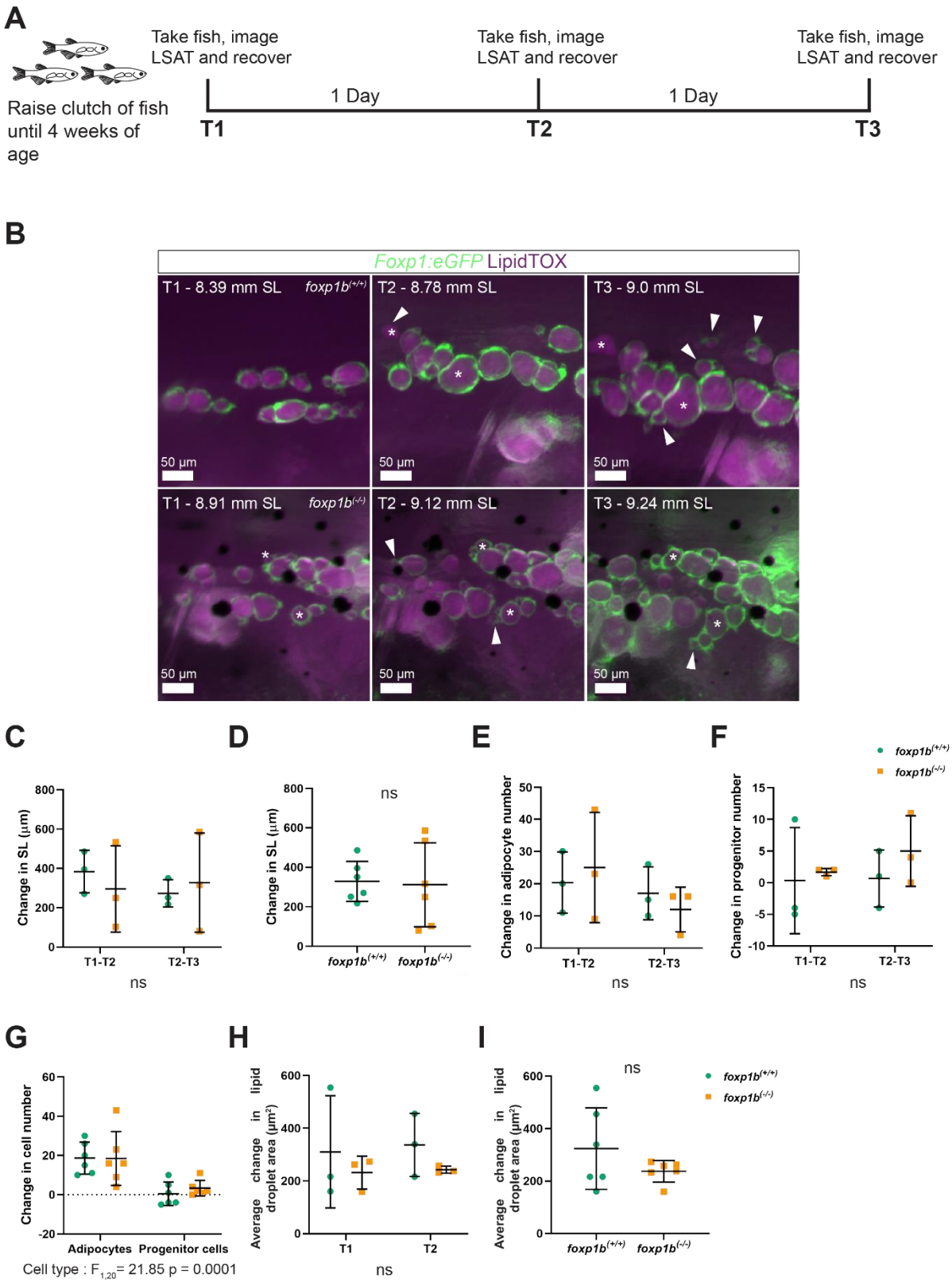

Figure 4.14 – *foxp1b*$^{(-/-)}$ mutants do not show altered rates of hyperplastic and hypertrophic growth.

Figure 4.14 – *foxp1b*$^{(-/-)}$ mutants do not show altered rates of hyperplastic and hypertrophic growth. A. Schematic showing the experimental protocol. **B.** Representative maximum intensity projections of a section of LSAT in the same WT and *foxp1b*$^{(-/-)}$ fish across 3 timepoints. White arrowheads highlight the appearance of new cells. Images are taken from the posterior end of the LSAT, the anterior end of the LSAT is found to the right of the images. **C.** Scatter dot plot showing change in SL across each experimental timepoint. n = 3. Each point shows the change in the SL of one fish across two timepoints. A two way ANOVA was performed and the difference between the groups was not found to be significant. **D.** Scatter dot plot showing change in SL for all fish across all timepoints. n = 3. Each point shows the change in the SL of one fish across two timepoints. A two tailed t-test was performed and the difference between the groups was not found to be significant, p = 0.8628. **E.** Scatter dot plot showing change in adipocyte number across each experimental timepoint. n = 3. Each point shows the change in the number of cells present in the LSAT of one fish across 2 timepoints. A two way ANOVA was performed and the difference between the groups was not found to be significant. **F.** Scatter dot plot showing change in progenitor number across each experimental timepoint. n = 3. Each point shows the change in the number of cells present in the LSAT of one fish across 2 timepoints. A two way ANOVA was performed and the difference between the groups was not found to be significant. **G.** Scatter dot plot showing change in cell number for all fish across all timepoints. Each point shows the change in the number of cells of one fish across two timepoints. A two way ANOVA was performed and the difference between cell types was found to be significant $F_{1,20} = 21.85$ p = 0.0001. **H.** Scatter dot plot showing the average change in cell area across each experimental timepoint. n = 3. Each point shows the change in the average area of the lipid droplets present in the LSAT of one fish across two timepoints. A two way ANOVA was performed and the difference between the groups was not found to be significant. **I.** Scatter dot plot showing the change in average lipid droplet area for all fish across all timepoints. Each point shows the change in the average lipid droplet area of one fish across two timepoints. A two tailed t-test was performed and the difference between the groups was not found to be significant. **C-I.** Error bars show mean and standard deviation.

4.2.17 – Changes in adipocyte number, progenitor number and lipid droplet area are not correlated with changes in SL in *foxp1b*$^{(-/-)}$ mutants

As a final measure of LSAT expansion in *foxp1b*$^{(-/-)}$ mutants, I looked at the relationship between somatic growth and changes in adipocyte and progenitor number and lipid droplet area within LSAT. I first plotted change in adipocyte number against change in SL and found no correlation between the two variables for either WT or *foxp1b*$^{(-/-)}$ mutant fish **(Figure 4.15A)**. I also found no correlation between change in progenitor number and change in SL for either genotype **(Figure 4.15B)**. This lack of correlation between changes in cell number and changes in SL has previously been observed in WT fish. Change in lipid droplet area was previously shown to be correlated with change in SL in WT fish, however this relationship was not found for either WT or mutant fish in this experiment **(Figure 4.15C)**. The lack of correlation between change in average lipid droplet area and change in SL in this experiment may be due to a small sample size **(Figure 4.15C)**. Change in adipocyte number was found not to be correlated with change in average lipid droplet area in both WT and *foxp1b*$^{(-/-)}$ mutant fish **(Figure 4.15D)**. Finally change in adipocyte number was not found to be correlated with change in progenitor number in either genotype **(Figure 4.15E)**. Change in adipocyte number has previously been shown to be negatively correlated with change in progenitor number in WT fish and the lack of observed correlation here may again be due to a small sample size **(Figure 4.15E)**. Taken together these data suggest that the relationship between somatic growth and changes in adipocyte number, progenitor number and lipid droplet area are not altered in *foxp1b*$^{(-/-)}$ mutant fish. Overall LSAT expansion does not appear to be altered in *foxp1b*$^{(-/-)}$ mutant fish.

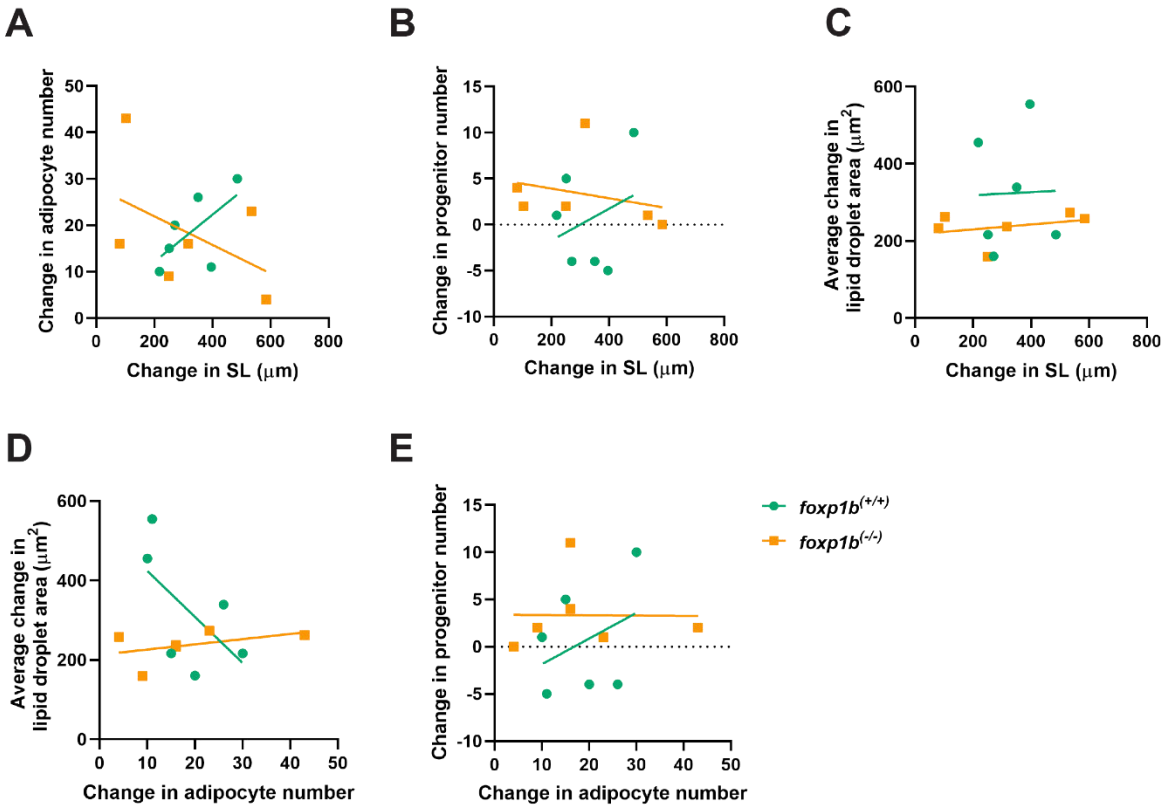

Figure 4.15 – Changes in, adipocyte number, progenitor number and lipid droplet area are not correlated with changes in SL in *foxp1b*$^{(-/-)}$ mutants.

Figure 4.15 – Changes in, adipocyte number, progenitor number and lipid droplet area are not correlated with changes in SL in *foxp1b*$^{(-/-)}$ mutants. A. Scatter graph comparing change in SL to change in adipocyte number. n = 3. Each point shows the change in adipocyte number vs the change in SL for 1 fish between 2 timepoints. *foxp1b*$^{(+/+)}$, R^2 = 0.3965. The slope of the line is not significantly non zero $F_{1,4}$ = 2.628 p = 0.1803. *foxp1b*$^{(-/-)}$, R^2 = 0.2289. The slope of the line is not significantly non zero $F_{1,4}$ = 1.187 p = 0.3371. **B**. Scatter graph comparing change in SL to change in progenitor number. n = 3. Each point shows the change in progenitor number vs the change in SL for 1 fish between 2 timepoints. *foxp1b*$^{(+/+)}$, R^2 = 0.08413. The slope of the line is not significantly non zero $F_{1,4}$ = 0.3674 p = 0.5771. *foxp1b*$^{(-/-)}$, R^2 = 0.0788 The slope of the line is not significantly non zero $F_{1,4}$ = 0.3422 p = 0.59. **C.** Scatter graph comparing change in SL to change in average lipid droplet area. n = 3. Each point shows the change in average lipid droplet area vs the change in SL for 1 fish between 2 timepoints. *foxp1b*$^{(+/+)}$, R^2 = 0.0007026. The slope of the line is not significantly non zero $F_{1,4}$ = 0.002812 p = 0.9602. *foxp1b*$^{(-/-)}$, R^2 = 0.1081. The slope of the line is not significantly non zero $F_{1,4}$ = 0.4849 p = 0.5246. **D.** Scatter plot comparing change in adipocyte number to change in average lipid droplet area. n = 3. Each point shows the change in adipocyte number vs the change in average lipid droplet area for 1 fish between 2 timepoints. *foxp1b*$^{(+/+)}$, R^2 = 0.3684. The slope of the line is not significantly non zero $F_{1,4}$ = 2.333 p = 0.2014. *foxp1b*$^{(-/-)}$, R^2 = 0.1897. The slope of the line is not significantly non zero $F_{1,4}$ = 0.9363 p = 0.388. **E.** Scatter plot comparing change in adipocyte number to change in progenitor number. n = 3. Each point shows the change in adipocyte number vs the change progenitor number for 1 fish between 2 timepoints. *foxp1b*$^{(+/+)}$, R^2 = 0.1347. The slope of the line is not significantly non zero $F_{1,4}$ = 0.6225 p = 0.4742. *foxp1b*$^{(-/-)}$, R^2 = 0.0001215. The slope of the line is not significantly non zero $F_{1,4}$ = 0.0004862 p = 0.9835.

4.2.18 - *foxp1a*$^{(-/-)}$*:foxp1b*$^{(-/-)}$ mutants do not have an altered LSAT appearance

I next examined LSAT expansion in *foxp1a*$^{(-/-)}$*:foxp1b*$^{(-/-)}$ double mutants. As *foxp1a*$^{(-/-)}$*:foxp1b*$^{(-/-)}$ mutants have previously been shown to have a more severe phenotype than either of the single mutants, I performed a shorter preliminary experiment using the *foxp1a*$^{(-/-)}$*:foxp1b*$^{(-/-)}$ double mutants **(Figure 4.16A)**. *Foxp1:eGFP:foxp1a*$^{(+/-)}$*:foxp1b*$^{(+/-)}$ fish were incrossed and their offspring raised until approximately 13 mm SL. Fish were then genotyped and *foxp1a*$^{(-/-)}$*:foxp1b*$^{(-/-)}$ mutant fish and WT siblings were incubated with LipidTOX and their LSAT imaged using a stereomicroscope **(Figure 4.16A)**. Following imaging all fish were recovered and used to establish breeding stocks **(Figure 4.16A)**. I first examined the appearance of LSAT in the *foxp1a*$^{(-/-)}$*:foxp1b*$^{(-/-)}$ mutants. The overall appearance of LSAT in the *foxp1a*$^{(-/-)}$*:foxp1b*$^{(-/-)}$ mutants was normal, with LSAT present as a long thin depot which extended primarily along the anterior-posterior axis. LSAT branching was also observed in the *foxp1a*$^{(-/-)}$*:foxp1b*$^{(-/-)}$ mutants **(Figure 4.16B)**. I next quantified the number of branching events per LSAT in both the WT and *foxp1a*$^{(-/-)}$*:foxp1b*$^{(-/-)}$ mutant fish **(Figure 4.16B & C)**. I found no correlation between branch number and SL in WT fish but a positive correlation was present in *foxp1a*$^{(-/-)}$*:foxp1b*$^{(-/-)}$ mutant fish **(Figure 4.16C)**. The lack of correlation in WT fish is likely due to a small sample size. No differences in the number of branching events were observed between WT and *foxp1a*$^{(-/-)}$*:foxp1b*$^{(-/-)}$ mutant fish **(Figure 4.16C)**. I then examined branch length and plotted the average number of cells per branch against SL **(Figure 4.16B & D)**. Here I found no correlation between branch length and SL for either genotype and again this is likely to be caused by a small sample size **(Figure 4.16D)**. No differences in the average number of cells per branch were observed between the two genotypes **(Figure 4.16D)**. Overall the LSAT depot appears to have a normal morphology in *foxp1a*$^{(-/-)}$*:foxp1b*$^{(-/-)}$ mutants and there are no changes in LSAT branching in *foxp1a*$^{(-/-)}$*:foxp1b*$^{(-/-)}$ mutants.

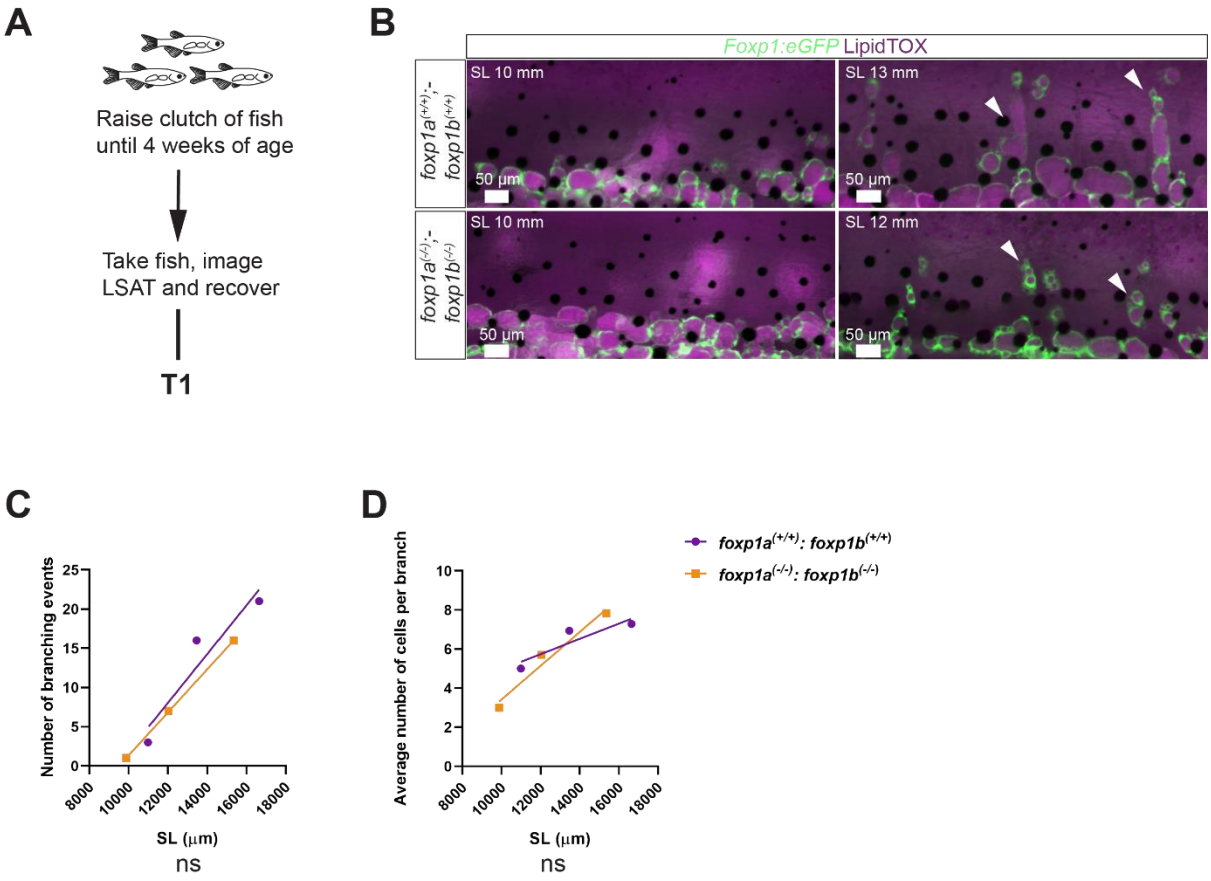

Figure 4.16 – *foxp1a*$^{(-/-)}$*:foxp1b*$^{(-/-)}$ mutants do not have an altered LSAT appearance.

Figure 4.16 – *foxp1a*$^{(-/-)}$*:foxp1b*$^{(-/-)}$ mutants do not have an altered LSAT appearance. A. Schematic showing the experimental protocol. **B.** Representative maximum intensity projections showing increasing number of branching events with increasing SL in both *foxp1a*$^{(-/-)}$*:foxp1b*$^{(-/-)}$ mutants and WT siblings. Each panel shows LSAT from a different fish. White arrowheads highlight branching events. Branches are defined as a chain of 3 or more adipocytes which branch away from the main line of the LSAT at a roughly 45° angle. The anterior end of the LSAT is found to the right of each image. **C.** Scatter graph comparing the number of branching events to SL. n = 3. *foxp1a*$^{(+/+)}$*:foxp1b*$^{(+/+)}$, R^2 = 0.899. The slope of the line is not significantly non zero $F_{1,1}$ = 8.901 p = 0.2059. *foxp1a*$^{(-/-)}$*:foxp1b*$^{(-/-)}$, R^2 = 1.00. The slope of the line is significantly non zero $F_{1,1}$ = 327467 p = 0.0038. An Ancova analysis was performed and the slopes of the lines were not found to be significantly different. **D.** Scatter graph comparing the average number of cells per branch to SL. N = 3. *foxp1a*$^{(+/+)}$*:foxp1b*$^{(+/+)}$, R^2 = 0.8077. The slope of the line is not significantly non zero $F_{1,1}$ = 4.2 p = 0.289. *foxp1a*$^{(-/-)}$*:foxp1b*$^{(-/-)}$, R^2 = 0.9636. The slope of the line is not significantly non zero $F_{1,1}$ = 26.47 p = 0.1222. An ancova analysis was performed and the slopes of the lines were not found to be significantly different $F_{1,14}$ = 2.776 p = 0.1179.

4.2.19 - *foxp1a*$^{(-/-)}$*;foxp1b*$^{(-/-)}$ mutants show no differences in adipocyte number, progenitor cell number or lipid droplet area.

Finally, I wanted to determine whether adipose progenitor numbers and adipose morphology were altered in the LSAT of *foxp1a*$^{(-/-)}$*;foxp1b*$^{(-/-)}$ mutants. To do this I measured adipocyte number, progenitor cell number and lipid droplet area in the LSAT of the *foxp1a*$^{(-/-)}$*:foxp1b*$^{(-/-)}$ mutant fish and their WT siblings **(Figure 4.17A.C.E & G)**. The SL of all fish was measured and no difference was found between the SL of *foxp1a*$^{(-/-)}$*:foxp1b*$^{(-/-)}$ mutants and WT fish **(Figure 4.17B)**. The number of adipocytes per LSAT was found to be positively correlated with SL in WT fish but not in *foxp1a*$^{(-/-)}$*:foxp1b*$^{(-/-)}$ mutants **(Figure 4.17C & D)**. The number of adipocytes per LSAT was not found to be significantly different in *foxp1a*$^{(-/-)}$*:foxp1b*$^{(-/-)}$ and WT fish **(Figure 4.17C & D)**. Progenitor number was also measured and this was found to be correlated to SL in *foxp1a*$^{(-/-)}$*:foxp1b*$^{(-/-)}$ mutants but not in WT fish **(Figure 4.17E & F)**. The lack of correlation between cell number and SL in both WT and *foxp1a*$^{(-/-)}$*:foxp1b*$^{(-/-)}$ mutants is likely due to a small sample size. The number of progenitor cells per LSAT was not found to be significantly different in *foxp1a*$^{(-/-)}$*:foxp1b*$^{(-/-)}$ mutants and WT fish **(Figure 4.17E & F)**. Finally, average lipid droplet area was plotted against SL and no correlation was observed for either genotype **(Figure 4.17G & H)**. Again, as a correlation between these variables has previously been observed in WT fish, the lack of correlation here is likely due to a small sample size. A significant difference in lipid droplet area between the two genotypes was not found. In conclusion *foxp1a*$^{(-/-)}$*:foxp1b*$^{(-/-)}$ mutants appear to have a normal LSAT morphology.

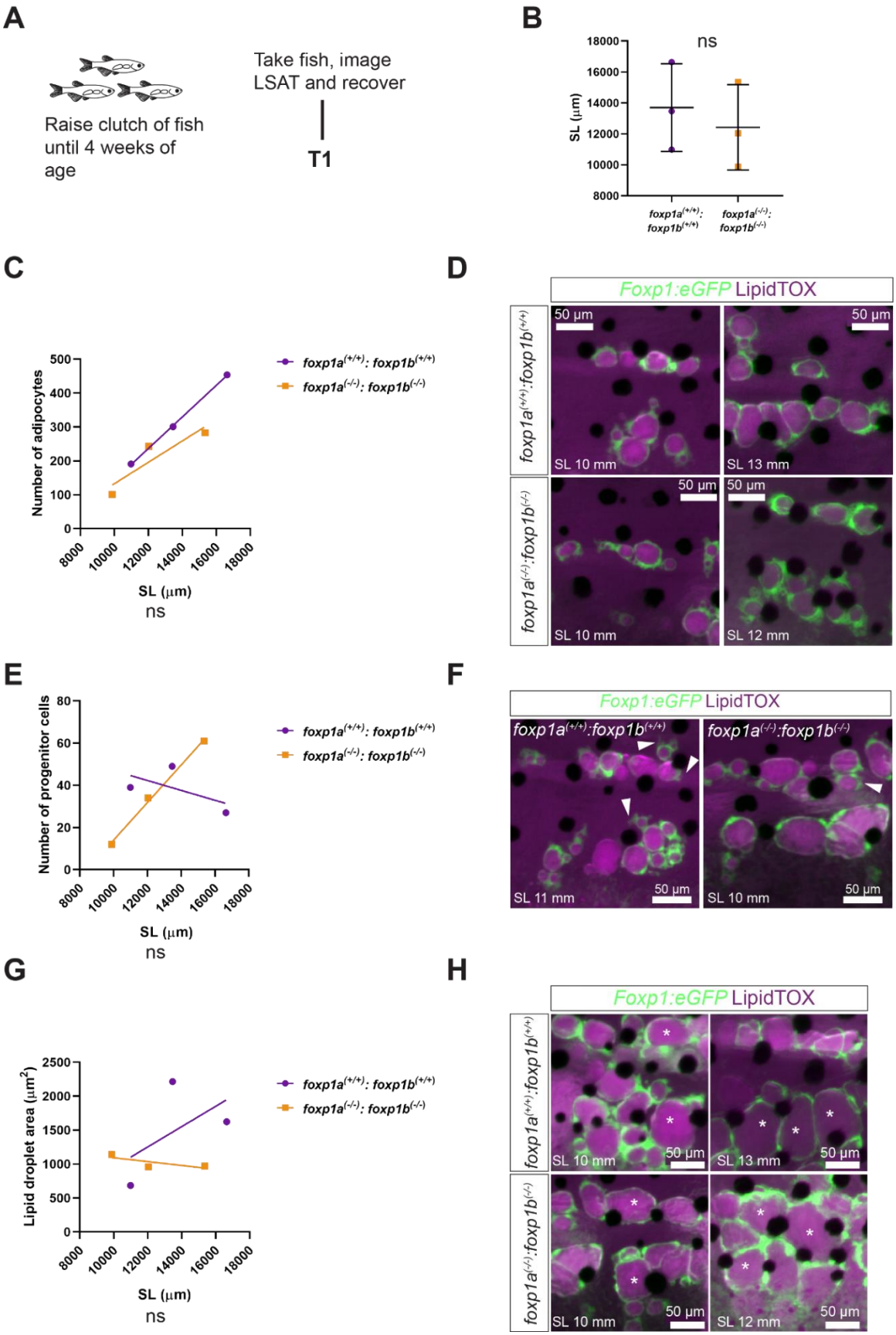

Figure 4.17 – *foxp1a*$^{(-/-)}$;*foxp1b*$^{(-/-)}$ mutants have a normal LSAT morphology

Figure 4.17 – *foxp1a*$^{(-/-)}$*;foxp1b*$^{(-/-)}$ mutants have a normal LSAT morphology. A. Schematic showing the experimental protocol. **B.** Scatter dot plot showing the SL of WT and *foxp1a*$^{(-/-)}$*:foxp1b*$^{(-/-)}$ mutants. n = 3 per genotype. A two tailed t-test was performed and the difference between the groups was not found to be significant, p = 0.6059. **C.** Scatter graph comparing number of adipocytes per LSAT to SL. n = 3. *foxp1a*$^{(+/+)}$*:foxp1b*$^{(+/+)}$, R^2 = 0.9995. The slope of the line is significantly non zero $F_{1,1}$ = 2086 p = 0.0139. *foxp1a*$^{(-/-)}$*:foxp1b*$^{(-/-)}$, R^2 = 0.8232. The slope of the line is not significantly non zero $F_{1,1}$ = 4.657 p = 0.2763. An Ancova analysis was performed and the slopes of the lines were not found to be significantly different. **D.** Representative maximum intensity projections showing increasing adipocyte number with increasing SL in both *foxp1a*$^{(-/-)}$*;foxp1b*$^{(-/)}$ mutants and WT siblings. Each panel shows LSAT from a different fish. The anterior end of the LSAT depot is found to the right of each image. **E.** Scatter graph comparing number of progenitor cells to SL. n = 3. *foxp1a*$^{(+/+)}$*:foxp1b*$^{(+/+)}$, R^2 = 0.3646. The slope of the line is not significantly non zero $F_{1,1}$ = 0.5738 p = 0.5873. *foxp1a*$^{(-/-)}$*:foxp1b*$^{(-/-)}$, R^2 = 0.9961. The slope of the line is significantly non zero $F_{1,1}$ = 258.2 p = 0.0396. An Ancova analysis was performed and the slopes of the lines were not found to be significantly different. **F.** Representative maximum intensity projections showing similar number of adipose progenitor cells in *foxp1a*$^{(-/-)}$*;foxp1b*$^{(-/-)}$ mutants and WT siblings. White arrow heads highlight adipose progenitor cells. The anterior end of the LSAT depot is found to the right of each image. **G.** Scatter graph comparing average lipid droplet area to SL. n = 3. *foxp1a*$^{(+/+)}$*:foxp1b*$^{(+/+)}$, R^2 = 0.3017. The slope of the line is not significantly non zero $F_{1,1}$ = 0.4319 p = 0.6298. *foxp1a*$^{(-/-)}$*:foxp1b*$^{(-/-)}$, R^2 = 0.5719. The slope of the line is not significantly non zero $F_{1,1}$ = 1.336 p = 0.454. An Ancova analysis was performed and the slopes of the lines were not found to be significantly different **H.** Representative maximum intensity projections showing increasing adipocyte area with increasing SL in both *foxp1a*$^{(-/-)}$*;foxp1b*$^{(-/-)}$ mutants and WT siblings. Each panel shows LSAT from a different fish. Asterisks highlight large lipid droplets. The anterior end of the LSAT is found to the right of each image.

4.3 - Discussion

In this chapter I have generated a novel zebrafish transgenic line which labels both adipocytes and adipose progenitor cells. This transgenic line has allowed LSAT growth in live zebrafish to be imaged and has allowed the dynamics of normal LSAT growth to be quantified. Using this transgenic line I have proposed a model of spatial LSAT expansion, in which new cells are added to the centre of the depot and LSAT then further expands by forming chains of adipocytes which branch away from the main LSAT body. I have also shown that LSAT expands by steady hypertrophic growth with bursts of hyperplastic growth. I then demonstrated that *foxp1a* but not *foxp1b* is required for normal LSAT expansion. LSAT was found to expand normally in *foxp1b*$^{(-/-)}$ mutants but new cells were not added to the centre of LSAT in *foxp1a*$^{(-/-)}$ mutants and the number of cells per branch was found to be increased in these mutants. Finally the morphology of the LSAT depot was found to be normal in *foxp1a*$^{(-/-)}$*:foxp1b*$^{(-/-)}$ mutants however further timecourse experiments are required to determine if LSAT expansion is impaired in these mutants. In this section I will discuss the limitations of the data I have presented, and a broader discussion can be found in the general discussion section (Chapter 6).

The *Foxp1:eGFP* line has GFP expression in both adipocytes and adipose progenitor cells and was used to measure LSAT expansion. Adipocytes were identified by their morphology and an individual adipocyte was defined as a cell with a GFP positive cytoplasm and a singular lipid droplet. However, during the analysis of LSAT growth it was sometimes difficult to determine if cells in close proximity constituted one cell or two. Furthermore, it is known that both mammalian and zebrafish white adipocytes may contain multiple small lipid droplets during early terminal differentiation (Flynn et al., 2009). However, due to the nature of the *Foxp1:eGFP* line, early terminally differentiated adipocytes could not be distinguished from multiple small adipocytes. One way to overcome this challenge would be to express a nuclear marker in the *Foxp1:eGFP* transgenic line. For example, mRNA of fluorescently tagged histone 2B (H2B) could be injected into *Foxp1:eGFP* embryos at the one cell stage (Imrie and Sadler, 2010). H2B localises fluorescent protein expression to chromatin and so acts as a nuclear marker (Imrie and Sadler, 2010). This strategy would mark all nuclei and would allow adipocytes with multiple lipid droplets and small adipocytes with a single lipid droplet to be distinguished.

Another limitation of the data presented is that the differentiation of adipose progenitor cells into adipocytes cannot be visualised and instead must be inferred. The timing of the LSAT imaging every 24 hours meant that the appearance of many adipose progenitor cells was missed. This could be observed by the lack of any cells at one timepoint and the appearance of mature adipocytes 24 hours later. This problem could be overcome by imaging at reduced intervals or by continuous imaging of the same fish over a set time period.

Finally, the data presented from the *foxp1* mutants suggests that *foxp1* may be involved in the spatial expansion of LSAT however no differences were observed in adipose progenitor cell behaviour. Strong phenotypes were not observed in the *foxp1a*$^{(-/-)}$ and *foxp1b*$^{(-/-)}$ single mutants during normal development. However, this is not too surprising as both mutants had normal levels of AT during normal development and only displayed a phenotype following exposure to a high fat diet. Furthermore, *foxp1b*$^{(-/-)}$ mutants showed normal LSAT expansion both during normal development and in response to a high fat diet and so the normal LSAT growth observed in the *Foxp1:eGFP:foxp1b*$^{(-/-)}$ mutants was not unexpected. The major limitation here is the lack of *foxp1a*$^{(-/-)}$*;foxp1b*$^{(-/-)}$ data. This could be overcome by performing more *foxp1a*$^{(-/-)}$*;foxp1b*$^{(-/-)}$ imaging and by ensuring that the imaging took place over a period of three days, i.e. following the same protocol as outlined in section 4.2.10.

In summary I have presented data which for the first time quantifies the cellular dynamics of AT expansion in zebrafish. I have also shown that *foxp1* may play a role in regulating the expansion of LSAT, however further work is required to uncover whether *foxp1* influences adipose progenitor cell behaviour. Here I have detailed the major limitations of the data presented, and a more comprehensive discussion can be found in chapter 6.

Chapter 5 – The role of *cebpa* as a master regulator of adipogenesis is conserved from mammals to zebrafish

5.1 – Introduction

Obesity is associated with adipose tissue dysfunction (Crewe et al., 2017). Adipose tissue (AT) dysfunction occurs when adipose tissue expands beyond its normal capacity (Lafontan, 2014). This leads to hypoxia, fibrosis, cellular senescence and necrotic adipocyte death (Crewe et al., 2017). The resulting dysfunctional adipose tissue is no longer able to store lipid, and this results in the ectopic deposition of lipid in the liver and insulin resistance (Lafontan, 2014). One factor known to influence adipose tissue dysfunction is adipose morphology. Adipose morphology is defined as the number and size distribution of adipocytes within adipose tissue (Hoffstedt et al., 2010). A hypertrophic adipose tissue, characterised by the presence of few large adipocytes, is associated with dysfunctional adipose tissue (Hoffstedt et al., 2010). In contrast a hyperplastic adipose tissue morphology, characterised by the presence of many small adipocytes, is associated with a normal metabolic profile (Hoffstedt et al., 2010). Therefore, obesity is associated with adipose tissue dysfunction and a hypertrophic adipose morphology is also associated with adipose tissue dysfunction.

Adipose tissue can expand via an increase in adipocyte number or an increase in adipocyte size. Changes in adipocyte size are controlled by lipid entering or leaving the cell, while changes in cell number are controlled by cell death and the differentiation of progenitor cells (Lapid and Graff, 2017, Siersbaek and Mandrup, 2011, Tsuboyama-Kasaoka et al., 2000). I will now expand on how increases in cell number can increase adipose tissue area and improve adipose tissue dysfunction. The hyperplastic growth of adipose tissue is controlled by the differentiation of progenitor cells into mature adipocytes in a process known as adipogenesis (Siersbaek et al., 2012). Adipogenesis is controlled by a network of transcription factors (Siersbaek et al., 2012). External factors initiate a first wave of transcription factors, and they in turn activate a second wave of transcription factors (Siersbaek et al., 2012). This second wave contains the master regulators peroxisome proliferator activated receptor gamma (*Pparg*) and CCAAT enhancer binding protein alpha (*Cebpa*), and these factors then bring about the expression of genes which result in the mature adipocyte phenotype (Siersbaek et al., 2012). Adipogenesis can therefore mediate adipose tissue expansion via hyperplastic growth.

One of the master regulators of adipogenesis, *Cebpa,* is capable of influencing adipose tissue levels *in vivo*. *Cebpa* is a basic leucine zipper transcription factor which

is most abundantly expressed in adipose tissue, the liver and the placenta (Linhart et al., 2001). Although much of the work on uncovering the transcriptional network which controls adipogenesis has been done *in vitro*, *Cebpa* has also been shown to influence adipose levels *in vivo* (Linhart et al., 2001, Siersbaek et al., 2012). As whole body *Cebpa* knock out mice die shortly after birth due to liver defects, a study by Linhart et al (2001) generated a transgenic mouse in which *Cebpa* expression was restricted to the liver (Flodby et al., 1996, Wang et al., 1995). The line was generated by crossing the *Cebpa* knockout line to a line in which *Cebpa* was expressed under the albumin promoter (Linhart et al., 2001). This produced a mouse in which *Cebpa* expression was limited to the liver and improved the survival of the mice (Linhart et al., 2001). The knockout mice were found to have no white adipose tissue which demonstrated that *Cebpa* is required for the commitment of preadipocytes to adipocytes *in vivo* (Linhart et al., 2001). The transgenic mice also had increased serum insulin levels, despite normal glucose levels, suggestive of peripheral insulin resistance (Linhart et al., 2001). In summary, one of the master regulators of adipogenesis is capable of modulating adipose levels and metabolic regulation *in vivo*. Therefore, identification of novel genetic factors which influence adipose tissue levels could lead to the development of treatments to alleviate the metabolic dysregulation associated with obesity.

Zebrafish are an emerging model of adipose tissue biology and have previously been used to test if novel candidate genes play a role in adipose tissue expansion (Minchin et al., 2015). Much is known about AT in zebrafish. For example, zebrafish are known to possess AT which is homologous to mammalian white AT, and which expresses many of the same molecular markers as mammalian WAT (Flynn et al., 2009). It is also known that zebrafish adipose tissue acts as an energy store, with adipose in zebrafish expanding in response to a high fat diet (Minchin and Rawls, 2017b). However, much of what is known about the molecular regulation of adipose tissue expansion in mammals is unknown in zebrafish. Therefore, a better understanding of the molecular regulation of adipose tissue expansion in zebrafish would help to further establish zebrafish as a model of adipose tissue expansion. As many aspects of adipose tissue biology are conserved from mammals to zebrafish, it seems likely this is also true of the molecular basis of adipose tissue expansion. This leads me to the hypothesis that *cebpa* controls adipose tissue expansion in zebrafish.

In this chapter I have generated two novel loss of function *cebpa* alleles, to investigate the hypothesis that *cebpa* controls adipose tissue expansion in zebrafish. I have used these mutants to test my hypothesis by measuring adipose levels in response to both a control and high fat diet. *cebpa* mutants were found to have reduced levels of adipose tissue on both a control and high fat diet. Mutants were also found to have a more hypertrophic adipose tissue morphology and increased levels of blood triglycerides. This phenotype closely mirrors that of the *Cebpa* knockout mice generated by Linhart et al (2001). Overall, I have found data which suggests a conserved role for *cebpa* in adipose tissue expansion in zebrafish. I have also used RNA Seq to identify novel candidate genes which may be involved in adipose tissue expansion.

5.2 – Results

5.2.1 - Zebrafish possess a gene homologous to mammalian *Cebpa*

In order to investigate if the molecular basis of adipogenesis is conserved in zebrafish, I have chosen to examine the role of the transcription factor *cebpa*. *Cebpa* is a master regulator of adipogenesis in mammals. To investigate the role of *cebpa* in zebrafish I first had to determine whether *Cebpa* is conserved in zebrafish and to what extent it is conserved. To do this I used the gene tree feature on Ensembl (ENSGT00940000162646). Briefly, gene tree shows the maximum likelihood phylogenetic tree for a given gene and represents the evolutionary history of that gene. Using gene tree, I traced the human ortholog of *CEBPA* to the zebrafish *cebpa* gene **(Figure 5.1A)**. I then made use of the Clustal Omega alignment software to determine how well the cDNA and protein sequences of *cebpa* were conserved. I compared the cDNA and protein sequences of human, mouse and *Xenopus cebpa* to that of zebrafish *cebpa* **(Figure 5.1B & C)**. Zebrafish *cebpa* seems to show moderate levels of conservation to human *CEBPA*, with 64.94% cDNA sequence homology and 61.81% protein sequence homology **(Figure 5.1B & C)**. Using the protein summary information on Ensembl I was also able to find that, like mammalian *Cebpa*, zebrafish *cebpa* is comprised of a single exon **(Figure 5.1D)**. Zebrafish *cebpa* also contains two TAD (Transactivation Domain) domains and a bZIP DNA binding domain **(Figure 5.1D)** (ENSP00000427514.1). The two TAD domains in Cebpa are thought to bind to transcriptional coactivators and binding of these cofactors is thought to be necessary for transcription of *cebpa* (Kovacs et al., 2003). The bZIP DNA binding domain shows higher conservation than the entire Cebpa protein, with 80.65% sequence homology between human and zebrafish sequences **(Figure 5.1D & E)**. In summary both the sequence and functional domains of the *Cebpa* gene are conserved to zebrafish.

A

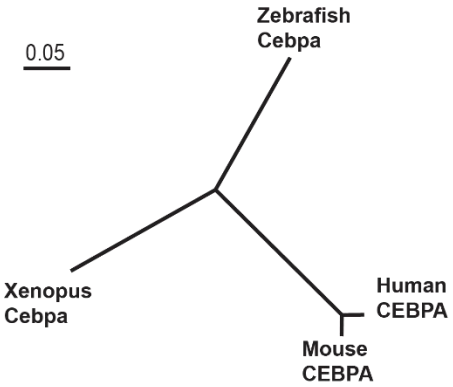

B

cDNA Sequence	Zebrafish *cebpa* (201)
Zebrafish *cebpa* (201)	100%
Xenopus *cebpa* (201)	66.19%
Mouse *Cebpa* (201)	64.59%
Human *CEBPA* (201)	64.94%

C

Protein Sequence	Zebrafish Cebpa (201)
Zebrafish Cebpa (201)	100%
Xenopus Cebpa (201)	65.34%
Mouse CEBPA (201)	62.15%
Human CEBPA (201)	61.81%

D

E

Figure 5.1 – Zebrafish possess a gene homologous to mammalian *Cebpa*. A. Unrooted phylogenetic tree. Amino acid sequences were aligned using Clustal Omega. Unrooted was used to generate the tree (Pole Bioinformatique Lyonnais). Scale bar shows amino acid changes per site. **B.** Comparison of *cebpa* isoforms homologous to the human isoform 201. Numbers correspond to isoforms as identified on Ensembl. Sequences were aligned using Clustal Omega **C.** Comparison of Cebpa protein sequences homologous to the human isoform 201. Numbers correspond to isoforms as identified on Ensembl. Sequences were aligned using Clustal Omega. **D.** Schematic showing the functional domains of Cebpa. Functional domains are shown in green. bZIP (Pfam). Percentage conservation of the bZIP domain is shown. **E.** Alignment of the protein sequences of the bZIP domains of human and zebrafish Cebpa. Alignment was generated using Clustal Omega. Red letters and asterisks show changed amino acids.

5.2.2 - CRISPR/Cas9 was used to generate zebrafish with heritable mutations in *cebpa*

To investigate the role of *cebpa* in adipose tissue expansion, I next wanted to generate loss of function *cebpa* alleles. To achieve this, I made use of the CRISPR/Cas9 system. I first designed a series of guide RNAs (gRNAs) targeting close to the translation start site of *cebpa* **(Figure 3.3A)**. The translation start site was targeted to try and disrupt as much protein function as possible. The gRNAs were then synthesised and injected into WT zebrafish embryos at the one cell stage, along with the Cas9 nuclease protein **(Figure 3.3A).** The mutagenic activity of each of the guides was then assessed using a T7 endonuclease 1 (T7E1) assay **(Figure 5.2A)**. gRNAs which produced a different banding pattern to that of uninjected fish were deemed to be active and inducing mutations **(Figure 5.2A)**. The active gRNAs were then reinjected into wild type (Cawthorn et al.) embryos, in order to generate stable lines. These embryos were raised until adulthood and became the G0 generation **(Figure 3.3A & B)**. In order to generate stable mutant lines, G0 fish with germline mutations were identified. Adult G0 fish were outcrossed to WT fish and their progeny screened by T7E1 assay for lesions at the CRISPR target locus **(Figure 3.3B & Figure 5.2B)**. G0 fish found to have germline mutations were again crossed to WT fish and their offspring raised to adulthood **(Figure 3.3B)**. These fish became the F1 generation. In summary this strategy generated a F1 generation of fish with heritable mutations in *cebpa.*

5.2.3 - The nature of the mutations generated by CRISPR/Cas9 were identified and mutations predicted to have a severe effect on protein function were selected

The CRISPR/Cas9 system does not induce mutations in all F1 fish and the effect of the mutations induced is also not likely to be the same. To determine if a mutation had occurred and the nature of the mutation, DNA from F1 fish was sent for sequencing **(Figure 3.3C - Stage 3)**. Tissue from the caudal fin of adult F1 fish was taken and gDNA extracted. This gDNA was then sent for sequencing. Predicted frameshift mutations were selected for, as these were predicted to severely disrupt protein function. The selected F1 mutants were then outcrossed to WT fish **(Figure 3.3D)**. This then produced a breeding stock, 50% of which were WT and 50% of which

were heterozygous for a known mutation **(Figure 3.3D)**. Overall, I was able to generate two mutant alleles which were predicted to have a severe effect on the function of Cebpa.

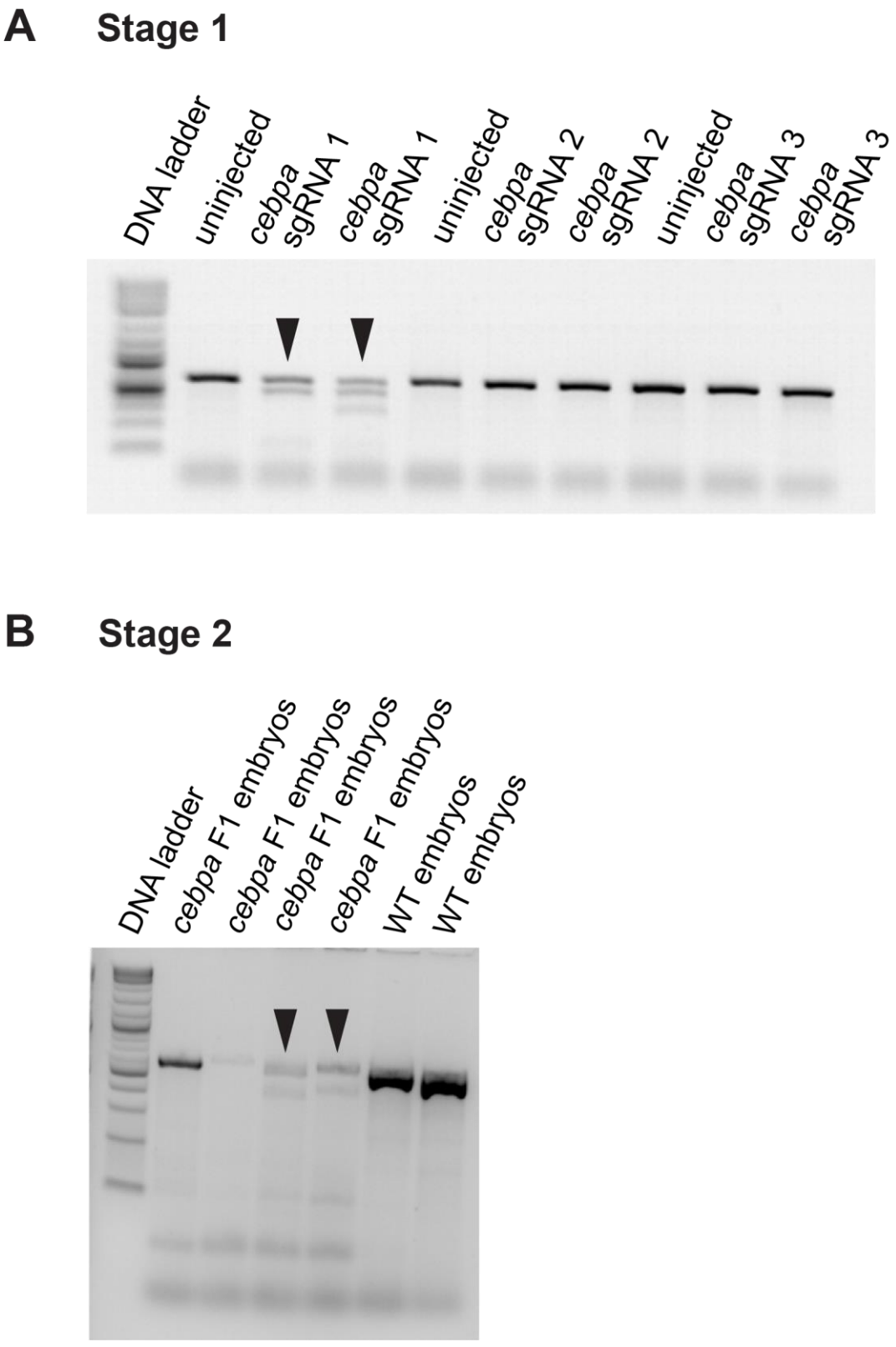

Figure 5.2 – CRISPR/Cas9 induces mutations in *cebpa*.

Figure 5.2 – CRISPR/Cas9 induces mutations in *cebpa*. A. T7E1 assay gels used to test CRISPR guide efficiency. See stage 1 of Figure 5.2. Guides are cutting if the banding pattern in the injected lane is different to that of the uninjected lane. Arrowheads highlight changes in the banding patterns in the injected fish. Pools of 10 embryos were tested. **B.** T7E1 assay gels used to test CRISPR activity in F1 embryos. See stage 2 of Figure 5.2. Guides are cutting if the banding pattern in the injected lane is different to that of the uninjected lane. Arrowheads highlight changes in the banding patterns in the injected fish. Pools of 10 embryos were tested.

5.2.4 - Two mutant alleles, predicted to have severe effects on protein function, were generated using CRISPR/Cas9

Using CRISPR/Cas9 and the strategy outlined above, I was able to generate two mutant alleles. The first allele, *cebpa*$^{(ed19/ed19)}$, is caused by a 38bp deletion close to the translation start site, which results in a frameshift and the introduction of an early stop codon **(Figure 5.3A, B & C)**. The mutant protein is predicted to have lost the bZIP DNA binding domain, and also the TAD2 domain **(Figure 5.3A)**. Therefore, the *cebpa*$^{(ed19/ed19)}$ allele is predicted to be non-functional. The second mutant allele, *cebpa*$^{(ed20/ed20)}$ is the result of a 7bp deletion **(Figure 5.3A &B)**. The 7bp deletion is predicted to cause a frameshift and to introduce an early stop codon **(Figure 5.3A, B & C)**. Like the *cepba*$^{(ed19/ed19)}$ allele, the *cepba*$^{(ed20/ed20)}$ allele is predicted to lack any functional domains and is therefore thought to be a loss of function mutant **(Figure 5.3A)**. In summary, using CRISPR/Cas9 I effectively induced mutations in *cebpa* and generated two predicted loss of function mutant alleles.

5.2.5 - *cebpa*$^{(ed19/ed19)}$ and *cebpa*$^{(ed20/ed20)}$ mutants do not show a decrease in *cebpa* transcript levels

Having generated two predicted loss of function *cebpa* alleles, I next wanted to determine to what degree the alleles were affected. It was hypothesised that alleles showing high levels of transcript degradation would show high levels of protein reduction and a severe phenotype. I therefore assessed *cebpa* mRNA levels in the *cebpa*$^{(ed19/ed19)}$ and *cebpa*$^{(ed20/ed20)}$ fish. To do this I fin clipped WT and mutant fish at 5 days post fertilisation (dpf) and extracted RNA from pools of embryos. Transcript levels were then measured by RT-qPCR **(Figure 5.3D & E)**. It was found that *cebpa* transcript levels were not reduced in either the *cebpa*$^{(ed19/ed19)}$ mutants or in the *cebpa*$^{(ed20/ed20)}$ mutants **(Figure 5.3D & E)**. *cebpa* transcript levels were increased in both *cebpa*$^{(ed19/ed19)}$ and *cebpa*$^{(ed20/ed20)}$ mutants when compared to WT siblings, and this difference was significant in *cebpa*$^{(ed19/ed19)}$ fish **(Figure 5.3D & E)**. *cebpa*$^{(ed19/ed19)}$ mutants showed a 1.5 fold increase in transcripts, while *cebpa*$^{(ed20/ed20)}$ mutants showed a 1.8 fold increase **(Figure 5.3D & E)**. This increase in transcript levels was unexpected, however it does not provide any information about protein levels in the mutants. Attempts were made to assess protein levels in the mutants using a Western blot and an antibody which recognised the human CEBPA protein. The antibodies

tested were not able to recognise the zebrafish Cebpa protein, and this may be due to a lack of homology between the two proteins. In summary *cebpa* mRNA levels are increased in *cebpa*$^{(ed19/ed19)}$ and *cebpa*$^{(ed20/ed20)}$ fish when compared to WT siblings however protein levels in these mutants remain unknown.

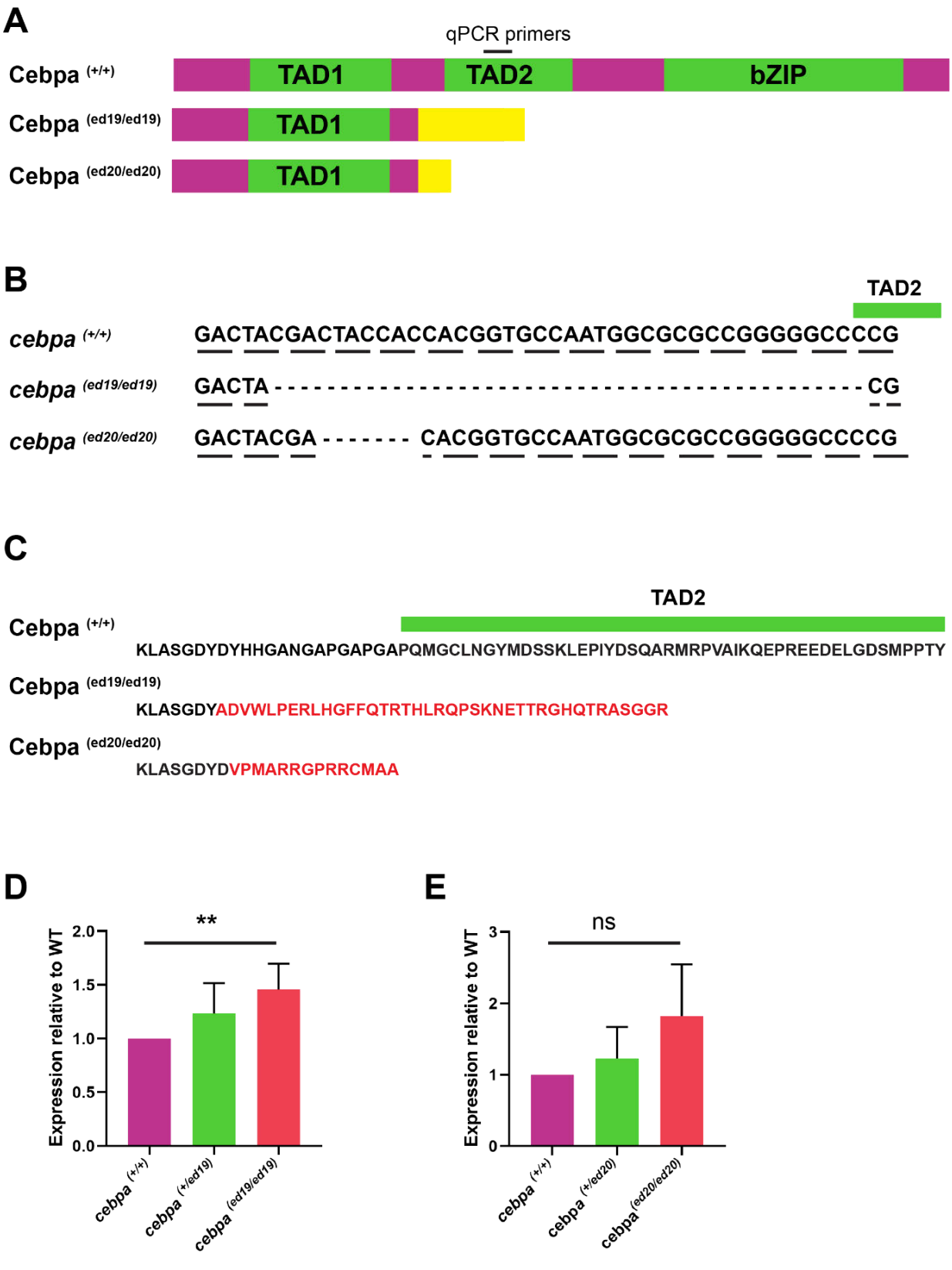

Figure 5.3 – *cebpa*$^{(ed19/ed19)}$ and *cebpa*$^{(ed20/ed20)}$ mutants do not show a reduction in *cebpa* transcript levels.

Figure 5.3 – *cebpa*$^{(ed19/ed19)}$ and *cebpa*$^{(ed20/ed20)}$ mutants do not show a reduction in *cebpa* transcript levels. A. Schematic showing the structure of the Cebpa protein in WT and in both *cebpa*$^{(ed19/ed19)}$ and *cebpa*$^{(ed20/ed20)}$ fish. Green bars show functional domains. TAD (Transactivation domain). bZIP (basic leucine zipper). Yellow bars indicate a change to the protein sequence in *cebpa*$^{(ed19/ed19)}$ and *cebpa*$^{(ed20/ed20)}$ mutants, as depicted in 5.4C. The location of qPCR primers is marked. **B.** Letters indicate DNA bases. Small dashed lines illustrate where a deletion has taken place. The thicker dashed lines show the reading frame. The green bar shows the start of the TAD2 domain. **C.** Letters represent amino acids. Letters in red are changed from the WT sequence. The green bar marks the TAD2 domain. **D.** n = 5-6. A two tailed t-test was performed to compare the *cebpa*$^{(+/+)}$ and *cebpa*$^{(ed19/ed19)}$ groups, p = 0.0011. Error bars show standard deviation. **E.** n = 6. Error bars show standard deviation. Ns (Not significant).

5.2.6 - *cebpa*$^{(ed19/ed19)}$ and *cebpa*$^{(ed20/ed20)}$ mutants show the same larval death phenotype as published zebrafish mutants

To further test if the *cebpa*$^{(ed19/ed19)}$ and *cebpa*$^{(ed20/ed20)}$ mutants are likely to be loss of function mutants, I compared their phenotype to that of previously published loss of function *cebpa* zebrafish mutants. A study in 2015 generated zebrafish *cebpa* mutants in which a premature stop codon had been introduced and this produced a truncated Cebpa protein, which lacked a bZIP domain (Yuan et al., 2015). A luciferase reporter assay was then used to demonstrate that the mutant protein had lost its transcriptional activity and that the mutant generated was a loss of function mutant (Yuan et al., 2015). I therefore compared the *cepba*$^{(ed19/ed19)}$ and *cebpa*$^{(ed20/ed20)}$ mutants to the previously published mutants, as evidence of a similar phenotype would lend support to the idea that the *cebpa*$^{(ed19/ed19)}$ and *cepba*$^{(ed20/ed20)}$ mutants are also loss of function mutants.

The most striking phenotype of the Yuan et al (2015) mutants was the early death of homozygous mutants. Homozygous mutants did not survive past 3 weeks of age (Yuan et al., 2015). To measure survival *cebpa*$^{(+/ed19)}$ and *cebpa*$^{(+/ed20)}$ fish were incrossed and the survival of all ungenotyped offspring monitored for 21 days **(Figure 5.4A)**. It was found that around 30% of the embryos from *cebpa*$^{(+/ed19)}$ incrosses and 15% of the embryos from *cebpa*$^{(+/ed20)}$ incrosses died **(Figure 5.4A)**. The amount of death was suggestive of a homozygous lethal phenotype. To determine if the death observed was in fact that of the homozygous embryos, the surviving fish were fin clipped at 21 dpf and genotyped. At 21 dpf no *cebpa*$^{(ed19/ed19)}$ mutants were present and very few *cebpa*$^{(ed20/ed20)}$ mutants were present **(Figure 5.4B)**. None of the *cebpa*$^{(ed20/ed20)}$ mutants present at 21 dpf survived to adulthood. Taken together these results show that like the *cebpa* mutants in the study by Yuan et al (2015) *cebpa*$^{(ed19/ed19)}$ and *cebpa*$^{(ed20/ed20)}$ mutants die during larval development, before 21 dpf.

5.2.7 - *cebpa*$^{(ed19/ed19)}$ mutants show the same small liver phenotype as published zebrafish mutants

As a second comparison I also looked at the second major phenotype reported of the Yuan et al (2015) mutants. The 2015 study reported that *cebpa* mutants showed defects in liver development, resulting in a small liver and suggested that it was this

defect which led to death in the mutants (Yuan et al., 2015). This liver defect has also been noted in *Cebpa* knock out mice (Flodby et al., 1996, Wang et al., 1995). To assess if the cause of death was likely to be similar in the mutants I had generated, I quantified the area of the livers in *cepba*$^{(ed19/ed19)}$ mutants **(Figure 5.4C & D)**. Fish were genotyped at 3 dpf and then imaged using brightfield microscopy. The liver was detected by its morphology, and it can be seen as a shadow over the top left hand corner of the swim bladder **(Figure 5.4C)**. When liver area was measured it was found that *cebpa*$^{(ed19/ed19)}$ fish had significantly smaller livers than their WT siblings **(Figure 5.4D)**. Therefore *cebpa*$^{(ed19/ed19)}$ fish show the same small liver phenotype as the Yuan et al (2015) mutants. In summary both *cebpa*$^{(ed19/ed19)}$ and *cebpa*$^{(ed20/ed20)}$ mutants reproduce the previously described phenotypes of loss of function mutants, and this gives confidence to the idea that these are indeed loss of function mutations.

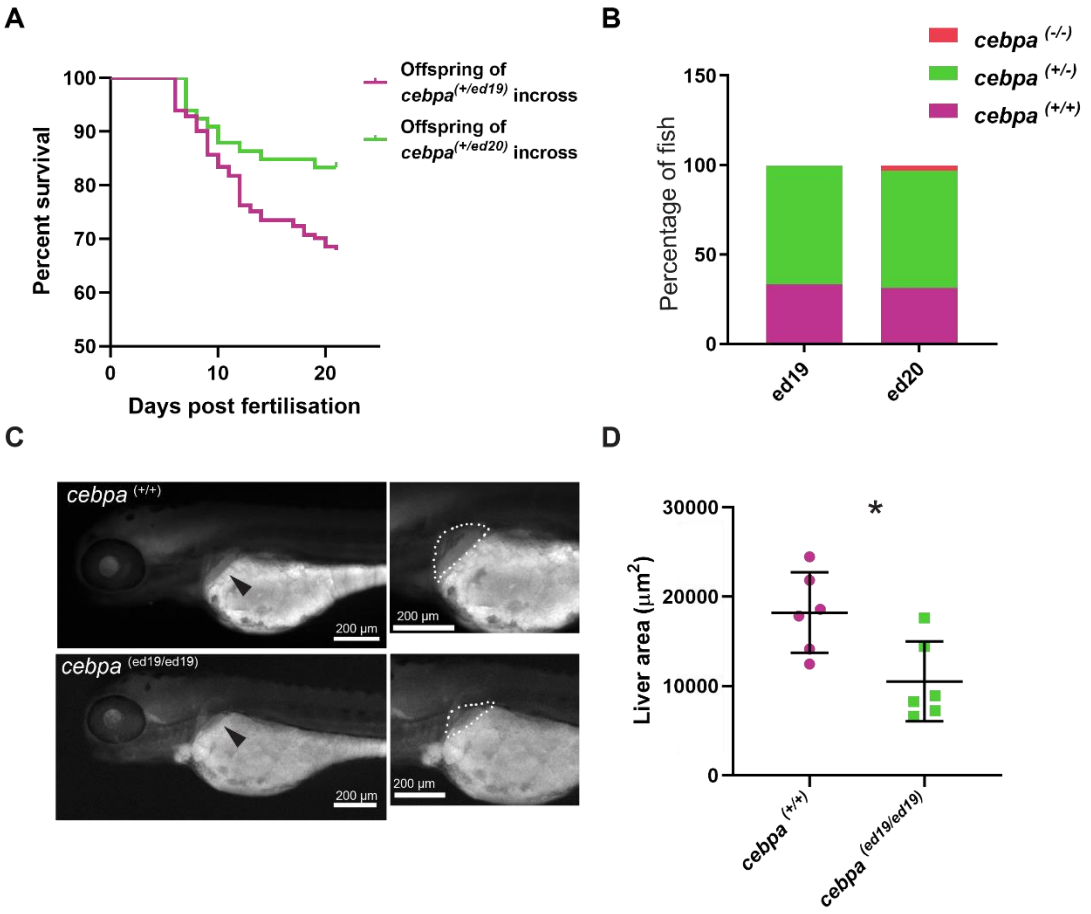

Figure 5.4 – *cebpa*$^{(ed19/ed19)}$ and *cebpa*$^{(ed20/ed20)}$ mutants show a phenotype similar to that of previously published *cebpa* mutants. A. Survival of fish generated from *cebpa*$^{(+/ed19)}$ and *cebpa* $^{(+/20)}$ incrosses. Ed19, n = 181. Ed20, n = 66. **B.** Genotypes of fish surviving past 21 dpf. **C.** Representative bright field images of 3 dpf embryos. Arrow heads show livers. White dotted line shows the liver area measured. **D.** Quantification of liver area. n = 6. Error bars show mean and standard deviation. A two tailed t-test was performed p = 0.014.

5.2.8 - *cebpa*$^{(+/ed19)}$ and *cebpa*$^{(+/ed20)}$ mutants have reduced levels of adipose tissue during normal development

Having determined the *cebpa*$^{(ed19/ed19)}$ and *cebpa*$^{(ed20/ed20)}$ alleles are likely to be loss of function alleles, I next wanted to examine the effect of loss of *cebpa* function on adipose tissue levels. Due to the fact that *cebpa*$^{(ed19/ed19)}$ and *cebpa*$^{(ed20/ed20)}$ homozygous mutants die before the development of AT, all experiments were carried out with *cebpa*$^{(+/ed19)}$ and *cebpa*$^{(+/ed20)}$ heterozygous mutants. To examine levels of adipose tissue, fish were raised until 30 dpf and then stained with Nile Red **(Figure 5.5A & D)**. The fish were then imaged using a fluorescence stereomicroscope and the total fluorescence area measured **(Figure 5.5A & D)**. The total fluorescence area, which acts as a proxy for total AT area, was then compared to standard length (SL) (Tingaud-Sequeira et al., 2011). Under normal fed conditions, both *cebpa*$^{(+/ed19)}$ and *cebpa*$^{(+/ed20)}$ fish had significantly less AT when compared to WT siblings **(Figure 5.5C & F)**. *cebpa*$^{(+/ed19)}$ fish were also found to be significantly smaller than WT siblings **(Figure 5.5B)**. In summary, *cebpa*$^{(+/ed19)}$ and *cebpa*$^{(+/ed20)}$ mutants have reduced levels of AT during normal development.

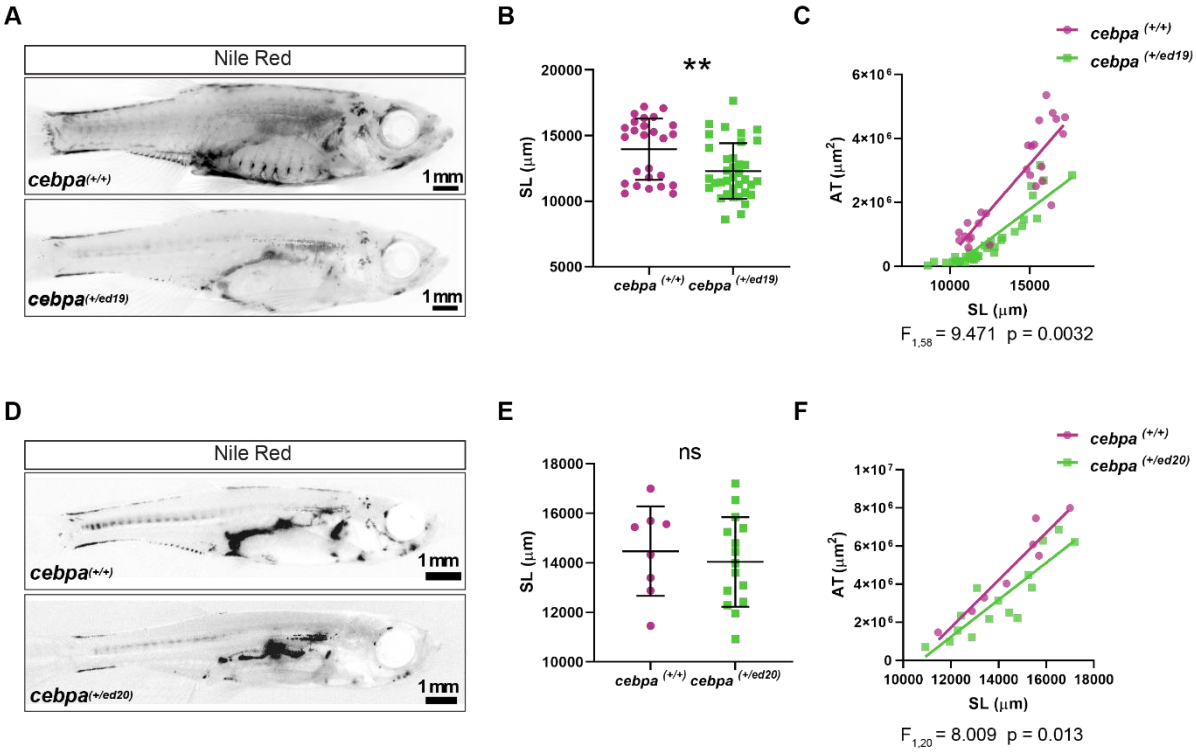

Figure 5.5 – *cebpa*$^{(+/ed19)}$ and *cebpa*$^{(+/ed20)}$ mutants show impaired adipose tissue expansion. A. Representative Nile red images. **B.** n = 26-36. A two tailed t-test was performed, p = 0.0051. Error bars show mean and standard deviation **C.** n = 26-36. An Ancova analysis was performed and the slopes of the lines were found to be significantly different. $F_{1,58}$ = 9.471. p = 0.0032. **D.** Representative Nile red images. **E.** n = 8-15. Error bars show mean and standard deviation **F.** n = 8-15. An Ancova analysis was performed and the elevation of the slopes was found to be significantly different. $F_{1,20}$ = 8.009. p = 0.013.

5.2.9 - *cebpa*$^{(+/ed19)}$ mutants gain less adipose tissue in response to a high fat diet

Cebpa knockout mice have almost no WAT and the effect of a high fat diet (HFD) on adipose tissue expansion has not been examined in these mice (Linhart et al., 2001). I therefore placed the *cebpa*$^{(+/ed19)}$ mutants on a HFD to determine whether AT expansion was altered in response to this stimulus. *cebpa*$^{(+/ed19)}$ mutants and WT siblings were placed on a 1 week HFD **(Figure 5.6A)**. The duration of the diet was shorter than for previous experiments due to the more severe phenotype of the *cebpa*$^{(+/ed19)}$ mutants at baseline. To perform the HFD, I incrossed *cebpa*$^{(+/ed19)}$ fish and raised their offspring until 4 weeks of age **(Figure 5.6A)**. Fish were then genotyped and separated into *cebpa*$^{(+/+)}$ and *cepba*$^{(+/ed19)}$ groups **(Figure 5.6A)**. At 8 weeks of age the fish were divided into two size matched groups, one control diet and one HFD group **(Figure 5.6A)**. Fish were then subjected to a 1 week HFD, consisting of a 2 hour immersion in a 5% egg yolk solution each day (Carten et al., 2011, Semova et al., 2012, Walters et al., 2012) **(Figure 5.6A)**. Following the HFD fish were stained with Nile Red to assess AT levels **(Figure 5.6A & B)**. It was found that *cebpa*$^{(+/+)}$ HFD fish had significantly more AT than *cebpa*$^{(+/+)}$ control diet (CD) fish **(Figure 5.6C & D)**. *cebpa*$^{(+/ed19)}$ HFD fish also gained adipose tissue and were found to have significantly more AT than *cebpa*$^{(+/ed19)}$ CD siblings **(Figure 5.6C & D)**. Strikingly *cebpa*$^{(+/ed19)}$ HFD fish had less AT than *cebpa*$^{(+/+)}$ CD fish **(Figure 5.6C & D)**. Together this shows that while *cebpa*$^{(+/ed19)}$ fish are capable of gaining AT in response to a HFD, this ability is severely limited and *cepba*$^{(+/ed19)}$ fish have less AT than *cebpa*$^{(+/+)}$ fish on a control diet.

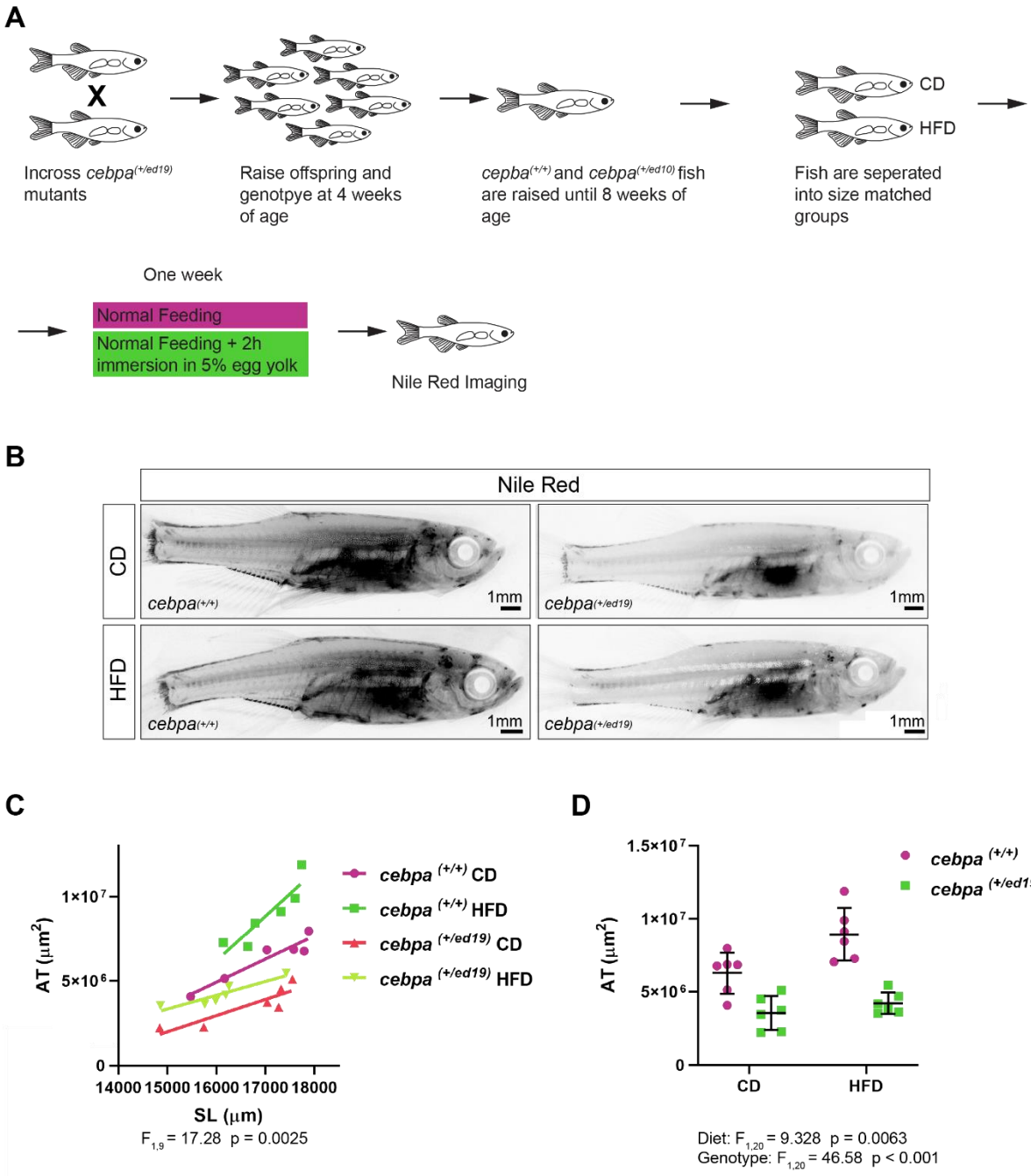

Figure 5.6 – *cebpa*$^{(+/ed19)}$ mutants gain less adipose tissue in response to a HFD.

Figure 5.6 – *cebpa*$^{(+/ed19)}$ mutants gain less adipose tissue in response to a HFD. **A.** Schematic showing protocol used for the HFD. **B.** Representative Nile Red images. **C.** n = 6. An Ancova analysis was performed. The elevation of the lines of the *cebpa*$^{(+/+)}$ CD and *cebpa*$^{(+/+)}$ HFD groups were found to be significantly different $F_{1,9}$ = 29.29 p = 0.0004. The elevation of the lines of the *cebpa*$^{(+/ed19)}$ CD and *cebpa*$^{(+/ed19)}$ HFD groups were also found to be significantly different, $F_{1,9}$ = 17.28 p = 0.0025. **D.** n = 6. Error bars show mean and standard deviation. A two way ANOVA was performed and the effect of diet and genotype were found to be significant. Diet, $F_{1,20}$ = 9.328 p = 0.0063. Genotype, $F_{1,20}$ = 46.58 p < 0.0001

5.2.10 - *cebpa*$^{(+/ed19)}$ and *cebpa*$^{(+/ed20)}$ mutants have a more hypertrophic visceral adipose tissue morphology

Adipose expands via hyperplastic and hypertrophic growth (Lapid and Graff., 2017). As adipose tissue expansion is impaired in *cebpa*$^{(+/ed19)}$ and *cebpa*$^{(+/ed20)}$ mutants, I next wanted to determine if adipose tissue morphology was altered in the mutants. As adipocytes are largely unilocular, lipid droplet number and size measurements were used as a proxy for adipocyte measurements. To examine adipose morphology PVAT was dissected from 2 month old *cebpa*$^{(+/ed19)}$ and *cebpa*$^{(+/+)}$ fish, following a 1 week HFD. The PVAT was then stained with LipidTOX and the whole depot imaged using confocal microscopy. This provided 3D information on lipid droplet size and allowed lipid droplet diameter to be accurately measured. The number and diameter of lipid droplets within the adipose depot was then measured **(Figure 5.7A. B. C. & D)**. The *cebpa*$^{(+/ed19)}$ fish were found to have a more hypertrophic PVAT morphology, with significantly fewer lipid droplets than WT siblings **(Figure 5.7C)**. *cebpa*$^{(+/ed19)}$ mutants were also found to have lipid droplets with a significantly greater average diameter, within PVAT, than WT siblings **(Figure 5.7D)**. This data shows that visceral adipose in *cebpa*$^{(+/ed19)}$ mutants expands via hypertrophic growth to a greater extent than in WT fish.

To further test whether adipose morphology is altered in *cebpa* mutants I also looked at morphology in adult fish. PVAT was dissected from *cepba*$^{(+/ed19)}$ and *cebpa*$^{(+/ed20)}$ fish and WT siblings and stained with LipidTOX. Confocal imaging was then used to image the depots and lipid droplet number and diameter was again measured **(Figure 5.7E &H)**. *cebpa*$^{(+/ed19)}$ fish were again found to have a more hypertrophic lipid droplet morphology, with significantly fewer lipid droplets and a significantly greater average lipid droplet diameter **(Figure 5.7F & G)**. In contrast *cebpa*$^{(+/ed20)}$ fish were found to have an unchanged adipose morphology, with no changes in lipid droplet number or average lipid droplet diameter **(Figure 5.7I & J)**. This difference could be due to the smaller n number of the *cebpa*$^{(+/ed20)}$ experiment or the *cebpa*$^{(+/ed20)}$ fish may have a more subtle phenotype. Overall *cebpa* mutants show a more hypertrophic visceral adipose tissue morphology than WT siblings.

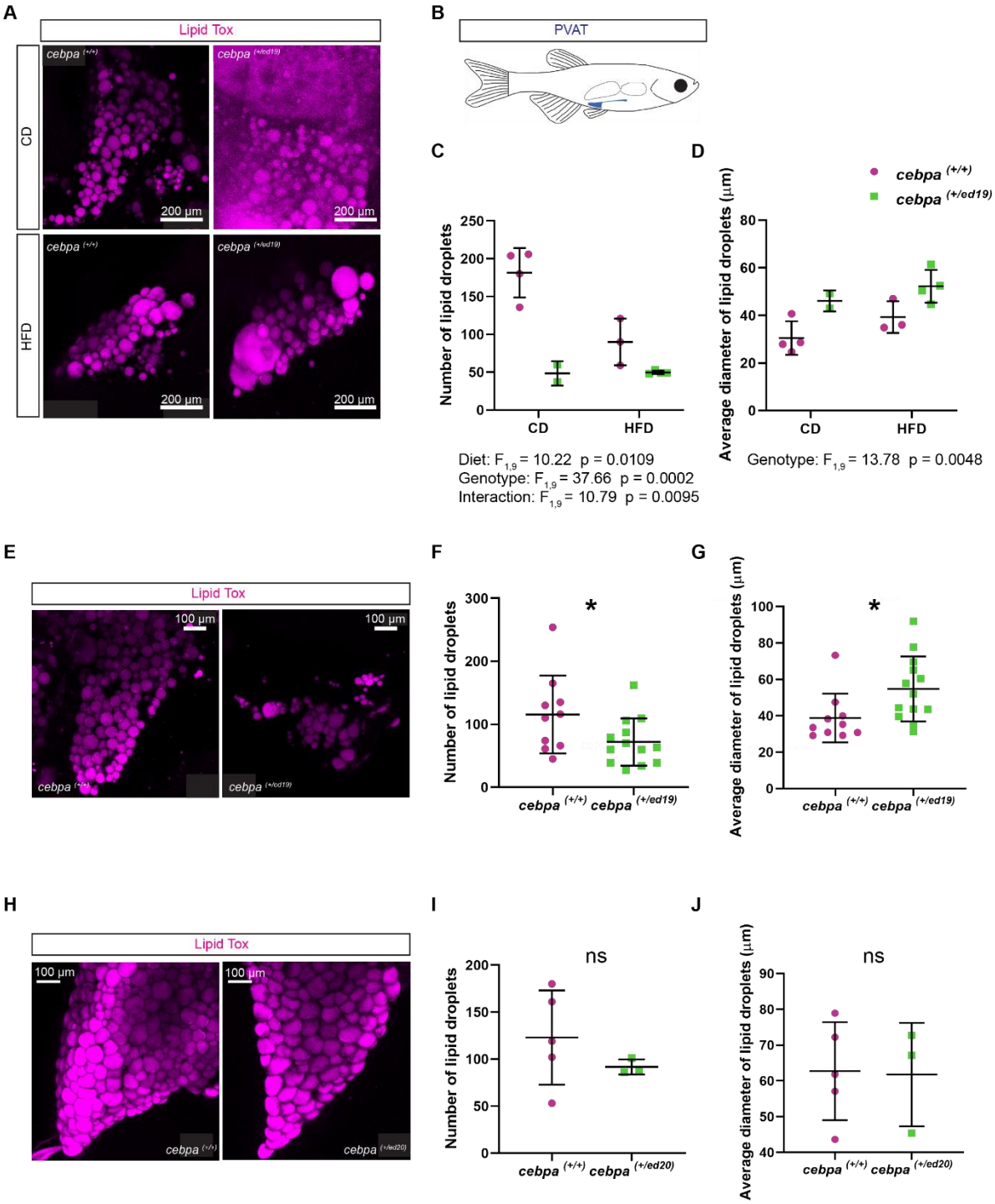

Figure 5.7 – *cebpa*$^{(+/ed19)}$ mutants have a more hypertrophic VAT morphology

Figure 5.7 – *cebpa*$^{(+/ed19)}$ mutants have a more hypertrophic VAT morphology. A. Representative maximum intensity projections of PVAT (Pancreatic VAT) depots. The anterior end of the depot is to the right of the image and the posterior to the left. **B.** Schematic showing location of the PVAT depot in zebrafish. **C.** n = 2-4. Error bars show mean and standard deviation. A two way ANOVA was performed. The effect of diet and genotype were found to be significant, as was the interaction between the two. Diet, $F_{1,9} = 10.22$ $p = 0.0109$. Genotype, $F_{1,9} = 37.66$ $p = 0.0002$. Interaction, $F_{1,9} = 10.79$ $p = 0.0095$. **D.** n = 2-4. Error bars show mean and standard deviation. A two way ANOVA was performed and the effect of genotype was found to be significant. $F_{1,9} = 13.78$ $p = 0.0048$. **E.** Representative maximum intensity projections of PVAT depots. The anterior end of the depot is to the right of the image and the posterior to the left. **F.** n = 10-13. Error bars show mean and standard deviation. A two tailed t-test was performed, $p = 0.0479$. **G.** n = 10-13. Error bars show mean and standard deviation. A two tailed t-test was performed, $p = 0.0276$. **H.** Representative maximum intensity projections of a section of the PVAT depots. **I.** n = 3-5. Error bars show mean and standard deviation. **J.** n = 3-5. Error bars show mean and standard deviation.

5.2.11- *cebpa*$^{(+/ed19)}$ mutants have a more hypertrophic subcutaneous adipose tissue morphology

To test if the changes observed in adipose morphology are confined to visceral adipose, I examined the adipose morphology of subcutaneous adipose tissue. To do this I stained live *cebpa*$^{(+/ed19)}$ fish and WT siblings with LipidTOX and then euthanised the fish. The LSAT depot was then imaged through the skin of euthanised fish using confocal microscopy **(Figure 5.8A & B)**. Lipid droplet number and diameter was then measured. *cebpa*$^{(+/ed19)}$ fish were found to have a more hypertrophic LSAT morphology than WT siblings **(Figure 5.8C & D)**. *cepba*$^{(+/ed19)}$ mutants had fewer lipid droplets and a greater average lipid droplet diameter **(Figure 5.8C & D)**. In summary the altered adipose morphology observed in *cepba*$^{(+/ed19)}$ fish is not confined to visceral adipose tissue and *cebpa*$^{(+/ed19)}$ fish have a more hypertrophic subcutaneous adipose tissue morphology.

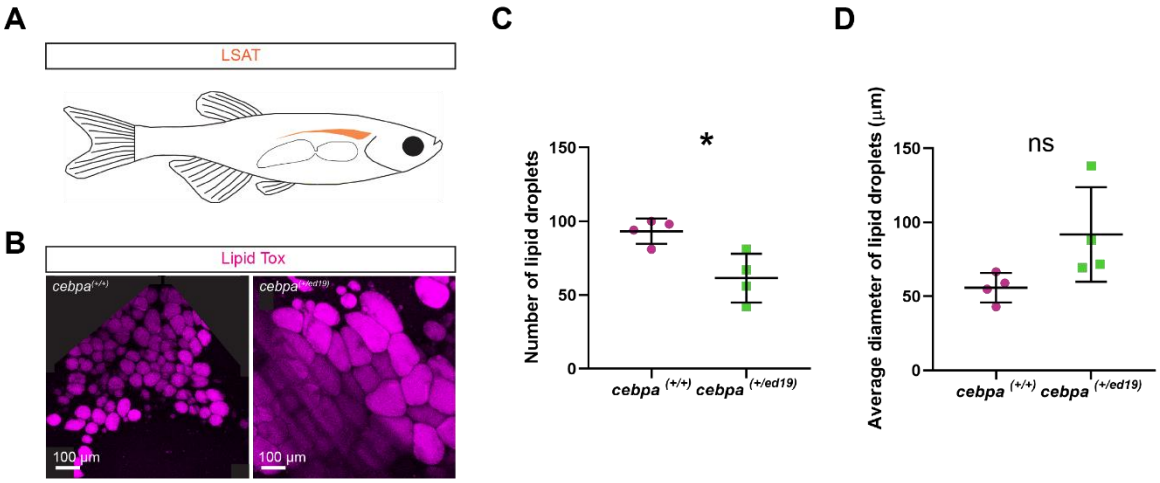

Figure 5.8 – *cebpa*$^{(+/ed19)}$ mutants have a more hypertrophic SAT morphology A. Schematic showing the location of the LSAT depot. **B.** Representative maximum intensity projections of a section of the LSAT depot. **C.** n = 4. Error bars show mean and standard deviation. A two tailed t-test was performed, p = 0.0143. **D.** n = 4. Error bars show mean and standard deviation

5.2.12 - *cebpa*$^{(+/ed19)}$ mutants have elevated levels of blood triglycerides

As *cebpa*$^{(+/ed19)}$ and *cebpa*$^{(+/ed20)}$ mutants are less able to store lipid in adipose tissue, it is expected that levels of blood metabolites may be altered in these mutants. *Cebpa* knockout mice, in which *Cebpa* is expressed only in the liver, show normal levels of glucose but elevated levels of insulin, suggestive of peripheral insulin resistance (Linhart et al., 2001). I therefore wanted to test if *cebpa*$^{(+/ed19)}$ and *cebpa*$^{(+/ed20)}$ mutants showed a similar phenotype to the mouse phenotype. To do this I measured levels of lipid metabolites in the blood. Adult fish were euthanised, blood extracted, and levels of glucose, triglyceride and cholesterol measured **(Figure 5.9A. B. C. D. E. & F)**. Levels of blood glucose in the *cebpa*$^{(+/ed19)}$ and *cebpa*$^{(+/ed20)}$ mutants were unchanged compared to WT fish, reflecting the phenotype of the mouse mutants **(Figure 5.9A & D)**. Levels of cholesterol were also unchanged in both mutants **(Figure 5.9C & F)**. However, levels of triglycerides were significantly increased in *cebpa*$^{(+/ed19)}$ mutants compared to WT siblings **(Figure 5.9B)**. Overall *cebpa*$^{(+/ed19)}$ mutants show increased levels of blood triglycerides.

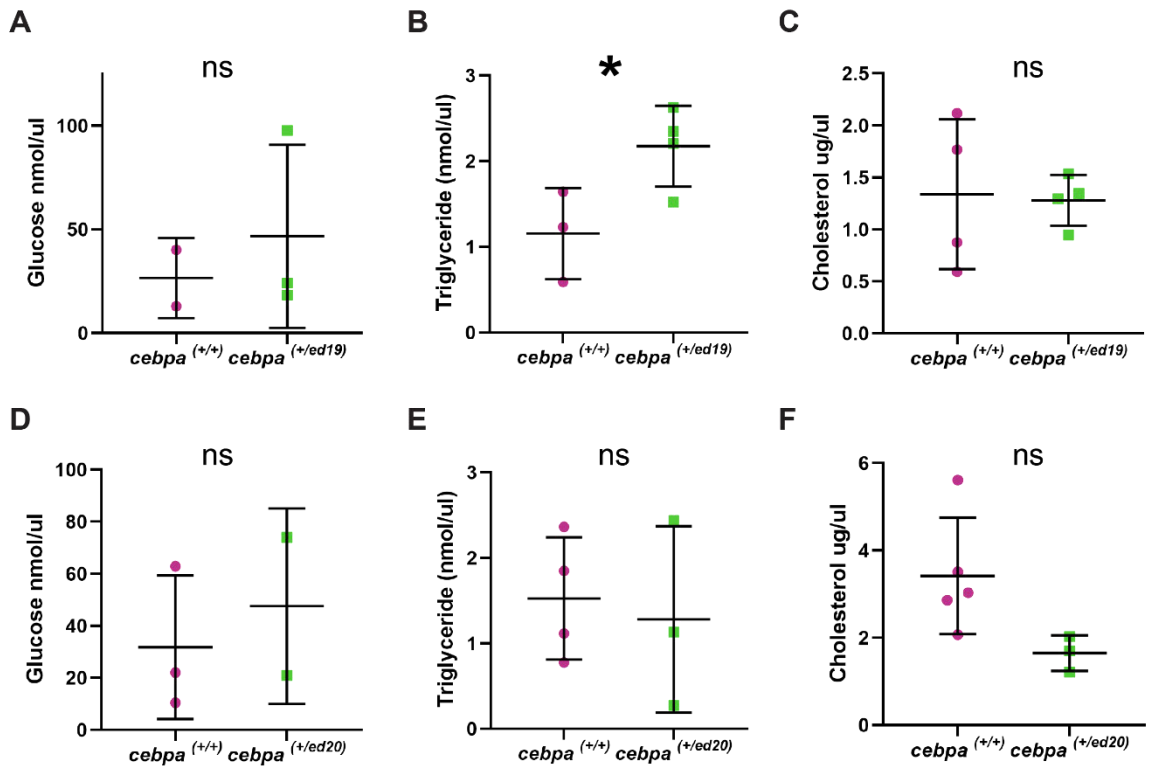

Figure 5.9 – *cepba*$^{(+/ed19)}$ mutants have elevated levels of blood triglycerides. A. n = 2-3 **B.** n = 3. A two tailed t-test was performed p = 0.0428 **C.** n = 4. **D.** n = 2-3 **E.** n = 3-4 **F.** n = 3-5 **A - F.** Error bars show mean and standard deviation.

5.2.13 - *cebpa*$^{(+/ed19)}$ mutants have fewer adipocytes, fewer adipose progenitor cells and show reduced levels of hyperplastic growth

The results presented so far suggest that *cebpa* is required for adipose tissue expansion in zebrafish, however the role of *cebpa* in adipogenesis has not been addressed. To examine this I made use of the *Foxp1:eGFP* line to assess adipose progenitor cell behaviour and adipose growth in the *cebpa*$^{(+/ed19)}$ mutants. Details of how the *Foxp1:eGFP* was generated can be found in chapter 4. Briefly the *Foxp1:eGFP* line expresses GFP in both adipose progenitor cells and mature adipocytes. *cebpa*$^{(+/ed19)}$ mutants were crossed to *Foxp1:eGFP* fish and then genotyped at 1 month of age. Following this GFP positive *cebpa*$^{(+/ed19)}$ fish and WT siblings were stained with LipidTOX and the whole LSAT depot imaged in live fish using a stereomicroscope. The fish were then recovered and the imaging was repeated 24 hours and 48 hours after the first timepoint. The number of adipocytes and adipose progenitor cells in the LSAT of each fish was measured, with adipose progenitor cells being classified as GFP positive cells which lacked a lipid droplet. Analysis of cell number and lipid droplet area showed that *cebpa*$^{(+/ed19)}$ mutants had a reduced number of both adipose progenitor cells and mature adipocytes **(Figure 5.10A & C)**. *cebpa*$^{(+/ed19)}$ mutants also had a greater average lipid droplet area **(Figure 5.10B & C)**. Together this shows that *cebpa*$^{(+/ed19)}$ fish have a more hypertrophic LSAT morphology and suggests that hyperplastic growth is impaired. To examine this, I looked at the growth of LSAT across the timepoints. Differences in the appearance of LSAT between fish allowed individual fish to be tracked throughout the experiment, and this allowed changes in adipocyte size and number to be measured **(Figure 5.10D. E. F. & G)**. *cebpa*$^{(+/ed19)}$ mutants showed a smaller increase in the number of progenitor cells and mature adipocytes over the timepoints than WT siblings **(Figure 5.10D. F. & G)**. Change in lipid droplet area was very similar between *cebpa*$^{(+/ed19)}$ fish and WT siblings **(Figure 5.10E. F. & G)**. Overall, the reduced number of adipose progenitor cells and the reduced increase in adipose progenitors and mature adipocytes in *cebpa*$^{(+/ed19)}$ mutants suggests that hyperplastic adipose growth and thereby adipogenesis is impaired in the mutants.

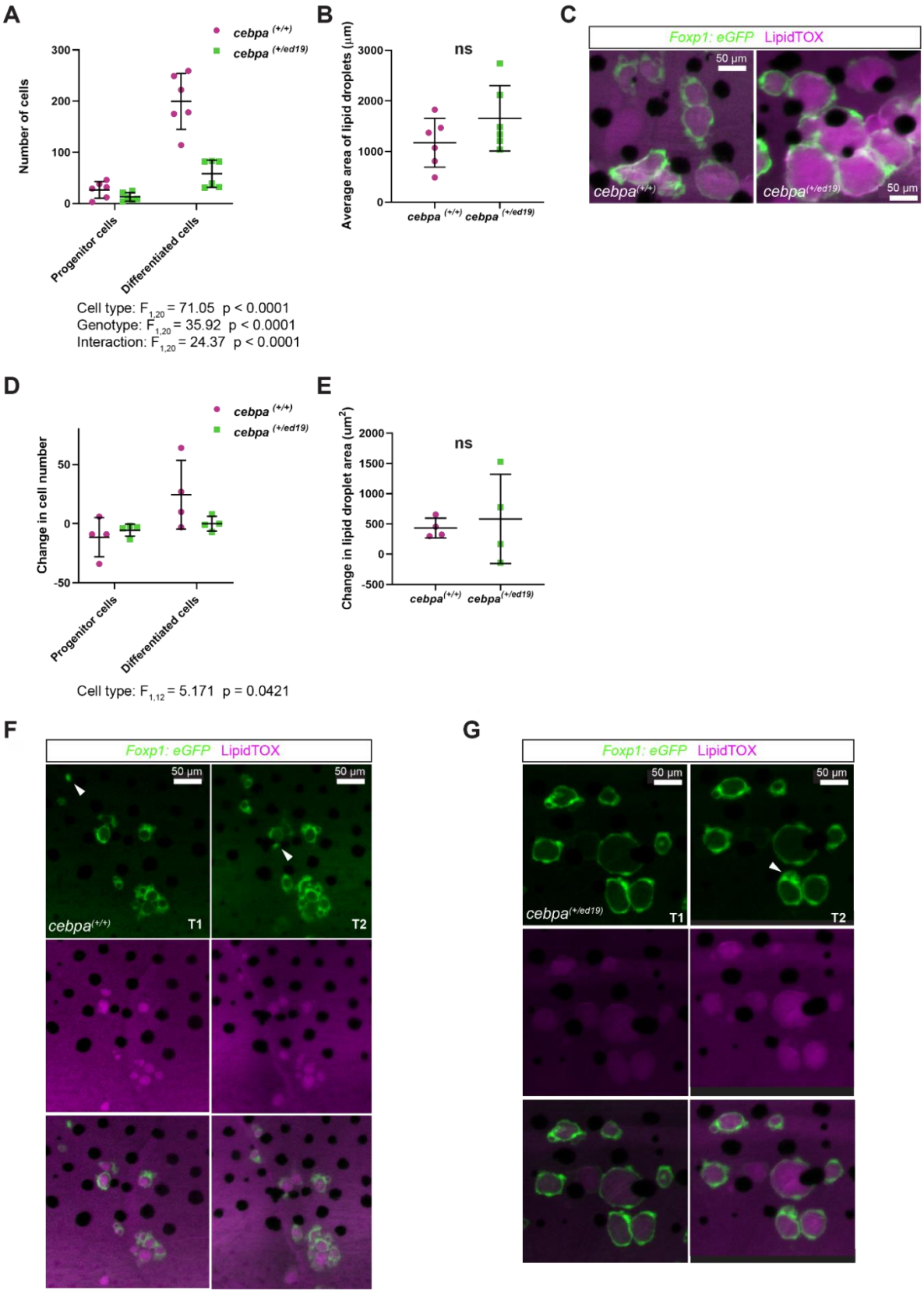

Figure 5.10 – *cepba*$^{(+/ed19)}$ mutants have a more hypertrophic adipose morphology and show reduced levels of hyperplastic growth.

Figure 5.10 – *cepba*$^{(+/ed19)}$ mutants have a more hypertrophic adipose morphology and show reduced levels of hyperplastic growth. A. n = 6 per group. Measurements taken from 4 fish at 3 timepoints. A two way ANOVA was performed and the effect of cell type, genotype and the interaction were all found to be significant. Cell type, $F_{1,20} = 71.05$ $p < 0.0001$. Genotype, $F_{1,20} = 35.92$ $p < 0.0001$. Interaction, $F_{1,20} = 24.37$ $p < 0.0001$. **B.** n = 6. Measurements taken from 4 fish at 3 timepoints. A two tailed t-test was performed, p = 0.1739. **C.** Representative maximum intensity projections. **D.** n = 4. Measurements taken from 4 fish at 3 timepoints and the differences between these measurements plotted. A two way ANOVA was performed and the effect of cell type was found to be significant, $F_{1,12} = 5.171$ $p = 0.0421$. **E.** n = 4. Measurements taken from 4 fish at 3 timepoints and the differences between these measurements plotted. A two tailed t-test was performed, p = 0.7059. **F.** Representative maximum intensity projections. Arrow heads show progenitor cells. T1 (Timepoint one). T2 (Timepoint 2). **G.** Representative maximum intensity projections. Arrow heads show progenitor cells. T1 (Timepoint one). T2 (Timepoint 2). **A.B.D & E.** Error bars show mean and standard deviation.

5.2.14 - Genes involved in tissue development, regeneration and cell differentiation are upregulated in *cebpa*$^{(+/ed19)}$ mutants

Analysis of the *cebpa*$^{(+/ed19)}$ and *cebpa*$^{(+/ed20)}$ mutants suggest a conserved role for *cebpa* in adipogenesis in zebrafish. This provides further evidence that zebrafish is a useful model for the study of adipose tissue expansion. As all the data I have presented so far in this chapter is already well established in mouse models I also wanted to use the novel zebrafish mutants generated to identify new candidate genes which may play a role in adipose tissue expansion. To do this I have used RNA-Sequencing (RNA-Seq). RNA-Seq is a technique used to determine the quantity and sequences of RNA in a sample (Wang et al., 2009). PVAT was dissected from *cebpa*$^{(+/+)}$ and *cebpa*$^{(+/ed19)}$ siblings at 2 months of age and RNA extracted. RNA quality was then assessed by measuring RNA concentration and RNA integrity number (RIN) value, and the samples were sent to BGI. There the RNA was reverse transcribed into cDNA and amplified by PCR. The DNA was then sequenced on a BGISEQ-5000 platform. Following sequencing, low quality reads were removed and HISAT (Hierarchical Indexing for Spliced Alignment of Transcripts) was used to map reads to the zebrafish genome. Gene expression levels were then calculated and differentially expressed genes reported. Overall, RNA Seq was used to detect genes differentially expressed in the PVAT of *cebpa*$^{(+/+)}$ and *cebpa*$^{(+/ed19)}$ fish.

The RNA-Seq revealed that 949 genes were significantly upregulated in *cebpa*$^{(+/ed19)}$ mutants when compared to WT siblings and that 177 genes were significantly downregulated **(Figure 5.11A)**. From this data set, genes which were upregulated were then grouped according to gene ontology (GO) term enrichment **(Figure 5.11B)**. Gene ontology is an initiative which aims to annotate genes and to enable functional interpretation of experimental data (Gene Ontology, 2008). GO term analysis using ZebrafishMine revealed an enrichment of terms relating to tissue development, lipid and steroid metabolism and cell differentiation **(Figure 5.11B)**. Of particular interest were genes categorised into the cell differentiation GO term **(Figure 5.11B)**. As *cebpa* is a key regulator of adipocyte differentiation, genes sorted into the cell differentiation GO term could be interesting candidate genes in the regulation of adipose tissue expansion. Interesting candidate genes will be expanded upon in the discussion. In summary the *cebpa*$^{(+/ed19)}$ mutants have facilitated the identification of novel candidate genes, which may play a role in adipose tissue expansion.

A

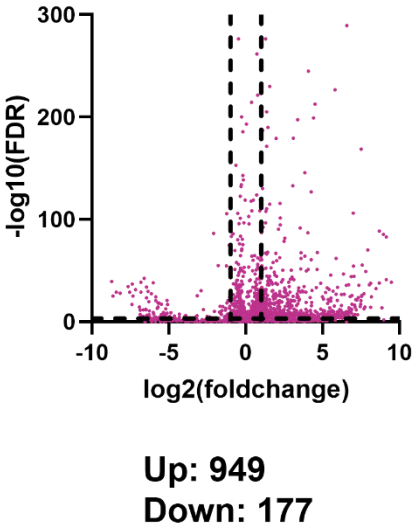

B

GO ID	Terms for genes upregulated in *cebpa*$^{(+/ed19)}$	p-value
GO:0009888	Tissue development	$9.402275e^{-18}$
GO:0008610	Lipid biosynthetic process	$1.524586e^{-17}$
GO:0006694	Steroid biosynthetic process	$3.345866e^{-17}$
GO:0005576	Extracellular region	$1.663486e^{-16}$
GO:0008202	Steroid metabolic process	$2.971015e^{-16}$
GO:0016126	Sterol biosynthetic process	$2.339697e^{-15}$
GO:0032502	Developmental process	$5.138370e^{-15}$
GO:0048856	Anatomical structure development	$3.757277e^{-14}$
GO:0009611	Response to wounding	$8.648902e^{-13}$
GO:0009653	Anatomical structure morphogenesis	$8.814166e^{-13}$
GO:0044421	Extracellular region part	$1.500760e^{-12}$
GO:0005615	Extracellular space	$2.034840e^{-12}$
GO:0016125	Sterol metabolic process	$2.491159e^{-12}$
GO:0031099	Regeneration	$3.641369e^{-12}$
GO:0030154	Cell differentiation	$7.868370e^{-12}$
GO:0048869	Cellular developmental process	$1.420667e^{-11}$
GO:0006629	Lipid metabolic process	$1.597085e^{-11}$
GO:0007275	Multicellular organism development	$1.699245e^{-11}$
GO:0044283	Small molecule biosynthetic process	$8.249150e^{-11}$
GO:0042060	Wound healing	$8.809466e^{-11}$

Figure 5.11 – RNA-Seq profiling of *cebpa*$^{(+/ed19)}$ mutants reveals an altered transcriptional signature. A. Volcano plot showing significantly up and downregulated genes. Dashed lines indicate significance. Log2(foldchange) ≤ -1 and ≥ 1. FDR ≤ 0.001. **B.** Top 20 GO terms in upregulated genes. Genes with log2(foldchange) ≥ 1 and FDR ≤ 0.001 were taken for GO term analysis using ZebrafishMine.

5.3 - Discussion

Zebrafish are an emerging model of adipose tissue expansion. Much is known about how AT behaves in zebrafish however it is currently unknown whether the molecular basis of adipose tissue expansion is conserved to zebrafish. Therefore, a better understanding of the molecular basis of adipose tissue expansion in zebrafish could help to further establish zebrafish as a model of adipose tissue expansion.

In summary, I have presented data which suggests that the role of *cebpa* in adipose tissue expansion is conserved to zebrafish. I have generated two *cebpa* mutant alleles, both of which show defects in AT expansion **(Figure 5.12A & B)**. *cebpa*$^{(+/ed19)}$ mutants have reduced levels of AT, a reduced response to a HFD, a more hypertrophic AT morphology and increased levels of blood triglycerides **(Figure 5.12A)**. While *cepba*$^{(+/ed20)}$ mutants have reduced levels of AT and a more hypertrophic adipose morphology **(Figure 5.12B)**. The phenotypes of both mutants also mirror those of published zebrafish and mouse mutants. Together this data is supportive of a conserved role of *cepba* in adipogenesis in zebrafish **(Figure 5.12C)**. In this section I will discuss the limitations of the data I have presented, and a full discussion can be found in the general discussion section (Chapter 6).

One major limitation of the data I presented is that it is currently unknown if levels of *cebpa* protein are changed in the *cebpa*$^{(ed19/ed19)}$ and *cepba*$^{(ed20/ed20)}$ mutants. Transcript levels were found to be unchanged in the *cebpa*$^{(ed20/ed20)}$ mutants and significantly increased in the *cebpa*$^{(ed19/ed19)}$ mutants. As the *cebpa* mutant transcripts do not appear to be degraded and as I was unable to assess protein levels it is unclear how or if Cebpa expression is altered in the mutants. The fact that *cebpa*$^{(+/ed19)}$ and *cebpa*$^{(+/ed20)}$ mutants show phenotypes consistent with both published zebrafish and mouse mutants gives confidence to the idea that *cepba* zebrafish mutants are indeed loss of function mutants. However, measuring protein levels would be helpful in determining the true nature of the *cebpa*$^{(+/ed19)}$ and *cebpa*$^{(+/ed20)}$ mutants.

Another limitation of the work I have presented is that all adipose phenotypes were assessed in the *cebpa*$^{(+/ed19)}$ and *cebpa*$^{(+/ed20)}$ heterozygous mutants. Both the *cebpa*$^{(ed19/ed19)}$ and the *cepba*$^{(ed20/ed20)}$ mutants die at 2 to 3 weeks of age due to a liver defect and as AT first develops in some fish at 12 dpf, I was unable to assess AT levels in these mutants. One way to overcome this problem would be to overexpress *cebpa* only in the liver, as was done in the *Cebpa* mouse mutants (Linhart et al., 2001).

This would allow me to assess the effect of total loss of *cebpa* on adipose tissue expansion in zebrafish. Overexpressing *cebpa* in the liver would also give confidence to the idea that adipose phenotypes in the *cebpa*$^{(+/ed19)}$ and *cebpa*$^{(+/ed20)}$ mutants are due to the effect of *cebpa* in adipose expansion and not a secondary effect of poor liver function.

In summary I have presented results which broadly agree with my hypothesis that the role of *cebpa* in adipogenesis is conserved to zebrafish and that *cebpa* is a key regulator of adipose tissue expansion in zebrafish. Here I have detailed the major limitations of the data presented and a fuller discussion can be found in chapter 6.

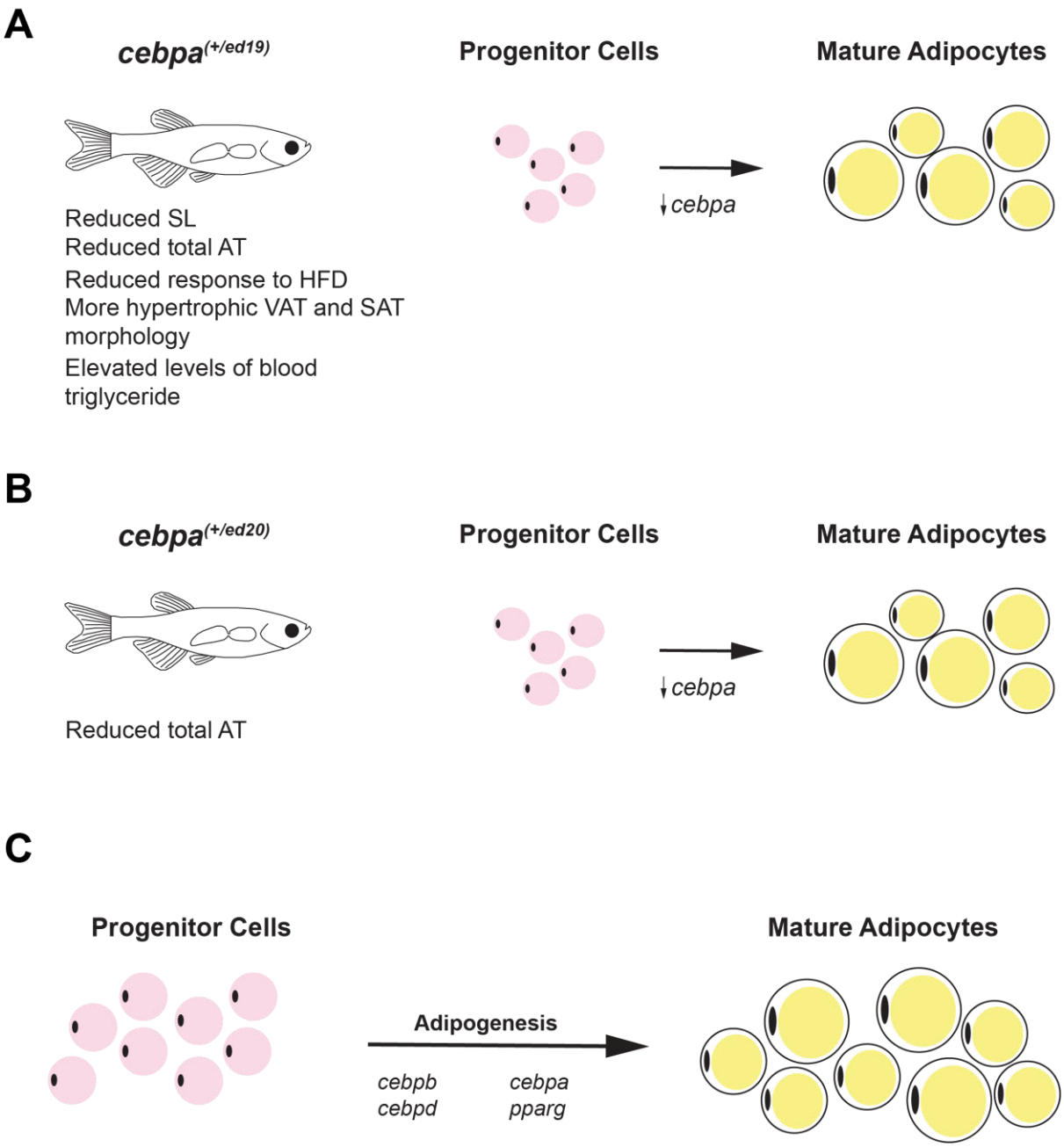

Figure 5.12 – The role of *Cebpa* in adipogenesis, and adipose tissue expansion, appears to be conserved in zebrafish. A. Summary of the phenotype of the *cebpa*$^{(+/ed19)}$ mutants and a model of the effect reduced levels of *cebpa* are thought to have on AT expansion. **B.** Summary of the phenotype of the *cebpa*$^{(+/ed20)}$ mutants and a model of the effect reduced levels of *cebpa* are thought to have on AT expansion. **C.** Schematic showing how adipogenesis is thought to proceed in zebrafish.

Chapter 6 – Discussion

6.1 – Summary of results

The findings in this thesis demonstrate three major points. Firstly, that *foxp1* is required for adipose tissue expansion, secondly that LSAT expands by steady hypertrophic growth with bursts of hyperplastic growth and finally that the genetic control of adipose tissue expansion is conserved between mammals and zebrafish. In chapter 3 I have provided evidence to support the hypothesis that *foxp1* is required for adipose tissue expansion. *Foxp1* has been implicated in the control of body weight and adiposity by multiple GWAS studies, and it is this gene which has been the primary focus of my thesis (Hoffmann et al., 2018, Kichaev et al., 2019, Speakman et al., 2018). *Foxp1* was identified as a factor which may influence adipose morphology and expansion and further research on the known roles of *Foxp1* led to the hypothesis that "*Foxp1* maintains AT progenitor cell populations and is required for AT expansion" **(Figure 6.1A)**. To investigate this hypothesis I used zebrafish as a model and using CRISPR mutagenesis generated three novel zebrafish mutants, *foxp1a*$^{(-/-)}$, *foxp1b*$^{(-/-)}$ and *foxp1a*$^{(-/-)}$;*foxp1b*$^{(-/-)}$. Using these new mutant lines, I found that *foxp1a* is not required for AT expansion during normal development but is required for AT expansion in response to a high fat diet. The reduced AT expansion of the *foxp1a*$^{(-/-)}$ mutants in response to a HFD was characterised by reduced SAT expansion and a more hypertrophic SAT morphology. Similarly, *foxp1b* was also found to be nonessential for AT expansion during normal development. However, in contrast to *foxp1a, foxp1b* was required for VAT expansion in response to a HFD, though reduced VAT expansion did not result in an altered adipose morphology. Finally, *foxp1a*$^{(-/-)}$;*foxp1b*$^{(-/-)}$ double mutants had reduced levels of adipose tissue both during normal development and in response to a high fat diet **(Figure 6.1B)**. The reduced AT expansion in the *foxp1a*$^{(-/-)}$;*foxp1b*$^{(-/-)}$ mutants led to a more hypertrophic adipose tissue morphology and increased levels of blood glucose, thus suggesting metabolic impairment. **(Figure 6.1B)**. Together these data demonstrated that *foxp1* is required for adipose tissue expansion.

In chapter 4 I set out to address the hypothesis that *foxp1* maintains progenitor cell populations in adipose tissue. To do this I generated a novel transgenic line, *Foxp1:eGFP*, in which both adipocytes and adipose progenitor cells express GFP. Using this line I was able to propose a model of spatial LSAT expansion, in which LSAT expands by adding new cells to the centre of the depot and then further expands by forming chains of adipocytes which branch away from the main LSAT body. I also

show that LSAT expands via steady hypertrophic growth with bursts of hyperplastic growth. I then examined the role of *foxp1* in LSAT expansion and found that, while *foxp1b* is not required for normal LSAT expansion, *foxp1a* does appear to be required for normal expansion. *foxp1a*$^{(-/-)}$ mutants were found to have altered spatial LSAT expansion and change in adipocyte number was not correlated with change in progenitor cell number, suggesting altered progenitor cell behaviour. Finally it was found that *foxp1a*$^{(-/-)}$*;foxp1b*$^{(-/-)}$ mutants showed no differences in adipose progenitor cell number. However further timecourse experiments are needed to fully examine LSAT expansion in *foxp1a*$^{(-/-)}$*;foxp1b*$^{(-/-)}$ mutants. Overall, this data suggests that *foxp1a* plays a role in LSAT expansion.

Finally, in chapter 5 I have presented evidence which suggests that the genetic control of adipose tissue expansion is conserved between mammals and zebrafish. Much is currently known about adipose tissue in zebrafish however the genetic regulation of adipose tissue expansion is still poorly understood. In contrast, the genetic control of adipose tissue expansion in mammals is well characterised however the question of whether this conservation is extended to zebrafish remains untested. To begin to investigate the genetic conservation of AT expansion in zebrafish, I examined the role of a master regulator of adipogenesis and proposed the hypothesis that *cepba* is a key regulator of adipose tissue expansion in zebrafish **(Figure 6.1D)**. To investigate this hypothesis, I generated two novel *cebpa* zebrafish mutants, *cebpa*$^{(ed19/ed19)}$ and *cebpa*$^{(ed20/ed20)}$. I showed that loss of *cebpa* in zebrafish has a very similar effect on adipose tissue expansion to the effect observed in mouse models **(Figure 6.1E)**. I found that *cebpa*$^{(+/ed19)}$ mutants had reduced levels of adipose tissue during normal development and following a high fat diet **(Figure 6.1E)**. Finally, I showed that *cebpa*$^{(+/ed19)}$ mutants had a more hypertrophic adipose tissue morphology, increased levels of blood triglycerides, and fewer adipose progenitor cells **(Figure 6.1E)**. Overall, I have provided data to support the hypothesis that *cepba* controls adipose tissue expansion in zebrafish.

In this chapter I will discuss my key findings and the significance of these findings. I will also discuss how this work could be taken forward and suggest follow up experiments. The major limitations of the work I have described are discussed in sections 3.3, 4.3 and 5.3.

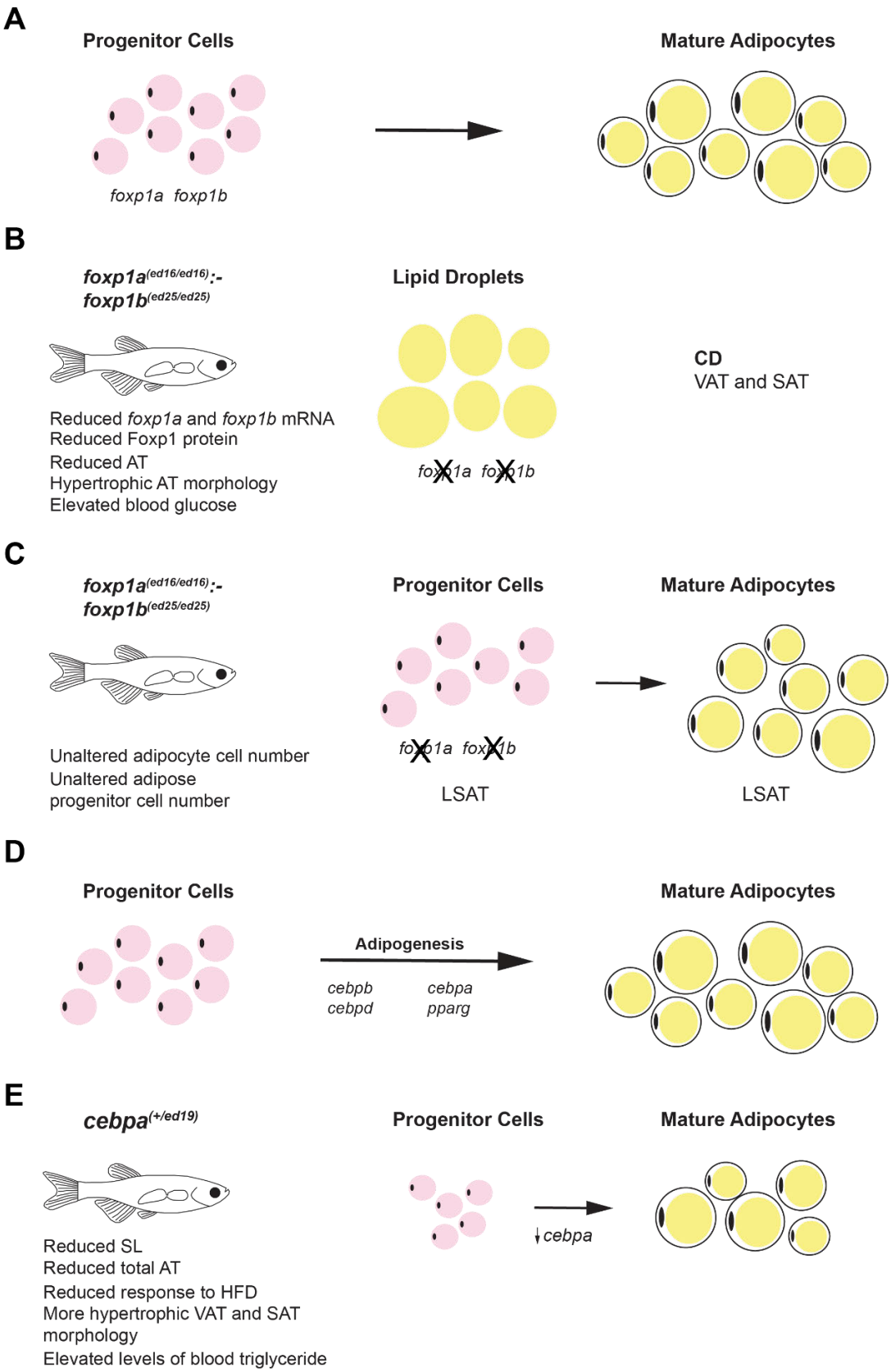

Figure 6.1 – Summary of key findings.

Figure 6.1 – Summary of key findings. A. Schematic of the hypothesis that *foxp1* maintains adipose progenitor cells and is required for adipose tissue expansion. **B.** Schematic showing the phenotype of *foxp1a*$^{(-/-)}$;*foxp1b*$^{(-/-)}$ mutants. **C.** Schematic showing the adipose progenitor phenotype of *foxp1a*$^{(-/-)}$;*foxp1b*$^{(-/-)}$ mutants. **D.** Schematic of the hypothesis that *cepba* is required for adipose tissue expansion in zebrafish. **E.** Schematic showing the phenotype of *cepba*$^{(+/ed19)}$ mutants.

6.2 – Key findings and significance

6.2.1 – Predicted loss of function *foxp1* zebrafish mutants are viable

To investigate the hypothesis that *foxp1* maintains adipose progenitor cell populations and is required for adipose tissue expansion, I first generated a series of predicted loss of function zebrafish mutants. All of the *foxp1* mutants described in this report, including the *foxp1a*$^{(-/-)}$, *foxp1b*$^{(-/-)}$ and the *foxp1a*$^{(-/-)}$;*foxp1b*$^{(-/-)}$ double mutants, were viable and survived to adulthood. This is in contrast to whole body *Foxp1* mouse mutants, which die at around embryonic day E14.5 due to defects in heart development (Wang et al., 2004). There are two possible explanations for the contrasting phenotypes observed, with the first being the different nature of the mutations generated. The mouse mutants described were generated by replacing the three exons of the forkhead DNA binding domain with a neomycin resistance cassette (Wang et al., 2004). The mouse mutants therefore contained no elements of the *Foxp1* forkhead DNA binding domain (Wang et al., 2004). In contrast the zebrafish mutants were generated using CRISPR and the induced mutations did not result in the loss of the entire FHD domain. While the *foxp1b*$^{(-/-)}$ mutants lacked all of the FHD apart from 4 amino acids, much of the FHD was retained in the *foxp1a*$^{(-/-)}$ mutants. Furthermore, although both mRNA and protein levels are reduced in both *foxp1a*$^{(-/-)}$ and *foxp1b*$^{(-/-)}$ mutants detectable levels still remained. Therefore, the less severe nature of the mutations generated in the zebrafish could explain the discrepancy between the observed phenotypes.

A second explanation for the difference between the viability of the mouse and zebrafish *foxp1* mutants could be the differing nature of mouse and zebrafish hearts. While zebrafish hearts can be thought of as comparable to mouse hearts, there are some key differences, not least their capacity for regeneration (Kikuchi, 2014). Furthermore, while zebrafish have two chambered hearts, mammals such as mice possess four chambered hearts (Andres-Delgado and Mercader, 2016). *Foxp1* is known to be required for cardiac outflow tract septation, a process which takes places during the formation of the four chambers of the heart and which does not take place in zebrafish (Wang et al., 2004). Therefore, it may be that while *Foxp1* is required for mouse heart development, it is not essential to zebrafish heart development. *foxp1* is also present as two paralogues in zebrafish and so another possibility is that the *foxp1a* and *foxp1b* genes may have undergone subfunctionalisation and only one

may be required for heart development. However, this theory has not been tested. Finally, it should be noted that while no obvious defects in heart function were observed in the zebrafish *foxp1* mutants, heart development and function were not examined. Therefore, the possibility remains that *foxp1* zebrafish mutants do show subtle defects in heart development or function. In summary the lack of a severe heart defect in the *foxp1* zebrafish mutants can be explained by the differing nature of the mutations in *foxp1* or by species specific differences in heart development.

6.2.2 – *foxp1b*$^{(-/-)}$ and *foxp1a*$^{(-/-)}$*;foxp1b*$^{(-/-)}$ mutants show altered somatic growth

One of the first phenotypic measures taken of the *foxp1* mutant zebrafish was standard length. *foxp1a*$^{(-/-)}$ mutants were found to have unaltered somatic growth when compared to WT siblings at 30 dpf. However, both *foxp1b*$^{(-/-)}$ and *foxp1a*$^{(-/-)}$*;foxp1b*$^{(-/-)}$ mutants were found to be significantly smaller than their WT siblings. These data suggest that *foxp1b* has a role in the somatic growth of zebrafish. As the whole body *Foxp1* mouse mutants died early in development no differences in size were reported, however adipocyte specific *Foxp1* knockout mice were reported to be normal in size (Liu et al., 2019, Wang et al., 2004). This difference in phenotype between the zebrafish and mouse mutants could be explained by the nature of the mutants. While mutation of *Foxp1* was restricted to adipocytes in the mouse model, the zebrafish mutants generated were whole body mutants (Liu et al., 2019). As *FOXP1* is known to be widely expressed in humans and has been shown to be widely expressed during zebrafish development, the reduced size of the zebrafish mutants could be explained by the action of *foxp1* on tissues other than adipose (Cheng et al., 2007, Fagerberg et al., 2014). For example, *Foxp1* is expressed in the brain in both humans and mice, however brain specific *Foxp1* knockout mice show no defects in locomotor activity (Bacon et al., 2015). In contrast *Foxp1* has been shown to be required for the formation of motor neuron circuits in mice (Arber, 2008). Therefore it is possible that the *foxp1b*$^{(-/-)}$ and *foxp1a*$^{(-/-)}$*;foxp1b*$^{(-/-)}$ fish show impaired locomotion and are outcompeted for food by their WT siblings. To test this mutant and WT could be raised separately and SL then measured to see if the reduced somatic growth phenotype of the mutants persists.

Another point to consider is that the reduced size of the *foxp1b*$^{(-/-)}$ and *foxp1a*$^{(-/-)}$*;foxp1b*$^{(-/-)}$ mutants could also be explained by a developmental delay. The stages at which *foxp1* mutant zebrafish reached developmental milestones were not characterised in depth. However, no obvious developmental delays were observed. Parichy et al (2011) have devised a method for staging postembryonic zebrafish and this could be utilised to determine whether *foxp1b*$^{(-/-)}$ and *foxp1a*$^{(-/-)}$*;foxp1b*$^{(-/-)}$ mutants are developmentally delayed (Parichy et al., 2009). Overall *foxp1b*$^{(-/-)}$ and *foxp1a*$^{(-/-)}$*;foxp1b*$^{(-/-)}$ mutants are significantly smaller than WT siblings and while this could be the result of reduced levels of *foxp1* throughout the fish, further experiments are needed to rule out any developmental delays in the mutant fish.

6.2.3 – *foxp1* is required for adipose tissue expansion

My hypothesis was that *foxp1* is required for adipose tissue expansion. Therefore, I next examined adipose tissue development in *foxp1* zebrafish mutants. Only the presence of white AT has been reported in zebrafish and so AT here refers only to WAT unless otherwise stated. *foxp1a*$^{(-/-)}$ and *foxp1b*$^{(-/-)}$ mutants were found to have normal levels of adipose tissue during normal development, while *foxp1a*$^{(-/-)}$*;foxp1b*$^{(-/-)}$ mutants were found to have reduced levels of AT relative to SL when compared to WT siblings. This suggests that no single *foxp1* paralogue is required for adipose tissue expansion but that *foxp1* itself is required for adipose tissue expansion. This finding is concordant with the recent study by Liu et al (2019). Liu et al (2019) showed that mice with conditional loss of *Foxp1* in adipose tissue had reduced levels of AT during normal development. This is in direct agreement with the results presented here, however the study proposed that the reduced levels of white adipose tissue observed in the mice were the result of increased brown/beige adipocyte differentiation (Liu et al., 2019). Zebrafish do not possess thermogenic adipose tissue and yet *foxp1* mutants still show defects in adipose tissue accumulation, suggesting that *foxp1* does play a role in white adipose tissue expansion. Furthermore, as the mouse mutants from the study by Liu et al (2019) were AT specific, together the mouse and zebrafish data support an adipose autonomous role of *foxp1*. However, an adipose autonomous role of *foxp1* in zebrafish is yet to be shown. In summary, the reduced levels of adipose tissue in the *foxp1a*$^{(-/-)}$*;foxp1b*$^{(-/-)}$ mutants supports the hypothesis that *foxp1 i*s required for adipose tissue expansion.

6.2.4 – *foxp1* is required for AT expansion in response to a HFD

To further examine the role of *foxp1* in adipose tissue expansion, I made use of a high fat diet to stimulate adipose tissue expansion. Briefly, fish were raised until 4 weeks of age and then stained with Nile Red to measured AT levels before the diet. The fish were then exposed to a 2 week HFD, which has previously been shown to result in significant AT accumulation in WT fish (Minchin and Rawls, 2017b). At the end of the diet the fish were again stained with Nile Red and this allowed AT accumulation in response to the diet to be calculated. All of the *foxp1* zebrafish mutants showed reduced AT expansion in response to the HFD. This is again in keeping with the results published by Lui et al (2019), which showed that adipocyte specific *Foxp1* knockout mouse mutants gained less adipose tissue in response to a high fat diet. Taken together these data show that *foxp1* is required for AT expansion in response to a HFD.

While all of the *foxp1* zebrafish mutants displayed reduced AT accumulation in response to the HFD, the *foxp1a*$^{(-/-)}$ and *foxp1b*$^{(-/-)}$ mutants showed differences in VAT and SAT accumulation. *foxp1a*$^{(-/-)}$ mutants showed reduced SAT accumulation in response to the HFD, while *foxp1b*$^{(-/-)}$ mutants showed reduced VAT accumulation. The different phenotypes observed in the two mutants is suggestive of gene subfunctionalisation and indicates that *foxp1a* may have a larger role in SAT, while *foxp1b* may have a stronger role in VAT. *foxp1a* and *foxp1b* may also show different expression patterns in different adipose tissues. While there is no direct evidence of this many duplicated genes in zebrafish have been shown to divide their expression between tissues in which the single gene is expressed in mammals (Kleinjan et al., 2008, Sharma et al., 2006). However, *foxp1a* and *foxp1b* expression in zebrafish needs to be further examined to determine if they show different patterns of expression. Overall, these data support the hypothesis that *foxp1* is required for AT expansion and suggests that *foxp1a* has a role in SAT expansion while *foxp1b* has a role in VAT expansion.

6.2.5 – *foxp1* mutants have a more hypertrophic adipose morphology

Having determined that *foxp1* is required for AT expansion I next examined whether the mode of adipose tissue expansion was altered in the *foxp1* mutants. AT can expand via hyperplastic growth, an increase in adipocyte number, or hypertrophic

growth, an increase in cell size (Hoffstedt et al., 2010). *foxp1a*$^{(-/-)}$ mutants were found to have a more hypertrophic LSAT, but not PVAT, morphology following a HFD. This meant that *foxp1a*$^{(-/-)}$ mutants had fewer but larger lipid droplets present in SAT than WT siblings, following a HFD. In contrast no differences in PVAT or LSAT morphology were observed in *foxp1b*$^{(-/-)}$ mutants. The lack of observed phenotype could be explained by a more subtle effect of a loss of *foxp1b* on VAT morphology and a sample size too small to see this effect. Finally *foxp1a*$^{(-/-)}$*;foxp1b*$^{(-/-)}$ mutants were found to have a more hypertrophic adipose morphology during normal development in the PVAT depot. Together this suggests that *foxp1* drives hyperplastic adipose tissue expansion. The hypertrophic AT morphology observed in the zebrafish mutants is reminiscent of the few very large adipocytes present in *Pparg* knockout mice (Wang et al., 2013a). *Pparg* knockout mice were found to have virtually no AT, and the adipocytes which were present were vastly enlarged (Wang et al., 2013a). The similarities between the *Pparg* knockout mice and the *foxp1* zebrafish mutants suggests that, like *pparg, foxp1* is an important driver of hyperplastic adipose tissue expansion. Furthermore, this suggests that *foxp1* may play a role in adipose progenitor proliferation and differentiation, and this role has been examined with the use of transgenic zebrafish. However, *Foxp1* adipocyte specific knockout mice do not share the hypertrophic adipose phenotype of the zebrafish mutants (Liu et al., 2019). The *Foxp1* mutant mice described by Lui et al (2019) were described as having a more hyperplastic adipose morphology than WT siblings, however this observation was made of a singular adipose depot and adipose morphology was not quantified. One explanation for this discrepancy could be that the reported browning of WAT in the *Foxp1* mutant mice may have led to mobilisation of lipid from white adipocytes and a more hyperplastic morphology (Liu et al., 2019). As zebrafish do not possess brown AT, the hypertrophic AT phenotype observed in the *foxp1* zebrafish mutants may therefore be due to the effect of *foxp1* on WAT only. In summary *foxp1* zebrafish mutants have a more hypertrophic adipose tissue morphology, which suggests that *foxp1* may drive hyperplastic adipose tissue expansion. However further experiments looking at adipocyte proliferation and differentiation are needed to test this.

6.2.6 – *foxp1a*$^{(-/-)}$*;foxp1b*$^{(-/-)}$ mutants have elevated levels of blood glucose

As adipose tissue expansion is impaired in the *foxp1* mutants and is characterised by a hypertrophic PVAT morphology, I examined levels of blood metabolites to get a better picture of the overall metabolic health of the mutants. *foxp1a*$^{(-/-)}$ and *foxp1b*$^{(-/-)}$ mutants were found to have normal levels of blood glucose, triglyceride and cholesterol. In contrast *foxp1a*$^{(-/-)}$*;foxp1b*$^{(-/-)}$ mutants were found to have increased levels of blood glucose compared to WT siblings, and this is reflective of the more severe phenotype of the *foxp1a*$^{(-/-)}$*;foxp1b*$^{(-/-)}$ mutants. The increased levels of blood glucose could be the result of increased gluconeogenesis in the liver or impaired glycogen storage by the liver and muscle (Stumvoll et al., 2005). With both being signs of reduced insulin secretion and peripheral insulin resistance (Stumvoll et al., 2005). This phenotype resembles the slightly more severe phenotype of *Cebpa* and *Pparg* mutant mice (Linhart et al., 2001, Wang et al., 2013a). Both *Cepba* and *Pparg* knockout mice have been reported to show peripheral insulin resistance (Linhart et al., 2001, Wang et al., 2013). Together this shows that similarly to loss of *Cepba* and *Pparg* expression, loss of *foxp1* expression leads to adverse metabolic outcomes.

In contrast to the adverse metabolic outcomes associated with loss of *foxp1* in zebrafish, loss of *Foxp1* in mouse models has been shown to improve glucose metabolism and insulin sensitivity (Liu et al., 2019). Adipose specific *Foxp1* knockout mice gained less weight than control littermates following a HFD and showed improved metabolic parameters (Liu et al., 2019). Loss of *Foxp1* in adipose tissue in mice therefore appears to improve metabolic parameters while loss of *foxp1* in zebrafish worsens them. This discrepancy could be explained by a number of factors, with the influence of brown adipose tissue being one such factor. In the *Foxp1* knockout mice described, the levels and activity of brown adipose tissue are increased (Liu et al., 2019). It could therefore be the case that the changes in BAT, and not WAT, are responsible for the improved metabolic profile of the *Foxp1* mutant mice. Zebrafish do not possess brown adipose tissue and so loss of *foxp1* in WAT is detrimental to metabolic health (Gesta et al., 2007). A second explanation for the difference in metabolic outcome is that while the *Foxp1* mouse mutants are adipose tissue specific, the zebrafish mutants are whole body mutants (Liu et al., 2019). *Foxp1* is known to play a role in the liver where it inhibits gluconeogenesis, and it may be that the loss of *foxp1* in this pathway leads to the increased blood glucose levels

observed in zebrafish mutants (Zou et al., 2015). Evidence to support this idea comes from a study in which increased *Foxp1* expression in the livers of mice, via tail vein injection of a recombinant adenovirus expressing *Foxp1*, leads to lower blood glucose levels (Zou et al., 2015). Therefore it may be the loss of *foxp1* expression in the liver, rather than in AT, that is responsible for the increased levels of blood glucose in *foxp1a*$^{(-/-)}$*;foxp1b*$^{(-/-)}$ mutants. In summary the differences in the metabolic health of *Foxp1* mouse and zebrafish mutants could be explained by either the lack of BAT in zebrafish or by the action of *foxp1* in the liver. Further experiments are needed to determine if the effects observed in the zebrafish mutants are adipose tissue autonomous and details of these proposed experiments can be found in sections 3.3 and 6.3

6.2.7 – Analysis of the *Foxp1:eGFP* transgenic line has provided novel information on LSAT growth and adipose progenitor behaviour in zebrafish

Having identified a role for *foxp1* in the expansion of zebrafish adipose tissue, I next looked at whether *foxp1* influences adipose progenitor cell behaviours. To do this I generated the *Foxp1:eGFP* transgenic zebrafish line, in which GFP is expressed by both adipocytes and adipose progenitor cells. This model allows for unprecedented imaging of adipose progenitor cells and adipose tissue growth *in vivo*. The *Foxp1:eGFP* line can be stained with lipophilic dyes to distinguish between mature adipocytes and progenitors. LSAT growth has previously been imaged in zebrafish, however this imaging relied entirely on the use of lipophilic dyes and so adipose progenitor cells could not be visualised (Minchin and Rawls, 2017b). The *Foxp1:eGFP* line therefore constitutes the first transgenic line capable of marking adipose progenitor cells in live fish. In addition to allowing for the visualisation of adipose progenitor cells, the *Fopx1:eGFP* line also allowed novel data on the cellular dynamics of LSAT expansion to be compiled. LSAT expansion has previously been described by Minchin and Rawls (2017), who showed that LSAT first appeared at 8.2 mm SL and that expansion of the depot occurred primarily along the anterior posterior axis. Expansion along the dorsal ventral axis was also reported and LSAT was reported to form a long thin depot (Minchin and Rawls, 2017b). These findings were corroborated by the findings in chapter 4. In addition, the cellular dynamics of LSAT expansion were described for the first time and cell number, average lipid droplet area and LSAT

branching were shown to correlate with SL. Furthermore, a model of the spatial expansion of LSAT was proposed. In this model LSAT expands by adding new cells to the centre of the depot and then further expands by forming chains of adipocytes which branch away from the main LSAT body. In summary LSAT expansion in zebrafish proceeds as previously described and the results described in chapter 4 are the most detailed quantification of zebrafish AT expansion to date.

6.2.8 – LSAT expands in zebrafish via steady hypertrophic growth with bursts of hyperplastic growth

In addition to providing novel information on LSAT growth, the *Foxp1:eGFP* line has also provided new insights into LSAT growth during development. It was shown that LSAT expands via steady hypertrophic growth, with bursts of hyperplastic growth and that the LSAT depot continues to expand over a period of at least 5 days. In contrast the development of SAT in mice has been shown to occur over a shorter timeframe, with the hyperplastic growth of SAT being confined to a 4 day time period (Wang et al., 2013b). Furthermore, due to the nature of mouse models, no data currently exists on the cellular nature of SAT expansion during mouse development. The differing nature of SAT development in zebrafish and mice can be explained by the differing developmental timings of adipose formation in the two species (Minchin and Rawls, 2017b, Wang et al., 2013b). In rodents subcutaneous adipose depots are formed during embryonic development while visceral depots are formed postnatally (Wang et al., 2013b). In contrast, all zebrafish AT depots are formed post embryonically and visceral adipose depots are known to be formed prior to subcutaneous depots (Minchin and Rawls, 2017b). Furthermore, the use of the *Foxp1:eGFP* line and lipophilic dyes allows LSAT development to be tracked in live zebrafish and therefore allows information on the cellular dynamics of LSAT growth to be compiled. This resolution however cannot be achieved in mice, as SAT development must be tracked using lineage tracing techniques (Wang et al., 2013b). Wang et al (2013) investigated SAT formation using a lineage tracing system in which mature adipocytes are indelibly marked by lacZ upon treatment with doxycycline. Pregnant mice were given doxycycline at various timepoints and the subcutaneous adipose tissue of their offspring examined (Wang et al., 2013b). Mice whose mothers were given doxycycline between E9-E16 showed heterogeneous LacZ expression, while mice whose mothers were given doxycycline between E9-E18 or E19-P10

showed nearly 100% lacZ positive cells (Wang et al., 2013b). This shows that in mice adipocyte commitment in SAT is initiated between E14-E18 and suggests SAT adipocytes are committed and differentiated early during adipogenesis (Wang et al., 2013b). In conclusion, hyperplastic growth of SAT in mice occurs over a shorter time period than in zebrafish and adipose tissue expands via steady hypertrophic growth with bursts of hyperplastic growth in zebrafish.

6.2.9 – *foxp1* doesn't appear to influence adipose progenitor cell maintenance

I next used the *Foxp1:eGFP* line to investigate the role of *foxp1* in adipose progenitor cell maintenance. SAT growth was imaged in *foxp1a*$^{(-/-)}$ and *foxp1b*$^{(-/-)}$ mutants over a period of five and three days, however no changes in adipose progenitor cell numbers or modes of adipose tissue growth were observed. In contrast the negative correlation between change in adipocyte number and change in progenitor cell number, which was observed in WT fish, was not observed in *foxp1a*$^{(-/-)}$ mutant fish. This suggests that progenitor cell behaviour is altered in *foxp1a*$^{(-/-)}$ mutants. *foxp1a*$^{(-/-)}$*;foxp1b*$^{(-/-)}$ double mutants however showed no significant difference in adipose progenitor cell number when compared to WT siblings. The *foxp1a*$^{(-/-)}$*;foxp1b*$^{(-/-)}$ data was taken from a single timepoint and so needs to be expanded upon in order to examine any differences in LSAT expansion. This preliminary data does not agree with the hypothesis that *foxp1* maintains adipose progenitor cells and is not in keeping with the known function of *foxp1* in other progenitor cell populations. For example, loss of *Foxp1* in bone marrow MSCs leads to a decline in their self-renewal capacity (Li et al., 2017). Furthermore, loss of *Foxp1* expression in the mammary gland leads to reduced mammary progenitor cell proliferation (Fu et al., 2018). In contrast lack of *foxp1* in adipose tissue does not appear to alter adipose progenitor cell number. However, while the *Foxp1:eGFP* line does mark adipose progenitor cells, the nature of the progenitor cells marked by the *Foxp1:eGFP* line remains untested. Therefore further work is needed to determine the nature of the progenitor cells marked by the *Foxp1:eGFP* line and this is discussed in the future directions section (Chapter 6.3.4). In summary *foxp1* does not appear to be required to maintain adipose progenitor cells however further work is needed to test this.

6.2.10 – The role of *cebpa* in liver development appears to be conserved to zebrafish

In addition to exploring the role of *foxp1* in adipose tissue expansion, I also examined the role of a master regulator of adipogenesis *cebpa*. To do this I investigated the hypothesis that *cebpa* is required for adipose tissue expansion in zebrafish. I generated two predicted loss of function zebrafish mutants, *cebpa*$^{(ed19/ed19)}$ and *cebpa*$^{(ed20/ed20)}$, and both mutants were found to die before 21 dpf. This early death phenotype is reminiscent of both published mouse and zebrafish *cebpa* mutants. *Cebpa* knockout mice die shortly after birth due to liver defects, and this defect has also been observed in zebrafish *cebpa* mutants (Siersbaek et al., 2012, Yuan et al., 2015). *cebpa* zebrafish mutants, described by Yuan et al (2015) died at around 3 weeks post fertilisation, had smaller livers than WT siblings and showed altered levels of liver cell proliferation. This small liver phenotype was also observed in the *cebpa*$^{(ed19/ed19)}$ mutants, suggesting that the role of *cebpa* in liver development is conserved to zebrafish. In summary the *cebpa*$^{(ed19/ed19)}$ and *cebpa*$^{(ed20/ed20)}$ mutants show that same early death phenotype as published mouse and zebrafish mutants and this phenotype also appears to be due to defects in liver development.

6.2.11 – The role of *cebpa* in adipose tissue expansion is conserved to zebrafish

I next examined the role of *cebpa* in adipose tissue expansion in zebrafish and found *cebpa*$^{(+/ed19)}$ and *cebpa*$^{(+/ed20)}$ mutants to have impaired adipose tissue expansion. As *cebpa*$^{(ed19/ed19)}$ and *cebpa*$^{(ed20/ed20)}$ mutants died before the development of adipose tissue, levels of adipose tissue were examined in *cebpa*$^{(+/ed19)}$ and *cebpa*$^{(+/ed20)}$ mutants. Levels of adipose tissue were found to be significantly reduced in both *cebpa* mutants when compared to WT siblings. This finding mirrors the phenotype of *Cebpa* knockout mice. In 2001 Linhart et al generated a mouse model in which *Cebpa* is expressed only by hepatocytes. These mice showed a complete absence of white adipose tissue, demonstrating that *Cebpa* is required for the commitment of preadipocytes to adipocytes *in vivo* (Linhart et al., 2001). This phenotype is also similar to that of the *Pparg* knockout mouse, with *Pparg* being another key regulator of adipogenesis (Wang et al., 2013a). In summary, the severely reduced levels of AT in *cebpa*$^{(+/ed19)}$ and *cebpa*$^{(+/ed20)}$ mutants mirrors previously

published mouse phenotypes and suggests that *cebpa* is a key regulator of AT expansion in zebrafish.

6.2.12 – *cebpa*$^{(+/ed19)}$ and *cebpa*$^{(+/ed20)}$ mutants have a more hypertrophic adipose tissue morphology than WT siblings

In addition to having reduced levels of adipose tissue, both *cebpa*$^{(+/ed19)}$ and *cebpa*$^{(+/ed20)}$ mutants showed a more hypertrophic adipose tissue morphology than WT siblings. Furthermore, use of the *Foxp1:eGFP* line revealed *cebpa*$^{(+/ed19)}$ mutants to have fewer adipose progenitor cells than their WT siblings. Taken together this suggests reduced rates of hyperplastic growth in *cebpa*$^{(+/ed19)}$ mutants and therefore potentially reduced rates of adipogenesis, all of which fits with *Cebpa's* known role as a master regulator of mammalian adipogenesis. Another known master regulator of mammalian adipogenesis is *Pparg* and *Pparg* knockout mice show a strikingly similar adipose morphology phenotype to that of the *cebpa*$^{(+/ed19)}$ mutants. *Pparg* knockout mice have nearly no AT but the adipocytes which are present are vastly enlarged (Wang et al., 2013a). This is a more severe but similar phenotype to the hypertrophic AT morphology observed in the *cebpa*$^{(+/ed19)}$ mutants. In summary the hypertrophic AT morphology of the *cebpa*$^{(+/ed19)}$ mutants and their reduced number of adipose progenitor cells provides further evidence to support the hypothesis that *cebpa* is a key regulator of zebrafish AT expansion.

6.2.13 – *cebpa*$^{(+/ed19)}$ mutants have elevated levels of blood triglycerides

Finally, I examined the levels of blood metabolites in *cebpa*$^{(+/ed19)}$ mutants to understand if the overall metabolic health of *cebpa*$^{(+/ed19)}$ mutants was altered. *cebpa*$^{(+/ed19)}$ mutants showed increased levels of blood triglycerides, while no changes were observed in levels of blood glucose or cholesterol. This phenotype precisely matches that of the *Cebpa* knockout mouse model, in which levels of blood triglyceride but not blood glucose were elevated (Linhart et al., 2001). This shows that, like in the mouse model, a reduction in *cebpa* levels results in a worsened metabolic outcome in zebrafish. The reduced levels of AT in *cebpa*$^{(+/ed19)}$ mutants and the increased levels of blood glucose are suggestive of AT dysfunction and ectopic lipid deposition. It would therefore be useful to examine levels of lipid in the livers of *cebpa*$^{(+/ed19)}$

mutants. Overall, the elevated levels of blood triglycerides in cebpa$^{(+/ed19)}$ mutants provides further evidence that the role of *cebpa* in adipose tissue expansion is conserved to zebrafish.

6.3 – Future directions

6.3.1 – Is the reduced adipose tissue expansion observed in *foxp1* mutants due to the effects of *foxp1* on adipose tissue alone?

All the zebrafish mutants described in this thesis are whole body mutants. This therefore leaves open the question of whether the phenotypes observed in these mutants are due to the loss of *foxp1* function in adipose tissue or if the phenotypes observed are caused by a lack of *foxp1* expression in other tissues. This problem has previously been discussed in section 3.3, with the generation of AT specific *foxp1* mutants and the *in vitro* culture of adipose progenitor cells given as examples of ways to overcome this issue. An additional avenue which has not yet been addressed is feeding behaviour in the *foxp1* zebrafish mutants. One explanation for the reduced levels of adipose tissue in the *foxp1* mutants, which is not an impaired ability of the adipose tissue to expand, could be reduced food consumption. Patients with mutations in the *FOXP1* gene have been reported to have intellectual disabilities and brain specific *Foxp1* knockout mice show broad brain morphology defects (Bacon et al., 2015). Therefore, due to the strong link between hunger and satiety signals from the brain and feeding behaviour, in addition to *Foxp1's* role in the brain, it is not unreasonable to suppose that feeding behaviour may be altered in *foxp1* mutants (Heisler and Lam, 2017). Food consumption was not monitored in the *foxp1* zebrafish mutants, however feeding behaviour can be assessed in zebrafish. One way to do this would be to isolate individual WT and *foxp1* mutant fish, give all fish the same amount of dry feed and monitor food consumption. Zebrafish also hunt live prey and so this could be filmed to observe if this behaviour is impaired in mutant fish (Shimada et al., 2012). In summary further experiments are needed to confirm that the phenotypes observed in *foxp1* mutants are due to the effect of *foxp1* on adipose only and assessing feeding behaviour would go some way to show this.

6.3.2 – Further characterisation of zebrafish *foxp1* expression is needed

FOXP1 is known to be expressed in adipose tissue in both humans and mice (Fagerberg et al., 2014, Liu et al., 2019). In chapter 3 I showed that *foxp1a* and *foxp1b* are expressed in a whole VAT depot and by cells of the SVF (section 3.2.3 & 3.2.4). However, whether *foxp1a* or *foxp1b* are expressed by adipocytes themselves or by

adipose progenitor cells remains unknown. One way to overcome this problem would be to make use of the *Foxp1:eGFP* line. Adipose tissue could be dissected from *Foxp1:eGFP* fish and the tissue digested and fractionated to separate adipocytes and the SVF. FACS (Fluorescence activated cell sorting) sorting could then be used to isolate GFP positive cells from each fraction and would give a pure population of adipocytes and adipose progenitor cells. RNA could then be extracted from these cells and *foxp1* expression measured. Overall there is a lack of data on *foxp1* expression in zebrafish and the *Foxp1:eGFP* line could be used to determine if *foxp1* is expressed in adipocytes and preadipocytes.

In addition to the uncertainty surrounding *foxp1* expression in adipose in zebrafish, it is also unclear which tissues express *foxp1* in juvenile zebrafish. Previously published expression data of *foxp1* in zebrafish comes from *in situ* hybridisations in embryos (Cheng et al., 2007). This data shows that *foxp1b* expression is dynamic in the early embryo and goes from being expressed ubiquitously at the 4 cell stage to being expressed in the mid-hindbrain and intestinal tract at 5 dpf (Cheng et al., 2007). This data however only exists for *foxp1b* and not *foxp1a* and the expression patterns of both genes are unknown at later stages of development. Crucially the expression of *foxp1* at the stages tested in this thesis, i.e. 4-5 weeks post fertilisation, are unknown. This is important information to gather as loss of *Foxp1* expression in mice results in heart, brain and liver phenotypes (Bacon et al., 2015, Wang et al., 2004, Zou et al., 2015). Therefore, knowing where in the zebrafish *foxp1* is expressed could help to interpret *foxp1* mutant phenotypes and to determine whether these phenotypes are likely due to loss of *foxp1* expression in AT. One way to determine where *foxp1* is expressed would be to perform *in situ* hybridisation against *foxp1a* and *foxp1b* in 4 week old fish. A better solution would be to find or generate antibodies which recognise zebrafish *foxp1* and use these to perform immunostaining on tissues of interest. In chapter 3 I measured Foxp1 protein levels in *foxp1a*$^{(-/-)}$, *foxp1b*$^{(-/-)}$ and *foxp1a*$^{(-/-)}$;*foxp1b*$^{(-/-)}$ mutants, all of which showed reduced levels of Foxp1 protein (Section 3.2.12, 3.2.21 & 3.2.30). Foxp1 protein levels were tested using protein lysate from the caudal fins of zebrafish and using an antibody which recognised human FOXP1 protein. There is currently no data as to whether Foxp1a, Foxp1b, or both paralogues are expressed in the caudal fin and the predicted protein sizes of Foxp1a and Foxp1b are very similar at 71 kDa and 74 kDa respectively. Therefore, it is unknown whether the FOXP1 antibody used recognises Foxp1a, Foxp1b or both paralogues. One way to overcome this problem would be to

have antibodies manufactured which recognise the zebrafish proteins themselves. In summary further information on the global expression of *foxp1* in zebrafish is needed, and this could be achieved through the use of *in situ* hybridisation or through the generation of antibodies which recognise the zebrafish Foxp1 proteins.

6.3.3 – Are the effects of the HFD in zebrafish due to overnutrition or due to increased levels of fat in the diet?

The 5% egg yolk based HFD used in this thesis has been shown to lead to significant AT accumulation over a two week period (Carten et al., 2011, Semova et al.,2012, Walters et al., 2012). However, the broader metabolic changes that the egg yolk based diet leads to have not been fully studied. Similarly, the use of HFDs in zebrafish is not widespread and there is little research into what constitutes a HFD for a zebrafish. In contrast the use of HFD's in mouse models is widespread and these diets are used to achieve an obesity like phenotype in a shorter timeframe than can be achieved through overfeeding (Speakman, 2019). However, there is still discussion as to how closely these diets resemble human diets, with differences in not only fat content between diets but also in levels of sucrose and fatty acids (Speakman, 2019). HFDs in mice commonly have a 40 or 60% fat content, this is in contrast to a standard chow diet which contains around 10% fat (Speakman, 2019). HFDs containing 40% fat have also been reported in zebrafish (Meguro et al., 2015). However lower fat content diets, at 22%, have been reported and result in metabolic changes (Oka et al., 2010). The 22% fat diet lasted for 8 weeks and led to a significant increase in levels of blood triglycerides (Oka et al., 2010). The 5% egg yolk diet also led to increased levels of blood triglycerides, though after only 2 weeks **(Figure 3.10)**. As there is uncertainty around the effects of different diets in zebrafish, further experiments are needed to test if the effect of the HFD used in this thesis results in an obesity like phenotype or if the observed phenotypes are due to changes in diet composition. This could be achieved by comparing the effects of the 5% egg yolk HFD with overfeeding and with other reported HFDs. Overall, little is known about how the composition of different diets affects AT expansion and metabolic phenotypes in zebrafish. Therefore further testing of the effects of diet on WT zebrafish is needed.

6.3.4 – Do zebrafish adipose progenitors resemble human or mouse adipose progenitor cells?

Adipose progenitor cells have been identified in zebrafish by Flynn et al (2009), which identified cells abundant in *fabp11a* transcript but lacking neutral lipid. *fabp11a* is a homologue of mammalian *Fabp4* which marks both adipocytes and adipose progenitors (Flynn et al., 2009). As the lipid negative cells described by Flynn et al (2009) were found close to *fabp11a* labelled lipid positive cells, the cells were determined to be adipose progenitor cells. In addition to the cells described by Flynn et al (2009), I have also identified adipose progenitor cells in chapter 4. The *Foxp1:eGFP* line marks lipid negative cells with GFP, and these cells were then observed to accumulate lipid and form mature adipocytes. However very little is known about adipose progenitor cells in zebrafish and the vast majority of our current knowledge of these progenitors comes from human and mouse data. Much of the data on adipose progenitor cells comes from *in vitro* cell culture work (Siersbaek et al., 2012). Normally adipose tissue is dissected, digested and the SVF isolated (Siersbaek et al., 2012). The SVF is then placed into culture and adipogenesis induced through the use of a hormonal cocktail (Siersbaek et al., 2012). This process has never been performed on zebrafish, however it has been performed using species of fish which are relevant to the aquaculture industry, such as Atlantic salmon and grass carp (Wafer et al., 2017). As isolation and differentiation of adipose progenitor cells has never been successfully demonstrated in zebrafish, it would be a useful experiment. It would be interesting to determine whether SVF cells from zebrafish could undergo adipogenesis in response to the normal hormonal cocktail of insulin, cAMP elevating agent, glucocorticoids and growth factors used on mammalian cell lines (Siersbaek et al., 2012). It would also be useful to test whether zebrafish cells express the same genes as mammalian cells do during the progression of adipogenesis. In summary little data exists on adipose progenitor cells in zebrafish and experiments using zebrafish *in vitro* cell culture models could help to expand the current understanding of adipose progenitor cells.

6.3.5 – Further characterisation of adipose progenitor cells marked by the *Foxp1:eGFP* line is needed

The *Foxp1:eGFP* line marks both mature adipocytes and adipose progenitor cells. However, the stage at which adipose progenitor cells are marked is unknown. Adipose progenitor cells are derived from mesenchymal stem cells, which have the ability to differentiate into osteoblasts, chondrocytes, and adipocytes (Merrick et al., 2019). Whether the *Foxp1:eGFP* line marks cells capable of differentiating into multiple lineages or whether it marks committed preadipocytes is currently unknown. One way to test this would be to isolate GFP positive adipose progenitor cells from *Foxp1:eGFP* zebrafish and to place the cells in culture. The cells could then be given hormonal cocktails which drive each of the different lineage specifications to see which cell types they are capable of differentiating into. Overall it is unknown at which stage of adipocyte commitment the *Foxp1:eGFP* line marks adipose progenitor cells, however *in vitro* cell culture experiments could be used to test this.

6.3.6 – Is zebrafish AT formed of a heterogeneous population of adipocytes

VAT and SAT in mammals are known to have distinct properties, with expression profiling revealing significant differences in the expression of 100s of genes between the two types of AT (Gesta et al., 2006, Vidal, 2001, Vohl et al., 2004). Furthermore, SAT in mammals is considered to be broadly protective, with numerous studies correlating increased SAT relative to VAT with preserved metabolic function, for subjects of similar weights (Ghaben and Scherer, 2019). However, while AT in zebrafish can be classified into VAT and SAT based on anatomical location, it is unclear whether these different depots have different properties (Minchin and Rawls, 2017b). Data from a study by Minchin et al (2015) showed that zebrafish with decreased levels of VAT relative to SAT had improved glucose tolerance following a HFD, suggesting that SAT is also protective in zebrafish. In order to further examine any differences in VAT and SAT in zebrafish RNA Seq could be used. VAT and SAT could be dissected from the *Foxp1:eGFP* line and GFP positive adipocytes and preadipocytes isolated. RNA Seq could then be used to look for genes differentially expressed between adipocytes and adipose progenitor cells from VAT and SAT. Additional data on the properties of VAT and SAT in zebrafish would be useful in

helping to interpret the phenotypes of *foxp1a*$^{(-/-)}$ and *foxp1b*$^{(-/-)}$ mutants, which gain less SAT and VAT in response to a HFD respectively. In summary not much is known about the differences between VAT and SAT in zebrafish, and RNA Seq could be used to look for differences in gene expression between the two types of WAT.

In addition to differences between adipose depots, multiple recent studies have highlighted the heterogeneous nature of adipose progenitor cells within single depots in mice and humans (Hepler et al., 2018, Merrick et al., 2019, Schwalie et al., 2018, Sempere et al., 2014). In particular single cell RNA-Seq has been utilised to identify subpopulations of adipose progenitor cells with differing adipogenic capacities (Hepler et al., 2018, Schwalie et al., 2018). For example, a study by Schwalie et al (2018) identified a subpopulation of adipose progenitor cells which were capable of inhibiting adipogenesis. No data currently exists on whether zebrafish adipose progenitor cells represent a homogeneous population of cells. Therefore, the next step would be to perform single cell RNA-Seq on zebrafish adipose progenitor cells to determine if the cells are a homogeneous population. The *Foxp1:eGFP* line could be utilised to isolate GFP positive adipose progenitor cells. In summary much is known about the nature of adipose progenitor cells in mammals which remains to be tested in zebrafish and the sequencing of zebrafish adipose progenitor cells would be one way in which to start to bridge this gap.

6.3.7 – Further characterisation of LSAT growth in zebrafish is needed

The *Foxp1:eGFP* line has been used to image LSAT expansion *in vivo*. From these experiments I have shown that LSAT appears to expand by steady hypertrophic growth with bursts of hyperplastic growth. However, all the imaging presented in this thesis was carried out over a period of five or fewer days and a lot of questions about LSAT growth remain to be addressed. Further experiments are needed to observe LSAT growth over longer periods of time, for example over two weeks. It would also be useful to see how LSAT grows in response to a dietary challenge such as a high fat diet. In addition, LSAT growth in response to starvation and refeeding could also be measured. In summary although imaging of the *Foxp1:eGFP* line allowed novel data about LSAT growth to be compiled, further experiments are needed to fully understand normal LSAT expansion.

6.3.7 – Identification of novel downstream effectors of *foxp1*

In chapters 3 and 4 I have presented data to support the hypothesis that *foxp1* maintains adipose progenitor cell populations and is required for adipose tissue expansion. As *foxp1* is a transcription factor, it is supposed that it influences the expression of many genes in order to maintain adipose progenitor cell populations. However which factors *foxp1* interacts with and how these interactions drive the proliferation and differentiation of adipose progenitor cells remains unknown. One way to learn more about downstream effectors of *foxp1* would be to use RNA-Seq. Adipose tissue could be dissected from *Foxp1:eGFP; foxp1a*$^{(-/-)}$*;foxp1b*$^{(-/-)}$ mutant fish and WT siblings. The SVF could then be isolated, GFP positive adipose progenitor cells removed and RNA extracted. Genes which are differentially expressed between the two groups could then be investigated as candidate downstream effectors. Overall additional experiments are required to identify downstream effectors of *foxp1* and to gain a better understanding of the transcriptional network surrounding *foxp1*.

6.3.8 – Identification of novel downstream effectors of *cebpa*

Finally, having demonstrated that the role of *cebpa* in adipose tissue expansion is conserved to zebrafish, I used *cebpa*$^{(+/ed19)}$ mutants to identify novel downstream effectors of *cebpa*. RNA Seq was performed on samples extracted from the PVAT of *cebpa*$^{(+/ed19)}$ mutants. The sequencing revealed that 949 genes were significantly upregulated in *cebpa*$^{(+/ed19)}$ mutants when compared to WT siblings and 177 were significantly downregulated. Further analysis by GO term analysis revealed an enrichment of terms relating to tissue development and cell differentiation. Of particular interest were genes found in the cell differentiation category. Genes in this category were chosen for further investigation as *cebpa* is a key regulator of the adipogenic cell differentiation pathway. Genes found within this category included *cxcr4b*. Chemokine receptor type 4 (CXCR4) is a chemokine receptor with potent chemotactic activity for lymphocytes (Lear et al., 2017). CXCR4 is a seven transmembrane G protein coupled receptor which is activated by the binding of one or more chemokines and which acts as the main receptor for CXCL12 (Lear et al., 2017). CXCR4 is known to be involved in processes such as chemotaxis and cell proliferation however a role for CXCR4 in adipose tissue is unknown (Lear et al., 2017). Loss of function *cxcr4b* zebrafish exist and could be used to investigate the

function of *cxcr4b* in adipose tissue expansion (Haas and Gilmour, 2006). One future experiment would be to cross the *cxcr4b* mutants to *cebpa*$^{(+/ed19)}$ mutants and examine whether this worsened or improved adipose tissue expansion. In summary I have used RNA-Seq to identify novel downstream candidate *cebpa* effectors, of which *cxcr4b* is an example.

Chapter 7 - Appendix

A

```
FOXP1    VRPPFTYASLIRQAILESPEKQLTLNEIYNWFTRMFAYFRRNAATWKNAV
Foxp1a   VRPPFTYAALIRQAILESPEKQLTLNEIYNWFTRTFAYFRRNAATWKNAV
Foxp1b   VRPPFTYASLIRQAILESPEKQLTLNEIYNWFTRMFAYFRRNAATWKNAV
                  *                                  *

FOXP1    RHNLSLHKCFVRVENVKGAVWTVDEVEFQKRRPQKIS
Foxp1a   RHNLSLHKCFVRVENVKGAVWTVDELEFQKRRPQKIT
Foxp1b   RHNLSLHKCFVRVENVKGAVWTVDELEFQKRRPQKIS
                                    *          *
```

B

```
FOXP1    CKWPGCEAVCEDFQSFLKHLNSEHAL
Foxp1a   CKWPGDEAVFGDFQSFLKHLNSEHAL
Foxp1b   CKWPGCEAVFEDFQSFLKHLNNEHAL
           *    **              *
```

Figure 7.1 – Alignment of the ZFD and FHD of zebrafish and human FOXP1. A. Alignment of the FHD of human FOXP1 with zebrafish Foxp1a and Foxp1b. The alignment was generated using Clustal Omega. Red letters and asterisks highlight amino acids changes. **B.** Alignment of the ZFD of human FOXP1 with zebrafish Foxp1a and Foxp1b. The alignment was generated using Clustal Omega. Red letters and asterisks highlight amino acids changes

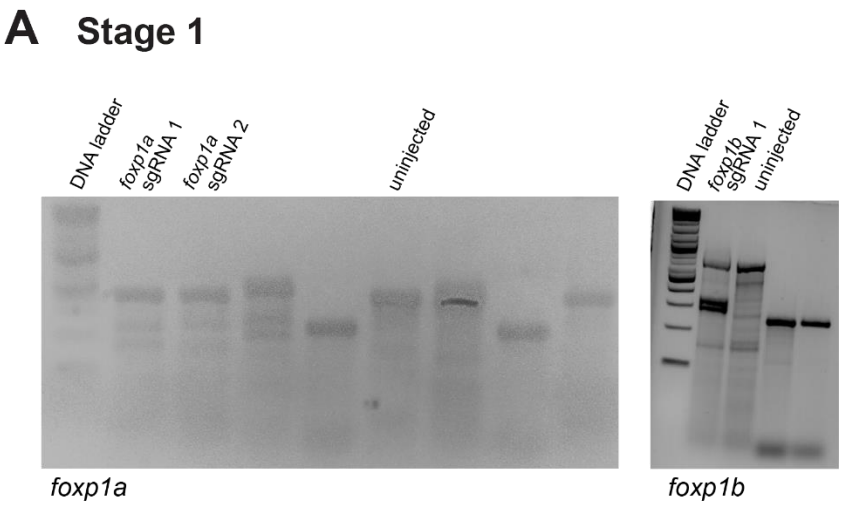

Figure 7.2 – Complete gels from Figure 3.4 (CRISPR/Cas9 induces mutations at the *foxp1a* and *foxp1b* loci).

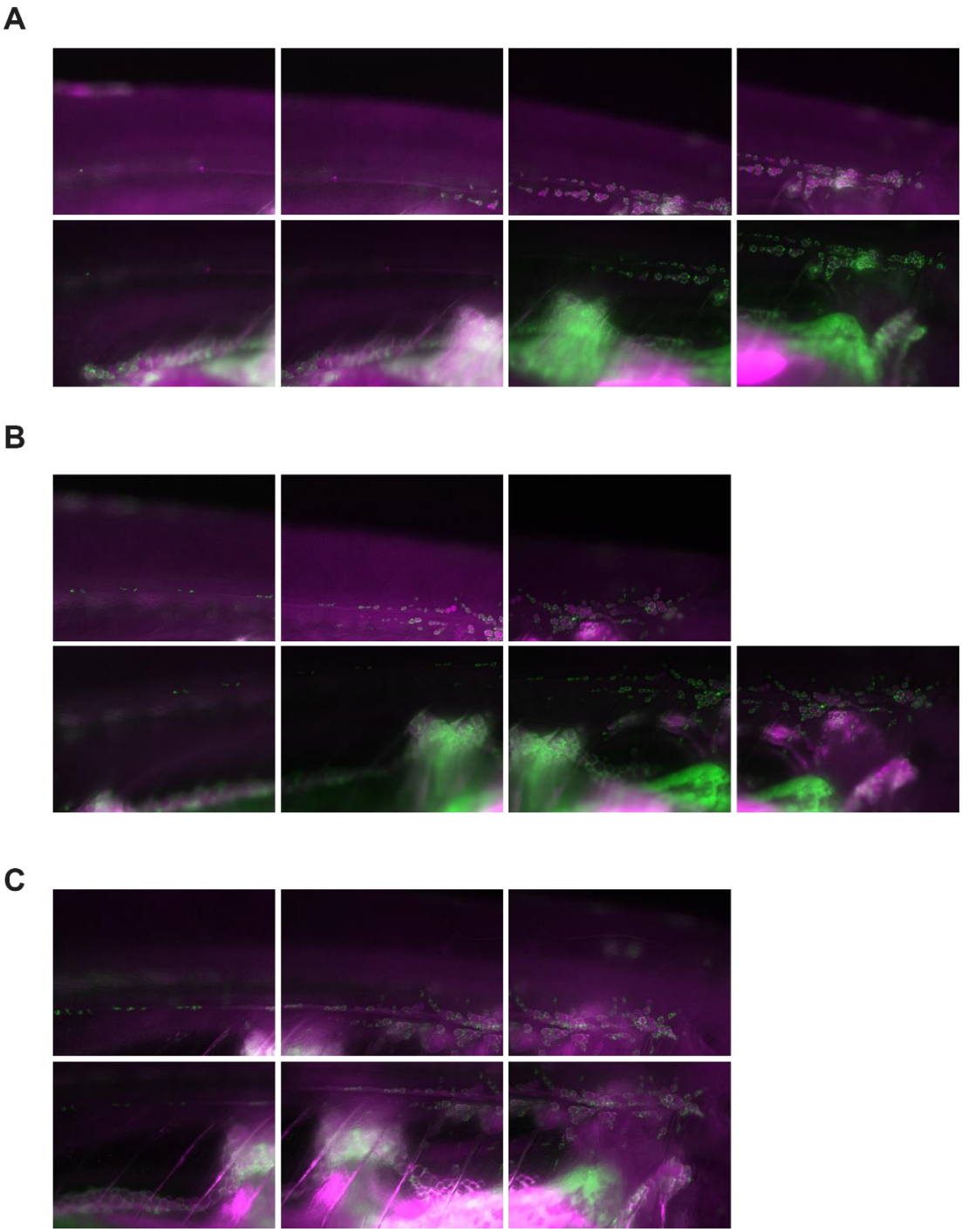

Figure 7.3 – Unprocessed images from chapter 4. A. Unprocessed images from figure 4.4B. **B.** Unprocessed images from figure 4.8B. Images are from the *foxp1a*$^{(-/-)}$ mutant upper panel. **C.** Unprocessed images from figure 4.8B. Images are from the *foxp1a*$^{(-/-)}$ mutant lower panel.

Chapter 8 – References

Agha, M., and Agha, R. (2017). The rising prevalence of obesity: part A: impact on public health. International journal of surgery Oncology *2*, e17.

Al-Goblan, A.S., Al-Alfi, M.A., and Khan, M.Z. (2014). Mechanism linking diabetes mellitus and obesity. Diabetes, metabolic syndrome and obesity : targets and therapy *7*, 587-591.

Andres-Delgado, L., and Mercader, N. (2016). Interplay between cardiac function and heart development. Biochimica et biophysica acta *1863*, 1707-1716.

Arber, S. (2008). FoxP1: conducting the Hox symphony in spinal motor neurons. Nature neuroscience *11*, 1122-1124.

Bacon, C., Schneider, M., Le Magueresse, C., Froehlich, H., Sticht, C., Gluch, C., Monyer, H., and Rappold, G.A. (2015). Brain-specific Foxp1 deletion impairs neuronal development and causes autistic-like behaviour. Molecular psychiatry *20*, 632-639.

Barak, Y., Nelson, M.C., Ong, E.S., Jones, Y.Z., Ruiz-Lozano, P., Chien, K.R., Koder, A., and Evans, R.M. (1999). PPAR gamma is required for placental, cardiac, and adipose tissue development. Molecular cell *4*, 585-595.

Barlow, W.E., White, E., Ballard-Barbash, R., Vacek, P.M., Titus-Ernstoff, L., Carney, P.A., Tice, J.A., Buist, D.S., Geller, B.M., Rosenberg, R.*, et al.* (2006). Prospective breast cancer risk prediction model for women undergoing screening mammography. Journal of the National Cancer Institute *98*, 1204-1214.

Barroso, I., Gurnell, M., Crowley, V.E., Agostini, M., Schwabe, J.W., Soos, M.A., Maslen, G.L., Williams, T.D., Lewis, H., Schafer, A.J.*, et al.* (1999). Dominant negative mutations in human PPARgamma associated with severe insulin resistance, diabetes mellitus and hypertension. Nature *402*, 880-883.

Berry, R., and Rodeheffer, M.S. (2013). Characterization of the adipocyte cellular lineage in vivo. Nature cell biology *15*, 302-308.

Bluher, M. (2010). The distinction of metabolically 'healthy' from 'unhealthy' obese individuals. Current opinion in lipidology *21*, 38-43.

Brzoska, M., Geiger, H., Gauer, S., and Baer, P. (2005). Epithelial differentiation of human adipose tissue-derived adult stem cells. Biochemical and biophysical research communications *330*, 142-150.

Calle, E.E., Rodriguez, C., Walker-Thurmond, K., and Thun, M.J. (2003). Overweight, obesity, and mortality from cancer in a prospectively studied cohort of U.S. adults. The New England journal of medicine *348*, 1625-1638

Carten, J.D., Bradford, M.K., and Farber, S.A. (2011). Visualizing digestive organ morphology and function using differential fatty acid metabolism in live zebrafish. Developmental biology *360*, 276-285.

Cawthorn, W.P., Scheller, E.L., and MacDougald, O.A. (2012). Adipose tissue stem cells meet preadipocyte commitment: going back to the future. Journal of lipid research *53*, 227-246.

Chen, Z., Torrens, J.I., Anand, A., Spiegelman, B.M., and Friedman, J.M. (2005). Krox20 stimulates adipogenesis via C/EBPbeta-dependent and -independent mechanisms. Cell metabolism *1*, 93-106

Cheng, L., Chong, M., Fan, W., Guo, X., Zhang, W., Yang, X., Liu, F., Gui, Y., and Lu, D. (2007). Molecular cloning, characterization, and developmental expression of foxp1 in zebrafish. Development genes and evolution *217*, 699-707.

Chu, Y.P., Chang, C.H., Shiu, J.H., Chang, Y.T., Chen, C.Y., and Chuang, W.J. (2011). Solution structure and backbone dynamics of the DNA-binding domain of FOXP1: insight into its domain swapping and DNA binding. Protein science : a publication of the Protein Society *20*, 908-924.

Civelek, M., Wu, Y., Pan, C., Raulerson, C.K., Ko, A., He, A., Tilford, C., Saleem, N.K., Stancakova, A., Scott, L.J., *et al.* (2017). Genetic Regulation of Adipose Gene Expression and Cardio-Metabolic Traits. American journal of human genetics *100*, 428-443.
Cleal, L., Aldea, T., and Chau, Y.Y. (2017). Fifty shades of white: Understanding heterogeneity in white adipose stem cells. Adipocyte *6*, 205-216.
Collaboration, N.C.D.R.F. (2016). Trends in adult body-mass index in 200 countries from 1975 to 2014: a pooled analysis of 1698 population-based measurement studies with 19.2 million participants. Lancet *387*, 1377-1396.
Collaborators, G.B.D.O., Afshin, A., Forouzanfar, M.H., Reitsma, M.B., Sur, P., Estep, K., Lee, A., Marczak, L., Mokdad, A.H., Moradi-Lakeh, M., *et al.* (2017). Health Effects of Overweight and Obesity in 195 Countries over 25 Years. The New England journal of medicine *377*, 13-27.
Crewe, C., An, Y.A., and Scherer, P.E. (2017). The ominous triad of adipose tissue dysfunction: inflammation, fibrosis, and impaired angiogenesis. The Journal of clinical investigation *127*, 74-82.
Drummond, I.A., and Davidson, A.J. (2016). Zebrafish kidney development. Methods in cell biology *134*, 391-429.
El-Brolosy, M.A., Kontarakis, Z., Rossi, A., Kuenne, C., Gunther, S., Fukuda, N., Kikhi, K., Boezio, G.L.M., Takacs, C.M., Lai, S.L., *et al.* (2019). Genetic compensation triggered by mutant mRNA degradation. Nature *568*, 193-197.
El-Gebali, S., Mistry, J., Bateman, A., Eddy, S.R., Luciani, A., Potter, S.C., Qureshi, M., Richardson, L.J., Salazar, G.A., Smart, A., *et al.* (2019). The Pfam protein families database in 2019. Nucleic acids research *47*, D427-D432.
Fagerberg, L., Hallstrom, B.M., Oksvold, P., Kampf, C., Djureinovic, D., Odeberg, J., Habuka, M., Tahmasebpoor, S., Danielsson, A., Edlund, K., *et al.* (2014). Analysis of the human tissue-specific expression by genome-wide integration of transcriptomics and antibody-based proteomics. Molecular & cellular proteomics : MCP *13*, 397-406.
Fisher, S., Grice, E.A., Vinton, R.M., Bessling, S.L., Urasaki, A., Kawakami, K., and McCallion, A.S. (2006). Evaluating the biological relevance of putative enhancers using Tol2 transposon-mediated transgenesis in zebrafish. Nature protocols *1*, 1297-1305.
Flodby, P., Barlow, C., Kylefjord, H., Ahrlund-Richter, L., and Xanthopoulos, K.G. (1996). Increased hepatic cell proliferation and lung abnormalities in mice deficient in CCAAT/enhancer binding protein alpha. The Journal of biological chemistry *271*, 24753-24760.
Floyd, Z.E., and Stephens, J.M. (2003). STAT5A promotes adipogenesis in nonprecursor cells and associates with the glucocorticoid receptor during adipocyte differentiation. Diabetes *52*, 308-314
Flynn, E.J., 3rd, Trent, C.M., and Rawls, J.F. (2009). Ontogeny and nutritional control of adipogenesis in zebrafish (Danio rerio). Journal of lipid research *50*, 1641-1652.
Fox, C.S., Liu, Y., White, C.C., Feitosa, M., Smith, A.V., Heard-Costa, N., Lohman, K., Consortium, G., Consortium, M., Consortium, G., *et al.* (2012). Genome-wide association for abdominal subcutaneous and visceral adipose reveals a novel locus for visceral fat in women. PLoS genetics *8*, e1002695.
Fu, N.Y., Pal, B., Chen, Y., Jackling, F.C., Milevskiy, M., Vaillant, F., Capaldo, B.D., Guo, F., Liu, K.H., Rios, A.C., *et al.* (2018). Foxp1 Is Indispensable for Ductal Morphogenesis and Controls the Exit of Mammary Stem Cells from Quiescence. Developmental cell *47*, 629-644 e628.
Gabut, M., Samavarchi-Tehrani, P., Wang, X., Slobodeniuc, V., O'Hanlon, D., Sung, H.K., Alvarez, M., Talukder, S., Pan, Q., Mazzoni, E.O., *et al.* (2011). An alternative splicing switch regulates embryonic stem cell pluripotency and reprogramming. Cell *147*, 132-146.

Gene Ontology, C. (2008). The Gene Ontology project in 2008. Nucleic acids research *36*, D440-444.
Gerin, I., Bommer, G.T., Lidell, M.E., Cederberg, A., Enerback, S., and Macdougald, O.A. (2009). On the role of FOX transcription factors in adipocyte differentiation and insulin-stimulated glucose uptake. The Journal of biological chemistry *284*, 10755-10763.
Gesta, S., Bluher, M., Yamamoto, Y., Norris, A.W., Berndt, J., Kralisch, S., Boucher, J., Lewis, C., and Kahn, C.R. (2006). Evidence for a role of developmental genes in the origin of obesity and body fat distribution. Proceedings of the National Academy of Sciences of the United States of America *103*, 6676-6681.
Gesta, S., Tseng, Y.H., and Kahn, C.R. (2007). Developmental origin of fat: tracking obesity to its source. Cell *131*, 242-256.
Ghaben, A.L., and Scherer, P.E. (2019). Adipogenesis and metabolic health. Nature reviews Molecular cell biology *20*, 242-258.
Gonzalez-Rosa, J.M., Burns, C.E., and Burns, C.G. (2017). Zebrafish heart regeneration: 15 years of discoveries. Regeneration *4*, 105-123.
Green, H., and Kehinde, O. (1976). Spontaneous heritable changes leading to increased adipose conversion in 3T3 cells. Cell *7*, 105-113.
Haas, P., and Gilmour, D. (2006). Chemokine signaling mediates self-organizing tissue migration in the zebrafish lateral line. Developmental cell *10*, 673-680.
Haczeyni, F., Bell-Anderson, K.S., and Farrell, G.C. (2018). Causes and mechanisms of adipocyte enlargement and adipose expansion. Obesity reviews : an official journal of the International Association for the Study of Obesity *19*, 406-420.
Haffner, S.M. (2006). Relationship of metabolic risk factors and development of cardiovascular disease and diabetes. Obesity *14 Suppl 3*, 121S-127S.
Hannenhalli, S., and Kaestner, K.H. (2009). The evolution of Fox genes and their role in development and disease. Nature reviews Genetics *10*, 233-240.
Heisler, L.K., and Lam, D.D. (2017). An appetite for life: brain regulation of hunger and satiety. Current opinion in pharmacology *37*, 100-106.
Hepler, C., Shan, B., Zhang, Q., Henry, G.H., Shao, M., Vishvanath, L., Ghaben, A.L., Mobley, A.B., Strand, D., Hon, G.C*., et al.* (2018). Identification of functionally distinct fibro-inflammatory and adipogenic stromal subpopulations in visceral adipose tissue of adult mice. eLife *7*.
Hepler, C., Vishvanath, L., and Gupta, R.K. (2017). Sorting out adipocyte precursors and their role in physiology and disease. Genes & development *31*, 127-140.
Hiller, M., Agarwal, S., Notwell, J.H., Parikh, R., Guturu, H., Wenger, A.M., and Bejerano, G. (2013). Computational methods to detect conserved non-genic elements in phylogenetically isolated genomes: application to zebrafish. Nucleic acids research *41*, e151.
Hinney, A., Vogel, C.I., and Hebebrand, J. (2010). From monogenic to polygenic obesity: recent advances. European child & adolescent psychiatry *19*, 297-310.
Hoffmann, T.J., Choquet, H., Yin, J., Banda, Y., Kvale, M.N., Glymour, M., Schaefer, C., Risch, N., and Jorgenson, E. (2018). A Large Multiethnic Genome-Wide Association Study of Adult Body Mass Index Identifies Novel Loci. Genetics *210*, 499-515.
Hoffstedt, J., Arner, E., Wahrenberg, H., Andersson, D.P., Qvisth, V., Lofgren, P., Ryden, M., Thorne, A., Wiren, M., Palmer, M*., et al.* (2010). Regional impact of adipose tissue morphology on the metabolic profile in morbid obesity. Diabetologia *53*, 2496-2503.
Hollenberg, C.H., and Vost, A. (1969). Regulation of DNA synthesis in fat cells and stromal elements from rat adipose tissue. The Journal of clinical investigation *47*, 2485-2498.

Hu, H., Wang, B., Borde, M., Nardone, J., Maika, S., Allred, L., Tucker, P.W., and Rao, A. (2006). Foxp1 is an essential transcriptional regulator of B cell development. Nature immunology *7*, 819-826.
Hubert, H.B., Feinleib, M., McNamara, P.M., and Castelli, W.P. (1983). Obesity as an independent risk factor for cardiovascular disease: a 26-year follow-up of participants in the Framingham Heart Study. Circulation *67*, 968-977.
Hwang, W.Y., Fu, Y., Reyon, D., Maeder, M.L., Kaini, P., Sander, J.D., Joung, J.K., Peterson, R.T., and Yeh, J.R. (2013). Heritable and precise zebrafish genome editing using a CRISPR-Cas system. PloS one *8*, e68708.
Ibrahim, M.M. (2010). Subcutaneous and visceral adipose tissue: structural and functional differences. Obesity reviews : an official journal of the International Association for the Study of Obesity *11*, 11-18.
Imrie, D., and Sadler, K.C. (2010). White adipose tissue development in zebrafish is regulated by both developmental time and fish size. Developmental dynamics : an official publication of the American Association of Anatomists *239*, 3013-3023.
Jiang, Y., Berry, D.C., Jo, A., Tang, W., Arpke, R.W., Kyba, M., and Graff, J.M. (2017). A PPARgamma transcriptional cascade directs adipose progenitor cell-niche interaction and niche expansion. Nature communications *8*, 15926.
Jiang, Y., Berry, D.C., Tang, W., and Graff, J.M. (2014). Independent stem cell lineages regulate adipose organogenesis and adipose homeostasis. Cell reports *9*, 1007-1022.
Kenchaiah, S., Evans, J.C., Levy, D., Wilson, P.W., Benjamin, E.J., Larson, M.G., Kannel, W.B., and Vasan, R.S. (2002). Obesity and the risk of heart failure. The New England journal of medicine *347*, 305-313.
Khera, A.V., Chaffin, M., Wade, K.H., Zahid, S., Brancale, J., Xia, R., Distefano, M., Senol-Cosar, O., Haas, M.E., Bick, A.*, et al.* (2019). Polygenic Prediction of Weight and Obesity Trajectories from Birth to Adulthood. Cell *177*, 587-596 e589.
Kichaev, G., Bhatia, G., Loh, P.R., Gazal, S., Burch, K., Freund, M.K., Schoech, A., Pasaniuc, B., and Price, A.L. (2019). Leveraging Polygenic Functional Enrichment to Improve GWAS Power. American journal of human genetics *104*, 65-75.
Kikuchi, K. (2014). Advances in understanding the mechanism of zebrafish heart regeneration. Stem cell research *13*, 542-555.
Kim, J.B., and Spiegelman, B.M. (1996). ADD1/SREBP1 promotes adipocyte differentiation and gene expression linked to fatty acid metabolism. Genes & development *10*, 1096-1107.
Kim, J.Y., van de Wall, E., Laplante, M., Azzara, A., Trujillo, M.E., Hofmann, S.M., Schraw, T., Durand, J.L., Li, H., Li, G.*, et al.* (2007). Obesity-associated improvements in metabolic profile through expansion of adipose tissue. The Journal of clinical investigation *117*, 2621-2637.
Kleinjan, D.A., Bancewicz, R.M., Gautier, P., Dahm, R., Schonthaler, H.B., Damante, G., Seawright, A., Hever, A.M., Yeyati, P.L., van Heyningen, V.*, et al.* (2008). Subfunctionalization of duplicated zebrafish pax6 genes by cis-regulatory divergence. PLoS genetics *4*, e29.
Koliaki, C., Liatis, S., and Kokkinos, A. (2019). Obesity and cardiovascular disease: revisiting an old relationship. Metabolism: clinical and experimental *92*, 98-107.
Kovacs, K.A., Steinmann, M., Magistretti, P.J., Halfon, O., and Cardinaux, J.R. (2003). CCAAT/enhancer-binding protein family members recruit the coactivator CREB-binding protein and trigger its phosphorylation. The Journal of biological chemistry *278*, 36959-36965.
Labun, K., Montague, T.G., Gagnon, J.A., Thyme, S.B., and Valen, E. (2016). CHOPCHOP v2: a web tool for the next generation of CRISPR genome engineering. Nucleic acids research *44*, W272-276.

Lafontan, M. (2014). Adipose tissue and adipocyte dysregulation. Diabetes & metabolism *40*, 16-28.
Lapid, K., and Graff, J.M. (2017). Form(ul)ation of adipocytes by lipids. Adipocyte *6*, 176-186.
Lear, T., Dunn, S.R., McKelvey, A.C., Mir, A., Evankovich, J., Chen, B.B., and Liu, Y. (2017). RING finger protein 113A regulates C-X-C chemokine receptor type 4 stability and signaling. American journal of physiology Cell physiology *313*, C584-C592.
Lefterova, M.I., and Lazar, M.A. (2009). New developments in adipogenesis. Trends in endocrinology and metabolism: TEM *20*, 107-114.
Lefterova, M.I., Zhang, Y., Steger, D.J., Schupp, M., Schug, J., Cristancho, A., Feng, D., Zhuo, D., Stoeckert, C.J., Jr., Liu, X.S.*, et al.* (2008). PPARgamma and C/EBP factors orchestrate adipocyte biology via adjacent binding on a genome-wide scale. Genes & development *22*, 2941-2952.
Leishman, E., Howard, J.M., Garcia, G.E., Miao, Q., Ku, A.T., Dekker, J.D., Tucker, H., and Nguyen, H. (2013). Foxp1 maintains hair follicle stem cell quiescence through regulation of Fgf18. Development *140*, 3809-3818.
Letunic, I., and Bork, P. (2018). 20 years of the SMART protein domain annotation resource. Nucleic acids research *46*, D493-D496.
Li, H., Liu, P., Xu, S., Li, Y., Dekker, J.D., Li, B., Fan, Y., Zhang, Z., Hong, Y., Yang, G.*, et al.* (2017). FOXP1 controls mesenchymal stem cell commitment and senescence during skeletal aging. The Journal of clinical investigation *127*, 1241-1253.
Li, S., Weidenfeld, J., and Morrisey, E.E. (2004). Transcriptional and DNA binding activity of the Foxp1/2/4 family is modulated by heterotypic and homotypic protein interactions. Molecular and cellular biology *24*, 809-822.
Lieschke, G.J., and Currie, P.D. (2007). Animal models of human disease: zebrafish swim into view. Nature reviews Genetics *8*, 353-367.
Linhart, H.G., Ishimura-Oka, K., DeMayo, F., Kibe, T., Repka, D., Poindexter, B., Bick, R.J., and Darlington, G.J. (2001). C/EBPalpha is required for differentiation of white, but not brown, adipose tissue. Proceedings of the National Academy of Sciences of the United States of America *98*, 12532-12537.
Liu, P., Huang, S., Ling, S., Xu, S., Wang, F., Zhang, W., Zhou, R., He, L., Xia, X., Yao, Z.*, et al.* (2019). Foxp1 controls brown/beige adipocyte differentiation and thermogenesis through regulating beta3-AR desensitization. Nature communications *10*, 5070.
Lowe, C.E., O'Rahilly, S., and Rochford, J.J. (2011). Adipogenesis at a glance. Journal of cell science *124*, 2681-2686.
Ma, X., Lee, P., Chisholm, D.J., and James, D.E. (2015). Control of adipocyte differentiation in different fat depots; implications for pathophysiology or therapy. Frontiers in endocrinology *6*, 1.
Maes, H.H., Neale, M.C., and Eaves, L.J. (1997). Genetic and environmental factors in relative body weight and human adiposity. Behavior genetics *27*, 325-351.
Manolio, T.A., Collins, F.S., Cox, N.J., Goldstein, D.B., Hindorff, L.A., Hunter, D.J., McCarthy, M.I., Ramos, E.M., Cardon, L.R., Chakravarti, A.*, et al.* (2009). Finding the missing heritability of complex diseases. Nature *461*, 747-753.
Manson, J.E., Colditz, G.A., Stampfer, M.J., Willett, W.C., Rosner, B., Monson, R.R., Speizer, F.E., and Hennekens, C.H. (1990). A prospective study of obesity and risk of coronary heart disease in women. The New England journal of medicine *322*, 882-889.
Martin, K.A., Mani, M.V., and Mani, A. (2015). New targets to treat obesity and the metabolic syndrome. European journal of pharmacology *763*, 64-74.

McMenamin, S.K., Minchin, J.E., Gordon, T.N., Rawls, J.F., and Parichy, D.M. (2013). Dwarfism and increased adiposity in the gh1 mutant zebrafish vizzini. Endocrinology *154*, 1476-1487.
Medina, E., Cordova, C., Villalobos, P., Reyes, J., Komives, E.A., Ramirez-Sarmiento, C.A., and Babul, J. (2016). Three-Dimensional Domain Swapping Changes the Folding Mechanism of the Forkhead Domain of FoxP1. Biophysical journal *110*, 2349-2360.
Meguro, S., Hasumura, T., and Hase, T. (2015). Body fat accumulation in zebrafish is induced by a diet rich in fat and reduced by supplementation with green tea extract. PloS one *10*, e0120142.
Merrick, D., Sakers, A., Irgebay, Z., Okada, C., Calvert, C., Morley, M.P., Percec, I., and Seale, P. (2019). Identification of a mesenchymal progenitor cell hierarchy in adipose tissue. Science *364*.
Minchin, J.E., Dahlman, I., Harvey, C.J., Mejhert, N., Singh, M.K., Epstein, J.A., Arner, P., Torres-Vazquez, J., and Rawls, J.F. (2015). Plexin D1 determines body fat distribution by regulating the type V collagen microenvironment in visceral adipose tissue. Proceedings of the National Academy of Sciences of the United States of America *112*, 4363-4368.
Minchin, J.E., and Rawls, J.F. (2011). In vivo analysis of white adipose tissue in zebrafish. Methods in cell biology *105*, 63-86.
Minchin, J.E., and Rawls, J.F. (2017a). In vivo imaging and quantification of regional adiposity in zebrafish. Methods in cell biology *138*, 3-27.
Minchin, J.E.N., and Rawls, J.F. (2017b). A classification system for zebrafish adipose tissues. Disease models & mechanisms *10*, 797-809.
Nica, A.C., and Dermitzakis, E.T. (2013). Expression quantitative trait loci: present and future. Philosophical transactions of the Royal Society of London Series B, Biological sciences *368*, 20120362.
Oishi, Y., Manabe, I., and Nagai, R. (2011). [Kruppel-like family of transcription factor 5 (KLF5). KLF5 is a key regulator of adipocyte differentiation]. Nihon rinsho Japanese journal of clinical medicine *69 Suppl 1*, 264-268
Oka, T., Nishimura, Y., Zang, L., Hirano, M., Shimada, Y., Wang, Z., Umemoto, N., Kuroyanagi, J., Nishimura, N., and Tanaka, T. (2010). Diet-induced obesity in zebrafish shares common pathophysiological pathways with mammalian obesity. BMC physiology *10*, 21.
Pandey, A., Patel, K.V., Vaduganathan, M., Sarma, S., Haykowsky, M.J., Berry, J.D., and Lavie, C.J. (2018). Physical Activity, Fitness, and Obesity in Heart Failure With Preserved Ejection Fraction. JACC Heart failure *6*, 975-982.
Parichy, D.M., Elizondo, M.R., Mills, M.G., Gordon, T.N., and Engeszer, R.E. (2009). Normal table of postembryonic zebrafish development: staging by externally visible anatomy of the living fish. Developmental dynamics : an official publication of the American Association of Anatomists *238*, 2975-3015.
Park, J., Morley, T.S., Kim, M., Clegg, D.J., and Scherer, P.E. (2014). Obesity and cancer--mechanisms underlying tumour progression and recurrence. Nature reviews Endocrinology *10*, 455-465
Poznanski, W.J., Waheed, I., and Van, R. (1973). Human fat cell precursors. Morphologic and metabolic differentiation in culture. Laboratory investigation; a journal of technical methods and pathology *29*, 570-576.
Preibisch, S., Saalfeld, S., and Tomancak, P. (2009). Globally optimal stitching of tiled 3D microscopic image acquisitions. Bioinformatics *25*, 1463-1465.
Raajendiran, A., Ooi, G., Bayliss, J., O'Brien, P.E., Schittenhelm, R.B., Clark, A.K., Taylor, R.A., Rodeheffer, M.S., Burton, P.R., and Watt, M.J. (2019). Identification of Metabolically Distinct Adipocyte Progenitor Cells in Human Adipose Tissues. Cell reports *27*, 1528-1540 e1527.

Rabkin, S.W., Mathewson, F.A., and Hsu, P.H. (1977). Relation of body weight to development of ischemic heart disease in a cohort of young North American men after a 26 year observation period: the Manitoba Study. The American journal of cardiology *39*, 452-458.
Rafferty, S.A., and Quinn, T.A. (2018). A beginner's guide to understanding and implementing the genetic modification of zebrafish. Progress in biophysics and molecular biology *138*, 3-19.
Rao, D.S., O'Connell, R.M., Chaudhuri, A.A., Garcia-Flores, Y., Geiger, T.L., and Baltimore, D. (2010). MicroRNA-34a perturbs B lymphocyte development by repressing the forkhead box transcription factor Foxp1. Immunity *33*, 48-59.
Rodeheffer, M.S., Birsoy, K., and Friedman, J.M. (2008). Identification of white adipocyte progenitor cells in vivo. Cell *135*, 240-249.
Rosen, E.D., Sarraf, P., Troy, A.E., Bradwin, G., Moore, K., Milstone, D.S., Spiegelman, B.M., and Mortensen, R.M. (1999). PPAR gamma is required for the differentiation of adipose tissue in vivo and in vitro. Molecular cell *4*, 611-617
Saez, E., Rosenfeld, J., Livolsi, A., Olson, P., Lombardo, E., Nelson, M., Banayo, E., Cardiff, R.D., Izpisua-Belmonte, J.C., and Evans, R.M. (2004). PPAR gamma signaling exacerbates mammary gland tumor development. Genes & development *18*, 528-540.
Salans, L.B., Cushman, S.W., and Weismann, R.E. (1973). Studies of human adipose tissue. Adipose cell size and number in nonobese and obese patients. The Journal of clinical investigation *52*, 929-941.
Sarusi Portuguez, A., Schwartz, M., Siersbaek, R., Nielsen, R., Sung, M.H., Mandrup, S., Kaplan, T., and Hakim, O. (2017). Hierarchical role for transcription factors and chromatin structure in genome organization along adipogenesis. The FEBS journal *284*, 3230-3244.
Schoettl, T., Fischer, I.P., and Ussar, S. (2018). Heterogeneity of adipose tissue in development and metabolic function. The Journal of experimental biology *221*.
Schwalie, P.C., Dong, H., Zachara, M., Russeil, J., Alpern, D., Akchiche, N., Caprara, C., Sun, W., Schlaudraff, K.U., Soldati, G.*, et al.* (2018). A stromal cell population that inhibits adipogenesis in mammalian fat depots. Nature *559*, 103-108.
Semova, I., Carten, J.D., Stombaugh, J., Mackey, L.C., Knight, R., Farber, S.A., and Rawls, J.F. (2012). Microbiota regulate intestinal absorption and metabolism of fatty acids in the zebrafish. Cell host & microbe *12*, 277-288.
Sempere, J.M., Martinez-Peinado, P., Arribas, M.I., Reig, J.A., De La Sen, M.L., Zubcoff, J.J., Fraga, M.F., Fernandez, A.F., Santana, A., and Roche, E. (2014). Single cell-derived clones from human adipose stem cells present different immunomodulatory properties. Clinical and experimental immunology *176*, 255-265.
Sharma, M.K., Liu, R.Z., Thisse, C., Thisse, B., Denovan-Wright, E.M., and Wright, J.M. (2006). Hierarchical subfunctionalization of fabp1a, fabp1b and fabp10 tissue-specific expression may account for retention of these duplicated genes in the zebrafish (Danio rerio) genome. The FEBS journal *273*, 3216-3229.
Shimada, Y., Hirano, M., Nishimura, Y., and Tanaka, T. (2012). A high-throughput fluorescence-based assay system for appetite-regulating gene and drug screening. PloS one *7*, e52549.
Shu, W., Yang, H., Zhang, L., Lu, M.M., and Morrisey, E.E. (2001). Characterization of a new subfamily of winged-helix/forkhead (Fox et al.) genes that are expressed in the lung and act as transcriptional repressors. The Journal of biological chemistry *276*, 27488-27497.
Siersbaek, R., Baek, S., Rabiee, A., Nielsen, R., Traynor, S., Clark, N., Sandelin, A., Jensen, O.N., Sung, M.H., Hager, G.L.*, et al.* (2014). Molecular architecture of transcription factor hotspots in early adipogenesis. Cell reports *7*, 1434-1442.

Siersbaek, R., Madsen, J.G.S., Javierre, B.M., Nielsen, R., Bagge, E.K., Cairns, J., Wingett, S.W., Traynor, S., Spivakov, M., Fraser, P.*, et al.* (2017). Dynamic Rewiring of Promoter-Anchored Chromatin Loops during Adipocyte Differentiation. Molecular cell *66*, 420-435 e425.
Siersbaek, R., and Mandrup, S. (2011). Transcriptional networks controlling adipocyte differentiation. Cold Spring Harbor symposia on quantitative biology *76*, 247-255.
Siersbaek, R., Nielsen, R., John, S., Sung, M.H., Baek, S., Loft, A., Hager, G.L., and Mandrup, S. (2011). Extensive chromatin remodelling and establishment of transcription factor 'hotspots' during early adipogenesis. The EMBO journal *30*, 1459-1472.
Siersbaek, R., Nielsen, R., and Mandrup, S. (2012). Transcriptional networks and chromatin remodeling controlling adipogenesis. Trends in endocrinology and metabolism: TEM *23*, 56-64.
Skurk, T., Alberti-Huber, C., Herder, C., and Hauner, H. (2007). Relationship between adipocyte size and adipokine expression and secretion. The Journal of clinical endocrinology and metabolism *92*, 1023-1033.
Song, Y., and Cone, R.D. (2007). Creation of a genetic model of obesity in a teleost. FASEB journal : official publication of the Federation of American Societies for Experimental Biology *21*, 2042-2049.
Spalding, K.L., Arner, E., Westermark, P.O., Bernard, S., Buchholz, B.A., Bergmann, O., Blomqvist, L., Hoffstedt, J., Naslund, E., Britton, T.*, et al.* (2008). Dynamics of fat cell turnover in humans. Nature *453*, 783-787.
Speakman, J.R., Loos, R.J.F., O'Rahilly, S., Hirschhorn, J.N., and Allison, D.B. (2018). GWAS for BMI: a treasure trove of fundamental insights into the genetic basis of obesity. International journal of obesity *42*, 1524-1531.
Speakman, J.R. (2019). Use of high-fat diets to study rodent obesity as a model of human obesity. International journal of obesity *43*, 1491-1492
Spiegelman, B.M., and Flier, J.S. (1996). Adipogenesis and obesity: rounding out the big picture. Cell *87*, 377-389.
Stroud, J.C., Wu, Y., Bates, D.L., Han, A., Nowick, K., Paabo, S., Tong, H., and Chen, L. (2006). Structure of the forkhead domain of FOXP2 bound to DNA. Structure *14*, 159-166.
Stumvoll, M., Goldstein, B.J., and van Haeften, T.W. (2005). Type 2 diabetes: principles of pathogenesis and therapy. Lancet *365*, 1333-1346.
Sugii, S., Olson, P., Sears, D.D., Saberi, M., Atkins, A.R., Barish, G.D., Hong, S.H., Castro, G.L., Yin, Y.Q., Nelson, M.C.*, et al.* (2009). PPARgamma activation in adipocytes is sufficient for systemic insulin sensitization. Proceedings of the National Academy of Sciences of the United States of America *106*, 22504-22509.
Tanaka, T., Yoshida, N., Kishimoto, T., and Akira, S. (1997). Defective adipocyte differentiation in mice lacking the C/EBPbeta and/or C/EBPdelta gene. The EMBO journal *16*, 7432-7443
Tang, Q.Q., Otto, T.C., and Lane, M.D. (2003). CCAAT/enhancer-binding protein beta is required for mitotic clonal expansion during adipogenesis. Proceedings of the National Academy of Sciences of the United States of America *100*, 850-855
Tang, W., Zeve, D., Suh, J.M., Bosnakovski, D., Kyba, M., Hammer, R.E., Tallquist, M.D., and Graff, J.M. (2008). White fat progenitor cells reside in the adipose vasculature. Science *322*, 583-586.
Teame, T., Zhang, Z., Ran, C., Zhang, H., Yang, Y., Ding, Q., Xie, M., Gao, C., Ye, Y., Duan, M.*, et al.* (2019). The use of zebrafish (Danio rerio) as biomedical models. Animal frontiers : the review magazine of animal agriculture *9*, 68-77.
Tingaud-Sequeira, A., Ouadah, N., and Babin, P.J. (2011). Zebrafish obesogenic test: a tool for screening molecules that target adiposity. Journal of lipid research *52*, 1765-1772.

Tran, K.V., Gealekman, O., Frontini, A., Zingaretti, M.C., Morroni, M., Giordano, A., Smorlesi, A., Perugini, J., De Matteis, R., Sbarbati, A*., et al.* (2012). The vascular endothelium of the adipose tissue gives rise to both white and brown fat cells. Cell metabolism *15*, 222-229.
Tran, T.T., Yamamoto, Y., Gesta, S., and Kahn, C.R. (2008). Beneficial effects of subcutaneous fat transplantation on metabolism. Cell metabolism *7*, 410-420.
Tsuboyama-Kasaoka, N., Takahashi, M., Tanemura, K., Kim, H.J., Tange, T., Okuyama, H., Kasai, M., Ikemoto, S., and Ezaki, O. (2000). Conjugated linoleic acid supplementation reduces adipose tissue by apoptosis and develops lipodystrophy in mice. Diabetes *49*, 1534-1542.
Untergasser, A., Nijveen, H., Rao, X., Bisseling, T., Geurts, R., and Leunissen, J.A. (2007). Primer3Plus, an enhanced web interface to Primer3. Nucleic acids research *35*, W71-74.
Van, R.L., Bayliss, C.E., and Roncari, D.A. (1976). Cytological and enzymological characterization of adult human adipocyte precursors in culture. The Journal of clinical investigation *58*, 699-704.
Varma, M.J., Breuls, R.G., Schouten, T.E., Jurgens, W.J., Bontkes, H.J., Schuurhuis, G.J., van Ham, S.M., and van Milligen, F.J. (2007). Phenotypical and functional characterization of freshly isolated adipose tissue-derived stem cells. Stem cells and development *16*, 91-104.
Veilleux, A., Caron-Jobin, M., Noel, S., Laberge, P.Y., and Tchernof, A. (2011). Visceral adipocyte hypertrophy is associated with dyslipidemia independent of body composition and fat distribution in women. Diabetes *60*, 1504-1511.
Vidal, H. (2001). Gene expression in visceral and subcutaneous adipose tissues. Annals of medicine *33*, 547-555.
Virtue, S., and Vidal-Puig, A. (2008). It's not how fat you are, it's what you do with it that counts. PLoS biology *6*, e237.
Vishvanath, L., MacPherson, K.A., Hepler, C., Wang, Q.A., Shao, M., Spurgin, S.B., Wang, M.Y., Kusminski, C.M., Morley, T.S., and Gupta, R.K. (2016). Pdgfrbeta+ Mural Preadipocytes Contribute to Adipocyte Hyperplasia Induced by High-Fat-Diet Feeding and Prolonged Cold Exposure in Adult Mice. Cell metabolism *23*, 350-359.
Visscher, P.M., Brown, M.A., McCarthy, M.I., and Yang, J. (2012). Five years of GWAS discovery. American journal of human genetics *90*, 7-24.
Vohl, M.C., Sladek, R., Robitaille, J., Gurd, S., Marceau, P., Richard, D., Hudson, T.J., and Tchernof, A. (2004). A survey of genes differentially expressed in subcutaneous and visceral adipose tissue in men. Obesity research *12*, 1217-1222.
Wafer, R., Tandon, P., and Minchin, J.E.N. (2017). The Role of Peroxisome Proliferator-Activated Receptor Gamma (PPARG) in Adipogenesis: Applying Knowledge from the Fish Aquaculture Industry to Biomedical Research. Frontiers in endocrinology *8*, 102.
Walters, J.W., Anderson, J.L., Bittman, R., Pack, M., and Farber, S.A. (2012). Visualization of lipid metabolism in the zebrafish intestine reveals a relationship between NPC1L1-mediated cholesterol uptake and dietary fatty acid. Chemistry & biology *19*, 913-925.
Wang, B., Lin, D., Li, C., and Tucker, P. (2003). Multiple domains define the expression and regulatory properties of Foxp1 forkhead transcriptional repressors. The Journal of biological chemistry *278*, 24259-24268.
Wang, B., Weidenfeld, J., Lu, M.M., Maika, S., Kuziel, W.A., Morrisey, E.E., and Tucker, P.W. (2004). Foxp1 regulates cardiac outflow tract, endocardial cushion morphogenesis and myocyte proliferation and maturation. Development *131*, 4477-4487.
Wang, F., Mullican, S.E., DiSpirito, J.R., Peed, L.C., and Lazar, M.A. (2013a). Lipoatrophy and severe metabolic disturbance in mice with fat-specific deletion of

PPARgamma. Proceedings of the National Academy of Sciences of the United States of America *110*, 18656-18661.
Wang, N.D., Finegold, M.J., Bradley, A., Ou, C.N., Abdelsayed, S.V., Wilde, M.D., Taylor, L.R., Wilson, D.R., and Darlington, G.J. (1995). Impaired energy homeostasis in C/EBP alpha knockout mice. Science *269*, 1108-1112.
Wang, Q.A., Tao, C., Gupta, R.K., and Scherer, P.E. (2013b). Tracking adipogenesis during white adipose tissue development, expansion and regeneration. Nature medicine *19*, 1338-1344.
Wang, Z., Gerstein, M., and Snyder, M. (2009). RNA-Seq: a revolutionary tool for transcriptomics. Nature reviews Genetics *10*, 57-63.
Watson, H.J., Yilmaz, Z., Thornton, L.M., Hubel, C., Coleman, J.R.I., Gaspar, H.A., Bryois, J., Hinney, A., Leppa, V.M., Mattheisen, M.*, et al.* (2019). Genome-wide association study identifies eight risk loci and implicates metabo-psychiatric origins for anorexia nervosa. Nature genetics *51*, 1207-1214.
White, R., Rose, K., and Zon, L. (2013). Zebrafish cancer: the state of the art and the path forward. Nature reviews Cancer *13*, 624-636.
Wueest, S., Rapold, R.A., Rytka, J.M., Schoenle, E.J., and Konrad, D. (2009). Basal lipolysis, not the degree of insulin resistance, differentiates large from small isolated adipocytes in high-fat fed mice. Diabetologia *52*, 541-546.
Xue, Y., Lim, S., Brakenhielm, E., and Cao, Y. (2010). Adipose angiogenesis: quantitative methods to study microvessel growth, regression and remodeling in vivo. Nature protocols *5*, 912-920.
Yuan, H., Wen, B., Liu, X., Gao, C., Yang, R., Wang, L., Chen, S., Chen, Z., de The, H., Zhou, J.*, et al.* (2015). CCAAT/enhancer-binding protein alpha is required for hepatic outgrowth via the p53 pathway in zebrafish. Scientific reports *5*, 15838.
Zou, Y., Gong, N., Cui, Y., Wang, X., Cui, A., Chen, Q., Jiao, T., Dong, X., Yang, H., Zhang, S.*, et al.* (2015). Forkhead Box P1 (FOXP1) Transcription Factor Regulates Hepatic Glucose Homeostasis. The Journal of biological chemistry *290*, 30607-30615.
Zwick, R.K., Guerrero-Juarez, C.F., Horsley, V., and Plikus, M.V. (2018). Anatomical, Physiological, and Functional Diversity of Adipose Tissue. Cell metabolism *27*, 68-83.